FLOOD ROUTING ON SMALL STREAMS: A REVIEW OF MUSKINGUM-CUNGE, CASCADING RESERVOIRS, AND FULL DYNAMIC SOLUTIONS

BY

William Joseph Heatherman

Submitted to the graduate degree program in Civil Engineering and the Graduate Faculty of the University of Kansas in partial fulfillment of the requirements for the degree of Doctor of Philosophy.

_____
Committee Co-Chair

_____
Committee Co-Chair

_____

_____

_____
Committee Members

Date defended: _____

The Dissertation Committee for William Joseph Heatherman certifies that this is the approved version of the following dissertation:

FLOOD ROUTING ON SMALL STREAMS: A REVIEW OF MUSKINGUM-CUNGE, CASCADING RESERVOIRS, AND FULL DYNAMIC SOLUTIONS

Committee:

_____
Co-Chair

_____
Co-Chair

_____

_____

_____

Date approved: _____

Abstract

Flood wave routing methods are adapted for small, naturally meandering streams. A simplified derivation of the Muskingum-Cunge equation is presented, based on Perumal and Kalinin-Milyukov's "characteristic reach length" concept. The derivation was extended to meandering streams, using the "parallel channels" analogy. "Cascading reservoirs", a second approximate method, is shown to be a special case of Muskingum-Cunge when properly formulated. Both approximate methods were evaluated against two "fully dynamic" solutions: the UNET-based solver in HEC-RAS and the National Weather Service's FLDWAV program.

The four models were tested on four natural streams in northeastern Kansas. Detailed procedures for creating "equivalent reaches" were developed. The sensitivity of model stability was tested against variations in distance step size and other controls. HEC-RAS and FLDWAV gave nearly identical results for all the test reaches. The two approximate methods also performed well, but with deviations which are discussed. Recommendations were given for setting distance steps in fully dynamic solutions.

Acknowledgements

There are many people who supported me in completing this dissertation. My co-advisors, Dr. David Parr and Dr. Bruce McEnroe, each gave encouragement to undertake this effort and had confidence that it would succeed. When I entered the Civil Engineering program as an undergraduate in 1990, I had no idea what enduring mentors I had found. I have also appreciated the guidance and input of my committee, including Dr. Bryan Young, Dr. Robert Parsons, and Dr. Carl McElwee.

I relied heavily on the support of my co-workers at the City of Overland Park. Mike Ross has been a mentor and friend, who launched me into the business of flood modeling and reminded me to stay curious. Doug Brown and Bill Ebel each offered countless words of support along the way.

To my mom and dad, Loretta and Harry, and to my brothers and sisters, Kim, Becky, Jim and Mark, thank you for all your help and patience, especially this last year. To my son, Diego, thank you for letting me get lost in floodplain thoughts so many times when I should have been paying attention. I wish you the best of luck on your own adventures.

Table of Contents

Abstract iii

Acknowledgements iv

List of Tables xii

List of Figures xvi

Chapter 1 Introduction 1

1.1 Problem Statement 1

1.2 Objectives 2

Chapter 2 Literature Review 4

2.1 Overview of the Flood Routing Problem 4

2.1.1 Background 4

2.1.2 Flow Classifications 6

2.1.3 Kinematic and Dynamic Wave Speed 7

2.1.4 Saint Venant Equations 10

2.1.5 Method of Characteristics 12

2.1.6 Simplified Methods 13

2.2 Development of Muskingum and Muskingum-Cunge Methods 14

2.2.1 Muskingum Method 14

2.2.2 Development of Variable Parameter Muskingum-Cunge 14

2.2.3 Perumal's Derivations 15

2.2.4 Extensions to Incorporate Inertial Effects 16

2.3 Other Hydrologic or Approximate Methods 18

2.3.1 Lag Method 18
2.3.2 Kinematic Routing 18
2.3.3 Kalinin-Milyukov Method 19
2.3.4 Cascading Reservoirs Approximation 20
2.4 Accuracy Criteria for Muskingum-Cunge 22
2.4.1 Measures of Accuracy 22
2.4.2 Limitations of the Diffusion Wave Assumption 24
2.4.3 Use of Variable Parameters and Averaging Schemes 26
2.4.4 Volume Conservation 27
2.4.5 Negative Outflow Values and Initial "Dip" 29
2.4.6 Computational Time and Distance Steps 30
2.4.7 Acceptable Range for the "*X*" Parameter 31
2.5 Computer Models 32
2.5.1 Hydrologic Models - HEC-1 32
2.5.2 HEC-RAS 33
2.5.3 Full Dynamic Models - General 34
2.5.4 HEC-RAS Unsteady Flow Model (uRAS) 37
2.5.5 NWS FLDWAV Model 37
2.5.6 USGS FEQ Model 38
2.6 Compound and Meandering Channels 39
2.6.1 General Tests 39
2.6.2 Discharge Estimates for Compound Channels 41

2.6.3 Meandering in Two-Dimensional Planform 43

Chapter 3 Basic Derivations of Muskingum-Cunge and Related Methods 45

3.1 Derivation of the Saint Venant Equations 45

3.2 Derivation of Muskingum Method 54

3.3 Derivation of Muskingum-Cunge 57

3.4 Physical Interpretation of *K* and *X*. 66

3.5 Muskingum-Cunge as Implemented in HEC-1 68

3.6 Cascading Reservoir Method 70

3.6.1 Routing Equation for a Single Reservoir 71

3.6.2 Modeling Rivers, Finding the Optimal Number of Subreservoirs (N) in Series 72

3.6.3 Direct Calculation of CR Input from HEC-RAS Data 73

3.6.4 Evaluation of Strelkoff's Guidance for N 76

3.6.5 Evaluation of Wave Speed-Time Step Method for Finding N. 79

3.7 Overview of Unsteady RAS (uRAS) 80

Chapter 4 Analyses of Meandering Channels within Overbanks 84

4.1 Conceptual Framework for Meandering Channels 84

4.2 Derivation of Muskingum-Cunge for Meandering Channels 85

4.3 Representative Reaches - Separate Lengths Method 91

4.4 Representative Reaches - Modified Overbank Method 91

4.5 Representative Reaches - Effective Length Method 95

4.6 Effective Lengths and Conveyance for Steady-State HEC-RAS 99

4.7 Effective Lengths for Unsteady RAS (uRAS) 107
4.7.1 Original uRAS Derivation 107
4.7.2 Corrections to the uRAS Derivation 114
Chapter 5 Preparation of Natural Stream Data 117
5.1 Overview 117
5.2 Selection of Stream Reaches and General Description 118
5.2.1 Data Sources and Reach Selection 118
5.2.2 General Description of the Selected Reaches 123
5.2.2.1 Reach No. 1 124
5.2.2.2 Reach No. 2 124
5.2.2.3 Reach No. 3 127
5.2.2.4 Reach No. 4 128
5.2.3 Standardization of Manning's Roughness Values 129
5.3 Hydrologic Inputs for Testing 130
5.3.1 Original Watershed Study Methods 131
5.3.2 Synthetic Hydrograph by Gamma Distribution 134
5.3.3 Inflow Peak Discharges and Times to Peak 136
5.4 Processing Software 139
5.4.1 Conventions for Describing Software Commands 142
5.5 Creation of the Base HEC-RAS Models 143
5.5.1 Detailed Procedures, Using Reach No. 3 as Example 144
5.5.1.1 Generating the Digital Elevation Model 145

5.5.1.2 Establishing the Stream Centerline and Cross-Section Alignments 146
5.5.1.3 Establishing the First Estimates of Valley Flow Path and Overbank Flow Lengths 148
5.5.1.4 Deriving the Basic HEC-RAS Geometry File from GeoRAS .. 150
5.5.1.5 Isolating an Equivalent Geometry File from the Original Watershed Study 154
5.5.1.6 Evaluating Cross-Sections and Setting Bank Stations 155
5.5.1.7 Assigning Manning's n Roughness 163
5.5.1.8 Calculating Bed Slope 164
5.5.1.9 Establishing a Family of Reference Flows 165
5.5.1.10 Running HEC-RAS for Initial Geometry and Steady-Flow ... 166
5.5.1.11 Revising the Valley Flow Path and Flow Distances 167
5.5.1.12 Finalizing the Base-Line Model 170
5.5.1.13 Calculating Sinuosity 171
5.5.2 Summary of Base HEC-RAS Model for Each Reach 172
5.5.2.1 Reach No. 1 172
5.5.2.2 Reach No. 2 174
5.5.2.3 Reach No. 3 184
5.5.2.4 Reach No. 4 184
5.6 Preparation of Tabular Output Summary 190
5.7 Preparation of the 8-Point Equivalent Reaches 198

Chapter 6 Application to Natural Streams 218

6.1 Testing Program for Natural Stream Reaches 218

6.2 Comparison of uRAS and FLW (Testing Round 6A) 220

6.2.1 Geometric and Hydrologic Parameters (Round 6A) 220

6.2.2 uRAS Model Setup (Round 6A) 223

6.2.3 FLW Model Setup (Round 6A) 228

6.2.4 Round 6A – Results 238

6.3 Comparison of VMC and CR to uRAS (Testing Round 6B) 253

6.3.1 Basic Geometric and Hydrologic Parameters (Round 6B) 253

6.3.2 uRAS Model Setup (Round 6B) 253

6.3.3 VMC Model Setup (Round 6B) 253

6.3.4 CR Model Setup (Round 6B) 259

6.3.5 Round 6B – Results 263

6.4 Comparing uRAS Results on Natural Reach Data vs. 8-Pt. Sections (Testing Round 6C) 284

6.4.1 uRAS Model for Natural Reach Data (Round 6C) 285

6.4.2 uRAS Model for Equivalent Reach (Round 6C) 289

6.4.3 Round 6C – Results 290

6.5 Analysis and Recommendations 300

Chapter 7 Sensitivity Testing of Modeling Controls 302

7.1 General Considerations 302

7.2 Distance Step and Minimum Baseflow Relationships, using uRAS (Testing Round 7A) 303
7.2.1 uRAS Model Setup (Round 7A) 306
7.2.2 Round 7A – Results 307
7.3 Distance Steps and Low-Flow Filter, using FLW (Testing Round 7B) 314
7.3.1 FLW Model Setup (Round 7B) 315
7.3.2 Round 7B – Results 317
7.4 Sensitivity to Time Step (Testing Round 7C) 325
7.4.1 uRAS Model Setup (Round 7D) 325
7.4.2 FLW Model Setup (Round 7D) 326
7.4.3 Round 7C – Results 326
7.5 Sensitivity to Theta (Testing Round 7D) 331
7.5.1 uRAS Model Setup (Round 7D) 331
7.5.2 FLW Model Setup (Round 7D) 332
7.5.3 Round 7D – Results 332
7.6 Analysis and Recommendations 338
Chapter 8 Summary, Conclusions and Recommendations 341
8.1 Summary and Conclusions 341
8.2 Recommendations for Further Research 345
References 347

List of Tables

Table 5-1. Stream Reaches Examined 122

Table 5-2. Hydraulic Reference Data for Stream Reaches 123

Table 5-3. Land Cover and Hydraulic Roughness of Stream Reaches 123

Table 5-4. Tabular Values of Dimensionless Inflow Hydrograph, Gamma Distribution, m=3.7 136

Table 5-5. Hydrologic Data from Watershed Studies 137

Table 5-6. Parameters for Synthetic Inflow Hydrographs to Simulate the 100-Year Flood 139

Table 5-7. Main-Channel Definition and Bank Stationing, Reach No. 3 161

Table 5-8. Flow Rates Relative to Q_{100}, Used for Steady-State Profiles 166

Table 5-9. Location of Valley Flow Midpoints, Reach No. 3 169

Table 5-10. Summary of Steady-State HEC-RAS Model Parameters, All Reaches 173

Table 5-11. Steady State Output, Reach No. 1 191

Table 5-12. Steady State Output, Reach No. 2 192

Table 5-13. Steady State Output, Reach No. 3 193

Table 5-14. Steady State Output, Reach No. 4 194

Table 5-15. Example Calculation of 8-Pt. Equivalent Reach Geometry, Reach No. 3 203

Table 5-16. Example of Discharge Calculations for the 8-Pt. Equivalent Reach, Reach No. 3 207

Table 5-17. Summary of Geometric and Hydraulic Properties for the 8-Pt. Equivalent Reaches 211

Table 5-18. Comparison of Roughness Values, Natural vs. 8-Pt. Equivalent Reaches 215

Table 6-1. Routing Lengths and Ratio to Characteristic Lengths, Rounds 6A and 6B 222

Table 6-2. Model Parameters, uRAS and FLW, Testing Round 6A 223

Table 6-3. FLDWAV Input File, Example for Reach No. 3..... 230

Table 6-4. Peak Flow Results and Relative Attenuation for Reach No. 1, Testing Round 6A 239

Table 6-5. Peak Flow Results and Relative Attenuation for Reach No. 2, Testing Round 6A 239

Table 6-6. Peak Flow Results and Relative Attenuation for Reach No. 3, Testing Round 6A 240

Table 6-7. Peak Flow Results and Relative Attenuation for Reach No. 4, Testing Round 6A 240

Table 6-8. Lag Time of Peak Outflow, Reach No. 1, Testing Round 6A..... 241

Table 6-9. Lag Time of Peak Outflow, Reach No. 2, Testing Round 6A..... 241

Table 6-10. Lag Time of Peak Outflow, Reach No. 3, Testing Round 6A..... 242

Table 6-11. Lag Time of Peak Outflow, Reach No. 4, Testing Round 6A..... 242

Table 6-12. Volume Losses During Outflow, Testing Round 6A 249

Table 6-13. HEC-1 Input File for VMC Routing, Example for Reach No. 3..... 255

Table 6-14. Values of N for CR Routing, Round 6B..... 260

Table 6-15. HEC-1 Input File for CR Routing, Example for Reach No. 3 261

Table 6-16. Peak Flow Results for Reach No. 1, Testing Round 6B 264

Table 6-17. Relative Attenuation Results for Reach No. 1, Testing Round 6B 264

Table 6-18. Peak Flow Results for Reach No. 2, Testing Round 6B 265

Table 6-19. Relative Attenuation Results for Reach No. 2, Testing Round 6B 265

Table 6-20. Peak Flow Results for Reach No. 3, Testing Round 6B 266

Table 6-21. Relative Attenuation Results for Reach No. 3, Testing Round 6B 266

Table 6-22. Peak Flow Results for Reach No. 4, Testing Round 6B 267

Table 6-23. Relative Attenuation Results for Reach No. 4, Testing Round 6B 267

Table 6-24. Lag Time of Peak Outflow, Reach No. 1, Testing Round 6B..... 268

Table 6-25. Lag Time of Peak Outflow, Reach No. 2, Testing Round 6B..... 268

Table 6-26. Lag Time of Peak Outflow, Reach No. 3, Testing Round 6B..... 269

Table 6-27. Lag Time of Peak Outflow, Reach No. 4, Testing Round 6B..... 269

Table 6-28. Volume Losses During Outflow, Testing Round 6B 280

Table 6-29. Volume Losses for VMC over Routing Length 280

Table 6-30. Peak Flow Results and Relative Attenuation, Reach No. 1, Testing Round 6C 292

Table 6-31. Peak Flow Results and Relative Attenuation, Reach No. 2, Testing Round 6C 293

Table 6-32. Peak Flow Results and Relative Attenuation, Reach No. 3, Testing Round 6C 294

Table 6-33. Peak Flow Results and Relative Attenuation, Reach No. 4, Testing Round 6C 295

Table 7-1. Computational Distance Steps to Evaluate, Reach No. 3, Testing Round 7A 304

Table 7-2. Sensitivity of Peak Flow Results to Distance Step Size, Based on uRAS Routing on Reach No. 3, Testing Round 7A 309

Table 7-3. Sensitivity of Volume Changes to Distance Step Size, Based on uRAS Routing on Reach No. 3, Testing Round 7A 309

Table 7-4. Sensitivity of Peak Flow Results to Distance Step Size, Based on FLW Routing on Reach No. 3, Testing Round 7B 319

Table 7-5. Sensitivity of Volume Changes to Distance Step Size, Based on FLW Routing on Reach No. 3, Testing Round 7B 319

Table 7-6. Sensitivity of Peak Flow Results to Time Step Size, Based on Routing of Reach No. 3 by uRAS and FLW, Testing Round 7C 328

Table 7-7. Sensitivity of Volume Changes to Time Step Size, Based on Routing of Reach No. 3 by uRAS and FLW, Testing Round 7C 328

Table 7-8. Sensitivity of Peak Flow Results to Weighting Factor, θ Based on Routing of Reach No. 3 by uRAS and FLW, Testing Round 7D 334

Table 7-9. Sensitivity of Volume Changes to Weighting Factor, θ, Based on Routing of Reach No. 3 by uRAS and FLW, Testing Round 7D 334

List of Figures

Figure 2-1. Typical Hydrographs for the Flood Routing Problem in River Channels 5

Figure 2-2. Monoclinal Rising Wave 9

Figure 2-3. Typical Box Scheme for Implicit Finite Difference Solutions 35

Figure 3-1. Definition Sketch for the Saint Venant Equations 46

Figure 3-2. Sum of Forces on Control Volume 49

Figure 3-3. Cross-Sectional Element of Flow 50

Figure 3-4. River Channel Over a Characteristic Length 58

Figure 3-5. Channel Extrapolated to Length Other Than L_u 63

Figure 3-6. Traditional Explanation off Prism-and-Wedge Storage 67

Figure 4-1. Characteristic Length for Parallel, Separate Length Channels 87

Figure 4-2. Cross-Section Adjustment for Equivalent Channel - Modified Overbanks Method 93

Figure 4-3. Discrepancy in Effective Lengths, Corrected Method vs. HEC-RAS Steady-State Method 103

Figure 4-4. Channel and Floodplain Flows in uRAS 109

Figure 5-1. Watersheds Examined for Study, Johnson County, Kansas 119

Figure 5-2. General Location of Stream Reaches Studied 119

Figure 5-3. Aerial View of Reach No. 1 125

Figure 5-4. Aerial View of Reach No. 2 125

Figure 5-5. Aerial View of Reach No. 3 126

Figure 5-6. Aerial View of Reach No. 4 126

Figure 5-7. Fitting Simulated Hydrograph to Watershed Study, Reach No. 1 140

Figure 5-8. Fitting Simulated Hydrograph to Watershed Study, Reach No. 2 140

Figure 5-9. Fitting Simulated Hydrograph to Watershed Study, Reach No. 3 141

Figure 5-10. Fitting Simulated Hydrograph to Watershed Study, Reach No. 4 141

Figure 5-11. Digital Terrain Model, Reach No. 3..... 146

Figure 5-12. Initial Estimate of Valley Flow Path, Reach No. 3 149

Figure 5-13. Cross-Section Index, Reach No. 3 156

Figure 5-14. Selected Cross-Sections, Reach No. 3 158

Figure 5-15. Profile of Left and Right Bank Stations, Reach No. 3 161

Figure 5-16. Top Width vs. Flow Depth for Cross-Sections in Reach No. 3 162

Figure 5-17. Bed Slope Profile, Reach No. 3 165

Figure 5-18. Valley Flow Midpoints and Revised Valley Path, Reach No. 3 169

Figure 5-19. Water Surface Profiles for Selected Discharges, Reach No. 3 171

Figure 5-20. Plan View and TIN, Reach No. 1..... 175

Figure 5-21. Cross-Section Index, Reach No. 1 175

Figure 5-22. Selected Cross-Sections, Reach No. 1 176

Figure 5-23. Top Width vs. Flow Depth for Cross-Sections in Reach No. 1 178

Figure 5-24. Water Surface Profiles for Selected Discharges, Reach No. 1 178

Figure 5-25. Plan View and TIN, Reach No. 2..... 180

Figure 5-26. Cross-Section Index, Reach No. 2 180

Figure 5-27. Selected Cross-Sections, Reach No. 2 181

Figure 5-28. Top Width vs. Flow Depth for Cross-Sections in Reach No. 2 183

Figure 5-29. Water Surface Profiles for Selected Discharges, Reach No. 2 183

Figure 5-30. Plan View and TIN, Reach No. 4..... 186

Figure 5-31. Cross-Section Index, Reach No. 4 186

Figure 5-32. Selected Cross-Sections, Reach No. 4 187

Figure 5-33. Top Width vs. Flow Depth for Cross-Sections in Reach No. 4 189

Figure 5-34. Water Surface Profiles for Selected Discharges, Reach No. 4 189

Figure 5-35. Dimensions for a Symmetrical 8-Pt. Cross-Sections 200

Figure 5-36. Surface Area vs. Volume Relationship for Reach No. 3..... 201

Figure 5-37. VSQ Plot, Reach No. 3 208

Figure 5-38. QCL Plot, Reach No. 3 210

Figure 5-39. VSQ Plot, Reach No. 1 212

Figure 5-40. QCL Plot, Reach No. 1 212

Figure 5-41. VSQ Plot, Reach No. 2 213

Figure 5-42. QCL Plot, Reach No. 2 213

Figure 5-43. VSQ Plot, Reach No. 4 214

Figure 5-44. QCL Plot, Reach No. 4 214

Figure 6-1. Outflow Hydrographs for Reach No. 1, after Routing by uRAS and FLW. 243

Figure 6-2. Outflow Hydrographs for Reach No. 2, after Routing by uRAS and FLW. 244

Figure 6-3. Outflow Hydrographs for Reach No. 3, after Routing by uRAS and FLW. 245
Figure 6-4. Outflow Hydrographs for Reach No. 4, after Routing by uRAS and FLW. 246
Figure 6-5. Hydrographs for Reach No. 1 after Routing 160,000 feet with uRAS and FLW 247
Figure 6-6. Hydrographs for Reach No. 2 after Routing 320,000 feet with uRAS and FLW 247
Figure 6-7. Hydrographs for Reach No. 3 after Routing 320,000 feet with uRAS and FLW 248
Figure 6-8. Hydrographs for Reach No. 4 after Routing 640,000 feet with uRAS and FLW 248
Figure 6-9. Outflow Hydrographs for Reach No. 1, after Routing by VMC and CR. 270
Figure 6-10. Outflow Hydrographs for Reach No. 2, after Routing by VMC and CR. 271
Figure 6-11. Outflow Hydrographs for Reach No. 3, after Routing by VMC and CR. 272
Figure 6-12. Outflow Hydrographs for Reach No. 4, after Routing by VMC and CR. 273
Figure 6-13. Hydrographs for Reach No. 1 after Routing with uRAS, VMC and CR. 274

Figure 6-14. Hydrographs for Reach No. 2 after Routing with uRAS, VMC and CR. 275
Figure 6-15. Hydrographs for Reach No. 3 after Routing with uRAS, VMC and CR. 276
Figure 6-16. Hydrographs for Reach No. 4 after Routing with uRAS, VMC and CR. 277
Figure 6-17. Decline of Peak Discharge over Distance, Reach No. 1, Comparing uRAS, VMC and CR..... 278
Figure 6-18. Decline of Peak Discharge over Distance, Reach No. 2, Comparing uRAS, VMC and CR..... 278
Figure 6-19. Decline of Peak Discharge over Distance, Reach No. 3, Comparing uRAS, VMC and CR..... 279
Figure 6-20. Decline of Peak Discharge over Distance, Reach No. 4, Comparing uRAS, VMC and CR..... 279
Figure 6-21. Volume Loss Over Routing Distance, Reach No. 2, using VMC Method..... 281
Figure 6-22. Volume Loss Over Routing Distance, Reach No. 4, using VMC Method..... 281
Figure 6-23. HEC-RAS Geometry Schematic for Reach No. 3, Natural Geometry, Unsteady Flow Routing 288
Figure 6-24. Decline of Peak Discharge over Distance, Reach No. 1, Comparing Natural vs. Equivalent Reach for uRAS Routing 296

Figure 6-25. Decline of Peak Discharge over Distance, Reach No. 2, Comparing Natural vs. Equivalent Reach for uRAS Routing 296
Figure 6-26. Decline of Peak Discharge over Distance, Reach No. 3, Comparing Natural vs. Equivalent Reach for uRAS Routing 297
Figure 6-27. Decline of Peak Discharge over Distance, Reach No. 4, Comparing Natural vs. Equivalent Reach for uRAS Routing 297
Figure 6-28. Natural vs. Equivalent Reach Routing by uRAS, Comparison of Select Hydrographs, Reach No. 1. 298
Figure 6-29. Natural vs. Equivalent Reach Routing by uRAS, Comparison of Select Hydrographs, Reach No. 2. 298
Figure 6-30. Natural vs. Equivalent Reach Routing by uRAS, Comparison of Select Hydrographs, Reach No. 3. 299
Figure 6-31. Natural vs. Equivalent Reach Routing by uRAS, Comparison of Select Hydrographs, Reach No. 4. 299
Figure 7-1. Outflow Hydrographs for Reach No. 3, after Routing 160,000 feet in uRAS, Various Distance Steps and Minimum Baseflows 310
Figure 7-2. Decline of Peak Discharge over Distance, Reach No. 3, Comparing uRAS Results for Select Distance Steps and Baseflows 311
Figure 7-3. Outflow Hydrographs for Reach No. 3, after Routing 160,000 feet in FLW, Various Distance Steps 320
Figure 7-4. Outflow Hydrographs for Reach No. 3, after Routing 160,000 feet in FLW, Comparison of Low-Flow Filter Options 321

Figure 7-5. Decline of Peak Discharge over Distance, Reach No. 3, Comparing FLW Results for Select Distance Steps and Filter Options 322

Figure 7-6. Outflow Hydrographs for Reach No. 3, after Routing 160,000 feet, Comparing FLW and uRAS Results for Δx = 20,000 ft. and 20% Baseflow 322

Figure 7-7. Outflow Hydrographs for Reach No. 3, after Routing 160,000 feet, Sensitivity to Time Step Size for uRAS and FLW 329

Figure 7-8. Decline of Peak Discharge over Distance, Reach No. 3, Comparing Sensitivity to Time Step Size for uRAS and FLW 330

Figure 7-9. Outflow Hydrographs for Reach No. 3, after Routing 160,000 feet, Sensitivity to Weighting Factor, θ for uRAS and FLW..... 335

Figure 7-10. Decline of Peak Discharge over Distance, Reach No. 3, Comparing Sensitivity to Weighting Factor, θ for uRAS and FLW..... 336

Figure 7-11. Effect of Increased θ on Routing Stability, Comparing Outflow Hydrographs for Reach No. 3 after Routing 160,000 feet with uRAS, Using Δx = 20,000 ft 337

Chapter 1

Introduction

1.1 Problem Statement

A fundamental step in the development of most hydrologic models is the estimation of travel time and attenuation for flood waves traveling in river channels. The governing equations in one-dimensional flow are the St. Venant's equations. Methods of river routing based on St. Venant's equations are referred to as "*hydraulic river routing*." Numerical solutions of the complete St. Venant's equations require extensive data and the solution of large systems of nonlinear equations, the solutions of which can become unstable or difficult solve with limited computational resources. To overcome this difficulty, most practical hydrologic models employ simplified numeric methods which produce translation and attenuation of the inflow hydrographs.

Perhaps the most widely used of the simplified methods is the Muskingum method. Cunge (1969) demonstrated that with the proper selection of coefficients, the Muskingum method is an approximation of the St. Venant equations. When used with these proper coefficients, the method is known as "*Muskingum-Cunge.*" Despite its popularity, the physical basis for the Muskingum-Cunge method is not well presented in most texts and not well understood by most practicing engineers. Several key myths exist about the nature of its performance and parameters. Most of

these myths have been dispelled in the academic literature, but references persist in textbooks and handbooks.

In addition, few studies address the unique aspects of flood routing in compound, meandering natural channels or that examine the performance of flood routing on streams of small drainage area. Typical values of input parameters for realistic, small natural streams are not readily available.

The Federal Emergency Management Agency (FEMA) is currently in the process of map modernization for floodplain studies throughout the nation. Incorrect applications of flood routing and Muskingum-Cunge could have practical impacts on the accuracy and efficiency of hydrology studies that support those maps. Over the last 10 years, the Johnson County government and cities of Johnson County have invested over $10 million dollars to develop new floodplain studies for the County. The data set available in Johnson County is unusually rich and provides an opportunity to explore the nature of the Muskingum-Cunge routing method on real streams.

1.2 Objectives

The objectives of this research project are to:

- Clearly establish the theoretical basis of the Muskingum-Cunge routing method, using a physically intuitive derivation and emphasizing the concept of the characteristic reach length.

- Clarify the relationship between Muskingum-Cunge and another important approximate method, the Cascading Reservoirs approach.
- Explicitly consider the nature of two-stage, meandering natural rivers and provide a derivation of Muskingum-Cunge for that case.
- Examine the performance of the variable-parameter Muskingum-Cunge method and the Cascading Reservoirs method, using actual stream data typical of small and mid-sized streams (48 square miles or less of drainage area), exploiting the data available in Johnson County, Kansas, and using the unsteady flow solver within the HEC-RAS modeling system as the full dynamic reference solution.
- Develop detailed methods for reducing geometric data on natural streams down to summary values that can be used efficiently in the Muskingum-Cunge methods.
- Compare the performance for this data of two fully dynamic flow solvers: the unsteady flow solver in HEC-RAS and the FLDWAV model developed by the National Weather Service.

Chapter 2

Literature Review

2.1 Overview of the Flood Routing Problem

Flood routing is the general name for methods used to estimate the travel time and attenuation of flood waves as they move downstream in a river or channel. It is among the most important and common forms of unsteady flow dealt with by engineers. Flood routing methods are applied to such problems as real-time flood forecasting, dam-breach analyses, modeling of watershed hydrology, peak flow estimation, and floodplain and flood insurance rates studies (USACE 1994, Henderson 1966).

2.1.1 Background

A "*hydrograph*" is the plot of discharge versus time as observed at a single point in a river system, reservoir or drainageway. As a flood wave moves downstream through a river channel, the peak flow rate and overall shape of the flood wave all change. These changes can be measured by plotting hydrographs at different stations downstream. The essence of the flood-routing problem is to predict the downstream hydrograph, using an input hydrograph upstream and information about the reach through which the wave travels. The two changes of primary interest are attenuation and translation of the floodwave. "*Attenuation*" is the relative decrease in the magnitude of the peak discharge. "*Translation*" is the delay in the time of peak discharge, based on travel time of the water mass moving downstream. Figure 2-1

depicts the inflow and outflow hydrographs for a typical flood routing problem in a river channel (USACE 1994, Bedient and Huber 1992).

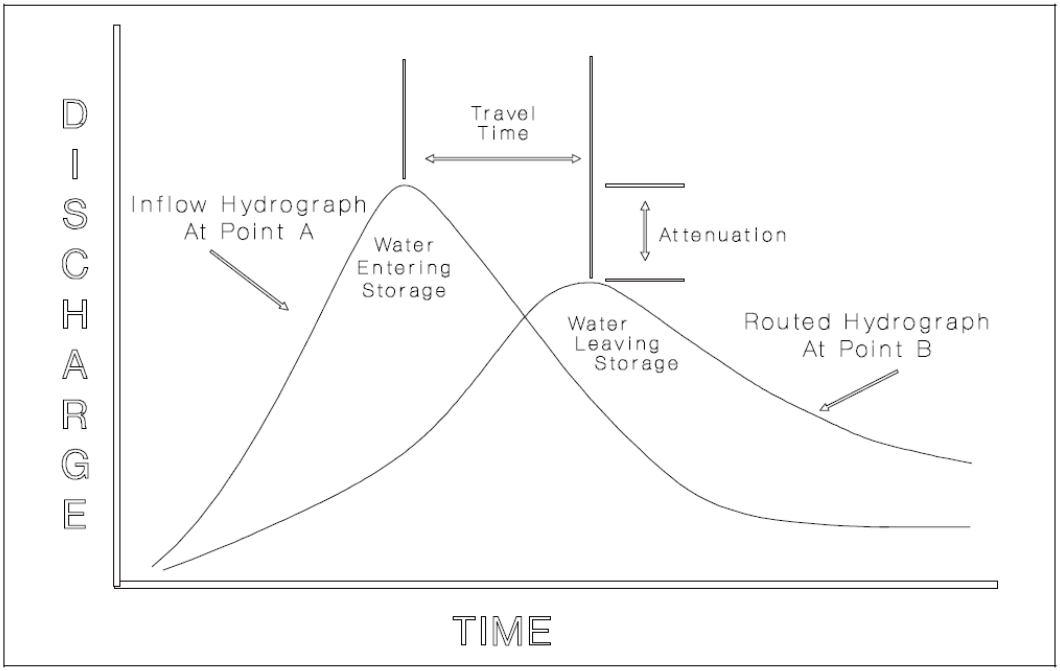

Figure 2-1. Typical Hydrographs for the Flood Routing Problem in River Channels
(*reprinted from USACE 1994)*

Hydraulic channel models like the Corps of Engineer's HEC-RAS model typically simulate a flood by assuming steady-state flow conditions based on simultaneous peaks all along the channel. In recent years, interest has increased in using unsteady models directly for flood modeling.

2.1.2 Flow Classifications

Open-channel flow is classified as "*unsteady*" when the depth or discharge at a fixed point changes with time. "*Steady flow*," by contrast, indicates that the depth or flow rate at a given location in a channel is constant with time. By definition, flood wave problems are a form of unsteady flow.

Unsteady flows are further classified as "*rapidly varied*" or "*gradually varied*." Rapidly varied flows are characterized by significant accelerations in the vertical direction and by large curvatures in the wave profile. During rapidly varied flow, the pressure distribution in the water column deviates from hydrostatic and discontinuities in the profile often emerge. In gradually varied flow, by contrast, the vertical acceleration of the flow is negligible and the pressure distribution is hydrostatic.

Flood routing problems typically involve long, gradual wave fronts that can be categorized as gradually varied, unsteady flow. The initial stages of a dam breach are one exception, when rapidly varied conditions dominate.

Flood waves can be also be described as *"translatory waves,"* meaning that as they propagate through an open channel, a significant movement of water mass downstream occurs. This is in contrast to "*oscillatory waves*" in which the water surface undulates, but for which very little net transport occurs (Chow 1959, pp. 4-7, 523).

A special form of translatory wave is the "*monoclinal rising wave*" which is a stable wave profile moves downstream at a constant velocity and without any change

in shape. It is a form of unsteady flow called *"uniformly progressive flow"* (Chow 1959, pp. 528-531). Although highly idealized, this wave type has proven a useful concept for analyzing flood waves in natural channels.

2.1.3 Kinematic and Dynamic Wave Speed

The speed at which a flood wave moves is termed its "*celerity.*" There are various types of waves in open-channel flow, each of which can have a unique celerity. The most familiar definition of celerity is dynamic celerity, c_d, which is the speed of a small disturbance in depth relative to the average velocity of flow in a channel. For waves to travel at this velocity, they must have low amplitudes, long periods, and travel with negligible losses of energy (Henderson 1966, pp. 38-40). The equation for dynamic celerity is:

$$c_d = \sqrt{gy} \text{ , for wide rectangular channels, or} \qquad (2\text{-}1)$$

$$c_d = \sqrt{gD} = \sqrt{g\frac{A}{T}} \text{ , for channels in general} \qquad (2\text{-}2)$$

where c_d is dynamic celerity, g is the acceleration due to gravity, A is the cross-sectional area of flow, T is the top width of the free surface, y is the depth of flow, and D is the hydraulic depth, which is equal to cross-sectional area divided by top width. For wide, rectangular channels, the hydraulic depth is equal to the flow depth (Henderson 1966, pp. 37-38; Chow 1959, pp. 13, 537-540).

Dynamic celerity is measured relative to the average velocity of the water, u. The disturbances move both upstream and downstream. To an observer standing on the bank, the apparent velocity of the disturbance would be given as $u \pm c_d$. The

most important dimensionless number in open-channel flow is the "*Froude number" (Fr)*, which is defined as the ratio of average water velocity to dynamic celerity, i.e.

$$Fr = \frac{u}{c_d} = \frac{u}{\sqrt{gD}} = \frac{u}{\sqrt{g\frac{A}{T}}}$$

When the Froude number is less than 1, the dynamic celerity is greater than the channel velocity, and the disturbance can travel both upstream and downstream. This condition is termed *subcritical flow* and is the most common condition over long runs of river. When the Froude number is greater than 1, the channel velocity is greater than the dynamic celerity, and all disturbances are swept downstream. This is known as *supercritical flow* and is typical of the swift flow found in river rapids or steep flumes. *Critical flow* is the condition when channel velocity and dynamic celerity are the same ($Fr = 1$) and is an important reference condition in many open-channel calculations.

While dynamic celerity describes the movement of small disturbances, it does not describe the rate of passage of the major portion of large flood waves. Seddon (1900, as reported in Chow 1959) found that for slow rates of rise in discharge, the velocity of the major flood wave observed from the bank is approximately that of a monoclinal rising wave. Seddon's findings were made through a study of gage records on the Missouri and Mississippi Rivers.

Figure 2-2 provides a diagram of the monoclinal rising wave as given by Chow (1959). The speed of this wave is often called the kinematic celerity c_k or Kleitz-Seddon celerity. Mathematically, the situation in the figure is converted to a

pseudo-steady-state condition by solving relative to an observer moving downstream alongside the flood wave.

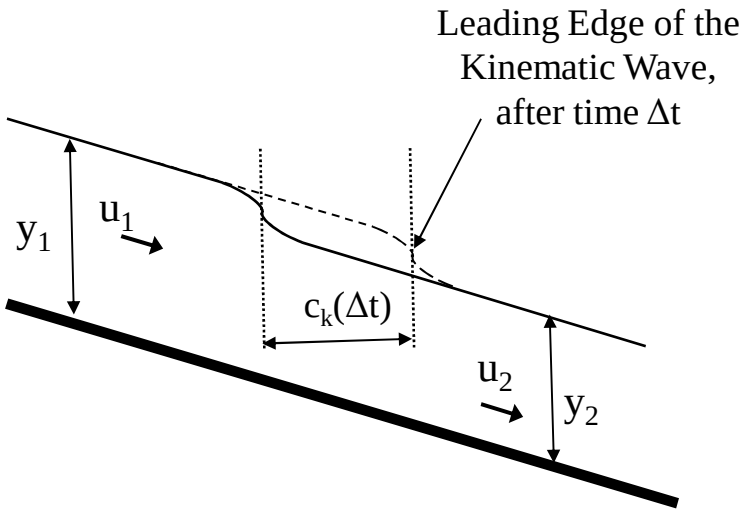

Figure 2-2. Monoclinal Rising Wave
(*adapted from Chow 1959)*

From Chow's derivation, the speed of this wave is approximated as (Chow 1959, pp. 528-531):

$$c_k = \frac{Q_1 - Q_2}{A_1 - A_2} = \frac{dQ}{dA}$$

where Q is discharge under steady-state conditions and A is the corresponding cross-sectional area of flow. The subscripts 1 and 2 refer to the locations upstream and downstream of the wave front. This form of wave speed can be calculated directly from steady-state conditions, and the relationship between Q and A depends only on the steady-state friction slope. The kinematic wave speed is reported relative to the bank, not the flow of water, and proceeds only in the downstream direction.

Henderson considered the differences between kinematic and dynamic celerity and reported that numerous studies had found that actual flood waves appear to travel at rates close to the kinematic celerity (1966, pp. 365-373). He also reported on theoretical studies by Lighthill and Whitham (1955), which described a connection between the two expressions. The kinematic celerity was understood to drive the bulk of the flood wave translation, while small disturbances moving at the dynamic celerity would emanate away from the primary flood wave, producing attenuation over time.

Both kinematic and dynamic celerity expressions are important in flood routing. Unfortunately, it has been common to use the single variable c for both, which can lead to confusion. In this paper, subscripts are used to distinguish between c_k and c_d. Where c alone is used, it always represents kinematic celerity c_k.

2.1.4 Saint Venant Equations

The classic hydraulic solution to the flood-routing problem was first proposed in 1848 by Barré de Saint-Venant (Chow 1959, p. 528). His approach solves both the continuity and momentum equations for a differential volume of one-dimensional flow, where the forces on the control volume are limited to the effect of gravity, pressure variation, and friction or roughness of the channel walls. Mass is conserved in the solution and the effect of acceleration within the control volume and momentum flux across the upstream and downstream faces are considered (Henderson 1966).

The resulting equations are known the *Saint Venant equations:*

Continuity:

$$\frac{\partial Q}{\partial x} + \frac{\partial A}{\partial t} = 0 \qquad (2\text{-}3)$$

Momentum:

$$S_f = S_o - \frac{dy}{dx} - \left(\frac{u}{g}\right)\frac{du}{dx} - \left(\frac{1}{g}\right)\frac{du}{dt} \qquad (2\text{-}4)$$

I II III IV V

where Q is discharge, A is cross-sectional area, x is distance measured along direction of flow, t is time, S_f is the friction slope, S_o is the bed slope, y is the depth of water above bed, and u is the longitudinal velocity of flow. The derivation of the Saint Venant equations is presented in Chapter 3, Section 3.1.

There is no general solution to the Saint Venant equations. One approach to practical computations is to simplify the equations by omitting one or more terms of the momentum equation, (indicated in Roman numerals under each). The "*kinematic equation*" arises when all terms and forces are omitted from the momentum equation except uniform friction and gravity (I and II). When the influence of changes in water-surface depth and pressure variation are retained (I, II and III), the equation is called "*diffusion equation*." For situations of extremely flat slope or for localized phenomena during rapidly varied flow, the role of momentum flux and acceleration become more important, while the influence of friction can be omitted, yielding the "*gravity equation*" (terms III, IV, and V only). Approaches that consider all forces and accelerations are termed "*full dynamic equations*" (Ponce and Simons 1977).

Until the advent of modern computing, direct use of the full Saint Venant equations was infeasible for all but the most limited or well crafted cases. Much of the early work on the Saint Venant equations utilized graphical techniques based on the "*method of characteristics.*" Much effort was also expended in developing simplified methods, some related loosely to the Saint Venant equations and others strictly empirical in nature. In recent decades, the emphasis on full Saint Venant solution has shifted to numeric methods, using finite difference techniques. Each of these approaches is mentioned in the following sections.

2.1.5 Method of Characteristics

The method of characteristics is a solution procedure in which the Saint Venant equations are transformed to ordinary differential equations (Chow 1959, Henderson 1966). The method relies on the idea that one can follow the pathway of an individual wave disturbance over time as it travels through the flow field. The traces of these pathways in a grid of time versus distance along the channel are called the "*characteristic curves*" or, more simply, the "*characteristics.*" There are two characteristics produced for any disturbance.

The wave disturbance travels relative to the flow field at a velocity equal to the dynamic celerity, $c_d = \sqrt{gy}$. By replacing flow depth *y* in the Saint Venant equations with the corresponding dynamic celerity, the number of independent variables is reduced and solutions can be calculated strictly in terms of velocity. This substitution is most useful when the acceleration terms (IV and V) of Eq. (2-4) are dominant. In subcritical flow, one characteristic moves upstream and the second

moves downstream. In supercritical flow, both characteristics are pointed in the downstream direction only.

The dynamic celerity is then calculated at specific intervals along the disturbance pathway or characteristic. The solutions can be complex, so semi-graphical techniques were developed to assist in the calculation.

2.1.6 Simplified Methods

For many problems, a full solution of the Saint Venant equations is unnecessary. A variety of simplified methods exist. Many of the early methods were empirical in nature and involved numeric techniques that introduce translation or attenuation to an inflow hydrograph. With time, attempts have been made to validate these empirical methods by relating their coefficients or structure to simplified forms of the Saint Venant equations. Methods that rely on empirical or highly simplified forms of the Saint Venant equations are typically termed *hydrologic methods* of flood routing, whereas full solutions to the Saint Venant equations are considered *hydraulic methods*. This evolution from empirical to theoretically justified methods can be traced in the development of the Muskingum-Cunge method.

2.2 Development of Muskingum and Muskingum-Cunge Methods

2.2.1 Muskingum Method

The Muskingum method is one of the best known and most widely adopted hydrologic methods for flood routing. It was introduced by McCarthy in 1938 for use by the Army Corps of Engineers in managing the Muskingum River basin in Ohio (Chow 1959, Henderson 1966, Roberson et al. 1988). Its original formulation was strictly empirical, with two coefficients that operated jointly to control translation and attenuation. It was recognized early that one of the coefficients, often termed *K*, is related to the travel time or translation of the wave through the channel, whereas the second coefficient, often written *X*, had the greatest impact on attenuation. The *X* coefficient was limited to the range 0 to 0.5 and graphical techniques were devised to estimate it from calibration data (Roberson et al. 1988). Because the original Muskingum method was empirical, it was limited for use to cases where calibration data existed. The Muskingum equation is derived in full in Section 3.2 and given at Eq. (3-13).

2.2.2 Development of Variable Parameter Muskingum-Cunge

Cunge (1969; Miller and Cunge 1975) advanced the use of the Muskingum method when he explained how the coefficients *K* and *X* could be related to the hydraulic properties of a simplified, prismatic channel. In doing so, Cunge used a linearized form of the diffusion equation, ignoring the effect of acceleration or momentum flux and eliminating second order-effects whenever possible. He described the Muskingum equation as a finite difference form of the kinematic

equation, in which the selection of time steps caused "artificial" diffusion. Formulations of Muskingum method based on Cunge's recommendations are now referred to as the *"Muskingum-Cunge method."*

Cunge's derivation resulted in the following values for K and X

$$K = \frac{\Delta x}{c_k} \tag{2-5}$$

$$X = \frac{1}{2}\left(1 - \frac{Q}{c_k T S_o \Delta x}\right) \tag{2-6}$$

where Q is a representative discharge, c_k is the kinematic wave speed, T is the top width of the channel, S_o is the bed slope, and Δx is the channel length or sub-length being calculated.

Ponce and Yevjevich (1978b) drew attention to the importance of allowing the values of K and X to vary with flow rate during Muskingum-Cunge simulations. Flood waves can be highly nonlinear and the use of constant values for the coefficients is a source of error.

2.2.3 Perumal's Derivations

Perumal (1992) provided an alternative derivation of the Muskingum-Cunge equation, tying it more closely to the diffusion equation. Perumal's greatest insight was to incorporate the concept of a *"characteristic length"* of channel as advanced in the Kalinin-Milyukov method. The characteristic length is that length over which one can assume a one-to-one relationship between the depth of flow at the midpoint and discharge at the downstream end. The Muskingum-Cunge X coefficient is then shown to be an extrapolation factor to estimate the discharge at the end of reaches

having a length different than the characteristic length. A complete review of this alternative derivation is given in Chapter 3 and forms an essential prerequisite for an improved understanding of the Muskingum-Cunge method.

Perumal (1994a and 1994b) went on to derive a form of the Muskingum-Cunge equation that could be used to simultaneously compute the stage and discharge hydrograph for a prismatic cross-section.

2.2.4 Extensions to Incorporate Inertial Effects

Attempts have been made to include a simplified form of the inertial (acceleration) terms in the Muskingum-Cunge and related methods. These approaches invariably involve the incorporation of the Froude number in the basic equations.

Perumal (1994a, Perumal and Ranga Raju 1999) gave a reorganized form the Saint Venant equation's momentum equation that is similar to the following:

$$S_f = S_o - \frac{dy}{dx}\left(1-\left(n\lambda Fr\right)^2\right) \qquad (2\text{-}7)$$

where n is the coefficient applied to the hydraulic radius in the velocity equation, λ is a shape factor to describe the channel section, Fr is the Froude number and all other terms are as defined previously for the Saint Venant equations. The friction equation and shape factor relationships are as follows:

$$u = C_f R_h^{\,n} \sqrt{S_f}$$

$$\lambda = P\frac{\partial R_h/\partial y}{\partial A/\partial y} = 1 - R_h\frac{\partial P}{\partial A}$$

where u is the mean longitudinal velocity, C_f is a friction factor for either Chezy or Manning's equation, A is the cross-sectional area of flow, P_w is the wetted perimeter, R_h is the hydraulic radius, equal to $\left(\frac{A}{P_w}\right)$, and S_f is the friction slope of the flow. The first equation for the shape factor λ matches Perumal's expression, whereas the second equation was used by Chow (1959, p. 210). With manipulation, Chow and Perumal's equations can be shown equal. When a wide, rectangular channel is assumed, the shape factor λ equals one.

The expression $(n\lambda Fr)$ is defined by Chow as the Vedernikov number, *Ved*. Ponce (1991) elaborates on the nature of the Vedernikov number, which he explains as the ratio of relative kinematic celerity (relative to the channel velocity) to the dynamic wave speed, as follows:

$$Ved = \frac{c_k - u}{c_d}$$

Wang (2003) arrived at modified forms of the Saint Venant momentum equation similar to that given at Eq. (2-7). For a wide rectangular channel using Chezy's friction formula $(n = ½)$, Wang gave an equation equivalent to

$$S_f = S_o - \frac{dy}{dx}\left(1 - \frac{Fr^2}{4}\right) \qquad (2\text{-}8)$$

Dooge (1973; Dooge et al. 1982) appears to have been the first to propose an inertial effects correction term of this type. Although his format is a little different that the equations above, the result was substantially the same.

Dooge et al. (1982) and Ponce and Lugo (2001) each developed a modified form of the Muskingum-Cunge X factor in terms that include these types of corrections. Neither presented their results in a manner entirely consistent with the remainder of the derivations in this study. Ponce and Lugo's formula is equivalent to the following:

$$X = \frac{1}{2}\left(1 - \frac{Q}{cTS_o\Delta x}\left[1 - Ved^2\right]\right) \qquad (2\text{-}9)$$

2.3 Other Hydrologic or Approximate Methods

Numerous other approximate methods have been developed for flood routing. While no longer in widespread use, several of these methods shed light on the nature of the flood routing problem.

2.3.1 Lag Method

The simplest method involves merely lagging the hydrograph in time based on an estimated travel time through the reach. In this method, no amount of attenuation is introduced and the shape of the hydrograph is preserved intact (USACE 1998). Although the effect of attenuation is slight compared to the translation of a hydrograph, the complete elimination of all attenuation is typically too crude an approach for practical studies.

2.3.2 Kinematic Routing

The next simplest method is considered *"kinematic routing"* and was developed by French hydraulicians Kleitz and Graeff in the late nineteenth century, as

reported by Montes (1998). The model was elaborated upon by Lighthill and Whitham (1955). It proceeds from joint consideration of the one-dimensional continuity equation and from the kinematic form of the momentum equation. In theory, kinematic routing should not produce any attenuation in the peak flow, but the shape of the hydrograph will change because the kinematic celerity at higher flow depths is greater than at lower depths. This leads to a steepening of the rising limb of the wave profile. If allowed to continue long enough, the steepening becomes as sharp as to create a surge wave or moving hydraulic jump, known as *"kinematic shock."*

2.3.3 Kalinin-Milyukov Method

As previously mentioned, the concept of a characteristic reach was born out of a method developed by Kalinin and Milyukov (1958). Developed in the Soviet Union in the 1950s, this method introduced the concept of characteristic reach length, upon which Perumal's modern understanding of Muskingum-Cunge is based. The characteristic reach is a conceptual length of channel for which a one-to-one relationship can be established between the depth in the midpoint and the discharge at the downstream end, at least for small deviations from steady-state flow. The final form of the Kalinin-Milyukov equations is distinct from Muskingum-Cunge, utilizing various exponential relationships for coefficients. Authoritative presentation of the method is given by Miller and Cunge (1975) and Montes (1998).

2.3.4 Cascading Reservoirs Approximation

Another approach to flood routing on rivers is to mimic the flood routing response of a stream with a series of reservoirs. The "*modified Puls river routing*" method described by the Corps of Engineers (USACE 1994, 1998, 2000) is a common formulation of this method. For simplicity, all methods that utilize this concept are collectively referred to as the *"Cascading Reservoirs Approximation."*

The river reach is approximated by a series of discrete routing elements, each of which is assumed to behave like a level-pool reservoir. Each storage node is presumed to represent a given segment of the channel, and each node is assumed to have identical properties. The storage associated with each node is representative of the volume of water under the steady-state profile for the given length of channel, and the stage-discharge curves are developed based on uniform steady flow. In this method, the channel must be divided into a whole number *N* of identical reservoirs.

By running the inflow hydrograph through a series of these reservoirs, cascading one into the other in series, an outflow hydrograph can be produced. The number of individual nodes used to divide the channel segment is a calibration parameter.

The greatest difficulty in applying this method is estimating the proper number of nodes needed to represent the routing in a reach. The more individual nodes used, the closer the outflow hydrograph appears to be pure translation, with peak discharge unchanged. The minimum number of nodes than can be used is one, in which the entire reach is treated like a single reservoir (USACE 1994).

The characteristic length described in the Kalinin-Milyukov method is intended to represent the length of river that can be routed as if it were a single reservoir, based on the steady-state volume and flow rate (Miller and Cunge, 1975, Montes 1998). As such, it would seem that N should be selected so that each storage node represented a segment of channel having a length equal to the characteristic reach length.

In an early presentation of the modified Puls method for river routing, the Corps of Engineers suggested that, as a first approximation, *N* should be estimated such that each individual reservoir represents the length of channel traveled by a flood wave in one model time step (USACE 1994). The results of this approach would be very different than when using the characteristic reach length, since it would imply that the value of *N* is not a fundamental channel property, but would change with different user-defined time steps. In the more recent HEC-HMS User's Manual (USACE 2000), an alternate formula is suggested, in which the number of steps is a function of the channel length, flow depth and slope, but not based on time step. These equations and issues are examined in more detail in Chapter 3.

A variation of the cascading reservoirs approach is to assume that the storage in each sub-reservoir is directly proportional to the discharge in each. This approximation is known as "*linear-storage models"* (Montes 1998), "*linear reservoirs"* (Ponce 1980), or as a "*cascade of linear reservoirs"* (Ponce 1989). The Streamflow Synthesis and Reservoir Regulation model (SSARR) developed for the

U.S. Army Corps of Engineers in 1956 also utilizes the LCR concept (Miller and Cunge, 1975).

2.4 Accuracy Criteria for Muskingum-Cunge

Beyond the derivation of Muskingum-Cunge, the greatest focus of the literature has been on estimating the accuracy and limits of the method. There is also a large commentary on several well known numerical inconsistencies that arise, such as negative outflows during early stages of routing and loss of volume when using variable values for the parameters K and X. Some of the accuracy limits are functions of the linear nature of the Muskingum-Cunge equation, while others are more fundamentally related to the use of the diffusion equation form of the momentum equation instead of the full dynamic form.

2.4.1 Measures of Accuracy

A variety of tests can be considered to assess the accuracy of a method. An ASCE task committee (ASCE 1993) reviewed the available methods for assessing accuracy of watershed models. For single-event models, the task force adopted the recommendations of Green and Stephenson (1986), who proposed that peak flow rate, flow volume, hydrograph shape and timing be the primary areas of evaluation. For peak flow rate, the simple percent error in peak (PEP) criterion was adopted:

$$PEP = \frac{\left(Q_{SIM} - Q_{OBS}\right)}{Q_{OBS}} \times 100 \qquad (2\text{-}10)$$

where Q_{OBS} is the observed peak flow rate and Q_{SIM} is the simulated peak flow rate.

Likewise, a simple index of deviation in runoff volume was considered sufficient for volume conservation. The index D_V is given by

$$D_V = \frac{(V_{SIM} - V_{OBS})}{V_{OBS}} \quad (2\text{-}11)$$

where V_{OBS} is the observed volume over the duration of the hydrograph and V_{SIM} is the simulated volume.

For shape and timing, an index "G" was proposed that involves a simple sum of the square of the residuals between actual or theoretical discharges and the modeled discharges, given by:

$$G = \sum_{i=1}^{n} \left(Q_{OBS}(t_i) - Q_{SIM}(t_i)\right)^2 \quad (2\text{-}12)$$

where $Q_{OBS}(t_i)$ and $Q_{SIM}(t_i)$ are the flow rates at each point in time (t_i) in the observed and simulated hydrographs, respectively.

An overall goodness-of-fit test based on results of multiple events was also strongly recommended. Green and Stephenson proposed using both the total overall sum of squared residuals (TSSR) and the total overall sum of absolute residuals (TSAR), similar to the index G. They also emphasized that graphical plots should be used to supplement statistical tests, that multiple events be tested, and that multiple criteria be evaluated, with emphasis then given to the test that best represents the purpose of the modeling. In particular, they noted,

> *"no single statistical goodness-of-fit criterion is sufficient to assess adequately for all purposes the fit between a computed and an observed hydrograph ... the criteria ultimately chosen should depend on the objective of the modeling exercise."*

Synchronization of the timing is a critical issue for those methods that involve residuals, such as the G, TSSR, and TSAR criteria. A mismatch in the timing of the peak flows can significantly increase the reported error terms.

2.4.2 Limitations of the Diffusion Wave Assumption

The first constraints to the Muskingum-Cunge equation lie in the limits of the diffusion equation. Ponce and Simons (1977) applied the theory of linear stability to a dimensionless form of the full dynamic equations, and to various simplified forms, including the kinematic, diffusion, steady dynamic, and gravity wave forms. By analyzing the impact of a small sinusoidal perturbation of flow in the channel, they defined expected ranges for given levels of accuracy in outflow calculations. They later expanded the consideration to define expected limits on the accuracy of the kinematic and diffusion wave assumptions, based on how physical dimensions of the channel and upon how slowly the inflow hydrograph rose and fell (Ponce et al. 1978a). The more slowly the hydrograph passed, the more applicable the kinematic or diffusion wave assumptions become, with the kinematic wave assumption having the most rigorous limit.

Ponce's criteria were:

Kinematic Waves,

$$\frac{PS_o u_o}{y_o} \geq 171 \qquad (2\text{-}13)$$

Diffusion Waves,

$$\frac{PS_o u_o}{y_o} \geq 30(Fr), \qquad \text{or} \qquad (2\text{-}14a)$$

$$PS_o\sqrt{\frac{g}{y_o}} \geq 30 \qquad \text{(2-14b)}$$

where P is the total wave period of the sinusoidal disturbance, S_o is the bed slope, u_o is the steady uniform flow velocity and y_o is the steady uniform flow depth, g is the acceleration due to gravity, and the Froude number Fr is given by $\frac{u_o}{\sqrt{gy_o}}$ (Ponce et al. 1978a, USACE 1994). Since Ponce's work was based on a sinusoidal disturbance with a peak that occurred in the middle of the wave period, the above test is often evaluated using the time to peak of the rising limb instead (t_p), assuming $P = 2t_p$ (Ponce 1989).

Ponce's criteria for the kinematic wave solution (Eq. 2-13) was intended to ensure that the peak flow rate was within 95% of the value from dynamic routing after the wave had been traveling for a duration equal to one full wave period. For the diffusion criteria, the test given at Eq. 2-14b is intended to ensure that the wave speed (celerity) with within 5% of the dynamic solution. A direct relationship to the error of attenuation was not made (Ponce et al. 1978a; Ponce 1989).

Crago and Richards (2000) reviewed Ponce's accuracy criteria, based in part on concerns that the small perturbation analyses used by Ponce may not adequately account for the large amplitude changes that occur during flood flows. They utilized the FEQ model (Franz and Melching 1997) which solves the full dynamic form of Saint Venant equations and analyzed the width of the looped rating curve that emerged. The presence of a large loop or hysteresis effect was considered indicative

of a non-kinematic wave, whereas a relatively single-valued relationship indicated a channel and slope condition that could be amenable to kinematic wave assumptions. Crago and Richards concluded that the width of the loop in the dimensionless rating curve was closely related to Ponce's wave period criteria.

2.4.3 Use of Variable Parameters and Averaging Schemes

Ponce and Yevjevich (1978b) compared a single routing event using both constant-parameter and variable-parameter formulations of Muskingum-Cunge. The inflow had a peak flow of 200 cubic feet per second (cfs) per unit width of channel and a time to peak of 48 hours and was routed using 12-hour time steps. The reference values for determining coefficients on the constant parameter case were based on flow characteristics at peak flow, 2/3 of peak flow, and 1/4 of peak flow.

On the variable-parameter case, the Muskingum-Cunge coefficients were evaluated at every time step, based on flow conditions at that time. Three different averaging schemes were employed: a 2-point scheme based on inflow and outflow values at the beginning of the time step only; a 3-point scheme which also incorporates the inflow value at the end of the time step, which is known before the routing takes place; and a 4-point scheme in which the unknown value of outflow at the end of the time step is estimated and included in the averaging, using an iterative process until adequate convergence is obtained.

Ponce found that the results of the constant value Muskingum-Cunge method were highly dependent on the reference value of discharge used in calculating the coefficients. Both travel time and attenuation (subsidence) were impacted. By

contrast, the variable parameter method gave results that fell within the middle of the constant parameter results. The 3-point and 4-point averaging schemes each worked well, but the 2-point scheme resulted in smaller peaks, slightly decreased rate of travel, and a loss of volume over the simulation.

No other sources in the literature were found that directly compare constant-parameter versus variable-parameter methods.

2.4.4 Volume Conservation

While allowing the Muskingum-Cunge parameters to vary improves the overall accuracy and shape of most hydrographs, Ponce and Chaganti (1994) noted that the main drawback of the variable parameter method is *"a small but perceptible loss of mass."* They found that the 3-point averaging methods suffered greater loss of mass than the 4-point methods and that the loss of mass increased as the ratio of peak flow to base flow increased. They concluded, however, that the mass loss was not strongly correlated with the resolution of the modeling time steps.

Ponce and Changanti did find the detailed method by which the 3-point and 4-point averages were calculated made a difference in volume conservation. Two key parameters were needed in Ponce's formulation of the equation: the kinematic celerity c_k, and the unit width discharge q. The kinematic celerity is a unique function of unit discharge. They defined the *"conventional"* method of averaging as one in which both c_k and q are calculated at each of the 3 or 4 computational points and averaged. By contrast, a *"modified"* method was proposed whereby the value of q was calculated and averaged, but the kinematic celerity for the system was then

calculated directly from the resulting average discharge. In a limited range of numerical experiments using wide, rectangular channels, Ponce and Changanti reported that the modified method produced a slight but consistent improvement in mass conservation. The constant-parameter Muskingum-Cunge method consistently showed perfect conservation of mass.

The overall range of mass retention for the conditions tested was 95% to 99%. For the worst-case condition of mass retention, the conventional 3-point technique retained 95.3% of its volume after routing, whereas the conventional 4-point iterative technique retained 97.4%. When the modified averaging methods were used, the volume accuracy improved very slightly, to 96.7% and 98.4% respectively.

Tang et al. (1999a) further explored the issue of volume conservation. They provided an analytic proof for the observation that constant-parameter Muskingum-Cunge conserves volume. They also conducted numeric experiments on various variable-parameter schemes, using a model based on a single rectangular channel with a Manning's coefficient *n* of 0.035, a synthetic inflow hydrograph with a peak discharge of 900 m^3/s, and a time to peak of 24 hours. The tests were conducted for a range of slopes between 0.2% and 0.01%. A single, extreme-value test was also conducted for a slope of 0.025%. Five different time steps, ranging from 0.25 hours to 2 hours, were tested. Several different computational distance steps were also evaluated. They tested both the 3-point and 4-point averaging schemes, and they used both the conventional and modified averaging techniques discussed by Ponce and Changanti. Tang also proposed an additional averaging technique that was a

variation on the conventional method, but for which the parameter X is evaluated based on the average value of the quotient q/c_k.

From this work, Tang confirmed Ponce's finding that the modified method of averaging gave better results than the conventional method, and that the 4-point average gave better results than the 3-point average. The results of the conventional method and Tang's variation were approximately equal for all cases, except in the case of very mild slopes (0.01%). The effect of different lengths of distance step were small for steep channels (greater than 0.2%) but increased for milder slopes. All of the 3-point averaging schemes were influenced by distance step, whereas the iterative 4-point schemes were relatively uninfluenced. By the same token, the time step influenced results on the 3-point averaging schemes, but had negligible effect on the iterative 4-point schemes, except in steeper channels.

2.4.5 Negative Outflow Values and Initial "Dip"

The Muskingum method is known to sometimes produce an initial dip in the outflow hydrograph at the beginning of a simulation. When the base flow is sufficiently low, this initial dip can cause the first several time steps to report a negative value for flow in the outflow hydrograph. Ponce and Theurer (1982) proposed a criterion for computational time and distance steps to avoid negative flows. To avoid a negative dip in the routing, they recommended that the distance step should be kept below a maximum value, as follows:

$$\Delta x \le \frac{1}{2}\left(c\Delta t + \frac{Q_o}{c_k T S_o} \right) \qquad (2\text{-}15)$$

where Δx is the computation distance step, Δt is the computational time step, c_k is the kinematic celerity (or kinematic wave speed), Q_o is the reference discharge, T is the top width at the water surface, and S_o is the bed slope. The first term in the parenthesis on the right side of the equation represents the distance that will be traveled by the kinematic wave during one computational time step, whereas the second term is the characteristic length, to be discussed in more detail in Chapter 3.

Perumal's (1992) derivation of Muskingum-Cunge explains this initial negative outflow or dip. The dip occurs when the computation distance step in the initial phases of routing is longer than the characteristic reach length. Because the outflow discharges are extrapolated based on the characteristic reach length, the initial outflow values can be extrapolated below the initial discharges. As noted above, this error is a function of the spatial resolution in the model.

2.4.6 Computational Time and Distance Steps

As already noted, avoidance of a negative outflow during the early stages of outflow routing has been one driver in setting limits to the size of the computation distance step. Tang and Knight (1999b) reported a separate numeric problem that occurs in steep channels of compound shape - oscillations during the falling limb. Whereas the control of the "dip" required an upper limit to the distance step, control of the oscillations required a lower boundary:

$$\Delta x \geq \left(c\Delta t - \frac{Q_o}{c_k T S_o} \right) \tag{2-16}$$

Other potential considerations include the shape of the inflow hydrograph and general timing. Nash (1959) proposed alternate formulations of Muskingum coefficients when the time step for the model was not small relative to the travel time of the kinematic wave through the reach. These coefficients are not used in most Muskingum-Cunge programs. To match the shape of the hydrograph, the HEC-1 User's Manual (USACE 1998) recommends that the time step be no larger than 1/20th of the time to peak. It further requires that the distance step not exceed the total travel time of a kinematic wave through the reach.

2.4.7 Acceptable Range for the "*X*" Parameter

One of the greatest myths surrounding Muskingum method has been the acceptable range for the *X* parameter. In its original formulation as a weighting scheme between inflow and outflow, it was understood to have a limit between 0 and 0.5 (Miller and Cunge 1975; Weinmann and Laurenson 1979). Based on Cunge's relationship, a requirement to keep the *X* value positive places a lower limit on the size of distance step that can be used (Weinmann and Laurenson 1979).

Ponce and Theurer's (1982) proposed accuracy criteria for time and distance steps suggested that as a practical measure, this limit was unnecessary and that negative values of *X* caused no computational difficulties. Recently, Szel and Gasper (2000) investigated the issue at length, and concluded that the concept of weighting parameters played no role in Muskingum-Cunge. Formulations with a negative X were acceptable, and in some cases, lead to improved stability and accuracy. It is Perumal's derivation of Muskingum-Cunge and its relationship to the Kalinin-

Milukov method, however, that clarified *X* as a length adjustment factor, with negative values simply indicating a characteristic length larger than the routing step. The proper range of Muskingum-Cunge *X* is now understood to be -∞ to 0.5.

2.5 Computer Models

A variety of computer models perform channel routing and flow analyses. Many of these program have been developed by various agencies of the federal government with responsibilities over water resources. The models used in this study and some related models of interest are summarized.

2.5.1 Hydrologic Models - HEC-1

HEC-1 is a computer model that packages many common hydrologic processes together in one modeling environment (USACE 1998). The original model was developed by the Hydrologic Engineering Center (HEC) of the U.S. Army Corps of Engineers and was first released in 1968. Various refinements were issued 1970, 1973, 1981, 1990 and 1998. HEC-1 includes procedures to input precipitation patterns and amounts, estimate net losses, convert precipitation to runoff, combine hydrographs from multiple tributaries and route flows using a variety of methods, including Muskingum-Cunge, modified Puls for river routing (hereinafter referred to as Cascading Reservoirs), and kinematic wave method. The program also contains models for flood damage analyses, parameter optimization, and multiple plan comparisons.

The HEC-1 model describes a watershed as a series of independent subareas or processes, and within a subarea calculations are made based on average or lumped values of the parameters. In 2000, HEC released HEC-HMS (Hydrologic Modeling System), which is the successor to HEC-1. Most of the same computational methods were included in HEC-HMS, but with more advanced user interface and programming (USACE 2000).

2.5.2 HEC-RAS

HEC-RAS is a widely-used model for open-channel hydraulic analyses. A successor to the original HEC-2 program, it allows for the calculation of stage and velocity for complex systems of natural streams, including routines for bridges, culverts, weirs, and other hydraulic structures. The basic traditional use of HEC-RAS has been for one-dimensional steady flow, with channel geometry and roughness characteristics input at various cross-sections.

Typically, a backwater analysis is performed for subcritical flows, in which a downstream boundary condition is set to establish the downstream flow depth, then an iterative method used to calculate the flow depth at the next upstream section, using the energy equation. Mixed-flow and supercritical solutions can also be found. In recent years, HEC-RAS has been expanded to include an unsteady flow solver, based on the older UNET program. The unsteady flow routines in HEC-RAS are discussed in greater detail in the next section. HEC-RAS has also incorporated additional subroutines for scour analyses at bridges and sediment transport (USACE 2002a and 2002b).

2.5.3 Full Dynamic Models - General

Specialized modeling routines are needed to solve the complete form of the Saint Venant equations. Because the equations are non-linear, analytical solutions do not exist for most practical needs. Finite difference schemes are needed, whereby values are calculated for the state variables at specific nodes along the channel at specific times. Finite difference schemes can be distinguished as "*explicit*" or "*implicit.*" Explicit schemes use the known values at a specific time step to estimate the derivatives, and those values and derivatives are used to extrapolate the state variable to the next time step. These methods are easiest to program but are only accurate or stable when extremely small time steps are used.

By contrast, implicit schemes develop a system of equations to describe the values of the state variables and derivatives for all spatial nodes in the system at both the beginning and ending time step. Implicit schemes allow for information from the entire river reach to influence the solution at every point, producing greater accuracy at larger time steps (Roberson et al. 1988, Barkau 1997, Fread and Lewis 1998).

One can think of any given point along the channel at a specified time as being bounded by a four-point box, or finite difference cell, as shown in Figure 2-3, which is reprinted from the HEC-RAS unsteady flow documentation (Barkau 1997, USACE 2002b). Part of the boundary is formed by two spatial nodes, one upstream and one downstream, signified by subscripts "j" and "j+1", and part of the boundary is formed by two discrete times, one prior and one later, signified by subscripts "n" and "n+1".

All such individual boxes are then assembled into a matrix and numerical solution techniques are used to simultaneously solve for all unknowns. Although significantly more complex, implicit schemes allow much larger time steps to be used in the solution (Franz and Melching 1997).

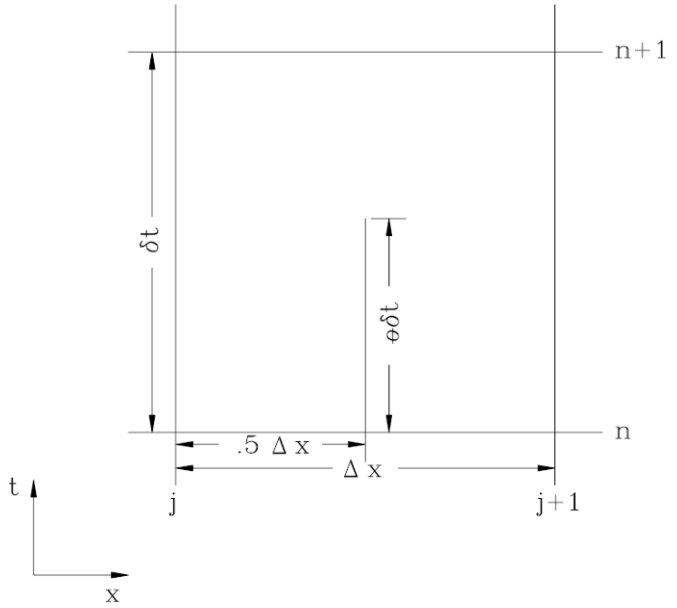

Figure 2-3. Typical Box Scheme for Implicit Finite Difference Solutions *(reprinted from USACE 2002b)*

To solve for conditions at the end of a given time step, the initial values and relationships for all the state variables must be specified at the beginning of the time step. In addition, relationships are required for conditions at the boundary of the solution at the end of the time step (time n+1) (Fread and Lewis 1998). For subcritical flow, one boundary condition must be specified at the downstream end and one at the upstream end. Those boundary conditions are typically inflow or outflow discharges or a specified head (Barkau 1997).

Implicit methods estimate the partial derivative between nodes differently for space and time. For the individual box shown in Figure 2-3, the derivative with respect to time for any given state variable (say *F*) is estimated directly as the average rate of change between the nodes:

$$\frac{\partial F}{\partial t} \approx \frac{1}{2}\left[\frac{\left(F_{j+1}^{n+1} - F_{j+1}^{n}\right) + \left(F_{j}^{n+1} - F_{j}^{n}\right)}{\delta t}\right] \tag{2-17}$$

where δt is the incremental time step between calculations steps, and *F* is any continuous state variable for which the partial derivative exists, with specific values designated or calculated at specific nodes of time and distance steps, the subscript indicating the spatial location of the node and the superscript indicating the temporal position (Barkau 1997).

By contrast, a pure average on the spatial derivative can sometimes produce unstable results. Instead, a weighted average is used, giving slightly more weight to the value of the state variables at the end of the time step. This extra weighting produces greater stability, but at the cost of reduced accuracy. In general, it is recommended that the weighting factor, typically denoted theta (θ), be set between 0.55 and 0.60 (Barkau 1997, Fread and Lewis 1998). Under this scheme, the partial derivative with respect to distance for a state variable is given as follows:

$$\frac{\partial F}{\partial x} \approx \theta\left[\frac{\left(F_{j+1}^{n+1} - F_{j}^{n+1}\right)}{\delta x}\right] + (1-\theta)\left[\frac{\left(F_{j+1}^{n} - F_{j}^{n}\right)}{\delta x}\right] \tag{2-18}$$

2.5.4 HEC-RAS Unsteady Flow Model (uRAS)

One common computer program for solving the dynamic wave problem in real rivers is the unsteady flow module incorporated in HEC-RAS Version 3.0 and later (USACE 2002a and 2002b). This module is based on the older UNET model, which was developed by Dr. Robert Barkau in cooperation with HEC. The original UNET model was specifically designed to use input data from HEC-2. The UNET solution routines have now been embedded as a solution option in HEC-RAS. Input data compatible for the unsteady solver is created directly from the basic geometry data input into HEC-RAS through the use of a pre-processing routine. The original UNET equations used a modified form of the St. Venant equations (Barkau 1997). The HEC-RAS unsteady module was selected as the benchmark model for routings in this study. For convenience, the unsteady flow option within HEC-RAS will be referred to as the (uRAS) model in this report. More detail on the uRAS model is given in Chapters 3 and 4.

2.5.5 NWS FLDWAV Model

The National Weather Service also developed a generalized flood routing model called FLDWAV (Fread and Lewis 1998). This model was a replacement of previous two previous models, DAMBRK and DWOPER, which focused on dam break and river routing problems, respectively. Similar to FEQ, FLDWAV also uses a modified form of the St. Venant equations and allows for input of natural channel cross-sections. An implicit solution procedure is used. Sinuosity factors are introduced to account for meandering streams, and the variable nature of compound

sections is handled by a table of depths versus top width. FLDWAV allows for the Manning's n value to vary by depth or discharge.

The FLDWAV model was used in a limited fashion in this study. It was used to validate the performance of the uRAS model in Chapter 6. In Chapter 7, certain operational features of the model are tested, as they relate to overall model stability. A major limitation of the model is the lack of a modern graphical interface and a cumbersome input routine. The FLDWAV program is not well-suited to use in complex, small streams. More detail on the input routines for FLDWAV are given in Chapter 6. For convenience, the FLDWAV program will often be abbreviated FLW in this report.

2.5.6 USGS FEQ Model

The FEQ (Full Equations) model was developed by the U.S. Geological Survey, in cooperation with the Illinois Department of Natural Resources. It was developed in part to handle the flat streams with broad floodplains that were characteristic of the Chicago area. It solves a modified form of the one-dimensional St. Venant equations for a sequence of open channels and can also handle empirical relationships for control structures such as bridges, culverts, dams, spillways, drop structures, etc. Channel characteristics are pre-processed into a series of tables, and an implicit numerical solution calculated (Franz and Melching 1997). The FEQ model was not evaluated in this report.

2.6 Compound and Meandering Channels

The majority of numeric comparisons of Muskingum-Cunge and other flood-routing method have been made on highly simplified, wide rectangular channels or on simple prismatic shapes, such a single stage trapezoidal channels. By contrast, most practical flood routing problems apply to natural streams, many of which are characterized by small main-flow channels meandering within wide floodplains, where the floodplains may be heavily vegetated with substantially greater roughness than the main-flow channel. Geometric properties may be highly variable from section to section.

2.6.1 General Tests

The Natural Resources Conservation Service (NRCS, formerly Soil Conservation Service) evaluated the routing characteristics of cross-sectional data drawn from 20 watersheds in 17 states (Younkin and Merkel 1988). A series of 12 typical sections were developed to represent a range of channel geometries under different flow conditions. Four of the typical sections represented a range of ratios in top-width to flow area at bankfull (in-bank) flow. Four of the typical sections included overbank floodplains with shallow flows, based on a 5- to 10-year storm flow rate. The final four sections represented deep overbank flows typical of 100-year storms. Dimensionless geometric data was based on composite results from 836 cross-sections drawn from these watersheds, and the cross-sections represented channels having between 8 to 375 square miles of contributing drainage. All data was derived from NRCS offices, based on local planning or flood insurance studies.

A series of hypothetical unsteady routings were made for each channel, comparing both a constant-parameter and variable-parameter diffusion routing method, each similar to Muskingum-Cunge. A dynamic model using an implicit four-point solution to the full St. Venant equations was used as a benchmark. The study found that the diffusion model results were sensitive to the time-to-peak of the hydrograph and length of channel, but were relatively uninfluenced by the Froude number. Over 80% of testing runs satisfied the accuracy criteria for match between diffusion and full dynamic models. Those criteria were (1) peak flows within 1%, (2) time to peak within one increment of the model time step, and (3) 95% correlation of the shapes of the discharge and area hydrographs. The study also found that the variable-parameter model predicted timing and shape better, and that accuracy was best on narrow, deep channels.

Tang and Knight (1999b) evaluated hypothetical compound channels with large overbank flows. They found that a significant delay can occur in the rising limb once bankfull flow is reached, creating what they termed a “shoulder” in the hydrograph. Mild slopes and rough overbanks each contributed to increased diffusion, and the roughened overbanks is associated with delayed travel times for the peak. Overall flood-wave diffusion did not appear dependent on the ratio of peak discharge to bankfull flow.

Garbrecht and Brunner (1991) also tested hypothetical compound cross-sections, comparing results from variable-parameter Muskingum-Cunge to a full dynamic solution from the DAMBRK program developed by the National Weather

Service. The overbank was modeled as an entirely separate channel with periodic junctions to allow rebalancing of flows between the overbank and main-channel. Under this scheme, they found that hydrograph peaks and times to peak were within 4% for most of the test cases, and that the Muskingum-Cunge approach represented the overall hydrograph shape well.

2.6.2 Discharge Estimates for Compound Channels

In compound channels, flow estimates are developed by separating main-channel and floodplain sections. Henderson (1966) described this approach, whereby the water-surface elevation is taken as level across the entire composite section, and a weighted average value of velocity head computed for the entire section to find the energy grade line. Henderson noted that this method does not consider the impact of exchanging flows between the main-channel and overbank sections. A hypothetical dividing line is needed to separate those flows, and the orientation of that line has an impact on calculation accuracy.

Stephenson and Kolovopoulos (1990) reviewed the dividing-line problem, considering the effect of momentum transfer directly, and provided a summary of the major dividing-line methods. The "*vertical division method"* uses a vertical line at each bank point to separate flows. It was noted that this method generally predicts too high a flow rate, which is attributed to an incorrect consideration of shear stress on the main channel. Because flow in the main channel is moving more rapidly than the overbanks, any mixing of flows should have a tendency to accelerate the floodplain flows and provide a drag on the main channel. A variation on the vertical

division method involves counting the length of the vertical division as part of the wetted perimeter on the main channel, but ignoring its length on the floodplain. They termed this the "*K-method*."

A second method tilts the vertical line at an angle towards the center of the channel, producing the "*diagonal division method*." This method is intended to approximate the effective location of the zero-shear-stress layer between the main-channel and floodplain.

A third method attempts to balance the momentum between the adjacent cross-sections based on an area correction, without defining a specific interface line. This method is termed the "*area method*." Stephenson and Kolovopoulos reported the tests of previous researchers and concluded that the area method was the most promising approach, because it yielded smaller deviations in total flow rate and main-channel to floodplain ratios. When momentum transfer effects are factored into the discharge formula for compound sections, it produces an increase in floodplain flow, a decrease in main-channel flow and greater diffusion of the hydrograph, particularly at lower depths.

Wormleaton and Merrett (1990) provided some of the experimental evidence used in Stephenson and Kolovopoulos's paper. Wormleaton and Merrett performed flume experiments on compound channels and gathered detailed data on point velocities and boundary shear stresses. They fitted their results to solutions using the vertical and diagonal interface method, with a correction factor proposed for each. They found that the vertical division method can produce significant inaccuracies in

total discharge and flow proportioning, but that those disparities could be reduced with their correction factor. The disparities were greatest where the floodplains were roughest. The diagonal division method generally performed better than the vertical method. The error in total discharge and main-channel proportions decreases with greater overall discharge and floodplain depths.

2.6.3 Meandering in Two-Dimensional Planform

The considerations given above to compound sections apply for straight reaches of river. Most natural streams have the additional complexity of a meandering plan form. Patra and Kar (2000) provide an overview of the literature on meandering floodplains, which they found to be limited. They reported that some researchers (Toebes and Sooky 1967) had proposed a horizontal fluid boundary as more realistic than a vertical division. Patra and Kar also conducted flume experiments for meandering channels, from which they developed various empirical formulas which they proposed could better estimate discharge. Each of their methods involved use of a diagonal division method, with the division angle based in part on floodplain flow depth and the sinuosity of the channel. Their experiments showed a significant difference in velocities between the main-channel and floodplain when overbank flood depths were low, but that mean velocities in the two segments become more similar at greater flow depths.

Ervine et al. (2000) also developed a series of discharge predictors based on a theoretical solution to the Navier-Stokes equation for turbulent flow in a sinuous

channel, which included consideration of relative roughness between main-channel and floodplain and the ratio of peak discharge to bankfull discharge.

At this point, it appears that predicting the impact of meandering geometry on discharge prediction is an area of ongoing research.

Chapter 3

Basic Derivations of Muskingum-Cunge and Related Methods

3.1 Derivation of the Saint Venant Equations

A complete description of one-dimensional unsteady open-channel flow is given by the Saint Venant equations (Chow 1959, Henderson 1966, Roberson et al. 1988).

The Saint Venant equations are based on the continuity and momentum equations for a segment of channel between two cross-sections, as shown in Figure 3-1. The channel segment has a length of Δx. The parameters for the upstream cross-section of Figure 3.1 are defined as y = depth of flow in the channel, z = bed elevation relative to a horizontal datum, A = area of flow, u = average velocity of the section and $Q = uA$ = discharge. Neglecting higher-order terms in the Taylor expansion, the corresponding variables at the downstream cross-section are

$y + \left(\frac{\partial y}{\partial x}\right)\Delta x$, $A + \left(\frac{\partial A}{\partial x}\right)\Delta x$, $u + \left(\frac{\partial u}{\partial x}\right)\Delta x$ and $Q + \left(\frac{\partial Q}{\partial x}\right)\Delta x$. The entire channel segment between the two cross-sections is the control volume for this system. All flow enters the segment through the upstream segment and leaves through the downstream segment.

The bed slope of the channel is S_o. It is assumed that the bed slope is very small, such that $S_o \approx \sin(\alpha)$ where α is the angle of inclination of the bed slope relative

to the horizontal plane. It is also assumed that the velocity vectors are nearly parallel to the bed and perpendicular to the upstream and downstream cross-sections.

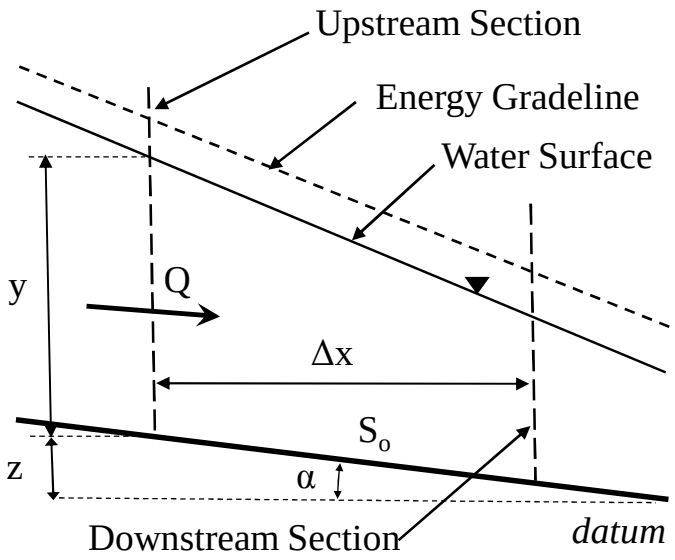

Figure 3-1. Definition Sketch for the Saint Venant Equations
(adapted from Roberson et al., 1988)

Continuity Equation

The flow is assumed to be incompressible, so conservation of mass is given by the continuity equation, as follows:

$$Q_{in} - Q_{out} = \frac{\partial VOL}{\partial t}$$

where Q_{in} = inflow discharge, Q_{out} = outflow discharge, VOL = volume of fluid stored within the channel segment and $\frac{\partial VOL}{\partial t}$ = rate of change in volume storage over time. Substituting the values for the channel in Figure 3-1 gives

$$Q - \left[Q + \left(\frac{\partial Q}{\partial x} \right) \Delta x \right] = \frac{\partial (A * \Delta x)}{\partial t}$$

$$\frac{\partial A}{\partial t} + \frac{\partial Q}{\partial x} = 0 \qquad \text{(3-1a)}$$

where Eq. (3-1a) is the first Saint Venant equation. It is often useful to expand this equation further into an alternate form, based on $Q = (uA)$:

$$\frac{\partial A}{\partial t} + u\frac{\partial A}{\partial x} + A\frac{\partial u}{\partial x} = 0 \qquad \text{(3-1b)}$$

Momentum Equation

The second Saint Venant equation comes from Newton's 2nd law of motion, which states that the sum of the forces acting upon on a system of mass are equal to the change in momentum of the system. For the condition in Figure 3-1, only the forces and momentum changes in the longitudinal direction of flow (x) are considered. In other words,

$$\sum F_x = \frac{\partial (momentum_x)_{system}}{\partial t} \qquad \text{(3-2)}$$

where the system is defined as a given quantity of mass.

To relate this to a fixed space, as shown in Figure 3-1, the control volume equation is used (Roberson and Crowe 1990). The control volume equation, also known as the Reynolds transport theorem, states that for any extensive property (i.e. a conservative property related to the total mass of the system, such as momentum or energy), the relationship between the property of a fixed system of mass can be

related to the properties within a control volume (CV) and to the flux across the boundaries of the control volume, known as the control surfaces (CS), as follows:

$$\frac{\partial B_{system}}{\partial t} = \frac{\partial}{\partial t}\int_{CV}(b\rho)dVOL + \int_{CS} b\rho\left(\vec{U}\bullet d\vec{A}\right) \qquad (3\text{-}3)$$

where B is any extensive property, b is the corresponding intensive property (defined as the amount of the extensive property per unit mass, or B/m where m is mass), ρ is the mass density or mass per unit volume, VOL is the volume within the control volume, $\vec{U}$ is the velocity vector of the total flow and $d\vec{A}$ is an area vector for each control surface, which has a magnitude equal to the size of the control surface and a direction normal to the area and pointing outwards. The dot product $\left(\vec{U}\bullet d\vec{A}\right)$ gives the total discharge across a given control surface (Roberson and Crowe 1990).

For the conditions in Figure 3-1, flow is only possible across the upstream and downstream sections, and all velocities are perpendicular to the cross-sections, so for each section, $\left(\vec{U}\bullet d\vec{A}\right) = (uA)_i = Q_i$.

Momentum is defined as mass times velocity $\left(m\vec{U}\right)$ and it is a vector quantity. As stated previously, all velocities (u) are assumed to be in the longitudinal (x) direction, so the momentum of the system is simply (mu) and the intrinsic form of momentum is simply the velocity u.

The volume of the control volume is approximated as $A(\Delta x)$ (neglecting the incremental change in area over distance). With these simplifications and substitutions, Eqs. (3-2) and (3-3) are combined as follows:

$$\sum F_x = \frac{\partial (momentum_x)_{system}}{\partial t} = \rho \Delta x \frac{\partial}{\partial t}[uA] + [\rho uQ]_{out} - [\rho uQ]_{in}$$

The last two terms on the right hand side represent the net efflux of momentum from the control volume, and can be further reduced,

$$[\rho uQ]_{out} - [\rho uQ]_{in} = \rho \left[uQ + \frac{\partial (uQ)}{\partial x} \Delta x - uQ \right] = \rho \left[\frac{\partial \left(u^2 A\right)}{\partial x} \right] \Delta x$$

which leaves,

$$\sum F_x = \rho \Delta x \frac{\partial}{\partial t}(uA) + \rho \Delta x \frac{\partial}{\partial x}\left(u^2 A\right) \qquad (3\text{-}4)$$

There are three forces acting on the control volume in the longitudinal or x-direction, as shown in Figure 3-2. Those forces are the component of gravity in the x-direction ($F_{g,x}$), the net pressure force acting on the upstream and downstream section faces (F_p), and the resistance or friction force acting against the flow at the channel sides (F_f). Forces are considered positive when they act in the downstream direction.

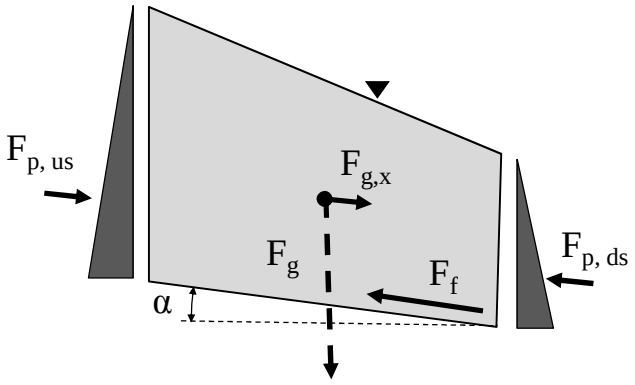

Figure 3-2. Sum of Forces on Control Volume
(adapted from Roberson et al., 1988)

The force of gravity in the longitudinal (x) direction is given by the component of the control volume weight acting in the direction parallel to the bed slope, i.e.

$$F_{g,x} = \gamma(A\Delta x)\sin\alpha \approx \gamma(A\Delta x)S_o$$

where γ is the unit weight of the fluid, noting that $\rho = \frac{\gamma}{g}$ where g is the acceleration due to gravity and ρ is the mass density. This force is always positive in the downstream direction.

To evaluate the net pressure force, an incremental element of flow is considered, based on the cross-section shown in Figure 3-3.

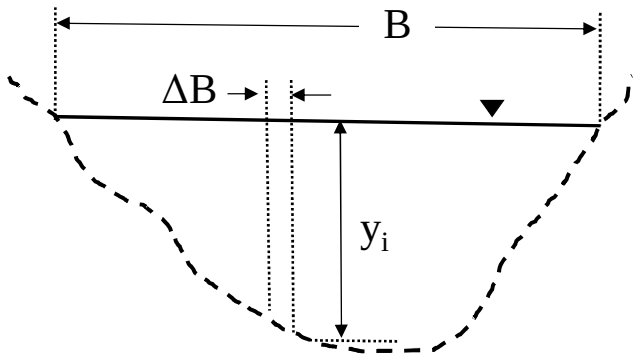

Figure 3-3. Cross-Sectional Element of Flow
(adapted from Henderson 1966)

The incremental element has a cross-sectional width of ΔB, a depth of y_i and a length of Δx. The hydrostatic thrust on the upstream end of the segment is $\frac{\gamma}{2}\Delta B(y_i)^2$ and on the downstream end is $-\frac{\gamma}{2}\Delta B\left(y_i + \frac{\partial y}{\partial x}\Delta x\right)^2$. Neglecting higher-

order terms, the net force due to hydrostatic pressure is therefore $-\gamma \Delta B\left(y_i \frac{\partial y}{\partial x} \Delta x \right)$.

Summing this term for all the increments of width yields

$$F_p = -\gamma \ A \frac{\partial y}{\partial x} \Delta x$$

If depth is increasing in the downstream direction, this force is negative. If depth is decreasing in the downstream direction, the force is positive.

The resistance or friction force represents the total of all non-conservative forces that cause energy loss in the system. It consists of an average frictional shear force (τ) applied over the entire channel wall of the segment that is in contact with the flow (i.e. wetted perimeter (P_w) times the channel length (Δx)), and it always acts in the negative (upstream) direction,

$$F_f = -\tau \ P_w \Delta x$$

The average shear force cannot be directly determined, so it is assumed that the friction force experienced during unsteady flow is the same as would be experienced during steady flow conditions, and is approximated as:

$$\tau = \gamma \ R_h S_f$$

where R_h is the hydraulic radius $\left(\frac{A}{P_w} \right)$ and S_f is the friction slope, or slope of the energy grade line as calculated for the given discharge using a standard resistance equation, such as Manning's or Chezy's formula (Henderson 1966). This friction force is given by the slope of the energy grade line,

$$F_f = \gamma(A\Delta x)S_f$$

Combining these three forces in Eq. (3-4) gives

$$\gamma(A\Delta x)S_o - \gamma A\frac{\partial y}{\partial x}\Delta x - \gamma(A\Delta x)S_f = \rho\Delta x\frac{\partial}{\partial t}(uA) + \rho\Delta x\frac{\partial}{\partial x}(u^2A)$$

which after rearranging and simplifying, gives

$$(gA)(S_o - S_f) = \frac{\partial}{\partial t}(uA) + \frac{\partial}{\partial x}(u^2A) + gA\frac{\partial y}{\partial x}$$

$$(gA)(S_o - S_f) = u\frac{\partial A}{\partial t} + A\frac{\partial u}{\partial t} + 2Au\frac{\partial u}{\partial x} + u^2\frac{\partial A}{\partial x} + gA\frac{\partial y}{\partial x}$$

$$(gA)(S_o - S_f) = A\frac{\partial u}{\partial t} + Au\frac{\partial u}{\partial x} + gA\frac{\partial y}{\partial x} + u\left[\frac{\partial A}{\partial t} + A\frac{\partial u}{\partial x} + u\frac{\partial A}{\partial x}\right]$$

From Eq. (3-1b), the term in the brackets on the right hand side of the last equation reduces to zero, leaving,

$$(S_o - S_f) = \left(\frac{1}{g}\right)\frac{\partial u}{\partial t} + \left(\frac{u}{g}\right)\frac{\partial u}{\partial x} + \frac{\partial y}{\partial x}, \qquad \text{or}$$

$$S_f = S_o - \frac{\partial y}{\partial x} - \left(\frac{u}{g}\right)\frac{\partial u}{\partial x} - \left(\frac{1}{g}\right)\frac{\partial u}{\partial t} \qquad (3\text{-}5)$$

I II III IV V

Eq. (3-5) is the standard form of the second Saint Venant equation. Term I arises from the friction force, Term II from the gravitation force, and Term III from the net pressure forces on the control volume.

Term IV was created by convective acceleration and is due to the difference in inertial between flows entering and leaving the control volume (momentum flux). It is positive when the velocity at the downstream end of the control volume is higher

than at the upstream end (i.e. when there is acceleration of the fluid as it passes through the control volume). Term V is based on the effect of temporal acceleration and represents the rate of change of momentum within the control volume. It is positive when the velocity is higher at the end of the time step than at the beginning (i.e. when there is a net acceleration of all fluid within the control volume over a time step).

In cases of long flood waves, the values of Terms IV and V are typically small in magnitude compared to the other terms and can be ignored (Henderson 1966). Even if not negligible, the last two terms are often generally opposite in sign during passage of a flood wave, which means that it is more accurate to ignore both terms than just one (Ponce 1990). On the rising limb of a flood wave, the convective acceleration term would be negative, since the velocity of the flow at the upstream end of the control volume would be greater than at the downstream end. The temporal acceleration, however, would be positive, since the velocities at both ends of the channel would be greater at the end of a time step than at the beginning. The situation is reversed on the falling limb.

For these reasons, these last two terms can often be neglected for long flood waves and Eq. (3-5) is approximated as:

$$S_f = S_o - \frac{dy}{dx} \tag{3-6}$$

This formula is known as the *diffusion equation* and represents the condition when the friction slope at a given cross-section is determined solely by the slope of

the water surface. This approximation is generally acceptable except in the following circumstances:

- in channels of very small slope;
- when the rate of change of discharge is very rapid;
- when the channel dimensions vary dramatically from upstream to downstream; or
- when there is a sharp curvature in the slope of the water surface (for instance, the leading edge of a dam-break wave or surge).

A resistance formula must be employed to calculate the friction slope (S_f) when using the Saint Venant or diffusion equations. In this study, Manning's formula was used:

$$Q = C(S_f)^2 = \frac{M}{n} A(R_h)^{1.67} (S_f)^2 \qquad (3\text{-}7)$$

where Q is the discharge, C is conveyance in the section, n is Manning's roughness coefficient, M is a coefficient of 1.0 in S.I. units and 1.486 in English units, A is the cross-sectional area of the flow, P_w is the wetted perimeter, and R_h is the hydraulic radius equal to $\frac{A}{P_w}$. Conveyance is denoted C instead of K in this study to avoid confusion with the Muskingum coefficient.

3.2 Derivation of Muskingum Method

The Muskingum method uses the continuity equation and an empirical term to relate outflow discharge to changes in volume over a routing interval. The continuity

equation in finite difference form as applied over a channel reach of length Δx is given by

$$\frac{dQ}{dx} + \frac{dA}{dt} \approx \frac{(O - I)}{\Delta x} + \frac{\Delta A}{\Delta t} = 0 \tag{3-8}$$

$$I - O = \Delta x\left(\frac{\Delta A}{\Delta t}\right) = \frac{\Delta VOL}{\Delta t} \tag{3-9}$$

where I is the inflow discharge rate, O is the outflow discharge rate, Δt is the time interval of a routing step, ΔA is the change in average area of flow in the reach over the time step, and ΔVOL is the change in volume stored within the reach over the time step. Expanding Eq. (3-9) across the time step gives

$$\frac{I_1 + I_2}{2} - \frac{O_1 + O_2}{2} = \frac{VOL_2 - VOL_1}{\Delta t} \tag{3-10}$$

where the subscripts *1* and *2* refer to the values of the given parameters at the beginning and end of the time step, respectively.

The values of I_1, I_2, O_1, and VOL_1 are known for any given time step, and the values of O_2, and VOL_2 must be determined. The Muskingum method assumes that the volume can be approximated as weighted average of the inflow and outflow (Roberson et al. 1988), given as

$$VOL = K\left[X(I) + (1 - X)(O)\right] \tag{3-11}$$

where K and X are constants to be determined for a given reach from available data or assumed based on prior experience. This empirical relationship, along with the continuity Eq. (3-10) can be used to solve for the two unknowns.

A better expression of Eq. (3-11) would be based on the difference in storage across the time step instead of the absolute value of storage at any time, as shown below:

$$VOL_2 - VOL_1 = K\left[X(I_2 - I_1) + (1 - X)(O_2 - O_1)\right] \tag{3-12}$$

If the values of *K* and *X* are constant over all the routing steps, then there is no difference between Eq. (3-11) and (3-12). However, for natural channels, the value of *K* and *X* are not constant. At any given routing step, it is the rate of change in the variables that is most needed, not the absolute value. In the remainder of this investigation, the coefficients *K* and *X* will always represent the incremental values as implied in Eq. (3-12).

If Eqs. (3-10) and (3-12) are combined and like terms gathered and rearranged, the traditional Muskingum equations (Roberson et al. 1988; Ponce and Yevjevich 1978b) are found to be:

$$O_2 = C_1 I_1 + C_2 I_2 + C_3 O_1 \tag{3-13}$$

where

$$C_1 = \left(\frac{\Delta t + 2KX}{2K(1 - X) + \Delta t}\right) \qquad C_2 = \left(\frac{\Delta t - 2KX}{2K(1 - X) + \Delta t}\right)$$

and $$C_3 = \left(\frac{2K(1 - X) - \Delta t}{2K(1 - X) + \Delta t}\right)$$

3.3 Derivation of Muskingum-Cunge

The key to Muskingum-Cunge is the establishment of a one-to-one relationship between the storage found in a given reach and the discharge at a given point within the reach, which is then related to the inflow and outflow discharges. Perumal (1992) began his derivation with the premise that such a relationship could be defined. His derivation relies on the following assumptions:

1. For any given flow in the channel, there exists a particular length of channel such that there is a unique, one-to-one relationship between the discharge at the downstream end of the channel and the depth of flow at the mid-point. This length is denoted the characteristic length, L_u, of the channel and is a function of discharge.
2. The channel section is prismatic, with a constant shape and roughness throughout.
3. The dynamic terms of St. Venant's equations can be ignored and the momentum equation is solved by using Eq. (3-6), the diffusion equation, which means that the friction slope for the flow (S_f) is equal to the slope of the water surface (S_w).
4. The water-surface slope is linear along the length of the reach.
5. The differences between the water-surface slope and bed slope are small enough that the rate of change in discharge during unsteady flow caused by a change in water-surface slope (S_w) is approximately the same as the rate of

change in steady-state discharge resulting from a similar change in bed slope (S_o).

6. The difference in flow depths throughout the reach are small enough that the effective values for kinematic celerity and top width are nearly the same everywhere.

7. The volume stored beneath the water-surface profile for any given water-surface profile is approximately equal to the volume stored beneath the steady-state profile having the same depth of water at the midpoint, y_m.

Figure 3-4 provides a schematic view of a river reach for which assumption (7) might hold.

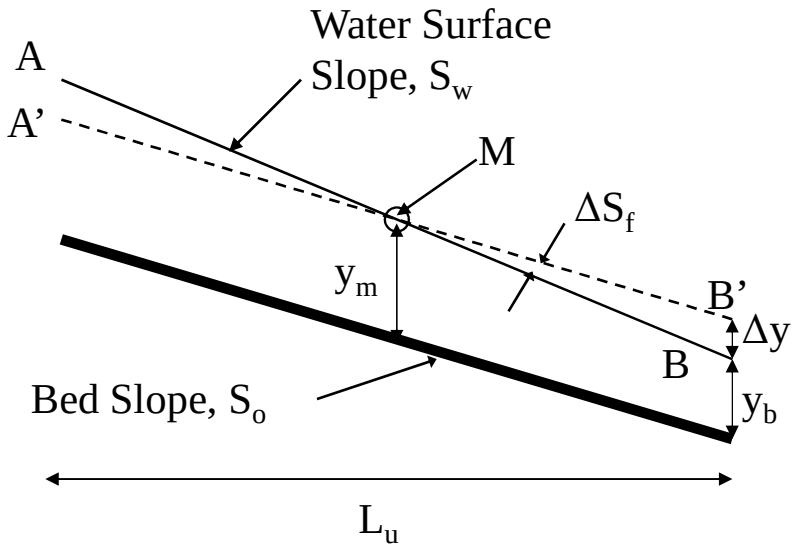

Figure 3-4. River Channel Over a Characteristic Length

The channel has a length of L_u and sections M at the midpoint and B at the downstream end are indicated. Figure 3-4 shows the typical case of a rising hydrograph, where S_f pivots around the midpoint of the reach and $S_f > S_o$. In this case, there is an extra volume stored in the wedge A-M-A', which makes up for the void in volume in the downstream end shown as wedge B-M-B'. The situation reverses when $S_f < S_o$.

This assumption is not strictly correct, since typical open-channel sections have banks and floodplains that slope outwards, so that there will always be slightly more volume in the half with the deeper flows than is offset by the void in the part with the shallower flows. For practical purposes, however, the difference is often small.

By assumption (3) and Eq. (3-7), the discharge at section B is a function solely of the water-surface slope S_f and of the section conveyance, which is assumed to be a function that varies solely with depth (y_b). In other words,

$Q_b = Q(y_b, S_w)$

If the depth of water at section M is held constant, then, by assumption (1), the value of Q at section B must remain constant. The following approximation can then be taken at section B:

$$dQ_b = \left(\frac{\partial Q_b}{\partial y}\right)\Delta y + \left(\frac{\partial Q_b}{\partial S_w}\right)\Delta S_w = 0 \qquad (3\text{-}14)$$

From Figure 3-4, the surface profile A'-B' shows the channel under steady-state flow. The profile A-B shows the channel under a rising-limb hydrograph where the depth in the middle of the section has not changed. At section B, the following relationship exists between flow depth and water-surface slope:

$$\Delta S_w = \frac{-\Delta y}{L_u/2} = (-2)\frac{\Delta y}{L_u} \tag{3-15}$$

By assumption (5)

$$\frac{\partial Q_b}{\partial S_w} \approx \frac{\partial Q_o}{\partial S_o} = \left(\frac{1}{2}\right) C_m (S_o)^{-0.5} = \frac{C_m S_o^{0.5}}{S_o} = \frac{Q_o}{2S_o} \tag{3-16}$$

The combination of terms and cancellation of Δy yields

$$\frac{\partial Q_b}{\partial y}\Delta y + \left(\frac{Q_o}{2S_o}\right)\left(-2\frac{\Delta y}{L_u}\right) = 0$$

$$\frac{\partial Q_b}{\partial y} = \frac{Q_o}{L_u S_o} \quad \text{, or} \tag{3-17}$$

In some cases, it is more useful to express Eq. (3-17) as:

$$\frac{\partial Q_b}{\partial y} = \frac{Q_o}{Z_u} \tag{3-18}$$

where $Z_u = L_u(S_o)$ is the vertical drop in the steady-state water-surface profile across the characteristic length of the river reach. The value of $\partial Q_b / \partial y$ can be evaluated as:

$$\frac{\partial Q_b}{\partial y} = \frac{\partial Q_b}{\partial A}\left(\frac{dA}{dy}\right) \tag{3-19}$$

The first term on the right hand side has been shown to be equal to the kinematic wave speed (c_k) and the second term is simply the top width of the channel (T), and

by assumption (5), the values of both can be evaluated based on steady-state conditions, so:

$$c_k = \frac{\partial Q_o}{\partial A} \tag{3-20}$$

$$T = \frac{dA}{dy} \tag{3-21}$$

$$\frac{\partial Q_b}{\partial y} = c_k \, T \tag{3-22}$$

Combining Eqs. (3-17) and (3-22) yields

$$c_k T = \frac{Q_o}{L_u S_o}$$

$$L_u = \frac{Q_o}{c_k T S_o} \tag{3-23}$$

For a channel with the given properties of c_k, T, and S_o, any given reach of length L_u will produce a one-to-one relationship between the stage of the water at the midpoint and the discharge at the downstream end. By assumption (6), this then also means that there will be a one-to-one relationship between the volume stored in the reach and the discharge at the downstream end.

To put this in more intuitive terms, if the water-surface slope across a reach is changed, but the depth remains the same in the center, one is in effect pivoting the water surface about the midpoint of the reach. If the water-surface slope is increased, the velocity of the water in the reach should increase, but the depth of flow and hence area downstream of the reach midpoint will decrease. Section B is by definition the specific location where these two effects are in balance, leading to no change in

discharge. If the water-surface slope decreases, then the velocity in the reach would decrease, but the depth and area of flow at the downstream would increase, again providing balance at section B. This balance is only strictly maintained for small variations of water-surface slope around the steady-state flow.

The values of c_k and T depend upon the discharge, so that the value of the characteristic reach length (L_u) is not constant for a channel, but also varies with discharge. As a general rule, L_u will increase with increasing Q.

Eq. (3-23) would be sufficient if a reach could always be divided into lengths of exactly L_u for calculation, but in many instances other values for a computation distance step, Δx, may be desired. Furthermore, since L_u varies by discharge, some means of adjusting the solution to report correct results for the given Δx over a range of flows would be desirable.

The procedure given above can be extended to the case of $\Delta x \neq L_u$. Assumptions 1 through 7 are taken as valid over the entire reach length Δx, not just the characteristic reach length L_u. Furthermore, an additional assumption (Perumal 1992) is made

8. The variation in discharge along the reach is linear, so that the discharge at any location within the reach can be given by linear interpolation between the inflow I and the outflow O.

In the strictest sense, assumptions (4) and (8) are incompatible. Discharge is not a linear function of depth, so the surface of the water and the rate of change of

discharge in a channel cannot both be linear. It is assumed, however, that the error introduced by making both assumptions simultaneously is tolerable.

Figure 3-5 shows the situation where Δx is greater than L_u. Section A refers to the inflow, section M refers to the midpoint of the reach, section B refers to the downstream end of the characteristic reach L_u, and section C refers to the downstream end of the routing reach Δx. The distance between sections B and C is denoted as r, and both L_u and Δx are centered on section M.

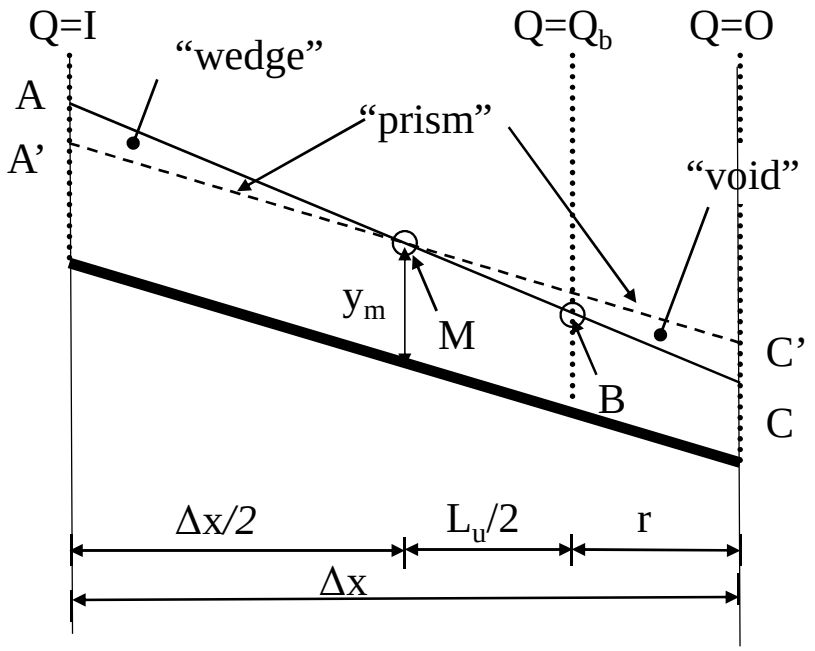

Figure 3-5. Channel Extrapolated to Length Other Than L_u

By assumption (8), the discharge at B is given by

$$\frac{I-O}{\Delta x} = \frac{Q_b - O}{r}$$

$$Q_b = \left(\frac{r}{\Delta x}\right)(I - O) + O$$

$$Q_b = X(I - O) + O = XI + (1 - X)O \tag{3-24}$$

where $X = r/\Delta x$ is a length adjustment factor to be used for linear interpolation. This definition of X is developed further, using Eq. (3-23):

$$X = \frac{1}{\Delta x}\left(\frac{\Delta x}{2} - \frac{L_u}{2}\right) = \frac{1}{2}\left(1 - \frac{L_u}{\Delta x}\right) \tag{3-25}$$

$$X = \frac{1}{2}\left(1 - \frac{Q}{cTS_o\Delta x}\right) \tag{3-26}$$

Eq. (3-26) is recognizable as Cunge's definition of Muskingum X (Cunge 1969, Roberson et al. 1988, Ponce and Yevjevich 1978b). A more general form for it is

$$X = \frac{1}{2}\left(1 - \frac{Q}{Z\dfrac{dQ}{dy}}\right) \tag{3-27}$$

where $Z = (S_o)\Delta x$ is the vertical drop in water-surface profile across the computational distance step Δx.

Because there is a one-to-one relationship between discharge at section B and the volume stored in the reach,

$$VOL_2 - VOL_1 = K\left[Q_{b2} - Q_{b1}\right] \tag{3-28}$$

where

$$K = \frac{dVOL}{dQ_b} \tag{3-29}$$

$$K = \frac{dA}{dQ_b}\Delta x$$

$$K = \frac{\Delta x}{c_k} \tag{3-30}$$

If the relationship between volume and discharge is linear, K will be a constant. Typically, the relationship is not linear and therefore K varies with discharge. This is the definition of K as proposed for Muskingum-Cunge (Cunge 1969, Roberson et al. 1988, Ponce and Yevjevich 1978b).

From Eq. (3-24), the difference in flow rate at section B at the beginning and end of a time step is given as:

$$Q_{b2} - Q_{b1} = X(I_2 - I_1) + (1 - X)(O_2 - O_1) \tag{3-31}$$

so

$$VOL_2 - VOL_1 = K\left[X(I_2 - I_1) + (1 - X)(O_2 - O_1)\right]$$

which is precisely the same as Eq. (3-12) used in the Muskingum equation. The relationships for *K* and *X* given by Eqs. (3-30) and (3-26) are also precisely the same as proposed by Cunge, and therefore it is shown that the Muskingum-Cunge is an approximate solution of St. Venant's equations based on the physical description shown on Figures 3-1 and 3-2 and from assumptions (1) through (8).

The author presented a detailed review of this derivation in a previous work (Heatherman 2004).

3.4 Physical Interpretation of *K* and *X*.

The value of *K* has units of time and represents the amount of time it takes for a flood wave, traveling at the kinematic celerity, to travel down the reach a distance equal to the computational distance step. The value of *K* depends upon the reference discharge. It generally decreases as discharge increases, except in regions where small increases in discharge open up expansive, slow-flowing floodplains. This concept of *K* is well established in the traditional understanding of Muskingum's method.

It is important to observe, though, that *K* did not arise in the equations from any explicit consideration of wave speed. It was merely a surrogate for the volume-discharge relationship. As noted by Henderson (1966), flood waves appear from empirical data to move at the kinematic wave speed, thus the relationship between K and travel time. If field calibration data, however, found a deviation between kinematic wave speed from theory and the actual progression speed at a station, one should not necessarily adjust the value of *K*.

The value for *K* discussed in the previous section was for the distance step used in the actual computations. In most computer models, the value of *K* is entered based on the travel time through the entire reach, and the computer internally subdivides the reach into smaller computational increments. Values of *K* are then calculated internally for each computational step.

Traditional explanations of *X* relied on the concept of prism storage and wedge storage, where wedge storage is defined as the volume of flow above a plane

that was established parallel to the stream bed and intersecting the flow depth at the channel outlet (Roberson et al. 1988, Montes 1998). Figure 3-6 presents the traditional understanding of prism and wedge storage, with the prism represented by that part below the dashed line.

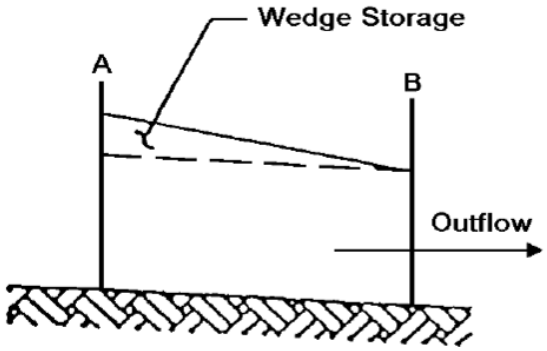

Figure 3-6. Traditional Explanation of Prism-and-Wedge Storage
(reprinted from USACE 1994)

The prism and wedge definition of X is incorrect. Assumption (7) asserts that the total of prism storage (as traditionally defined) within a reach of characteristic length L_u is approximately equal to the value of steady-state storage in the reach having a discharge equal to that of the outflow discharge. The plane of the *"prism"* is properly drawn to intersect the water-surface at the midpoint of the channel, as shown in Figure 3-5, rather than the outlet. The *"wedge"* on the half of the reach that lies above this plane is more or less offset by the *"void"* found below that plane on the opposite half.

Instead, X should be understood to be a length-adjustment factor, where the results for the characteristic length L_u are interpolated or extrapolated to the user-defined computational distance step Δx. A positive value of X indicates that the user-defined Δx is longer than L_u. It has a limiting value approaching + ½ as Δx becomes very large. A negative value of X simply means that Δx as smaller than L_u and that the results are being interpolated to a point interior to the characteristic reach. There is no limit to the negative value of X, it will approach -∞ as Δx becomes very small.

One might speculate that values of X close to zero should give the best results, as this would involve the least amount of interpolation or extrapolation. This would mean that the distance steps used in a model should optimally be set to L_u.

The values of K and X are not fundamental properties of a channel, but are dependent upon the computational distance step Δx. The fundamental variables of importance in defining a reach are the values of kinematic celerity (c_k) and the characteristic reach length (L_u).

3.5 Muskingum-Cunge as Implemented in HEC-1

HEC-1 provides several different options for using Muskingum-Cunge in routing. The most versatile method is the variable-parameter Muskingum-Cunge (VMC) method utilizing a user-input cross-section. The user-input cross-section is defined by eight station/elevation coordinates, and is therefore known as an 8-point cross-section (USACE 1998).

The VMC is invoked using an "RD" card in HEC-1, then by inputting the relevant parameters for the 8-point cross-section in a sequence of "RC", "RX" and "RY" cards. The eight station/elevation pairs describe the main-channel (bounded by the third and sixth input pairs), the left overbank (bounded by the 1st to 3rd points) and the right overbank (6th through 8th points). Single values for channel length and slope are input, as are roughness values for each overbank and the main-channel. Alternatively, several simpler, pre-defined cross-sectional shapes are available, such as trapezoidal, circular, triangular, and rectangular.

HEC-1 then uses an internal algorithm to divide the input channel into time and distance steps, based on the accuracy criteria set forth by Ponce and Theurer (1982). The time step (Δt) is first determined and is set equal to the overall model time step, unless it made shorter to ensure that it is: (a) no more than 1/20th of the time to peak of the inflow hydrograph, or (b) no more than the travel time through the reach. The distance step is then set equal to

$$\Delta x = c\Delta t$$

unless it needs to be set smaller to satisfy the following constraint:

$$\Delta x \leq \frac{1}{2}\left(c\Delta t + \frac{Q_{ref}}{c_k T S_o} \right)$$

where Q_{ref} was set $Q_{ref} = Q_{base} + (½)\ (Q_{peak} - Q_{base})$ and Q_{base} is the baseflow taken from the inflow hydrograph (USACE 1998). These time and distance steps are set by the program and are not subject to adjustment by the modeler.

The HEC-1 solution to VMC relies on a four-point iterative averaging scheme where the values of *K* and *X* are evaluated separately for each node in the "space-time" box (inflow and outflow points, both at beginning and end of time step). Since the outflow at the end of the time step is an unknown, the method requires an iterative solution.

Another method by which Muskingum-Cunge can be implemented is through direct use of Muskingum's method using the "RM" card. As such, the user can input the value of *K* for the reach and the value of *X*. The HEC-1 "RM" card allows the user to subdivide a reach into multiple sub-reaches. When this is the case, the value of *X* is entered based on what is appropriate for each individual sub-reach, whereas the value of *K* is for the entire series of subreaches. HEC-1 internally divides *K* by the number of sub-reaches to find the K_i to use in each reach.

HEC-1 guidance for Muskingum's method does not directly discuss the selection of values for *K* and *X*, but the previous derivation of Muskingum-Cunge's equations suggest that both are found using Cunge's derivation, and that the ideal combination would be to set sub-reaches so that *X* is approximately zero. This form of the Muskingum equation does not allow for any of the parameters to adjust with discharge, and can therefore be considered a "*constant-parameter*" model.

3.6 Cascading Reservoir Method

The Cascading Reservoir (CR) method treats the channel as a series of reservoirs. The routing through each reservoir is handled by using a level-pool

routing, usually called the modified Puls method (USACE 1994, 1998). For each individual reservoir, the modified Puls method involves combining the continuity equation and a table or graph that relates the volume in the reservoir to the elevation (stage) of a flat water surface and a table or graph that relates the same stage to the discharge through an outlet control structure, typically a weir or orifice. In this situation, there is a one-to-one relationship between the volume of storage in the reservoir and the outlet discharge.

3.6.1 Routing Equation for a Single Reservoir

Returning to the continuity equation as shown in Eq. (3-10) and re-arranging, one would have:

$$(I_1 + I_2) - (O_1 + O_2) = \frac{2(VOL_2 - VOL_1)}{\Delta t}$$

$$(I_1 + I_2) - 2(O_1) + \left[O_1 + 2\frac{(VOL_1)}{\Delta t} \right] = \left[O_2 + 2\frac{(VOL_2)}{\Delta t} \right] \quad (3\text{-}32)$$

$$(I_1 + I_2) - 2(O_1) + P_1 = P_2 \quad (3\text{-}33)$$

where

$$P_i = \left[O_i + 2\frac{(VOL_i)}{\Delta t} \right] \quad (3\text{-}34)$$

Because the outlet flow (O) and the stored volume (VOL) are uniquely related, there is a one-to-one relationship as well between P and O. A curve of P vs. O is developed directly and used with Eq. (3-33) to solve for each subsequent time step. All of the terms on the left are known at the beginning of a time step, so the value of P_2 can be calculated and related back to the values of O_2 and VOL_2.

3.6.2 Modeling Rivers, Finding the Optimal Number of Subreservoirs (N) in Series

The routing characteristics of a level-pool reservoir are significantly different than those of a prismatic open-channel river reach. In a river, the water-surface elevation over the reach is not flat, the discharge at the outlet is not uniquely related to storage volume, nor is the discharge controlled by a simple structure such as a weir or orifice. A series of cascading reservoirs, however, can be made to mimic the results of a river routing provided that suitable selections are made for the overall volume-discharge curve and for the number of identical reservoirs in series (USACE 1994).

To apply CR to a river routing situation, the first step is to define the relationship between storage and discharge for a stream reach over a range of steady-state flows, which is expressed in a table of volume versus discharge for the entire reach. This relationship can be derived from an existing backwater model, such as HEC-RAS (USACE 1994).

The reach is then broken up into a number (N) of identical sub-reservoirs, where each sub-reservoir contains $1/N^{th}$ of the entire reach's storage for any given outflow. Depending upon the number of sub-reservoirs used, the model can be made to represent anything between a reservoir routing (N=1) to a basin approaching pure translation with no attenuation (as N approaches infinity).

From the previous discussion of the Muskingum-Cunge equation, it should be clear that, by definition, each sub-reservoir used in the Modified Puls method should

represent a segment of the river having a length equal to the characteristic length. This would result in a Muskingum's X equal to zero, and therefore a routing in which the storage in the reach was uniquely tied to the outflow. Based on this, the number of sub-reservoirs needed is given by:

$$N_o = \frac{L_r}{L_u} = \frac{L_r\left(c_k T S_o\right)}{Q_o} \tag{3-35}$$

where N_o is the optimal number of sub-basins for the reach, L_r is the total length of the river reach being modeled, and L_u = characteristic length for the reach, as given in Eq. (3-23).

In the CR method, the value of Muskingum K is not explicitly determined, but is implicit in the storage-discharge table. Recalling Eq. (3-28), the effective value K for a discharge between the ith and jth entry in the storage discharge table is approximately:

$$K \approx \frac{VOL_j - VOL_i}{Q_j - Q_i} \tag{3-36}$$

3.6.3 Direct Calculation of CR Input from HEC-RAS Data

Eq. (3-23) provides the value of characteristic length based on the evaluation of known cross-sectional values of c_k, T, and K. The primary use of the CR technique is in natural river channels where values are evaluated over an entire reach, as opposed to at any single cross-section. Typically, the individual cross-sections in the reach vary significantly, making the determination of representative values of c_k, T, and K difficult. It would be useful to have a means of calculating X using only overall reach data, such as that typically available from HEC-RAS.

For a reach of length L_r, the optimal number of sub-reaches N_o will be selected so that each sub-reach has a length nearly equal to the characteristic reach length, L_u. Substituting Eq. (3-35) into Eq. (3-17)

$$\frac{\partial Q}{\partial y} = \frac{Q}{\left(L_r \big/ N_o \right) S_o}$$

$$\frac{\partial Q}{\partial y} = \frac{Q(N_o)}{Z_r}$$

$$N_o = \left(\frac{\partial Q}{\partial y} \right) \frac{Z_r}{Q} \tag{3-37}$$

where $Z_r = L_r(S_o)$ is total vertical drop in bed elevation (or steady-state water-surface profile) over the total reach. Using Eq. (3-29), $\frac{dQ}{dy}$ can be broken down as follows:

$$\frac{dQ}{dy} = \left(\frac{dQ}{dVOL} \right) \left(\frac{dVOL}{dy} \right) = \frac{SA}{K} \tag{3-38}$$

where $\frac{dVOL}{dy}$ equals the surface area (SA) of the steady-state water surface calculated over the entire reach length. Eq. (3-37) can therefore be written as:

$$N_o = \left(\frac{SA}{K} \right) \frac{Z_r}{Q} = \frac{SA(Z_r)}{Q\left(\Delta VOL \big/ \Delta Q \right)} \tag{3-39}$$

The values of SA, Z_r, and Q can all be found directly from HEC-RAS output tables for any given river reach. The value of K can be calculated from the values of Q and VOL for any two given steady-state profiles run for slightly different values of Q.

The values of N_o given in Eq. (3-39) are not based on any direct input of reach length. This avoids the problem of determining an "effective length" when dealing with natural channels for which the values of length for channel, left overbank and right overbank may be different. The differences instead become implicit in the values of volume and surface area. In Chapter 4, the issue of evaluating Muskingum-Cunge for meandering channels in which channel and overbank lengths are different is revisited, and it is found that Eq. (3-39) is supported in theory.

The Muskingum-Cunge method itself was derived by assuming that the channel is prismatic, meaning that shape and roughness do not change between sections. This is clearly not the case when dealing with most natural channel systems. However, all of the approximate routing methods implicitly assume the use of some type of representative reach containing a prismatic section that can be substituted for the actual reach with variable geometry and roughness.

Presumably, any idealized river section with a specified length and slope that matched the natural channel reach for the various terms in Eqs. (3-36) and (3-39) over the entire range of flow could be defined as the representative section. Use of these equations avoids the need to explicitly define the representative section; one can use the composite reach properties only.

If K and N_o are defined from reach data, one can also work backwards from Eqs. (3-30) and (3-35) to define nominal values for kinematic celerity and characteristic length. A reference length of channel, L_{ref}, would need to be specified, and these nominal values would be relative to that length. The length of the main

channel, L_{mc}, is the most likely reference value to use. The relationships would be as follows:

$$c_k = \frac{L_{ref}}{K} \tag{3-40}$$

$$L_u = \frac{L_{ref}}{N_o} \tag{3-41}$$

3.6.4 Evaluation of Strelkoff's Guidance for N

As mentioned in Chapter 2, the HEC-HMS Reference Manual (USACE 2000) suggests an alternate equation for determining the optimal number of sub-reservoirs (N) in the cascading reservoirs method:

$$N = 2 L_r \frac{S_o}{y_o} \tag{3-42}$$

where L_r is the total length of the river reach being modeled, S_o is the bed slope of the channel and y_o is the normal flow depth associated with baseflow in the channel. Baseflow is not defined in the manual.

The equation is based on work by Strelkoff (1980). Strelkoff's research was based on numerous unsteady routing simulations using the modified Puls (cascading reservoirs), kinematic wave, and full dynamic (St. Venant's equation) solutions. Two simplified cross-sections were evaluated: a simple rectangular section and a composite section with rectangular main-channel and a gently sloping overbank. Three downstream boundary were examined: normal depth, critical depth (free outfall conditions), and imposed backwater depths.

All channel properties were reduced to dimensionless parameters for comparison. In his study, the term "*baseflow*" simply meant the reference discharge used to evaluate channel properties. Inflow hydrographs were then routed and the attenuation and wave speeds evaluated. Inflow hydrographs had peak discharges that were either 5 or 20 times the baseflow.

For the modified Puls (cascading reservoirs) method, Strelkoff experimented with various numbers of subdivisions (N) on each reach, including N=1, 2, 4, 10 etc. He found that there was an "optimal" number of subdivisions for each reach that appeared to match the fully dynamic solution the best. He further found that number of subdivisions *"proved to be unrelated to the travel time through the subreach"* (Strelkoff 1980).

Strelkoff proposed an equation for the optimal number of subdivisions for a reach that is mathematically equivalent to Eq. (3-42), where the coefficient 2 was an average value but actually ranged from 1.0 to 3.3 depending upon the flow scenario. (Strelkoff's original equation and coefficients were the inverse of Eq. (3-42). The optimal coefficients ranged between 1/3 and 1, and ½ was selected as the average). Strelkoff cautioned that *"this information is strictly empirical; no theoretical basis has been found for the existence of such an 'optimal' value."*

In fact, a relationship between Strelkoff's equation and the characteristic reach length can be established. To do so, one must use the more fundamental definition of characteristic reach length given in Eq. (3-17)

$$\frac{\partial Q}{\partial y} = \frac{Q}{L_u S_o} \tag{3-17}$$

For simple cross-sectional shapes, the following equation can often be fitted to the discharge-stage relationship:

$$Q = \alpha\, y^m \tag{3-43}$$

where α and m are coefficients dependent upon the channel shape. If Manning's equation were used, an idealized triangular channel would have m = 2.67, whereas a very wide, rectangular channel would have m = 1.67. The partial derivative of discharge with respect to depth is thus,

$$\frac{\partial Q}{\partial y} = m\alpha\, y^{m-1} \tag{3-44}$$

so

$$\frac{Q}{\left(\frac{\partial Q}{\partial y}\right)} = \frac{\alpha\, y^m}{\left(m\alpha\, y^{m-1}\right)} = \frac{y}{(m)}$$

Rearranging (3-17) and substituting the above gives a new relationship for the characteristic reach length, L_u,

$$L_u = \frac{Q}{\left(\frac{\partial Q}{\partial y}\right) S_o} = \frac{y}{(m) S_o} \tag{3-45}$$

This expression can be substituted into Eq. (3-35) to yield an equation almost identical to Strelkoff's relationship given previously as Eq. (3-42),

$$N_o = \frac{L_r}{L_u} = m\, L_r \frac{S_o}{y} \tag{3-46}$$

Strelkoff's empirical coefficient ranged from 1.0 to 3.33. This range encompasses the theoretical range for *m* for semi-infinite rectangular channels and for triangular sections. Because Strelkoff arrived at his coefficients empirically, they may also contain an embedded adjustment for the reference discharge Q_o used and for the various different boundary conditions he examined.

Most natural channels consist of compound sections with a narrow main-channel and wide overbanks. These channels do not generally follow the simple discharge relationship given in Eq. (3-43). There is also uncertainty as to the best values to use for the coefficient *m* (Strelkoff's range covers a factor of 3.33) and for the reference depth at "baseflow." It is sufficient to note that the structure of Strelkoff's empirical equation lends support to the previous finding that characteristic reach length be used to define the optimal number of subreservoirs in the CR method.

3.6.5 Evaluation of Wave Speed-Time Step Method for Finding *N*.

In contrast to the methods derived previously for *N* based on the characteristic reach length, Corps of Engineer's guidance (USACE 1994, 2000) has also suggested the following expression as an initial estimate for *N*,

$$N = \frac{K}{\Delta t} = \frac{L_r}{c_k \, \Delta t} \tag{3-47}$$

where *K* is the travel time through the reach, based on kinematic wave speed as given in Eq. (2-5), and Δt is the user-defined time-step for the model. In other words, the number of reservoirs (*N*) would be set such that the wave will travel the length of one sub-reach during each time interval. Under this formula, the value *N* is dependent

upon the time step used in the model. Since no corresponding limits are provided for time step, one would expect the method work equally well for any reasonable choice of Δt. This is in distinct contrast to the methods based on characteristic length, where time step of the model was not a factor in establishing N.

There is no theoretical justification for Eq. (3-47). The development of Muskingum-Cunge relies on two separate relationships: one for K (based on c_k) and one for X (based on L_u). Unless a specific constraint were placed on the time step, Eq. (3-47) would reduce the routing to only one relationship, that given for K.

Eq. (3-47) can easily be checked using any model developed for cascading reservoirs. Various models could be developed, varying N and Δt as appropriate, and the sensitivity of modeling results examined. This test was performed early in the study (detailed results not presented) and it was found that Eq. (3-47) is not valid. The degree of diffusion in the hydrograph is very sensitive to the value of N but relatively uninfluenced by reasonable changes in model time step.

3.7 Overview of Unsteady RAS (uRAS)

To verify the accuracy of calculations made using these approximate routing methods, their results are compared against those derived from a complete solution to the St. Venant equations, as implemented by the HEC-RAS unsteady flow model.

As mentioned previously, the unsteady model in HEC-RAS was based on the UNET program originally written by Dr. Robert L. Barkau for the U.S. Army Corps

of Engineers (Barkau 1997, USACE 2002a, and USACE 2002b). In the remainder of this study, the unsteady flow model within HEC-RAS is referred to as uRAS.

uRAS simulates one-dimensional flow in open-channel reaches. It provides for separate specification of main-channel and overbank reaches and can accommodate a number of complex features often found in river engineering, such as split flow and junctions, off-line storage basins, energy losses due to bridge piers, weirs, and other flow obstructions, and lateral inflows.

The solution proceeds by breaking the river system into discrete geometric nodes, consisting either of river cross-sections or special structures, such as bridges, culverts, weirs, storage ponds, etc. Cross-sections are defined using station/elevation pairs and roughness coefficients, from which cross-section properties of conveyance and area per elevation are calculated. The distance between adjacent cross-sections is specified. Each cross-section in uRAS can be divided into a main channel and an overbank, with separate lengths defined for each.

Unlike the HEC-RAS steady-state solution, uRAS does not account for separate left and right overbanks. The input routines allow for separate specifications of each, but they are combined into a single overbank prior to calculation. The effective value of overbank length is taken as the average between right and left overbanks, regardless of the weighted area or conveyance in each overbank.

Special structures such as off-line storage, bridges, and culverts are input between the appropriate cross-sections, and empirical formulas are used to define their stage/discharge and stage/storage relationships.

The time-dependent features of unsteady flow are introduced by establishing boundary conditions, such as inflow hydrographs, hydrographs at junctions, and downstream stage or flow hydrographs.

A set of initial conditions for all the geometric nodes is established. This is typically done by using a steady-state discharge and calculating the initial conditions using standard backwater techniques.

uRAS solves the continuity and momentum equations over a time step using an implicit finite-difference scheme, as described in Chapter 2. The partial derivatives for each variable with respect to distance and time are written as finite differences between the four bounding nodes.

The two basic unknowns handled by uRAS are ΔQ (change in discharge during time step) and Δz (change in water-surface elevation during the time step). All other variables, such as area and velocity, are related to values of Q and z through the use of tables for each node. These tables are calculated prior to the uRAS run by using a geometry pre-processor. During the actual uRAS calculations, approximate values are interpolated from the previously established tables.

The equations for all geometric nodes are written and assembled into a system of equations that are solved simultaneously for all the unknowns at the end of the time step. The process is repeated for every subsequent time step to be modeled. Because St. Venant's equations are non-linear, a number of simplifying assumptions are made and a non-linear iterative technique is used to solve the system of equations.

In general, the iterations continue until the total error of the entire system of equations is minimized.

The matrix which is assembled for the non-linear system of equations can become very large, with many zero entries. For simple channels without off-line storage areas or special structures, the matrix remains banded, but when these structures exist, non-zero entries emerge outside the banded structure, complicating the solution. A direct application of traditional matrix solutions would involve numeric and memory storage difficulties. To efficiently handle the solution, Barkau developed a "skyline solution algorithm" in which the size of the matrix is compressed and pointers are used to define the proper location of occasional sparse entries outside the primary band (Barkau 1997, USACE 2002b).

Chapter 4

Analyses of Meandering Channels within Overbanks

4.1 Conceptual Framework for Meandering Channels

The basic derivation for Muskingum-Cunge was presented in Chapter 3. This derivation proceeded from the assumption of a simple prismatic channel with a single overall reach length.

Natural rivers are typically sinuous, having a meandering main channel within a broader floodplain. Important components of flow are found in both the main channel and the overbanks. The length of flow in the main-channel and each overbank will be different due to meanders. This difference in lengths impacts the calculations of both volume and effective conveyance. If not accounted for, this difference in lengths leads to errors in calculations of both wave speed and attenuation. An appropriate consideration of the difference in channel and overbank lengths must be made so that a proper "representative" channel reach can be defined.

This section provides a derivation specifically for the case of meandering streams and describes three means by which the resulting equations could be coded into models. It also explores the approximation made in both HEC-RAS and uRAS for solving meandering flow situations, and discovers problems with the formulation of each.

4.2 Derivation of Muskingum-Cunge for Meandering Channels

A derivation is needed for Muskingum-Cunge for the special case of an idealized compound channel consisting of a meandering channel within a straight floodplain. The most common approach to the meandering channels problem is to separate the main-channel and each overbank into separate, parallel sections (Henderson 1966).

The sections are assumed prismatic in the sense that the shape of the main channel and the overbanks each do not change over the length of the reach. The overbank and the main channel each have a separate length specified. The main channel can be thought of as running parallel to the overbank, with equal stages being maintained between the main channel and overbank at proportional distances along each. The water-surface elevation in the upstream end is assumed to be the same in both channel and overbank, and the same is true at the downstream end. The total drop in water-surface elevations across the reach for both the main channel and the overbank are assumed to be equal.

Water is assumed to flow freely between the main channel and the overbank as needed to maintain the equivalent stage, but without loss or gain of momentum. Because the main channel and overbanks are assumed to occupy separate channels, there is no turbulence or mixing of flows assumed by virtue of having the meandering channel running in a different direction than the dominant overbank flows, or from the momentum losses that might occur when overbank flows cross over the meandering channel beneath. In reality, as indicated in the literature, losses do occur

at the interface between main-channel flows and overbanks. For the parallel channels approach, it must be assumed that those losses are reflected in the choice of Manning's roughness factor.

For this type of system, the value of surface area, volume, and discharge will each be given as the sum of the respective values for the channel and overbank, as follows:

$$SA = T_{mc}(L_{mc}) + T_{ob}(L_{ob}) \tag{4-1}$$

$$VOL = A_{mc}(L_{mc}) + A_{ob}(L_{ob}) \tag{4-2}$$

$$Q = C_{mc}\sqrt{S_{w,mc}} + C_{ob}\sqrt{S_{w,ob}} = C_{mc}\sqrt{Z/L_{mc}} + C_{ob}\sqrt{Z/L_{ob}} \tag{4-3}$$

where *SA* is the surface area of the flow in the reach, *VOL* is volume of water, *Q* is the steady-state discharge, *T* is the top width of the channel or overbank, *L* is the length of the channel or overbank, *C* is the conveyance of the channel or overbank, *Z* is the total vertical drop in water-surface profile through the reach, and subscripts *mc* and *ob* refer to the channel and overbanks, respectively. For these equations, the friction slope is assumed equal to the slope of the water surface, as given by the diffusion equation.

Following the same procedure as used in Chapter 3 to derive Muskingum-Cunge, one begins with the continuity equation,

$$\frac{I_1 + I_2}{2} - \frac{O_1 + O_2}{2} = \frac{VOL_2 - VOL_1}{\Delta t} \tag{3-10}$$

and recognizes that

$$\Delta VOL = \Delta A_{mc}(L_{mc}) + \Delta A_{ob}(L_{ob})$$

$$\Delta VOL = \Delta y\,[T_{mc}(L_{mc}) + T_{ob}(L_{ob})] \qquad (4\text{-}4)$$

It is then assumed that there is a specific reach length ($L_{u,mc}$ for the channel and $L_{u,ob}$ for the overbank) for the meandering channel over which there is a one-to-one relationship between stage at the middle of the reach and discharge at the end, which is pictured in Figure 4-1.

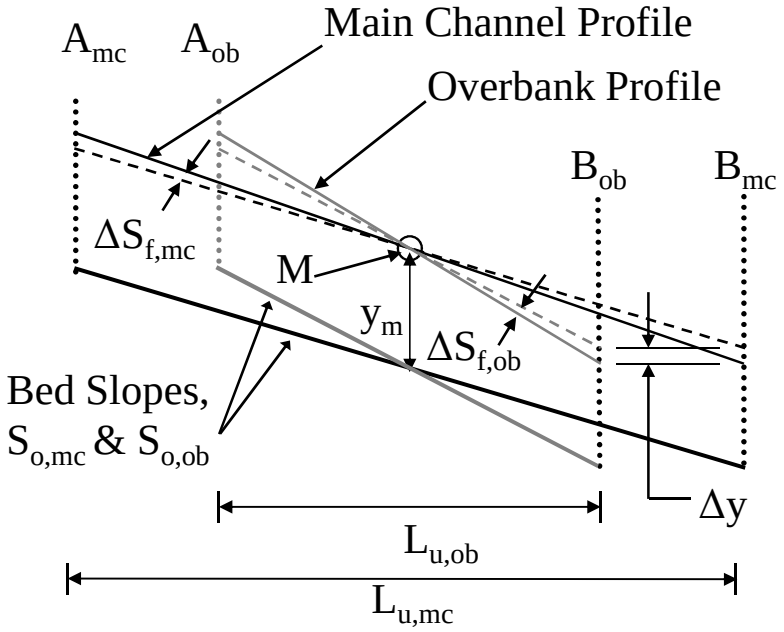

Figure 4-1. Characteristic Length for Parallel, Separate Length Channels

The same argument that led to Eq. (3-14) is used to define the following equation for discharges at section B in a compound meandering system:

$$\left(\frac{\partial Q_{b,mc}}{\partial y}\right)\Delta y + \left(\frac{\partial Q_{b,mc}}{\partial S_{w,mc}}\right)\Delta S_{w,mc} + \left(\frac{\partial Q_{b,ob}}{\partial y_{ob}}\right)\Delta y + \left(\frac{\partial Q_{b,ob}}{\partial S_{w,ob}}\right)\Delta S_{w,ob} = 0 \qquad (4\text{-}5)$$

where $S_{f,mc}$ is the water-surface slope in the main-channel, $S_{f,ob}$ is the water-surface slope in the overbank, and Δy is the change in depth of flow at the downstream end of the characteristic reach.

Because the stage at the downstream end of the channel remains the same for both channel and overbank, the value of Δy is also the same for both. For each given part of the flow, then, the following relationships hold:

$$\Delta S_{w,mc} = \frac{-\Delta y}{L_{u,mc}/2} = (-2)\frac{\Delta y}{L_{u,mc}} \tag{4-6}$$

$$\Delta S_{w,ob} = \frac{-\Delta y}{L_{u,ob}/2} = (-2)\frac{\Delta y}{L_{u,ob}} \tag{4-7}$$

By assumption (5) and Eq. (3-16) in the original derivation of Muskingum-Cunge derivation,

$$\frac{\partial Q_{mc}}{\partial S_{w,mc}} = \frac{Q_{mc}}{2S_{o,mc}} \tag{4-8}$$

$$\frac{\partial Q_{ob}}{\partial S_{w,ob}} = \frac{Q_{ob}}{2S_{o,ob}} \tag{4-9}$$

Finally, since changes in downstream stage (Δy) are the same for both overbank and the main-channel:

$$\frac{\partial Q_{mc}}{\partial y} + \frac{\partial Q_{ob}}{\partial y} = \frac{\partial Q}{\partial y} \tag{4-10}$$

Combining these terms yields:

$$\frac{\partial Q}{\partial y} = \frac{Q_{mc}}{L_{u,mc}S_{o,mc}} + \frac{Q_{ob}}{L_{u,ob}S_{o,ob}} \tag{4-11}$$

The total drop in water-surface elevation across the reach was constant, so the following equality holds:

$$Z_u = L_{u,mc}(S_{o,mc}) = L_{u,ob}(S_{o,ob}) \tag{4-12}$$

which means that Eq. (4-11) can be simplified as:

$$\frac{\partial Q}{\partial y} = \frac{Q_{mc} + Q_{ob}}{Z_u} = \frac{Q}{Z_u} \tag{4-13}$$

where Eq. (4-13) is precisely the general form of the solution for characteristic length of channel shown in Eq. (3-18).

This is also the same form as was developed in Section 3.6.3 for evaluating K and X directly from reach data. In cases of meandering, multi-part channels, it may be easiest to evaluate the reach based on total reach data, instead of by cross-section.

It should be noted that the derivations leading up to Eq. (4-13) would generally hold true for any number of separate parallel channels and is not limited to two channels. Therefore, for any given overbank and meandering channel condition, Eq. (4-13) would be considered a valid conclusion of the parallel channel analogy.

If the characteristic reach length is referenced in terms of channel length as $L_{u,mc}$ then

$$\frac{\partial Q}{\partial y} = \frac{Q_{total}}{L_{u,mc} S_{o,mc}}$$

$$L_{u,mc} = \frac{Q_{total}}{\left(\frac{\partial Q}{\partial y}\right) S_{o,mc}} \tag{4-14}$$

Eq. (4-14) defines the characteristic length in terms of channel length instead of overbank length. Eq. (4-12) shows that length and slope terms are combined in the equation to yield *Z*, which is the same for both the channel and the overbank. Either one could be used as the measure of characteristic length, provided that the appropriate slope is then included in the equation.

The final step in applying Muskingum-Cunge is to interpolate or extrapolate flows to the modeled outlet point when $L_{u,mc} \neq \Delta x_{mc}$. As with the previous derivation in section 2, section B is defined as the outlet from the characteristic channel. If the assumption of linear change in discharge from inflow to outflow point is maintained, and if it understood that each point along the length of the overbank is related to a point in the main-channel the same proportional distance from the outlet, then just as with the original derivation of Muskingum-Cunge:

$$Q_b = X(I - O) + O = XI + (1 - X)O$$

where X is the relative distance of section B from the outlet as compared to the total reach length. This relative proportion is the same in the overbank as it is for the main-channel. Using the same derivation as led to Eq. (3-25),

$$X = \frac{1}{2}\left(1 - \frac{L_{u,mc}}{\Delta x_{mc}}\right), \text{ if evaluated for the main channel,} \qquad (4\text{-}15)$$

$$\text{or } X = \frac{1}{2}\left(1 - \frac{L_{u,ob}}{\Delta x_{ob}}\right), \text{ if evaluated for the overbank} \qquad (4\text{-}16)$$

4.3 Representative Reaches - Separate Lengths Method

In theory, one could apply Muskingum-Cunge to meandering channels directly using the equations in sections 4.2. The representative sections would need to be defined, including the location of the bank stations separating the main-channel from the overbanks. Separate values for channel length and overbank length would be specified.

This method of specifying the geometry of a reach will be referred to as the *"separate lengths method."* Unfortunately, most computer programs for conducting hydrologic flood routing, including HEC-1 and HEC-HMS, do not allow for the specification of separate lengths in the main channel and overbank. Other methods of specifying representative reaches that utilize non-meandering equivalent cross-sections must be found.

4.4 Representative Reaches - Modified Overbank Method

Two new methods are presented for specifying an equivalent, non-meandering channel that is capable of acting as a representative reach. The first is termed the *"modified overbank method."*

For the modified overbank method, the main-channel length is selected as the representative length and applied to both main channel and overbank in the modified section; i.e,. L_{mce} and L_{obe} are each set equal to L_{mc}.

The shape and roughness of the overbank will be modified to maintain equivalence at every flow depth between all the necessary variables, thus ensuring the final results of flood routing are equivalent to those prepared from the original, *"separate lengths method"* cross-section. Those variables are: surface area (*SA*), volume (*VOL*), rate of change in volume (*K*), and discharge (*Q*).

The values of the various parameters in the original cross-section are subscripted "*mc*" and "*ob*" for main-channel and overbank, respectively, and "*mce*" and "*obe*" for the main channel and overbank in the effective cross-section.

To simplify the calculations the ratio between the channel length and the overbank length is defined as sinuosity, *SN*:

$$SN = L_{mc} / L_{ob}$$

The surface area in the modified section is then:

$$SA = SA_{mce} + SA_{obe} = SA_{mc} + SA_{ob}$$

$$(T_{mce} + T_{obe})L_{mc} = T_{mc}L_{mc} + T_{ob}L_{ob}$$

$$(T_{mce} + T_{obe}) = T_{mc} + \left(T_{ob} \middle/ SN\right) \qquad (4\text{-}17)$$

which is satisfied if:

$$T_{mce} = T_{mc} \text{ (i.e. no change) and } T_{obe} = \left(T_{ob} \middle/ SN\right)$$

For the volume of storage in the modified sections:

$$VOL = VOL_{mce} + VOL_{obe} = VOL_{mc} + VOL_{ob}$$

$$(A_{mce} + A_{obe})L_{mc} = A_{mc}L_{mc} + A_{ob}L_{ob}$$

$$\left(A_{mce} + A_{obe}\right) = A_{mc} + \left(A_{ob}/SN\right) \tag{4-18}$$

which likewise requires that

$$A_{mce} = A_{mc} \text{ (i.e. no change) and } A_{obe} = \left(A_{ob}/SN\right)$$

To create a section that satisfies Eq. (4-17), the width of the overbank in the equivalent section must be reduced from that in the original section by the proportion *SN* for every flow depth above bankfull. This would result in an overall contraction of the overbank, with every elevation point shifting towards the channel, as shown in Figure 4-2.

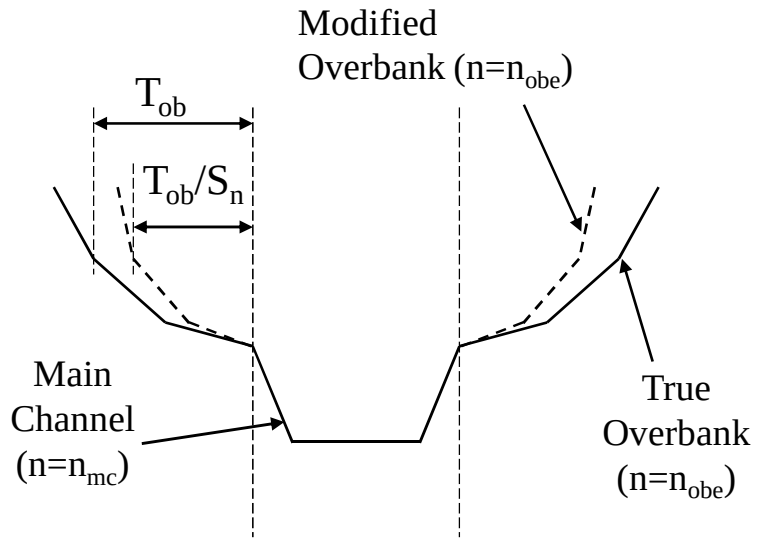

Figure 4-2. Cross-Section Adjustment for Equivalent Channel - Modified Overbanks Method

Since the area of the overbank can be expressed as an integration of depth and topwidth,

$$A = \int T dy$$

the modification of overbank widths to meet Eq. (4-17) would also produce an area-depth relationship that satisfies Eq. (4-18).

Moving on to the discharge relationship,

$$Q = Q_{mce} + Q_{obe} = Q_{mc} + Q_{ob}$$

$$\left(C_{mce} + C_{obe}\right)\sqrt{Z/L_{mc}} = C_{mc}\sqrt{Z/L_{mc}} + C_{ob}\sqrt{Z/L_{ob}}$$

where Z is the vertical drop in water-surface elevations across the reach, which is the same for both main-channel and overbanks. Further manipulation gives:

$$\left(C_{mce} + C_{obe}\right) = C_{mc} + \left(C_{ob}\sqrt{L_{mc}/L_{ob}}\right)$$

$$\left(C_{mce} + C_{obe}\right) = C_{mc} + \left(C_{ob}\sqrt{SN}\right) \qquad (4\text{-}19)$$

which requires

$C_{mce} = C_{mc}$ (again, no change) and $C_{obe} = C_{ob}\sqrt{SN}$

Since the geometry of the overbank is completely specified by Eqs. (4-17) and (4-18), the only remaining way of satisfying Eq. (4-19) is by adjustment of the Manning's roughness factor in the overbank.

$$C_{obe} = C_{ob}\sqrt{SN}$$

$$\frac{1.486}{n_{obe}} A_{obe}\left(\frac{A_{obe}}{P_{w,obe}}\right)^{2/3} = \frac{1.486}{n_{ob}} A_{ob}\left(\frac{A_{ob}}{P_{w,ob}}\right)^{2/3}\sqrt{SN} \qquad (4\text{-}20)$$

where P_w is the wetted perimeter.

Generally, the depth of flow in the overbank will be very small in relationship to the width of flow and the wetted perimeter can be taken as approximately equal to the top width, so that $P_{ob}/P_{obe} \approx T_{ob}/T_{obe}$; which by Eq. (4-17) yields $T_{ob}/T_{obe} = SN$. Also, by Eq. (4-19), $A_{ob}/A_{obe} = SN$. After rearrangement and simplification,

$$n_{obe} = \frac{n_{ob}}{(SN)^{3/2}} \qquad (4\text{-}21)$$

In summary, an equivalent section can be defined such that the length is equal to the main-channel length, the main-channel cross-section is unchanged, and the overbank shape and roughness is modified in accordance with Eqs. (4-17) and (4-21). This modified cross-section will provide reasonable agreement between the original section and the modified reach for the values of surface area, storage, and discharge for any given flow depth This section will not, however, provide an appropriate estimate of the velocity or velocity head in the overbank.

4.5 Representative Reaches - Effective Length Method

In some instances, it may not be possible to modify the shape of the representative cross-section and the modeler would prefer instead to achieve the continuity requirement by using the original cross-section and specifying an *"effective length," L_e,* instead.

Since the shape of the cross-section is not altered, the top widths will be same in both the original and equivalent section; i.e., $T_{mc} = T_{mce}$ and $T_{ob} = T_{obe}$ at all depths. The relationship for surface area becomes:

$$SA = SA_{mce} + SA_{obe} = SA_{mc} + SA_{ob}$$

$$(T_{mce} + T_{obe})L_e = T_{mc}L_{mc} + T_{ob}L_{ob}$$

$$(T_{mc} + T_{ob})L_e = T_{mc}L_{mc} + T_{ob}L_{ob}$$

which therefore dictates the value of L_e as

$$L_e = \frac{T_{mc}L_{mc} + T_{ob}L_{ob}}{T_{mc} + T_{ob}}$$

$$L_e = \frac{L_{mc}\left(T_{mc} + {T_{ob}}/{SN}\right)}{T_{mc} + T_{ob}} \qquad (4\text{-}22)$$

The effective length is based on the weighted value of top width with length. Since top width varies with discharge, L_e is not a constant but varies with flow.

To use this method, a reference value of discharge for determining L_e must be selected. The method will not necessarily route flows correctly for other discharges. Also, the same overall drop in water surface, Z, across the reach is the same as for the original channel, which means that the effective slope used in the conveyance calculation of the effective section will not match the original slope. The continuity equation becomes

$$Q = Q_{mce} + Q_{obe} = Q_{mc} + Q_{ob}$$

$$(C_{mce} + C_{obe})\sqrt{{Z}/{L_e}} = C_{mc}\sqrt{{Z}/{L_{mc}}} + C_{ob}\sqrt{{Z}/{L_{ob}}}$$

$$\left(C_{mce}+C_{obe}\right)=C_{mc}\sqrt{L_e/L_{mc}}+C_{ob}\sqrt{L_e/L_{ob}} \tag{4-23}$$

Because length and cross-sectional shape are fully specified, the discharge relationship can be met only by modifying Manning's roughness coefficient in both the overbank and main channel. Pairing terms from each side of the equation,

$$C_{mce}=C_{mc}\sqrt{L_e/L_{mc}}$$

$$\frac{1.486}{n_{mce}}A_{mce}\left(\frac{A_{mce}}{P_{w,mce}}\right)^{2/3}=\frac{1.486}{n_{mc}}A_{mc}\left(\frac{A_{mc}}{P_{w,mc}}\right)^{2/3}\sqrt{L_e/L_{mc}}$$

$$n_{mce}=n_{mc}\sqrt{L_{mc}/L_e} \tag{4-24}$$

Likewise

$$C_{obe}=C_{ob}\sqrt{L_e/L_{ob}}$$

$$\frac{1.486}{n_{obe}}A_{mce}\left(\frac{A_{obe}}{P_{w,obe}}\right)^{2/3}=\frac{1.486}{n_{ob}}A_{ob}\left(\frac{A_{ob}}{P_{w,ob}}\right)^{2/3}\sqrt{L_e/L_{ob}}$$

$$n_{obe}=n_{ob}\sqrt{L_{ob}/L_e} \tag{4-25}$$

Manning's "n" is adjusted in both the main-channel and the overbank to preserve the equivalent relationship between discharge and flow depth.

Since the channel length will typically be larger than the overbank length, the above equations result in an increase in the roughness of the main channel and a decrease in the roughness of the overbanks. It can be visualized that an artificial roughness is needed to compensate for friction length that is lost in the effective

main-channel section, as well as for the increase in slope of the effective main-channel. Conversely, an artificial lowering of the roughness is needed to compensate for the excess friction length imposed on the effective overbank section and for the drop in effective slope.

The final relationships to consider are volume and the rate of change in volume with discharge. The volume in the original reach using the separate lengths method (subscripted "*sep*") is given by:

$$VOL_{sep} = VOL_{mc} + VOL_{ob}$$

$$VOL_{sep} = A_{mc}(L_{mc}) + A_{ob}(L_{ob})$$

Volume in the representative reach using the "effective lengths" method (subscripted "*eqv*") is given by:

$$VOL_{eqv} = (A_{mc} + A_{ob})L_e$$

The weighting based on top width and a weighting based on cross-sectional area would not generally yield equivalent results, so in general

$$VOL_{eqv} \neq VOL_{sep}$$

However, the absolute value of volume is not directly an input into the routing equations. It is only the rate of change in volume with discharge that dictates the value of *K*. Returning to Eq. (3-29):

$$\frac{dVOL}{dQ} = \left(\frac{dVOL}{dy}\right)\left(\frac{dy}{dQ}\right) = K \qquad (3\text{-}29)$$

If L_e can be taken as approximately constant for small changes in depth, then

$\frac{dVOL}{dy} = SA$, as given in Eq. (3-38), which has the same for both the effective length and separated length methods (for small changes in depth).

Likewise, $\frac{dQ}{dy}$ as given in Eq. (4-13) will be the same for both methods. For that reason, $\frac{dQ}{dVOL}$ can be considered similar for the two methods, despite the fact that absolute value of volume is not.

Since L_e is not truly constant over the entire range of flows, it would be expected that the plot of discharge versus volume between the original section and the representative one would yield slightly different curves and thus different values for K. This is a potential error which is inherent in the effective lengths method.

4.6 Effective Lengths and Conveyance for Steady-State HEC-RAS

Eq. (4-3), which describes the total flow rate through the meandering channel/overbank system, is a consequence of the basic assumption of parallel flow. It corresponds to the classic case of split flow through two parallel conduits, where the total flow is divided between the two channels in such a way as to ensure an equal drop in head over each path. When the channels are each of the same length, the flow will be split between each in proportion to their cross-sectional conveyance. When the two channels are of different lengths, the proportion of the flow carried by the shorter channel will be greater than its relative conveyance.

HEC-RAS users face this issue when developing steady-state models for cases where the main channel meanders within an overbank or for where an entire channel and valley bend towards a new direction. In these cases, there will be different lengths of flow in the main channel and each overbank. In steady-state HEC-RAS, this situation is handled by dividing the channel into three separate conduits: main channel, left overbank and right overbank, each with a different length specified. HEC-RAS assumes that these three separate channel components can be consolidated into a single cross-section having an effective length which is a weighted average of the individual lengths specified for each component.

Maintaining a volume balance is not necessary for steady-state models. For that reason, the continuity equation can be ignored and an effective length defined to satisfy only the energy loss equation. The effective length defined under these conditions will be denoted L_{e*}. The equations for this case use three channel segments: main channel, left overbank and right overbank, which are subscripted "*mc*", "*lob*" and "*rob*," respectively. The relationship is as follows:

$$Q = Q_{lob} + Q_{mc} + Q = C_{lob}\sqrt{H/L_{lob}} + C_{mc}\sqrt{H/L_{mc}} + C_{rob}\sqrt{H/L_{rob}}$$

$$= \left(C_{lob} + C_{mc} + C_{rob}\right)\sqrt{H/L_{e*}} \qquad (4\text{-}26)$$

$$L_{e*} = \left(\frac{C_{lob} + C_{mc} + C_{rob}}{C_{lob}/\sqrt{L_{lob}} + C_{mc}/\sqrt{L_{mc}} + C_{rob}/\sqrt{L_{rob}}} \right)^2 \qquad (4\text{-}27)$$

where H is the total drop in the elevation of the energy grade line, including changes in the steady-state velocity head. For steady-state HEC-RAS, both the energy grade line and the water surface are assumed to be level across a cross-section, separated by a conveyance-weighted value for velocity head.

Using these equations, the effective length could be calculated directly from channel and overbank conveyance and length data. In a steady-state calculation, the value of Q is known, and the value of H (energy head loss across the reach) is the unknown. The values of C_{lob}, C_{mc}, C_{lob}, and thus L_{e*} are functions of depth. The depth is known for the downstream section, and unknown at the upstream section. The program would use an iterative solution to find a value for upstream depth that provides the closest balance to all the variables.

The effective length L_{e*} is only used to calculate the overall drop in energy grade line elevation between adjacent sections. Once the upstream energy grade line is established, the discharges and velocities in each of the distinct channels segments would be calculated based on the actual slope of each segment, using the total drop in flow line divided by the actual length of the channel or overbank. This operation would have the effect of allocating flows to the different channel segments in proportion to the value of $C_i \Big/ \sqrt{L_i}$ for each.

In actuality, HEC-RAS does not use Eq. (4-27) to determine effective lengths for steady-state solutions. Instead, the program assumes that the appropriate length is a simple conveyance weighted average, which will be designated as (L_w) (USACE 2002b).

$$L_{w(hec-ras)} = \frac{L_{lob}C_{lob} + L_{lob}C_{mc} + L_{lob}C_{rob}}{C_{lob} + C_{mc} + C_{rob}} \quad (4\text{-}28)$$

Once the drop in energy grade line is calculated, HEC-RAS assigns the discharges to the main-channel and overbanks in direct proportion to their conveyance, instead of by proportion to $C_i / \sqrt{L_i}$ as suggested by Eq. (4-27)

These two approaches are obviously different. Available reference materials do not explain the original source of Eq. (4-28), nor does it appear to be justified by the physical assumptions of parallel flow.

If Eqs. (4-27) and (4-28) are simplified to consider only two channel segments, the difference between the two can be examined graphically. The segment having the longer flow path is subscripted "*long*" and the segment with the shorter path subscripted "*short*". Each equation can then be expressed in terms of three dimensionless parameters: (1) the ratio of the shorter flow path to the longer flow path $\left(L_{short}/L_{long}\right)$; (2) the ratio of the conveyance in the longer segment to the combined conveyance of both segments $\left(C_{long}/C_{total}\right)$; and (3) the ratio of effective length to the length of the longer segment, which will be termed the effective length ratio (ELR). The first ratio is a function of the geometry alone, while the second two ratios vary by flow rate. The ELR is equal to $\left(L_{e^*}/L_{long}\right)$ for the proposed corrected method and $\left(L_w/L_{long}\right)$ for original HEC-RAS method.

Figure 4-3 shows a plot of these relationships for both Eq. (4-27) and (4-28) for various values of $\left(L_{short}/L_{long}\right)$. For cases where the difference between lengths is

low, the difference between the methods is obviously low. Likewise, the methods converge if one or the other channel segments tends to carry nearly all the flow (i.e. conveyance ratio close to 0 or 1.0).

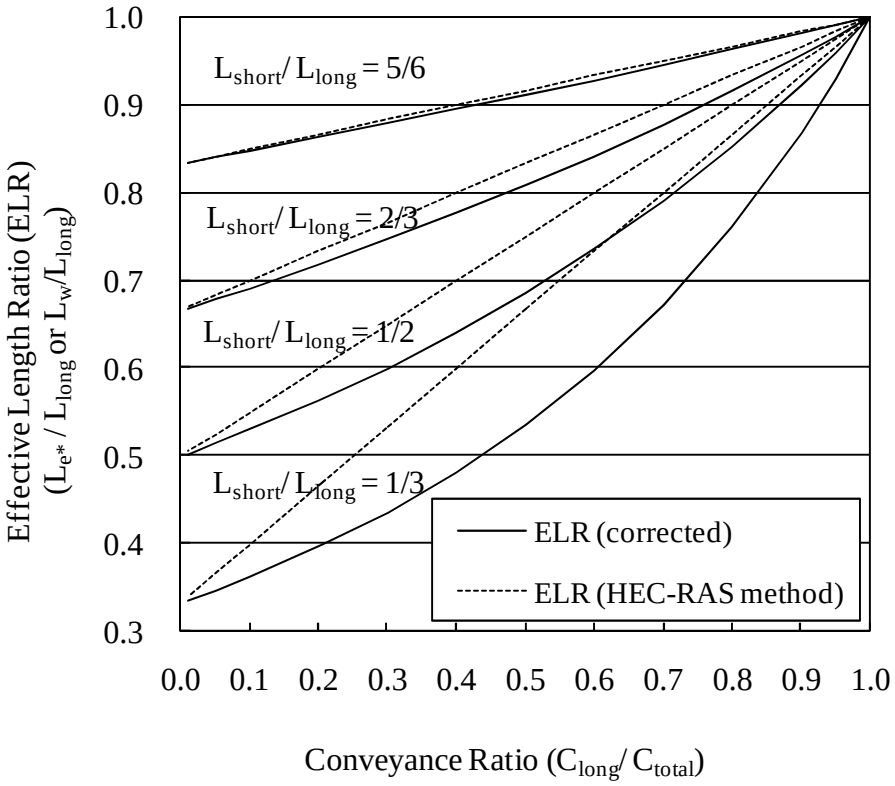

Figure 4-3. Discrepancy in Effective Lengths, Corrected Method vs. HEC-RAS Steady-State Method

When the difference in lengths is large and the flows are such that each channel segment carries a portion of the load, the differences in the methods are more pronounced. The HEC-RAS method over-estimates the effective length in all cases, which would lead to an under-estimation of the flow that can be conveyed for any given stage (or conversely, to an over-estimation of flow depths needed to convey a

given discharge). For example, if $\left(L_{short}/L_{long}\right)$ is (1/3) and the conveyance ratio $\left(C_{long}/C_{total}\right)$ is (0.5), the ratio of $\left(L_{e*}/L_{long}\right)$ is approximately (0.54), whereas the ratio of $\left(L_{e*(hec-ras)}/L_{long}\right)$is (0.67), a difference of approximately 25%. Since discharges vary in inverse proportion to the square root of length, this leads to an underestimation of the discharge rate at the given stage of approximately 10% $\left(\sqrt{1/1.25}=0.89\right)$.

From a theoretical point of view, Eq. (4-27) is superior, and it is recommended that USACE consider adding it to future versions of HEC-RAS.

There is also an alternative method available for making the appropriate adjustments within HEC-RAS. This second method involves setting all channel segments equal in length to the main-channel, and modifying the roughness in the overbanks to compensate. Beginning again with Eq. (4-26) and using the subscripts "*mce*," "*lobe*," and "*robe*" to indicate the values in a modified cross-section in which the overbank lengths have each been set to equal the main-channel length:

$$Q = C_{lob}\sqrt{H/L_{lob}} + C_{mc}\sqrt{H/L_{mc}} + C_{rob}\sqrt{H/L_{rob}} = \left(C_{lobe} + C_{mc} + C_{robe}\right)\sqrt{H/L_{mc}}$$

$$C_{lobe} + C_{mce} + C_{robe} = C_{lob}\sqrt{L_{mc}/L_{lob}} + C_{mc} + C_{rob}\sqrt{L_{mc}/L_{rob}}$$

which is accomplished if

$C_{mc} = C_{mc}$ (i.e. no change),

$C_{lobe} = C_{lob}\sqrt{L_{mc}/L_{lob}}$, and $C_{robe} = C_{rob}\sqrt{L_{mc}/L_{rob}}$

For steady-state solutions, the continuity equation can be ignored and no special constraints are placed on the area or volume of the sections. For that reason, all the adjustments can be made to the roughness coefficient alone. Changes are required only on the overbanks, since the main channel stays the same. For the left overbank:

$$\frac{1.486}{n_{lobe}} A_{lobe} \left(\frac{A_{lobe}}{P_{w,lobe}} \right)^{2/3} = \frac{1.486}{n_{lob}} A_{lob} \left(\frac{A_{lob}}{P_{w,lob}} \right)^{2/3} \sqrt{L_{mc} / L_{lob}}$$

$$n_{lobe} = n_{lob} \sqrt{L_{lob} / L_{mc}} \qquad (4\text{-}29)$$

By similar treatment, for the right overbank:

$$n_{robe} = n_{rob} \sqrt{L_{rob} / L_{mc}} \qquad (4\text{-}30)$$

Henderson (1966) suggested this technique in his discussion of flow between two adjacent sections on a curve, as follows:

> *"The easiest way of allowing for this effect is to vary the Manning n; thus if a berm has a smaller value of Δx than the main channel, we imagine its length to be increased to that of the main channel and the value of n reduced in proportion to $(\Delta x)^{1/2}$."*

As with the effective length method described in Section 4.5, this approach would only be used to determine the head loss between sections. Discharges and velocities would need to be apportioned to each channel segment on the basis of actual lengths and slopes.

Because Eqs. (4-29) and (4-30) rely on all lengths being the same, they do not run into errors due to HEC-RAS's use of Eq. (4-28). Modifications of this type may

be especially appropriate when modeling unusually sinuous reaches or areas with complicated and divergent overbank flow paths. Based on Figure 4-3, it appears that caution is warranted anytime a significant fraction of the conveyance is found in both channel and overbank sections and the ratio of flow lengths between overbank and channel segments is greater than 1.5.

The error in assigning flow between main-channel and overbanks may also be of concern. By assuming that flow is assigned to each segment in proportion to conveyance, HEC-RAS assigns less of the flow to the shorter segments (such as the inside of bends) than the parallel channel analogy suggests. As such, the corresponding average overbank velocity calculated for the inside bends would be too low, which may have consequences for sediment transport, scour, or channel protection calculations.

The error in the velocity calculation may also introduce some errors in the calculated head losses due to contractions or expansions, as the contraction and expansion loss terms are calculated based on changes in velocity head.

One should acknowledge that the underlying assumption of treating main-channel and overbank flows as parallel conduits is itself an approximation that ignores the complicated hydraulics of meandering flows. Main-channel flows above bankfull stage will be heavily influenced by the crossing and merging of overbank flows. Centripetal acceleration may cause the flow on the inside of river bends to be less than expected, despite the apparent decrease in flow distance. The entire flow condition is affected by the two- and three-dimensional nature of the flow path, all of

which are beyond the explicit capability of one-dimensional models to directly predict. On the other hand, Manning's n values based on empirical data likely include these effects.

4.7 Effective Lengths for Unsteady RAS (uRAS)

The uRAS unsteady flow calculation software also uses the concept of discrete, parallel channels in the development of its governing equations. To simplify the calculations and allow for the grouping of terms, it is necessary in uRAS to make an assumption about how the flow is divided between the channel and overbank. uRAS makes the assumption that flow is distributed to the channel and overbank in proportion to their conveyance, irrespective of whether the channel lengths are different. This assumption is inconsistent with the theory of parallel flows and would likely lead to errors when applied to channels of high sinuosity. In the following sections, the major concepts of the original uRAS derivation are presented, followed by a recommended correction that better conforms to the parallel channel analogy.

4.7.1 Original uRAS Derivation

The uRAS derivation was originally presented in the UNET User's Manual (Barkau, 1997) and has since been re-presented in a reorganized but identical fashion in the latest available HEC-RAS Hydraulic Reference Manual, Version 3.1 (USACE 2002b). Where parenthetical references are made to page numbers in the remainder of this section, the references are to the USACE (2002b) reference document only.

The uRAS derivation begins with a modified form of the St. Venant equations (ibid, p. 2-23, equation 2-44 and p. 2-28, equation 2-67):

Continuity:

$$\frac{\partial A}{\partial t} + \frac{\partial Q}{\partial x} + q_L = 0 \qquad (4\text{-}31)$$

Momentum:

$$\frac{\partial Q}{\partial t} + \frac{\partial (Qu)}{\partial x} + gA\left(\frac{\partial z}{\partial x} + S_f\right) = 0 \qquad (4\text{-}32)$$

where Q is discharge, A is cross-sectional area, q_L is the lateral inflow per unit length, u is the longitudinal velocity of flow, z is the elevation of the water surface, S_f is the friction slope given by Manning's equation, g is the acceleration due to gravity, x is distance measured along direction of flow, and t is time.

Under this form of the equation, the effects of bed slope (S_o) and flow depth (y) are combined together into a single expression $\frac{\partial z}{\partial x}$ for water-surface slope, which is a more convenient form when dealing with irregular cross-sections.

uRAS then conceptualizes the river as having two separate channels with a horizontal water surface across the entire cross-section (ibid, p. 2-29, figure 2-10) as reprinted in Figure 4-4. A finite-difference scheme is used to solve the continuity and momentum equations between any two cross-sections using a modified form of the St. Venant's equations developed separately for each individual channel.

There are apparent inaccuracies in the uRAS derivation as presented by Barkau. In this section, an attempt will be made to follow the major concepts and

style of the original derivation, but selected corrections will be made and discussed as they arise. Also, some nomenclature is adjusted to better conform to the conventions used in this study. For example, in the uRAS documentation, the main-channel and floodplain subscripted "*c*" and "*f*" respectively, while in this study the terms "*main channel*" and "*overbank*" are used and are subscripted "*mc*" and "*ob*". Terms without subscripts indicate that the values apply for the total system; however, the subscript "*total*" will be used in a limited fashion for clarity or emphasis.

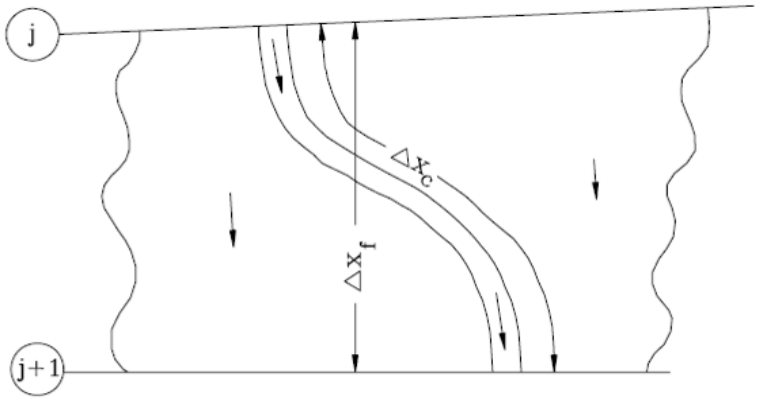

Figure 4-4. Channel and Floodplain Flows in uRAS
(reprinted from USACE 2002b)

For continuity, uRAS presents a set of equations for the main-channel and overbanks separately in implicit finite difference form (ibid, p. 2-33 and 2-34, equations 2-78, 2-79, 2-80 and 2-81), as follows:

Continuity for the Main-channel:

$$\frac{\Delta A_{mc}}{\Delta t} + \frac{\Delta Q_{mc}}{\Delta x_{mc}} = q_{mc} \tag{4-33}$$

Continuity for the Overbank:

$$\frac{\Delta A_{ob}}{\Delta t} + \frac{\Delta Q_{ob}}{\Delta x_{ob}} = q_{ob} \tag{4-34}$$

where Δx_{mc} and Δx_{ob} are the lengths between computational cross-sections for the main-channel and overbanks, respectively, and q_{mc} and q_{ob} are the average lateral exchanges of flow between the main-channel and the overbank, per unit length of each. In the uRAS manual, it appears that the appropriate subscripts for q_{mc} and q_{ob} are reversed (shown in the uRAS derivation as q_c and q_f). The algebra used to combine the equations, however, supports the form given here for Eq. (4-33) and (4-34). The uRAS derivation also contains terms for the storage from nonconveying portions of the cross-section and for lateral inflow from adjacent areas into the overbank. Those terms are not a part of the general derivation of the Muskingum-Cunge equation and are not subject to testing in this study. For that reason, they have been neglected here.

Eq. (4-33) and (4-34) are combined by recognizing that the net lateral exchange of flow between the main-channel and overbanks over a given segment is zero.

$$q_{mc}\Delta x_{mc} + q_{ob}\Delta x_{ob} = 0 \tag{4-35}$$

$$\Delta Q_{mc} + \Delta Q_{ob} + \frac{\Delta A_{mc}}{\Delta t}\Delta x_{mc} + \frac{\Delta A_{ob}}{\Delta t}\Delta x_{ob} = 0$$

$$\Delta Q_{total} + \frac{\Delta A_{mc}}{\Delta t}\Delta x_{mc} + \frac{\Delta A_{ob}}{\Delta t}\Delta x_{ob} = 0 \qquad (4\text{-}36)$$

This is the basic finite-difference form of the equation used by uRAS to express the continuity relationship. A separate expression for continuity is mentioned in the uRAS documentation (ibid, p. 2-30, equation 2-69). That particular form uses a problematic flow conveyance ratio (discussed later) and is less clear on the handling of the main-channel and overbank cross-sectional areas. It is unclear at this point to what degree that alternative form is used by uRAS in actual computations.

For momentum, Eq. (4-32) can be presented separately for the main-channel and overbank and converted to implicit finite-difference form (ibid, pp. 2-34 to 2-35, equations 2-84, 2-85, 2-86, and 2-87), as follows:

Momentum for the Main-channel:

$$\frac{\Delta Q_{mc}}{\Delta t} + \frac{\Delta\left(Q_{mc}u_{mc}\right)}{\Delta x_{mc}} + gA_{mc}\left(\frac{\Delta z}{\Delta x_{mc}} + S_{f,mc}\right) = M_{mc} \qquad (4\text{-}37)$$

Momentum for the Overbanks:

$$\frac{\Delta Q_{ob}}{\Delta t} + \frac{\Delta\left(Q_{ob}u_{ob}\right)}{\Delta x_{ob}} + gA_{ob}\left(\frac{\Delta z}{\Delta x_{ob}} + S_{f,ob}\right) = M_{ob} \qquad (4\text{-}38)$$

where A_{mc} and A_{ob} are the average cross-sectional areas of the main-channel and overbanks; Δz is the total drop in elevation of the water surface between computational cross-sections; $S_{f,mc}$ and $S_{f,ob}$ are the friction slopes for the main-channel and overbanks given by Manning's formula, and M_{mc} and M_{ob} are the

momentum fluxes between the main-channel and overbanks, per unit width of each. As with the continuity equation, there is an apparent error in the uRAS documentation regarding the subscripts of M_{mc} and M_{ob} (shown in uRAS as M_c and M_f). A corrected form consistent with the rest of the uRAS derivation is shown above.

The net exchange of momentum flux between the two channels is zero, which allows the two equations above to be combined (ibid, p. 2-35, equation 2-88),

$$M_{mc}\Delta x_{mc} + M_{ob}\Delta x_{ob} = 0 \tag{4-39}$$

$$\frac{\Delta Q_{mc}\Delta x_{mc}}{\Delta t} + \frac{\Delta Q_{ob}\Delta x_{ob}}{\Delta t} + \Delta\left(Q_{mc}u_{mc}\right) + \Delta\left(Q_{ob}u_{ob}\right) + gA_{mc}\left(\Delta z + S_{f,mc}\Delta x_{mc}\right) + gA_{ob}\left(\Delta z + S_{f,ob}\Delta x_{ob}\right) = 0 \tag{4-40}$$

$$\frac{\Delta Q_{mc}\Delta x_{mc} + \Delta Q_{ob}\Delta x_{ob}}{\Delta t} + \Delta\left(Q_{mc}u_{mc}\right) + \Delta\left(Q_{ob}u_{ob}\right) + g\Delta z\left(A_{mc} + A_{ob}\right) + \left(gA_{mc}S_{f,mc}\Delta x_{mc}\right) + \left(g\Delta A_{ob}S_{f,ob}\Delta x_{ob}\right) = 0 \tag{4-41}$$

In the original uRAS derivation, the first term of Eq. (4-41) is written instead as $\frac{\Delta\left(Q_{mc}\Delta x_{mc} + Q_{ob}\Delta x_{ob}\right)}{\Delta t}$. Both forms are numerically equivalent since Δx_{mc} and Δx_{ob} are each constants. It is a subtle transformation, however, that can be misleading. In the formulation of the matrix coefficients to solve uRAS, the actual calculation appears to be handled in a manner closer to that shown in Eq. (4-41), and so that form will continue to be used.

In order to further combine the second and third terms in Eq. (4-41), uRAS defines a velocity distribution factor, β, as follows (ibid, p. 2-35, equation 2-90 and 2-91):

$$\beta = \frac{Q_{mc}u_{mc} + Q_{ob}u_{ob}}{Q_{total}u_{total}} \tag{4-42}$$

which yields

$$\Delta\left(Q_{mc}u_{mc}\right) + \Delta\left(Q_{ob}u_{ob}\right) = \Delta\left(\beta\, Q_{total}u_{total}\right) \tag{4-43}$$

uRAS also defines a term Δx_e as the equivalent flow path (ibid, p. 2-35, equation 2-89), which is used to combine the friction terms (fifth and sixth terms) given in Eq. (4-41):

$$\left(gA_{mc}S_{f,mc}\Delta x_{mc}\right) + \left(gA_{ob}S_{f,ob}\Delta x_{ob}\right) = \left(gA_{total}S_f\Delta x_e\right)$$

$$\Delta x_e = \frac{\left(A_{mc}S_{f,mc}\Delta x_{mc}\right) + \left(A_{ob}S_{f,ob}\Delta x_{ob}\right)}{A_{total}S_f} \tag{4-44}$$

where S_f is an effective friction slope to be used in Manning's equation for the entire section. Before proceeding further, the meaning of each of the three friction slopes should be made clear (ibid, p. 2-26, equation 2-60):

$$S_f = \frac{Q_{total}^2}{C_{total}^2}, \qquad S_{f,mc} = \frac{Q_{mc}^2}{C_{mc}^2}, \quad \textit{and } S_{f,ob} = \frac{Q_{ob}^2}{C_{ob}^2} \tag{4-45}$$

Combining Eqs. (4-41), (4-42) and (4-44) and dividing all by the new term Δx_e gives the following relationship (ibid, p. 2-35 and 2-36, equations 2-92 and 2-93)

$$\frac{\Delta Q_{mc}\Delta x_{mc} + \Delta Q_{ob}\Delta x_{ob}}{\Delta t\Delta x_e} + \frac{\Delta\left(\beta Qu\right)}{\Delta x_e} + gA\left(\frac{\Delta z}{\Delta x_e} + S_f\right) = 0 \tag{4-46}$$

which is the finite-difference form of the momentum equation used by uRAS.

As of this point, however, the value of Δx_e is not yet defined. To solve for it, one must make some determination of the relative values of the friction slope terms (S_f, $S_{f,mc}$,and $S_{f,ob}$).

Barkau made the assumption that flow would be distributed in the main-channel and overbank sections in strict proportion to the conveyance widths of the two channels, so that

$$\frac{Q_{mc}}{Q_{total}} = \frac{C_{mc}}{C_{total}} = \Phi \text{, and} \qquad \frac{Q_{ob}}{Q_{total}} = \frac{C_{ob}}{C_{total}} = (1-\Phi) \tag{4-47}$$

where Φ is a flow distribution factor and represents the fraction of the total flow found in the main-channel (ibid, p. 2-29 and 2-30). One consequence of this assumption is that friction-slope terms used for each of the individual channels are the same as for the full channel:

$$\frac{Q_{mc}}{C_{mc}} = \frac{Q_{ob}}{C_{ob}} = \frac{Q_{total}}{C_{total}} \text{, so} \qquad S_{f,\,mc} = S_{f,\,ob} = S_f \tag{4-48}$$

which means that that equivalent flow path defined at Eq. (4-44) simplifies an area-weighted flow length (ibid, p. 2-43, equations 2-103 through 2-108) :

$$\Delta x_e = \frac{(A_{mc}\Delta x_{mc}) + (A_{ob}\Delta x_{ob})}{A_{total}} \tag{4-49}$$

4.7.2 Corrections to the uRAS Derivation

If the parallel-channel analogy is fully developed for uRAS, Barkau's assumption regarding flow distribution via Eq. (4-47) is incorrect and unneeded. In the parallel-channel analogy, the total drop in either energy head or water surface between computation nodes is assumed to be the same across all channels, but the friction slope varies based on the difference in flow lengths. Just as with the energy loss equation in HEC-RAS, the optimal definition for effective length in the uRAS momentum equation is given by a form of Eqs. (4-26) and (4-27)

$$Q = Q_{mc} + Q_{ob} = C_{mc}\sqrt{\Delta z / \Delta x_{mc}} + C_{ob}\sqrt{\Delta z / \Delta x_{ob}}\,, \tag{4-50}$$

but also, $Q = C_{total}\sqrt{\Delta z / \Delta x'_e}$, so

$$\Delta x'_e = \left(\frac{C_{mc} + C_{ob}}{C_{mc} / \sqrt{\Delta x_{mc}} + C_{ob} / \sqrt{\Delta x_{ob}}} \right)^2 \tag{4-51}$$

where $\Delta x'_e$ is a corrected form of the equivalent flow-length factor that could have been used in RAS. Unlike the steady-state HEC-RAS formula, the vertical drop Δz in Eq. (4-50) is referenced against the water-surface slope, not the energy grade line. That is because changes in velocity head due to local or convective acceleration are handled in uRAS by other terms in the momentum equation, whereas velocity head changes are included in the iterative calculations for the energy equation used by HEC-RAS in steady-state mode.

If this corrected flow length would have been used in uRAS, the relationship shown at Eq. (4-44) would have reduced to a simple identity, as follows:

$$\Delta x'_e = \frac{\left(A_{mc} S_{f,mc} \Delta x_{mc}\right) + \left(\Delta A_{ob} S_{f,ob} \Delta x_{ob}\right)}{\Delta A_{total} S_f}$$

$$\Delta x'_e = \frac{\left(A_{mc}\left(\frac{z}{\Delta x_{mc}} \right)\Delta x_{mc} \right) + \left(\Delta A_{ob}\left(\frac{z}{\Delta x_{ob}} \right)\Delta x_{ob} \right)}{\Delta A_{total}\left(\frac{z}{\Delta x'_e} \right)}$$

$$\Delta x'_e = \frac{(A_{mc} z) + (A_{ob} z)}{A_{total}\left(\frac{z}{\Delta x'_e}\right)}$$

$$\Delta x'_e = \Delta x'_e \frac{A_{mc} + A_{ob}}{A_{total}} = (\Delta x'_e)$$

If this correction is used, then Φ' could be used to represent the corrected flow distribution coefficient, as follows:

$$\Phi' = \frac{Q_{mc}}{Q_{total}} = \frac{C_{mc}}{C_{total}} \sqrt{\frac{\Delta x_e}{\Delta x_{mc}}},$$

$$\text{and } (1 - \Phi') = \frac{Q_{ob}}{Q_{total}} = \frac{C_{ob}}{C_{total}} \sqrt{\frac{\Delta x_e}{\Delta x_{ob}}} \qquad \text{(4-52)}$$

Because the derivation presented here is more consistent with the parallel-channel analogy than the derivation presented by Barkau, it is recommended that uRAS be re-configured to base its calculations of effective length as shown in Eq. (4-51) and flow distribution based on Eq. (4-52).

Chapter 5

Preparation of Natural Stream Data

5.1 Overview

Steady-state, multiple-profile HEC-RAS models were developed for four natural stream reaches in order to generate V versus Q and A versus Q relationships for each stream. Each stream reach was then used for testing. These HEC-RAS models also serve as a basis for unsteady HEC-RAS models developed in the next chapter.

The reaches are all located in Johnson County, Kansas. Data for each of the stream reaches was reduced to a format appropriate to the various models used in this study. The base data were obtained from a full HEC-RAS model developed as part of regional flood studies undertaken for Johnson County. From these base models, several forms of simplified data were developed, including direct tabular output of reach data and an 8-point typical section. The hydrology of each reach was also evaluated, using data from the regional flood studies. A simplified input hydrograph was developed for each reach, based on the peak flow and volumes of the estimated 100-year flood.

This chapter details the data evaluation and preparation process. Summary results for all four channels are presented. Detailed calculations for Reach No. 3 are provided to illustrate the methodology.

5.2 Selection of Stream Reaches and General Description

5.2.1 Data Sources and Reach Selection

The four natural channel reaches were represented using data from two watershed flood studies prepared for several cities and the county government within Johnson County, Kansas, a suburban area of the Kansas City metropolitan region. The streams chosen represented a range of conditions found in suburban and rural areas of Johnson County. The streams are small to moderate in size, with tributary drainage areas ranging from 1 to 48 square miles.

The first watershed study was prepared for the Tomahawk Creek basin (PEI 1997), which comprises a 23.4-square-mile drainage area in the east-center part of the County, including portions of the cities of Overland Park, Leawood and Olathe.

The second watershed study was performed for the Blue River basin, which has a drainage area of 86 square miles at the state line between Kansas and Missouri, of which 76 square miles lie within Johnson County. The Blue River basin lies to the south of the Tomahawk Creek Basin and includes the tributaries Negro Creek, Coffee Creek, Wolf Creek, and Camp Branch (CDM 2005). Figure 5-1 shows the general location of both watersheds in Johnson County. Figure 5-2 shows the location of the four stream reaches within those watersheds. Reach No. 1 is in the Tomahawk Creek watershed and the other reaches are in the Blue River watershed.

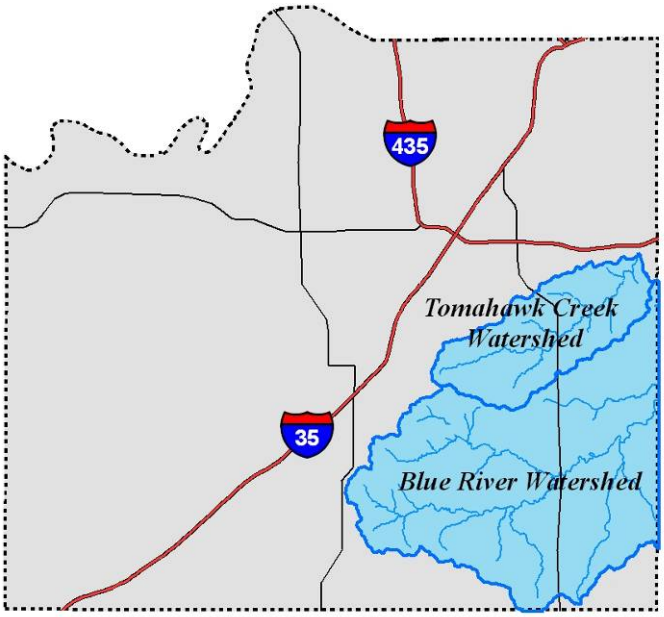

Figure 5-1. Watersheds Examined for Study, Johnson County, Kansas

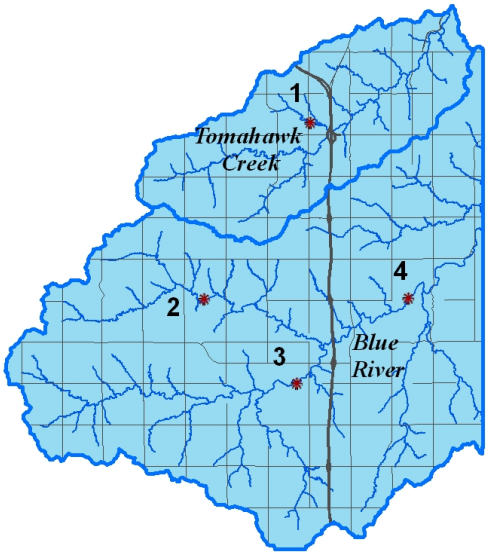

Figure 5-2. General Location of Stream Reaches Studied

Both watershed studies were prepared as part of a master program of floodplain remapping in Johnson County. The program was led by the Johnson County Stormwater Management Program (JCSMP), which provided copies of the study data.

Planimetric data for the Blue River watershed was obtained from the Johnson County Automated Information Mapping System (AIMS). Data included elevation points and aerial photography. Access to the data was provided courtesy of the JCSMP and AIMS. Aerial photography was available for various years between 1996 and 2006. Elevation models were developed from aerial flights conducted between 1998 and 2000 as part of the support work for the Blue River study and the other County-led watershed studies. The elevation data is referenced to the NAVD 1988 datum (Kent Lage, Johnson County Public Works, personal communication, July 10, 2008).

Except as noted in the discussion of the individual reaches, the original cross-sections from the Blue River study were used for this study, using methods similar to those discussed in this chapter. The AIMS planimetric data were used as a supplement. The Tomahawk Creek Flood Study was based on an earlier planimetric data set that was not easily recoverable for this study. The newer Johnson County AIMS data from 1998 to 2000 was used to recreate the elevation data in the Tomahawk Creek basin.

The four stream reaches were selected based on visual assessments of the work maps from the two watershed studies. Potential reaches were eliminated if they

appeared to have been channelized, straightened, leveed or armored in a significant way. Reach limits were also set to avoid having confluences with significant tributaries within the study reaches. From the pool of potential stream reaches remaining, the final four reaches were then selected to represent a range of contributing watershed area, slopes, and meander patterns.

The lengths of potential stream reaches to be tested were kept between 3,700 feet and 10,200 feet, or between 0.7 and 1.8 miles. This provided sufficient length to average out individual section parameters, while remaining short enough to retain uniform hydrologic conditions. Reach lengths that are too long risk incorporating channel segments with systematic changes from upstream to downstream, given that contributing drainage area and flow rates are increasing over the given length of channel. The average cross-section spacing varied between 400 to 1,000 feet, depending upon the stream reach.

Reaches were also selected to avoid large embankments associated with road crossings and to avoid any unique geometries that would tend to produce excessive backwater. While natural streams frequently contain these features, they are ignored in the Saint Venant equations and in the derivation of Muskingum-Cunge. Any small bridges, in-line weirs or other unique structures encountered in the reaches were removed from the HEC-RAS model.

A summary of the location information and watershed drainage area for the four natural channel reaches is given in Table 5-1. Table 5-2 provides an overview of the hydraulic characteristics of each. Estimates of sinuosity and bed slope for each reach were calculated using the methods described later in this chapter. Table 5-3 summarizes the land cover conditions of each reach as they currently exist and reports the Manning's n roughness values as used in the original watershed studies. As described later, a standardized roughness condition for main-channel and overbanks was established for the detailed testing conducted in this study.

Table 5-1. Stream Reaches Examined

Reach No.	Reach Name and General Location	Drainage Area at Upstream Boundary (sq. miles)	Water-shed Study
1	Trib. 12 of Tomahawk Creek, West of Antioch Road and South of 131st St.	1.02	Tomahawk Creek
2	Coffee Creek, East of Pflumm Road and South of 159th St.	8.31	Blue River
3	Wolf Creek, West of Antioch Road and South of 175th St.	24.5	Blue River
4	Blue River, between Metcalf Ave. and Mission Road, near 167th St.	47.9	Blue River

Table 5-2. Hydraulic Reference Data for Stream Reaches

Reach No.	Stationing of Reach Boundaries	Main-Channel Length (ft)	Sinu-osity	Main-Channel Slope
1	104+87 to 68+21 (in feet)	3,666	1.73	0.54%
2	13.664 to 12.428 (in miles)	6,523	1.52	0.17%
3	10.937 to 9.583 (in miles)	7,149	1.38	0.21%
4	6.870 to 4.938 (in miles)	10,199	1.36	0.084%

Table 5-3. Land Cover and Hydraulic Roughness of Stream Reaches

Reach No.	Typical Land Cover Conditions Along Main Channel and Riparian Area	Typical Manning's n used in Original Watershed Study	
		Main Channel	Overbanks
1	Wooded park in residential area.	0.045	0.06 to 0.08
2	Partially wooded, undeveloped.	0.035 to 0.040	0.035 and 0.090
3	Heavily wooded nature reserve.	0.030 to 0.035	" "
4	Partially wooded, mostly undeveloped.	0.030 to 0.035	" "

5.2.2 General Description of the Selected Reaches

This section contains a general description of each of the four selected stream reaches. Figures 5-3 through 5-6 present an aerial view of each stream reach area, based on Johnson County AIMS photography taken in 2006. These figures provide an overview of the physical conditions in each location and give reference to surrounding landmarks. The figures also display the stream centerline and cross-

section locations, which are used later in this study. More detailed topographic information for each of the four reaches follows later in this chapter.

5.2.2.1 Reach No. 1

This reach is located on a tributary of Tomahawk Creek within an urbanized portion of Overland Park, in the vicinity Antioch Road and 135th Street. The tributary was labeled Tributary 12 in the Tomahawk Creek Flood Study (PEI 1997). The specific reach to be examined begins immediately downstream of 131st Street and ends at a point approximately 410 feet west (upstream) of Antioch Road, as measured perpendicular to the road. Flow proceeds from west to east. The main channel has a length of 3,666 feet between the upstream and downstream bounding cross-sections of the study reach.

The stream primarily lies within Windham Creek Park, a public park owned by the City of Overland Park. The surrounding land uses are largely residential, with the 100-year floodplain extending into surrounding lawns.

5.2.2.2 Reach No. 2

This reach comprises a portion of Coffee Creek, one of the two tributaries that form the headwaters of the Blue River in Johnson County. It is located on various tracts of private property in an undeveloped area of Overland Park, between Pflumm Road and Quivira Road, south of 159th Street. Flow proceeds from west to east.

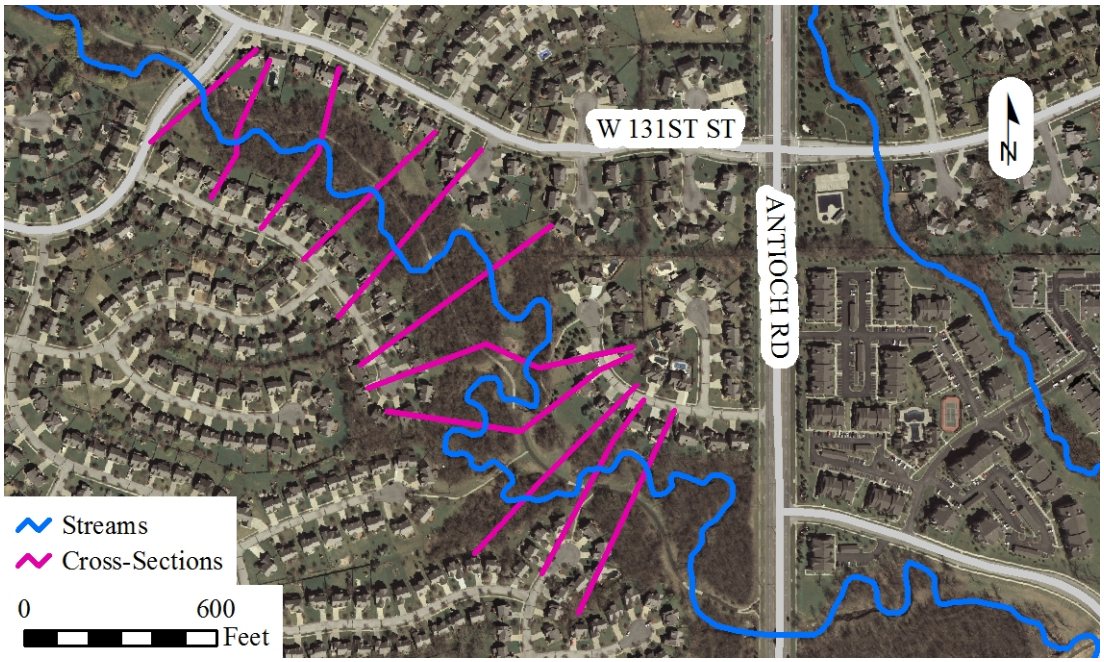

Figure 5-3. Aerial View of Reach No. 1

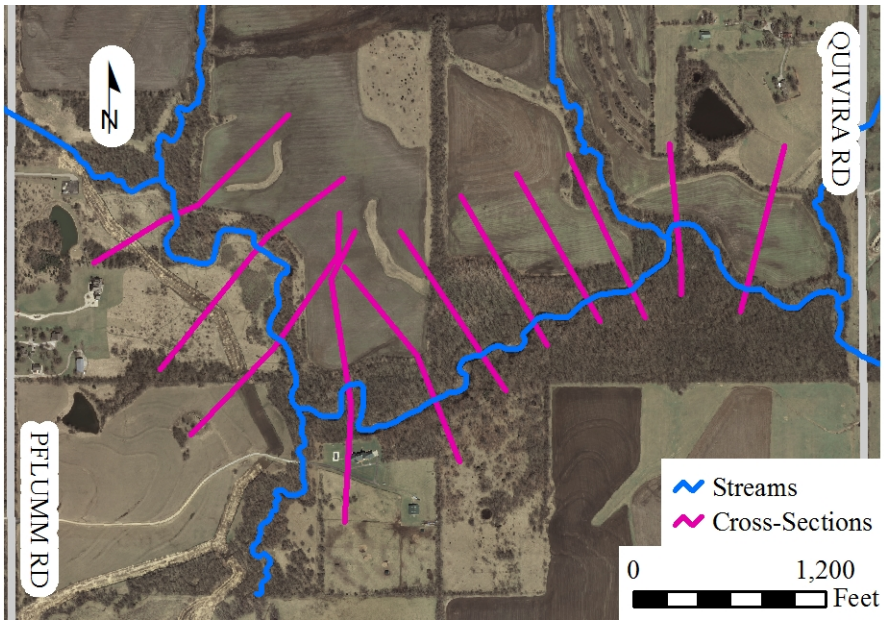

Figure 5-4. Aerial View of Reach No. 2

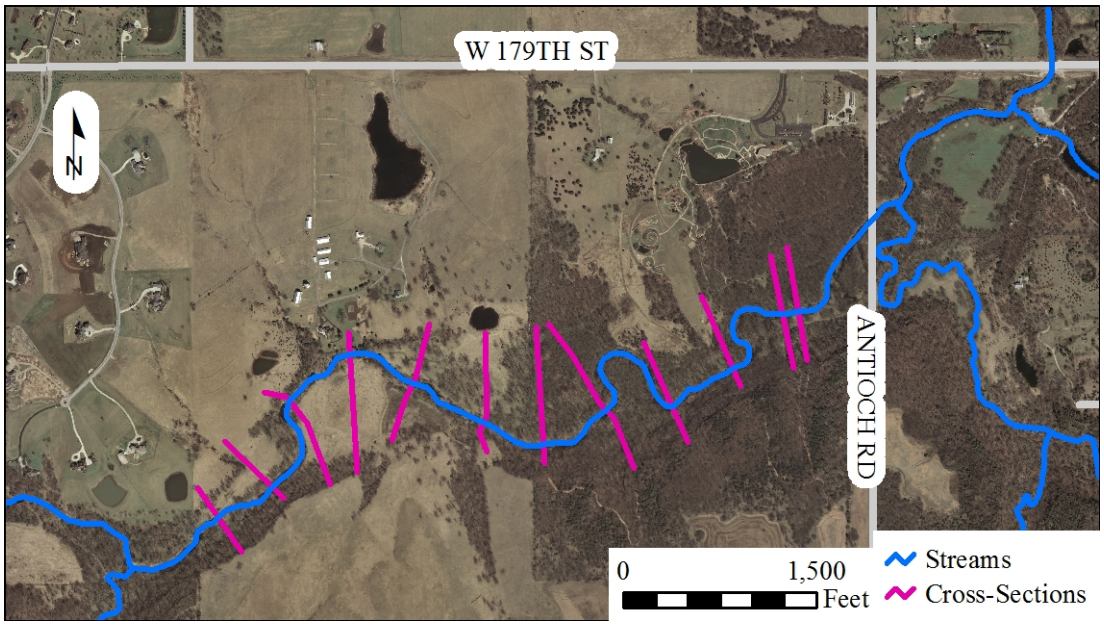

Figure 5-5. Aerial View of Reach No. 3

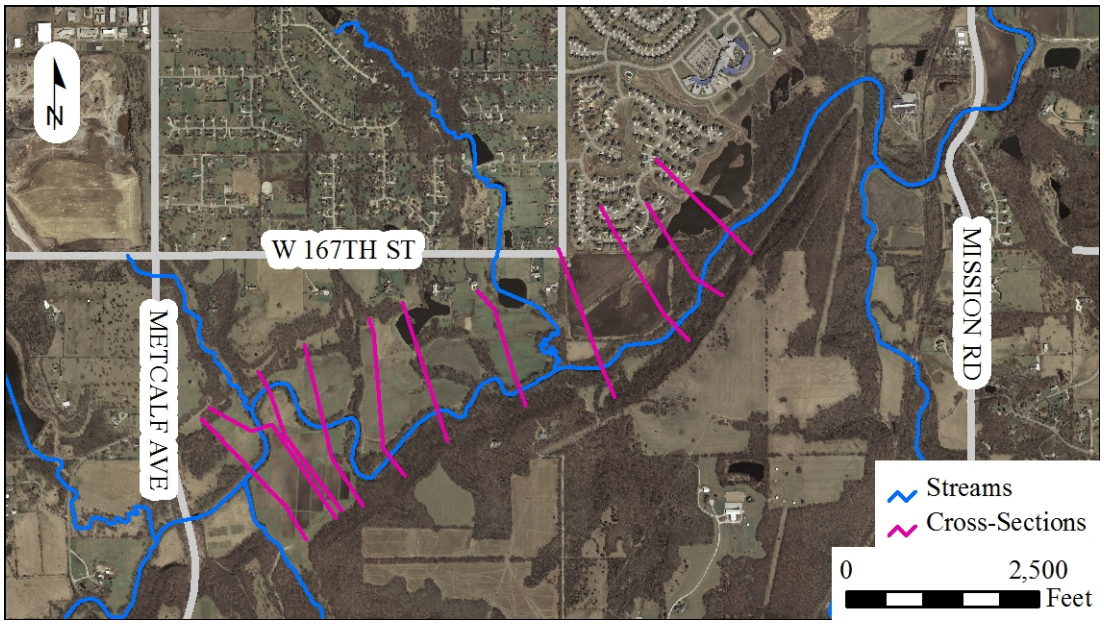

Figure 5-6. Aerial View of Reach No. 4

Land cover appears to be a mixture of wooded stream-side zones, pasture, and farm fields. Upstream of Pflumm Road lies Heritage Park, a large regional park owned by Johnson County. The detailed examination of Reach No. 2 begins at a point in the channel approximately 1,000 feet due east (downstream) of Pflumm Road and ends at a point approximately 730 feet due west of Quivira Road. The main-channel length between bounding cross-sections is 6,523 feet.

5.2.2.3 Reach No. 3

Reach No. 3 is a portion of Wolf Creek that flows through two large tracts of land owned and preserved by the City of Overland Park. Wolf Creek is a major stream that runs through southern Johnson County. Along with Coffee Creek, it forms the headwaters of the Blue River.

The lower portion of Reach No. 3 lies along a heavily forested area that is currently preserved as the Overland Park Arboretum. This portion of river appears to be largely untouched by agriculture or development. The upper portion of the river runs through a separate tract owned by Overland Park known as the Kemper Farm. This tract is also maintained by the City of Overland Park and is currently undeveloped. The Kemper Farm area shows more evidence of past agricultural activity, and the stream-side corridor is a mixture of woodland and cleared pasture or grassland. The downstream limit of this Reach No. 3 is located approximately 1,900 feet south of 179th Street and 580 feet west of Antioch Road. Between these

bounding sections, Reach No. 3 has a main-channel flow length of 7,149 feet. As with the other reaches in this study, flow is from west to east.

5.2.2.4 Reach No. 4

Reach No. 4 is a portion of main stem of the Blue River, downstream of the confluence of its headwaters, Coffee Creek and Wolf Creek. The specific reach analyzed in this study comprises a portion of the Blue River between Metcalf Avenue and Mission Road. The study reach begins at a point approximately 1,000 feet east (downstream) of Metcalf Avenue, which is also approximately 2,300 feet due south of 167th Street. The study reach ends approximately 3,100 feet west (upstream) of Mission Road. This location is also approximately 4,000 feet upstream (measured along the stream) of the confluence of Blue River with a major tributary, Camp Branch. The stream runs in a northeasterly direction. Reach No. 4 has a main-channel flow length of 10,199 feet.

The river in this area runs primarily through private property. Land uses vary from agricultural land, sod farming, and undisturbed forested areas. A portion of the left overbank in the downstream reach of this river had been developed, with a portion of the floodplain being converted into a wetland mitigation area. Since the time of the study, additional development has occurred along a portion of the left overbank in the downstream reaches, resulting in some fill placement at the outer edge of the floodplain fringe. This later development is not reflected in the modeling conducted for this study.

5.2.3 Standardization of Manning's Roughness Values

The original Blue River Watershed Study assigned roughness values to main-channels based on stream order and degree of meandering. The range specified was generally between 0.030 and 0.050, with engineering judgment applied to strongly meandering sections. For Reach No. 2, the main-channel Manning's n was generally assigned 0.035. For Reaches No. 3 and No. 4, the main-channel Manning's n varied between 0.030 and 0.035.

Roughness values in the overbank were assigned based on land cover. For Reaches No. 2 through No. 3, the values generally alternated between 0.090 assigned for trees and brush and 0.035 assigned for pasture and small grasses. Horizontal variations in values were established, so individual cross-sections contained multiple regions of both in each overbank (CDM 2005).

For Reach No. 1, which was studied as part of the Tomahawk Creek Flood Study, the original main-channel Manning's n was assigned as 0.045, with overbank roughness ranging between 0.06 and 0.08. These values were based on a consideration of stream size and sinuosity for the main-channel and land cover for the overbanks (Phelps 1998).

To simplify this study and allow for a more meaningful comparison of results between the reaches, a single reference condition was selected to apply to all four channels. Reach No. 3 is the least impacted by man-made activities and is generally in a forested state. Land cover conditions for Reach No. 3 were taken as the reference condition. Like the other three reaches, Reach No. 3 shows a moderate degree of

sinuosity. Using the HEC-RAS Hydraulic Reference (USACE 2002b) as a guide, the main-channel roughness for Reach No. 3 was set to 0.040, which corresponds to a main-channel on a natural stream that is "*clean, winding, some pools and shoals.*" The same main-channel roughness was also applied to Reaches No. 2 and No. 4. All three of these reaches are of sufficient size to maintain a baseflow in the center channel.

Reach No. 1 is an intermittent stream with more significant vegetation growth within the main-channel. A slightly larger main-channel roughness of 0.045 was selected for this location. This would fall within the range for main-channels similar to Reach No. 3, but with "*weeds and stones, lower stages, more ineffective slopes and sections*."

The overbank roughness for all four reaches was set to 0.100, which is consistent with HEC-RAS guidance for floodplain areas containing "*heavy stand of timber, few down trees, little undergrowth, flow below branches.*"

5.3 Hydrologic Inputs for Testing

Inflow hydrographs were developed to simulate flood events in each of the four stream reaches. The objective was to provide a baseline hydrograph to give a reasonable simulation of the inflow conditions during a 100-year flood in that reach. This would require that the peak of the hydrograph have a discharge equal to an estimated 100-year peak discharge (Q_{100}) and that the overall volume and shape of the hydrograph be reflective of realistic flood conditions. Synthetic hydrographs that

closely matched the watershed studies' hydrographs were developed using gamma distributions. These gamma-distribution hydrographs closely matched the peak discharge and the hydrograph width at the half-peak discharge. The hydrograph tails of the watershed study hydrographs were cut off as will be discussed and illustrated in Section 5.3.3.

5.3.1 Original Watershed Study Methods

Both the Tomahawk Creek Flood Study (PEI 1997) and the Blue River Watershed Study (CDM 2005) were developed as part of a floodplain remapping effort for Johnson County. Both studies had the following characteristics in common:

- HEC-1 was used as the hydrologic modeling platform.
- County-wide aerial photography, planimetric data, and elevation models were used to define watershed characteristics, including watershed boundaries, stream networks, impervious surfaces, and watershed slopes.
- Watersheds were divided into subareas of approximately 160 acres.
- NRCS soil types and data were used to classify pervious areas.
- Master-plan and land-use data from local governments were used to supplement land-use data for urbanized areas.
- The precipitation estimates were based on a synthetic design storm option in HEC-1, which defines a "balanced" or symmetrical design storm using the intensity-duration-frequency curves for Johnson County and a range of return periods, including 100-year.

- Net rainfall was transformed to runoff using the standard NRCS unit hydrograph for subareas.
- Lag times for individual subareas were calculated using watershed characteristics such as maximum flow length, watershed slope, and degree of imperviousness or improved channels.
- Hydrographs from individual subwatersheds were routed and combined based on the stream network and characteristics. Significant detention structures and ponds, if present, were analyzed as reservoirs.
- Modeled projections were calibrated using available data, including gage records from the US Geological Survey (where available) and the Overland Park and Johnson County ALERT flood warning system (www.stormwatch.com).

Key differences between the two studies include the following:

- The Tomahawk Creek study used the Green-Ampt formula to calculate losses from rainfall. Individual subbasins were divided into three sub-components, one each for the proportion of the area covered by silt loams, silty clay loams, and impervious surface. The Blue River study used the NRCS curve number (CN) method, based on the composite of the pervious and impervious surfaces.
- The Tomahawk Creek study used a 6-hour total duration for the design precipitation event; the Blue River study used a 24-hour storm duration.

- The Tomahawk Creek study defined the antecedent moisture conditions (AMC) for the Green-Ampt formula as “field capacity”, which is a moderately moist initial condition. The Blue River Watershed Study set the AMC condition for the NRCS CN method as a function of design storm length and return period. For the 100-year event, the AMC was set to 2.75.
- Lag times for subwatersheds were calculated using different methods. The Blue River study used a method in which the flow path is separated into four components: sheet flow, shallow concentrated flow, secondary channel flow, and primary channel flow. For each of these four elements, GIS procedures were used to define the longest flow path, average slope, and geometric shape. The Tomahawk Creek study used a generally similar methodology, but the flow components were based on more idealized flow path, with GIS procedures used to extract longest flow path and basin slopes.
- The Tomahawk Creek study used the variable-parameter Muskingum-Cunge method for channel routing, based on an idealized 8-point cross-section having a main-channel sized for the 1.5-year storm and a 10:1 constant side slope for overbank flows. The Manning’s roughness values were established by calibration and were approximately double the traditional text-book values. For tributaries, the values used were 0.120 for the main-channel at 0.200 for the overbanks. The Blue River study used the "modified Puls" method for channel routing as defined in the HEC-1 User's Manual (USACE 1998). Volume-discharge tables were developed from HEC-RAS data for the actual

reach, as part of an iterative process. The number of subreaches was defined using the recommendation in the HEC-1 User's Manual that the length of an individual reach be the distance that a kinematic wave speed would travel during one time-step of the model. This form of channel routing is similar to the Cascading Reservoirs method described in Chapter 3, except that the number of hypothetical reservoirs chosen was not based the characteristic length.

5.3.2 Synthetic Hydrograph by Gamma Distribution

This study required a simple, synthetic hydrograph to simulate inflows, one that could produce a single-peak, curvilinear shape, and positive skew (rising limb shorter and steeper than the falling limb).

The probability density function for the "*gamma distribution*" generates hydrographs with these attributes. The gamma distribution has been shown equivalent to a reorganized form of the "*Pearson Type III distribution*" (Bras 1990). Both terms are used interchangeably in the literature.

The standard NRCS curvilinear unit hydrograph was originally developed by graphical means, but it can be closely fitted to the gamma distribution. When used to define an inflow hydrograph, the NRCS (2007) form of the gamma distribution equation is:

$$\frac{I}{I_p} = \left(\frac{t}{t_p}\right)^m \exp\left[m\left(1-\frac{t}{t_p}\right)\right] \qquad (5\text{-}1)$$

where t is the time from the beginning of direct runoff to a specific ordinate on the hydrograph, I is the inflow discharge at that time, I_p is the peak (maximum) inflow given by the hydrograph, t_p is the time from the beginning of direct runoff to when the peak discharge occurs, also referred to as the "*time to peak*", and m is a skewness or shape factor. This form of the equation is dimensionless, with only one variable, m, being required to define the dimensionless shape.

Values of I_p and t_p are used to scale the hydrograph to fit the simulation. The traditional NRCS dimensionless unit hydrograph can be approximated by Eq. (5-1) with m set equal to 3.70. Tabular values of this gamma distribution hydrograph are given in Table 5-4.

Full dynamic solutions to St. Venant's equation require the specification of a baseflow or minimum stream discharge for computational stability. In Chapter 7, it is shown that the minimum baseflow value has an influence on model stability and accuracy. In each of three flood routing computer programs used in this study, baseflow values can easily be superimposed on previously calculated hydrographs. For these reasons, Eq. (5-1) was used to define all hydrographs in this study, with baseflow values superimposed afterwards. A single hydrograph shape with m =3.7 was used for all calculations.

Table 5-4. Tabular Values of Dimensionless Inflow Hydrograph, Gamma Distribution, m=3.7

t/t_p	I/I_p
0.0	0.000
0.2	0.050
0.4	0.310
0.6	0.664
0.8	0.918
1.0	1.000
1.2	0.937
1.4	0.791
1.6	0.618
1.8	0.456
2.0	0.321
2.2	0.218
2.4	0.144
3.0	0.036
4.0	0.003
5.0	0.000

5.3.3 Inflow Peak Discharges and Times to Peak

An input hydrograph was defined to simulate the 100-year storm in each reach. Hydrographs from the simulations in the Tomahawk Creek Flood Study (PEI 1997) and the Blue River Watershed Study (CDM 2005) were extracted for each reach. Table 5-5 provides a summary of the hydrologic parameters extracted from the studies for each reach. The hydrologic calculation node nearest the upstream cross-section was used to characterize the reach.

Table 5-5. Hydrologic Data from Watershed Studies

Reach No.	Data at Hydrologic Reference Point Nearest the Upstream Boundary of Reach				
	Drainage Area (sq. miles)	100-Yr. Discharge, Q_{100} (cfs)		Watershed Model	Hydrologic Model Reference Point ID
		per model	as rounded		
1	1.02	2,902	2,900	Tomahawk	C12D
2	8.31	11,002	11,000	Blue River	CCC035
3	24.5	23,502	24,000	Blue River	CWC112
4	47.9	35,409	36,000	Blue River	CBR015

Reach No. 2 was a special case. A major side tributary of Coffee Creek upstream of this reach is controlled by storage in a recreational lake in Heritage Park. The Blue River Watershed Study incorporated the storage effect of this lake in its model, which dramatically lowered peak flow conditions in this tributary and introduced delay in the release of a significant component of the flow volume into Reach No. 2. In order to better generalize the results of this study, the hydrology for Reach No. 2 was modified by eliminating the storage node and modeling the upstream conditions as uncontrolled. The peak discharge reported in Table 5-5 is based on this modified version of the Blue River Watershed study model.

An equivalent synthetic hydrograph using the gamma distribution was then developed to provide the same peak discharge and a reasonable fit of hydrograph shape and volume to those in the original watershed studies. For testing purposes, the actual values of the peak discharge were rounded to two significant digits. By error, the peak discharge for Reach No. 4 was rounded upwards to 36,000 cubic feet per second (cfs) instead of 35,000 cfs.

The time to peak was then adjusted to provide a reasonable match of the shape and volume of each hydrograph. A spreadsheet was constructed in which the completed hydrograph for the 100-year storm from the original watershed study could be plotted relative to a synthetic gamma-distribution hydrograph. The time base of the plot was adjusted so that *t=0* occurs at the beginning of direct runoff in the synthetic gamma-distribution hydrograph. Trial values of time to peak, t_p, were then used to find a hydrograph that matched the volume in the upper half of the original hydrograph.

The original watershed study hydrographs contained long leading and lagging extensions of lower flow that could not be simulated with a single gamma-distribution plot. This additional flow volume was not considered important for peak flow routing and was ignored.

All time-to-peak values were rounded to the nearest two-minute increment. Goodness of fit was determined by visual examination of the hydrograph, with particular emphasis on the overall fit of volume and shape in the range of flow above the 50% of the hydrograph peak. The relative location of the time to peak varied slightly between the synthetic hydrographs and the original study.

Table 5-6 presents a summary of the peak discharges and times to peak for input hydrographs to each reach. Figures 5-7 through 5-10 present the fitted hydrographs for all four reaches in this study.

The total volume of each synthetic hydrograph is also presented, in terms of net runoff relative to the basin size. The synthetic hydrographs in this study produce runoff discharges between 3.5 and 4.2 inches.

Table 5-6. Parameters for Synthetic Inflow Hydrographs to Simulate the 100-Year Flood

Reach No.	Peak Discharge, I_p (cfs)	Time to Peak, t_p (minutes)	Hydrograph Volume (acre-ft)	Contributing Watershed Size (sq. miles)	Net Runoff Represented by Hydrograph (inches)
1	2,900	36	192	1.02	3.53
2	11,000	88	1,780	8.31	4.02
3	24,000	124	5,460	24.5	4.18
4	36,000	160	10,600	47.9	4.15

5.4 Processing Software

Various computer programs were used to process the data for this study. Planimetric and spatial data were manipulated using ArcGIS™ , version 9.2. ArcGIS is a geographic information system (GIS) platform available from Environmental Systems Research Institute (ESRI). It consists of a suite of programs, including ArcMAP™ for displaying and manipulating data and ArcCatalog™ for managing files. A variety of data file formats can be managed within ArcGIS, including geodatabases and shapefiles (Ormsby et al. 2004).

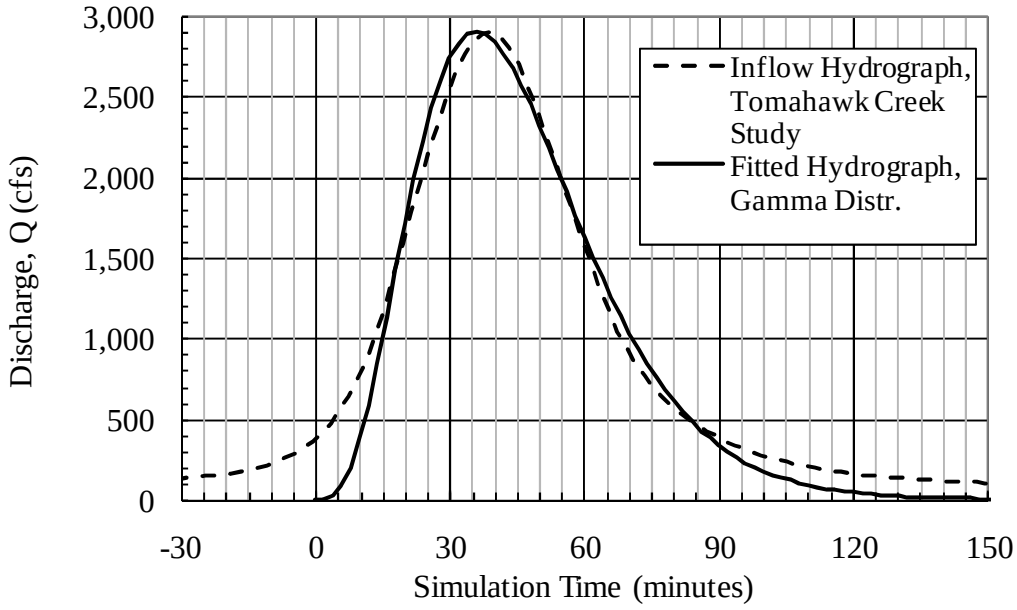

Figure 5-7. Fitting Simulated Hydrograph to Watershed Study, Reach No. 1

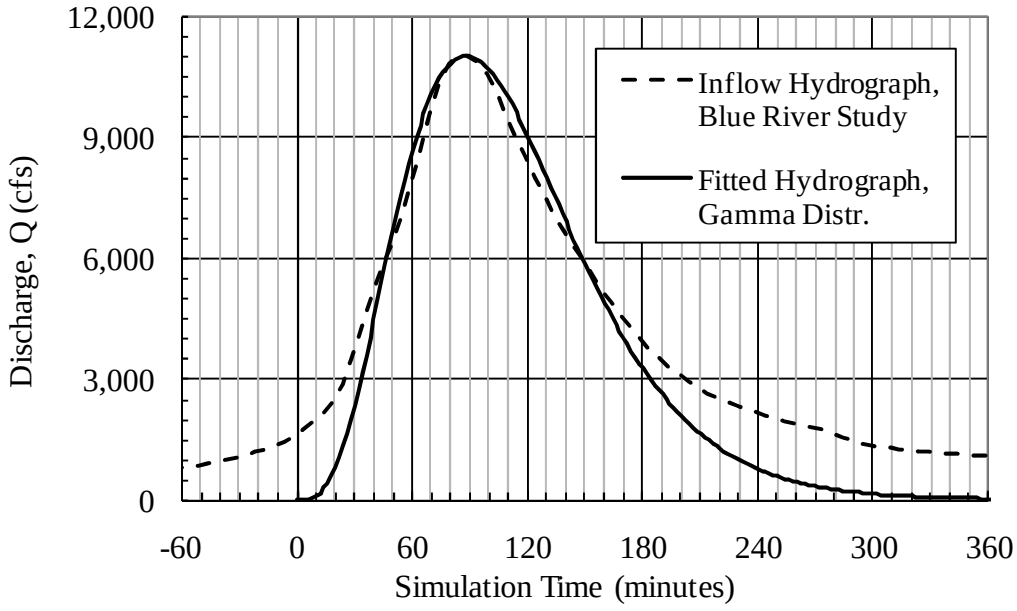

Figure 5-8. Fitting Simulated Hydrograph to Watershed Study, Reach No. 2

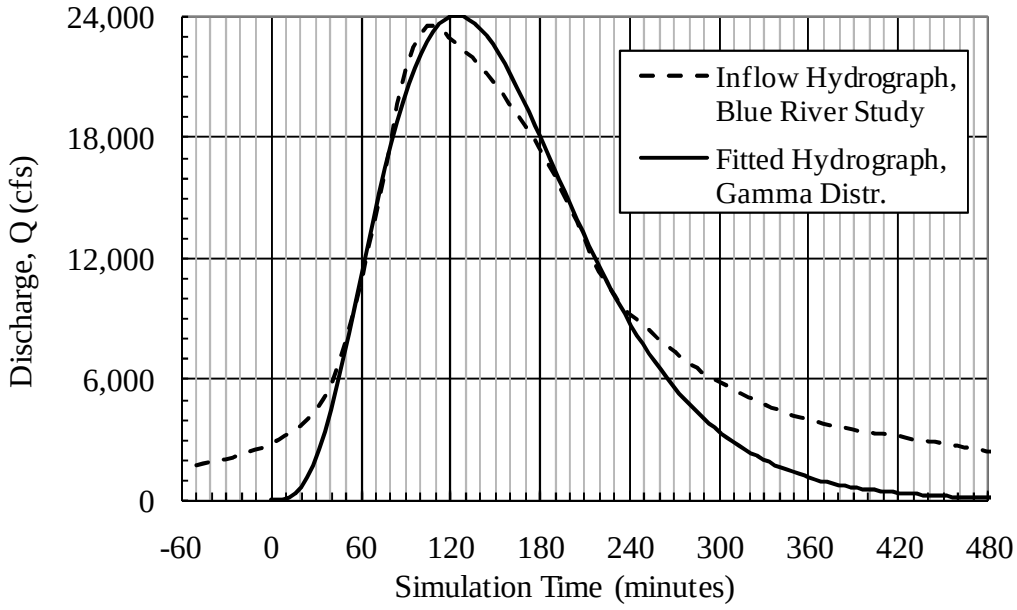

Figure 5-9. Fitting Simulated Hydrograph to Watershed Study, Reach No. 3

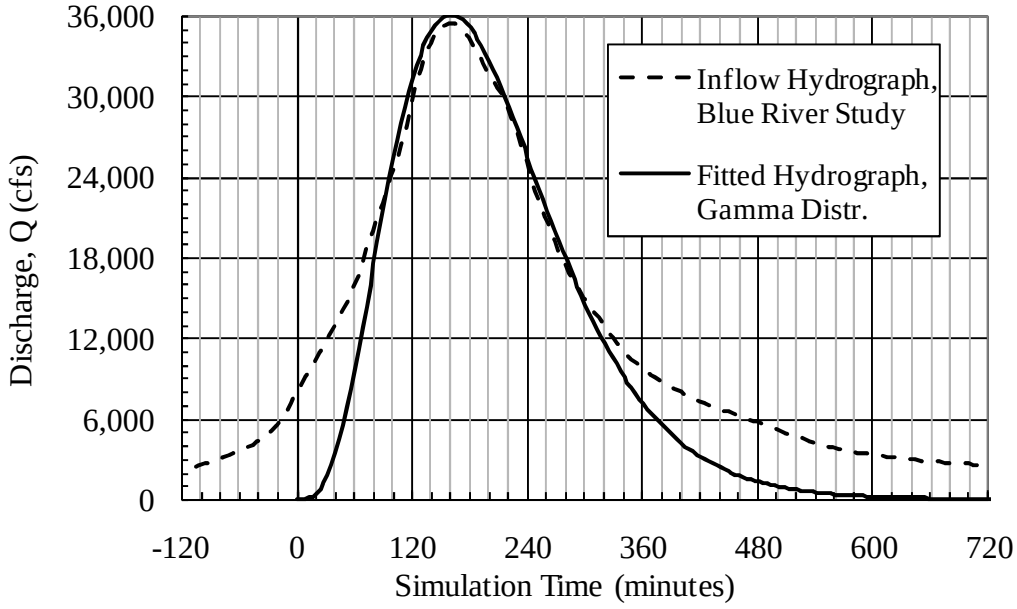

Figure 5-10. Fitting Simulated Hydrograph to Watershed Study, Reach No. 4

Sophisticated planimetric modeling requires the use of various extensions to ArcGIS. 3D Analyst™ provides specialized tools for three-dimensional terrain analysis, including creation of digital elevation models (Booth 2000). Spatial Analyst™ provides tools for analyzing raster data (Ormsby et al. 2004).

HEC Geo-RAS (version 4.0) is an extension jointly developed by ESRI and the Hydrologic Engineering Center of the U.S. Army Corps of Engineers. It provides customized tools for building HEC-RAS models from ArcGIS data and for converting HEC-RAS results back to ArcGIS formats (USACE 2005). Geo-RAS requires 3D Analyst and Spatial Analyst to run.

HEC-RAS models for the Blue River Watershed Study were originally developed using earlier versions of HEC-Geo RAS that used the ARC/INFO program as the GIS platform (CDM 2005).

HEC-RAS (version 3.1.3) is a hydraulic analysis program developed by the Hydrologic Engineering Center of the U.S. Army Corps of Engineers. It offers tools for both steady and unsteady analyses, as described previously. Several internal data management and graphing routines were also employed to process and review data (USACE 2002a and 2002b).

Finally, Microsoft® Office Excel® 2007 is a multi-purpose spreadsheet that was used extensively for data management and graphing.

5.4.1 Conventions for Describing Software Commands

Software procedures in this study are described in general terms when they are reasonably well-known to the hydraulic engineering community. Detailed

descriptions are given when procedures are less well-known. For Windows-based programs, menu options or commands are displayed in bold format. Specific sequences of menu choices, command buttons, or dialog box options are described in a narrative format or shown in sequential order, separated by the | (pipe) symbol. When this abbreviated format is used, the name of the program itself may be shown as the first step, if needed for clarity. Controlled phrases within a dialog box are shown in bold, whereas user-input text, such as a computer file name, are given in italics.

For example, the command to run a steady-state analysis in HEC-RAS could be described as **HEC-RAS | Run | Steady Flow Analysis | Compute**. Additional explanations of dialog box choices (such as "chose **Subcritical Flow Regime**" or "select *flow.f01* as the **Steady Flow File**") follow in narrative format.

In general, the names of computer software are shown in bold only if they are being used as part of a detailed explanation of commands.

5.5 Creation of the Base HEC-RAS Models

A base model of the geometry of each reach was created in HEC-RAS. The primary tools were **ArcGIS,** including the **3D Analyst** and **Spatial Analyst** extensions, the **HEC Geo-RAS (Geo-RAS)** extension, **HEC-RAS** calculations in steady-state mode, and **Microsoft Excel** spreadsheets. In general, the following process was followed:

- Create a digital elevation model (DEM) of the existing reach.

- Create the basic HEC-RAS geometry, including main-channel alignment and cross-section alignment and elevations. For Reaches No. 2, No. 3 and No. 4, the previously prepared geometry from the Blue River Watershed study was retained and modified.
- Set the initial alignment of the valley flow path and overbank flow lengths. Set initial left and right bank stations.
- Set the Manning's roughness values for the main-channel and overbank conditions.
- Calculate the bed slope.
- Define a family of reference discharges to use in steady-state flow to evaluate reach geometry.
- Produce the initial HEC-RAS run for steady-state conditions.
- Revise the valley flow alignment based on the center of overbank flow. Revise the left and right bank stations.
- Finalize the HEC-RAS geometry file, through iterative processing.

5.5.1 Detailed Procedures, Using Reach No. 3 as Example

The detailed procedures used to develop the base steady state HEC-RAS models are presented in this section. The processing of Reach No. 3 is given as an example because many of the basic processing steps are well represented. Additional details on site processing steps then follows in the discussions of Reaches Nos. 1, 2, and 4.

5.5.1.1 Generating the Digital Elevation Model

A digital elevation model of the region around each reach was developed using Johnson County AIMS data. The mass points and 3-dimensional breakline files were extracted from the Johnson County master set. A clip boundary was delineated by drawing a polygon in **ArcGIS** that encompassed the upper and lower limits of the reach and which extended laterally a sufficient distance to completely contain the floodplains. The boundary was also drawn to provide a visual context of the surrounding topography. Mass points were extracted by selecting those points within the polygon and exporting as a shapefile. Breaklines were extracted using **ArcToolbox | Analysis Tools | Extract | Clip.**

3D Analyst was then used to generate a triangular irregular network (TIN) of the region since a TIN is required by HEC GeoRAS. A second clip boundary polygon was drawn inside the original. The TIN was created using the **3D Analyst | Create/Modify TIN | Create TIN From Features** function, with the mass points, breaklines, and clip boundary as input. An image of the resulting TIN is shown in Figure 5-11. The figure also shows the stream centerline and cross-section locations.

The outer edges of the TIN for Reach No. 3 contained areas of erroneous zero elevation. These areas do not affect the remaining analysis and were ignored. To improve visualization of the TIN, the elevation ranges were reclassified into nine "quartiles" using the **Layer Properties | Symbology | Classify | Classification Method** option (accessed by right-clicking on the TIN layer in the display menu and selecting **Properties**). After reclassification, the TIN for Reach No. 3 illustrates

topography having an elevation range generally between 914 and 987 feet of elevation.

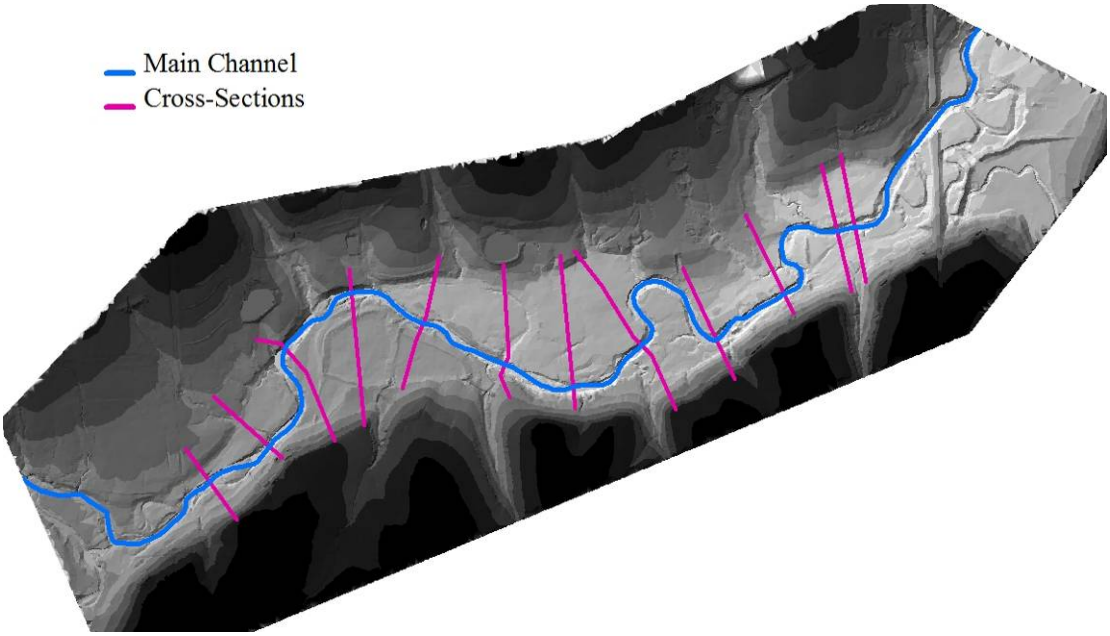

Figure 5-11. Digital Terrain Model, Reach No. 3

Contours at 10-foot and 2-foot intervals were then generated from the TIN using the **3D Analyst | Surface Analysis | Contour**. These contours were compared with contour data from the Johnson County AIMS master set. Contours generally matched, except for slight deviations and in the regions at the outer edges of the TIN with zero elevations.

5.5.1.2 Establishing the Stream Centerline and Cross-Section Alignments

A stream centerline was defined through the reach. For all four reaches, the centerline previously delineated in the Blue River Watershed Study or Tomahawk

Creek Flood Study was used. Each study's centerline data was available as an ArcGIS polyline shapefile. The polylines were extracted from the master data set and clipped so that they extended only short distances upstream and downstream of the reach boundaries and so that they remained within the boundaries of the TIN coverage. All tributary centerlines were removed from the data set. The location of the stream centerline was confirmed against the TIN.

Cross-sections were then delineated. In general, the cross-sections established in the original watershed study were used if appropriate. Cross-sections should be aligned perpendicular to the anticipated flow path and extend laterally a sufficient distance to fully contain the flood inundation limits. They should be spaced closely enough to accurately depict those changes in topography that may affect flow. In addition, HEC GeoRAS uses the end points of the cross-sections to define a bounding polygon that controls delineation of the floodplain between sections. Cross-sections must extend laterally a sufficient distance to ensure that the bounding polygon does not exclude intermediate areas, as can happen if cross-sections are not closely spaced through curves. Where main-channel or overbank flows curve, the cross-sections should be bent or "dog-legged" to remain perpendicular to flow across the entire range (USACE 2002). The cross-sections should be perpendicular to the contour lines in the overbanks.

Reach No. 3 is bounded by cross-section 10.937 on the upstream side and section 9.583 downstream. Stationing for Reach Nos. 2, 3 and 4 were all given in river miles, since these three reaches were part of the Blue River Watershed Study.

Reach No. 1 was stationed in feet. The original cross-section alignments for Reach No. 3 appeared adequate and were shown in Figure 5-11. These alignments were reviewed against the aerial photographs, the TIN, the contours, and the 100-year floodplains as previously delineated in the Blue River Watershed Study.

Geo-RAS requires that stream centerlines be drawn upstream-to-downstream and that cross-sections be drawn left-to-right, as observed looking downstream. The orientation of these data sets was verified by symbolizing the polylines with end arrows. All polylines were properly oriented.

5.5.1.3 Establishing the First Estimates of Valley Flow Path and Overbank Flow Lengths

HEC-RAS accommodates meandering channels by allowing separate flow path lengths to be established for the left overbank, the right overbank and the main-channel. It is customary in floodplain studies to delineate three separate pathways, with the left overbank flowpath remaining leftward of the stream centerline and the right overbank flow path always remaining rightward.

For natural meandering streams, this traditional method of flow delineation would tend to over-estimate the average travel path of the overbank flows, insofar as the overbank pathways are lengthened by the need to avoid crossing the main-channel. For this study, an alternate conceptualization of the flow was used, in which all the overbank flow is assumed to travel along a valley flow path which may cross above the stream centerline flow path. Although HEC-RAS does not analyze flow in this manner, the scenario will be simulated as closely as possible by setting the left

and right overbank flow paths equal to the valley flow path. The delineation of the valley flow path is discussed below.

The first estimate of the valley flow path was made by visually tracing a pathway through the center of the valley. Figure 5-12 presents the first estimate of valley flow path for Reach No. 3. The TIN and the 100-year floodplain limits from the original Blue River Watershed study models were used as backgrounds during the tracing to allow for better visualization and perspective of the proper flow path. Between the upstream and downstream bounding cross-sections, this initial valley path has a length of 5,039 feet.

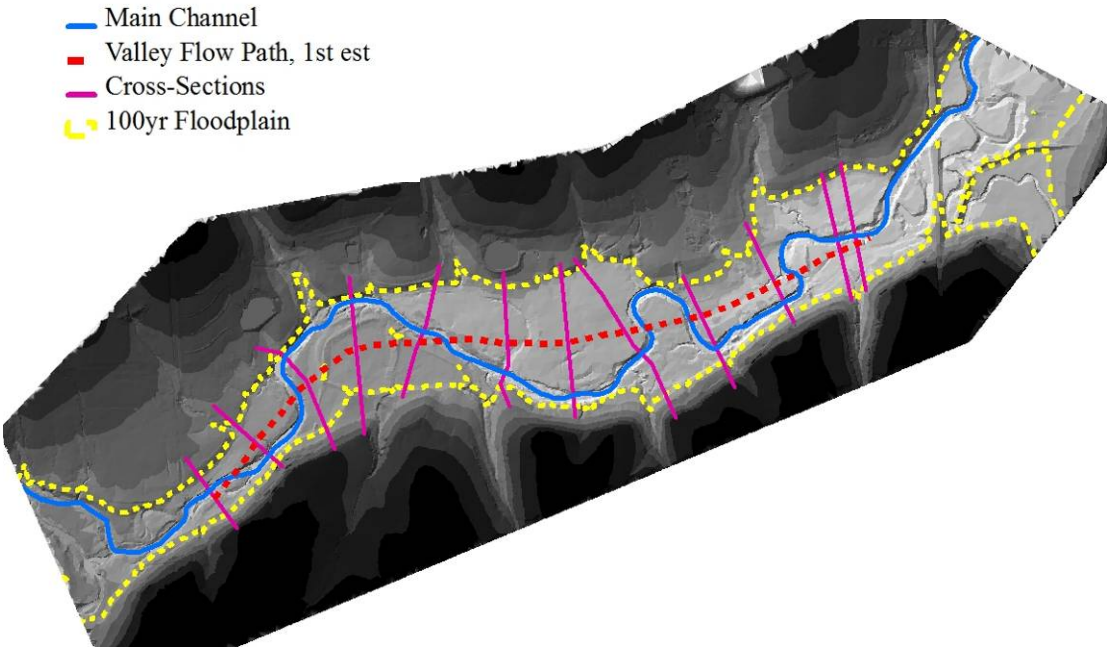

Figure 5-12. Initial Estimate of Valley Flow Path, Reach No. 3

This first estimate was inherently subjective. Perceptions of appropriate valley pathway vary in part on the depth of flow being considered. Once an initial HEC-RAS model is created, the estimates of area and depth of flow in the floodplains are used to revise the valley flow length estimates. The revision involves an iterative cycle of HEC-RAS modeling.

5.5.1.4 Deriving the Basic HEC-RAS Geometry File from GeoRAS

The basic HEC-RAS geometry file was then created for each reach, using the planimetric data derived thus far and the **RAS Geometry** tools in **GeoRAS**. A summary of the processing steps is presented below. Detailed software procedures are given in Chapters 4, 5 and 7 of the GeoRAS User's Manual (USACE 2005).

a) Open a new **ArcMap** project file *(*.mxd*) to store data for the work session.

b) Load a new data frame using the **GeoRAS | ApUtilities | Add Map** menu function.

c) Load the ground surface TIN. This action also sets the projected coordinate system for the data frame to match that of the TIN.

d) Use the **GeoRAS | RAS Geometry | Create RAS Layers | All** menu tool to create an ArcGIS geodatabase *(*.mdb)* file to house all the geometric data to be used by GeoRAS. Although a large number of feature class categories are generated, the only three needed for this study were the stream centerline (*River*), flow path centerlines (*Flowpaths*), and cross-section alignments (*XS CutLines*) features.

e) Open **ArcCatalog** and find the geodatabase *(*.mdb)* file. Use the **Load Data** command (right-click menu under each feature) to launch the **Simple Data Loader** dialog box. Load the stream centerline as the *River* feature. Load the stream a second time, this time as a *Flowpath* feature. Load the valley flow path (initial estimate) as an additional *Flowpath* feature. Load the cross-section alignments as the *XS CutLines* feature.

f) Reopen the **ArcMap** project *(*.mxd*) file again and confirm that the geometric elements have been loaded correctly. Assign the HydroID reference identifier to each element in the geodatabase with the **GeoRAS | ApUtilities | Assign UniqueID** menu option.

g) Use the **GeoRAS | River ID** menu tool to assign a river and reach name to the stream centerline.

h) Use the **GeoRAS | Assign LineType** menu tool to identify the stream centerline and valley flow paths. Define the stream centerline as a **Channel** linetype and the valley flow path as a **Left** linetype (the **Right** line type is not assigned). The GeoRAS tool assumes a traditional method of overbank delineation in which three alignments are defined. The Geo-RAS manual cautions that overbank alignments should not cross the main-channel, a condition which is clearly violated by the valley flow path. However, no problems were experienced in using the tool with the valley flow path crossing the main channel.

i) Open the **GeoRAS | RAS Geometry | Layer Setup** dialog box and designate

the TIN file and the layers for *Stream Centerline*, *XS Cut Lines*, and *Flow Path Centerlines*.

j) Use the **GeoRAS | RAS Geometry | Stream Centerline Attributes | Topology** and **Stream Centerline Attributes | Lengths/Stations** menu tools to assign remaining attribute data to the *River* feature.

k) Use the **GeoRAS | RAS Geometry | XS Cut Line Attributes | Reach/River Names** and **XS Cut Line Attributes | Stationing** menu tools to assign reach and river data to each section and to calculate the relative stationing of each section. Use the **XS Cut Lines | Downstream Reach Lengths** menu tool to calculate the stream centerline and valley flow path distances between sections. Bank stationing was not assigned using GeoRAS.

l) Use the **GeoRAS | RAS Geometry | XS Cut Line Attributes | Elevations** menu tools to extract the elevation data from the TIN and store it within a feature class called *XSCutLines3D*. View the cross-sections for initial data verification using the **GeoRAS | XS Plot** menu tool.

m) Use the **GeoRAS | RAS Geometry | Extract GIS Data** menu tool to export the data to an intermediate ASCII file that is read by HEC-GeoRAS. The export file carries the extension (**.RASExport.sdf)*.

n) Start **HEC-RAS** and create a new project. Open the Geometric Data editor and use the **HEC-RAS | Edit | Geometric Data | File | Import Geometry Data | GIS Format** menu tool to import the GeoRAS data *(*.RASExport.sdf)*. The **Import Options** dialog box regulates the process. Save the imported

geometry as a new HEC-RAS geometry file *(*.g01*). The import process provides the basic cross-section and reach data for HEC-RAS modeling. It also provides the coordinate data needed to show the stream centerline and cross-sections schematically in the **Geometric Data** plan view screen.

o) Complete the downstream flow length assignments. Use the **HEC-RAS | Edit | Geometric Data | Tables | Reach Lengths** dialog box to review the calculated downstream flow path lengths. The entries under the Channel and LOB (left overbank) columns match the stream centerline and valley flow path lengths. The ROB (right overbank) column is blank since these were not defined in GeoRAS. The LOB values are pasted into the ROB column.

The above procedure was performed for each of the four reaches analyzed in this study.

For Reaches No. 2 through No. 4, however, the results of this process were not directly used to create the baseline HEC-RAS model. Instead, the actual baseline model was extracted from the original Blue River Watershed Study data, with this latest processing being used for quality assurance review and to extract particular pieces of supplemental data. The master HEC-RAS models used in the Blue River Watershed Study were derived from similar GIS processes as described above. The next section describes the alternate procedure that was used to extract a geometric file from the previously developed Blue River Watershed Study. Use of this alternate procedure simplified the management of data models and preserved the connections in naming conventions and stationing that has been set forward in the original study.

Reach No. 1 was developed using the procedures in this section because the Tomahawk Creek Flood Study was developed from an earlier planimetric data source which was not easily recoverable and because it was developed without the benefit of GeoRAS tools.

5.5.1.5 Isolating an Equivalent Geometry File from the Original Watershed Study

For the three reaches derived from the Blue River Watershed Study, an alternate procedure was used to isolate and update the original study data. The original master geometry file was copied and all tributaries and unneeded river reaches were deleted using the **HEC-RAS | Edit | Geometric Data | Edit | Delete Reach** and **Delete Junction** tools. New dummy reaches and junctions were then inserted using the **HEC-RAS | Edit | Geometric Data | River Reach** button to break up the remaining reach into segments. Upstream and downstream segments were then deleted, along with the dummy reaches and junctions. Any remaining cross-sections upstream or downstream of the target reaches were deleted using the **HEC-RAS | Edit | Geometric Data | Cross Section Data | Options | Delete Cross Section** tool.

The original reach locations were selected to avoid bridges and embankments that create complications in the volume and backwater conditions. Any remaining small obstructions or special structures were removed from the model. Likewise, all levees and areas of blocked or ineffective flow were removed. Any necessary blocked-flow areas were then reassigned. No significant modifications were needed

for Reach No. 3.

Finally, the overbank flow lengths were updated using the distances for the valley flow path as described previously. The left overbank and right overbank values in the new geometry file were overwritten using the values calculated by GeoRAS for the initial valley flow path. The main-channel lengths were not changed, because the original stationing of the cross-sections was based on those values. The differences were negligible.

5.5.1.6 Evaluating Cross-Sections and Setting Bank Stations

The cross-sections in each reach were evaluated for appropriateness. To the extent possible, stations were used without significant adjustment. Blocked-flow areas were established if a cross-section had intercepted a major side tributary or contained other unusual features that would have overstated the area available for flow. No blocked-flow areas were required for Reach No. 3.

Left and right bank stations were also set for each section, using the **HEC-RAS | Edit | Geometric Data | Tools | Graphical Cross Section Edit** tool. Bank stations are used in HEC-RAS to separate conveyance calculations between the main-channel, left overbank, and right overbank regions. The bank stations also define the limits between the Manning's n roughness values established for each region. A series of factors were considered for each section, including:

a) Location of the most obvious slope breaks on each side of the main-channel;

b) Consistency of channel width between bank stations;

c) Consistency in flow depths below the bank stations, with elevations being set

on both sides of the channel to match the beginning of overbank flow on the lowest side.

No single factor governed the setting of bank stations. For Reaches No. 2 through 4, the bank stations assigned in the original Blue River Watershed Study were used as the initial estimate. For Reach No. 1, the location of the obvious slope break was used for the initial estimate. Bank stations were then adjusted as the model was further developed, using the steady-state profiles generated from modeling runs (described later) to better evaluate inconsistent areas.

An index of the cross-section locations and station identifiers for Reach No. 3 is shown in Figure 5-13.

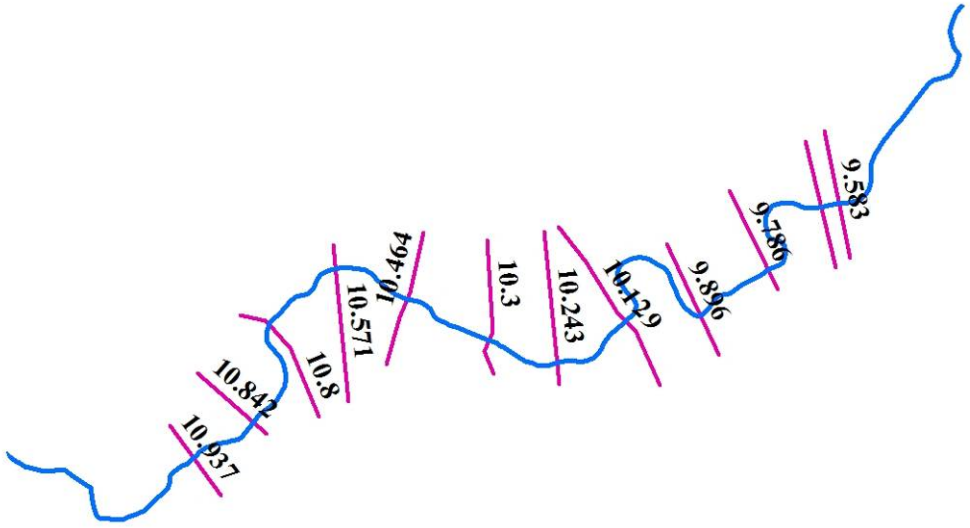

Figure 5-13. Cross-Section Index, Reach No. 3

A sample of six cross-sections from Reach No. 3 is given in Figure 5-14. The final bank station locations are shown as modeled. Also shown on these cross-sections are the water surfaces from two steady-state discharge profiles. The upper surface corresponds to the Q_{100} flow rate, and the lower surface corresponds to the profile for a steady-state discharge of 3,840 cfs, which is 16% of Q_{100}.

As discussed in more detail later, a series of steady-state discharge profiles were developed for each reach. For Reach No. 3, the discharge rate of 3,840 cfs appeared to represent the "*bankfull discharge*" ($Q_{bankfull}$) over a majority of the reach, with the depth of flow lying near the top of bank elevation on the lower bank, and with the inundation limits either being contained within the main channel or just beginning to spread out into the floodplain. Due to the natural variability of the cross-sections, no single discharge fits "bankfull" at all cross-sections. The ratio of Q_{100} that best approximation of $Q_{bankfull}$ will be evaluated separately for the other three reaches.

Figure 5-15 presents a profile view of the final left and right overbank elevations for Reach No. 3, as assigned. The $Q_{bankfull}$ discharge profile is also shown, illustrating the overall fit. Table 5-7 summarizes the main-channel width for each cross-section, based on the final assignment of bank stations. The average main-channel width between assigned bank stations was 85.8 feet. The average depth from the lowest assigned bank station was 9.0 feet.

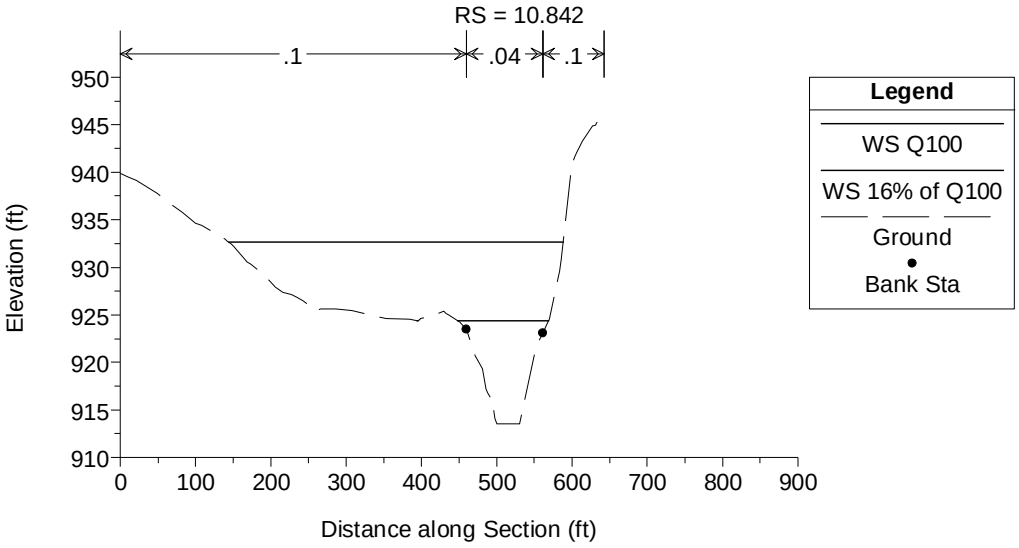

(a) Station 10.842 (miles)

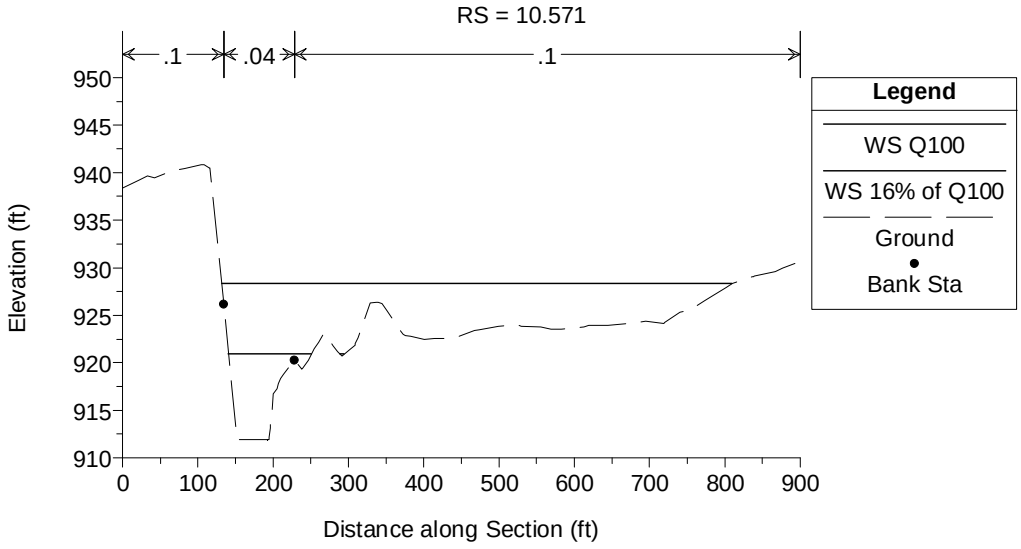

(b) Station 10.571 (miles)

Figure 5-14. Selected Cross-Sections, Reach No. 3

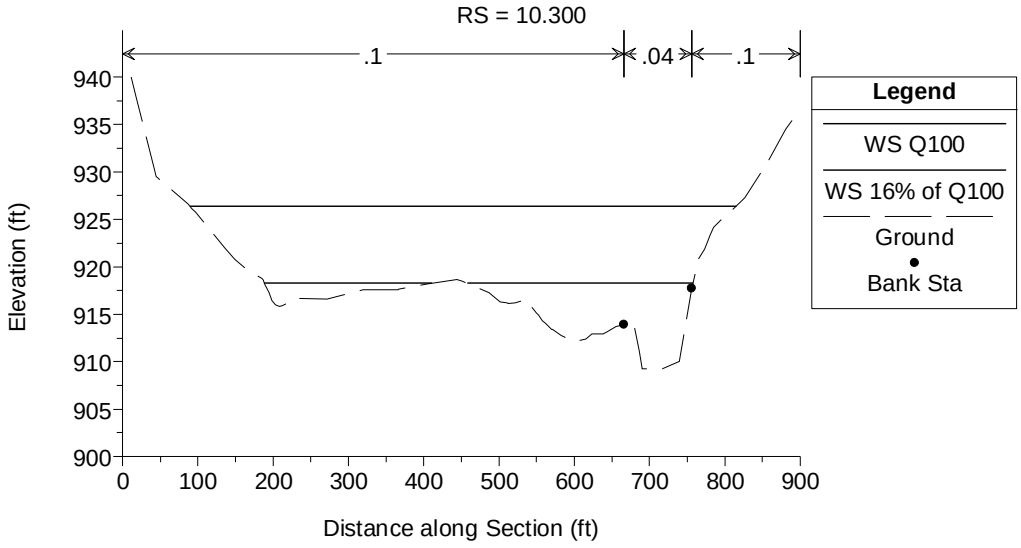

(c) Station 10.300 (miles)

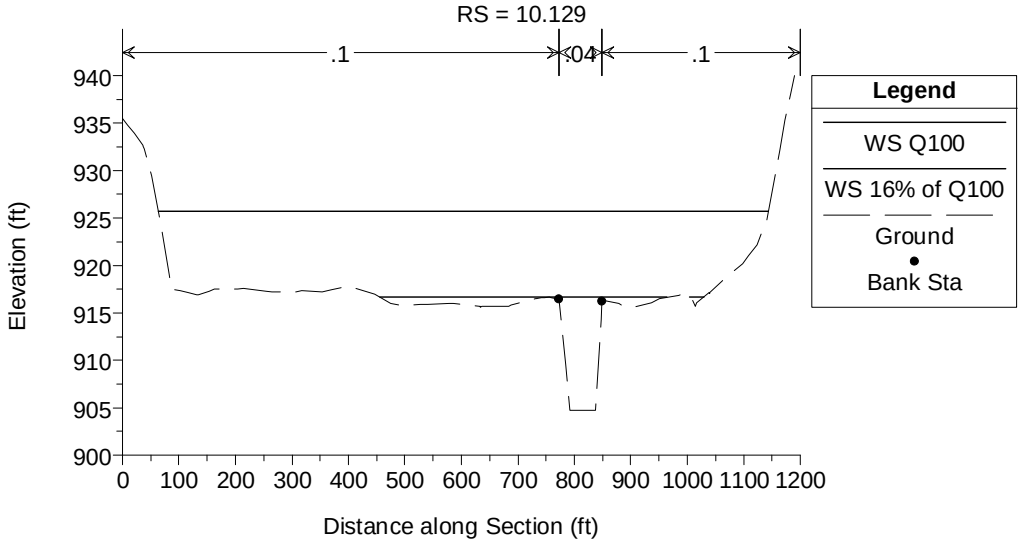

(d) Station 10.129 (miles)

Figure 5-14. Selected Cross-Sections, Reach No. 3 (cont.)

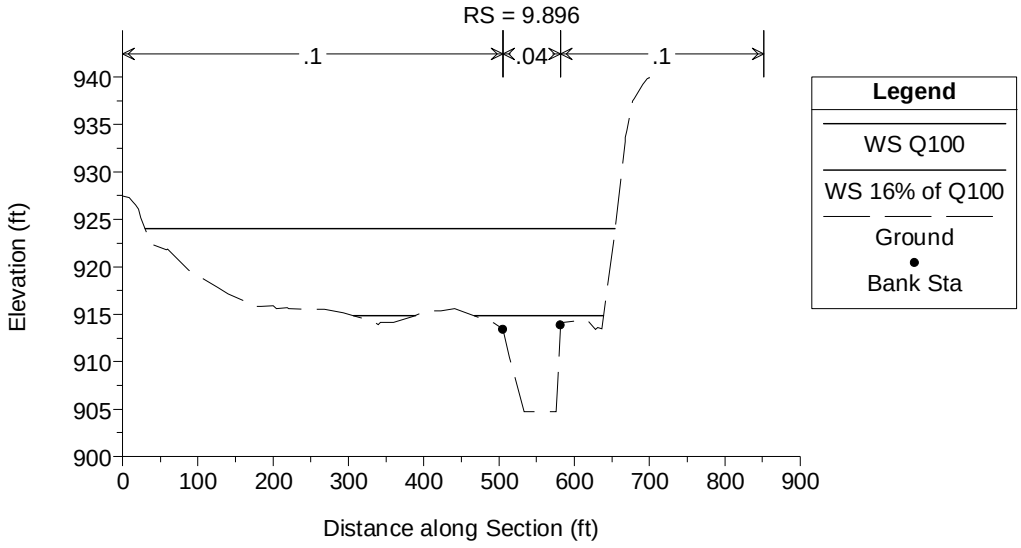

(e) Station 9.896 (miles)

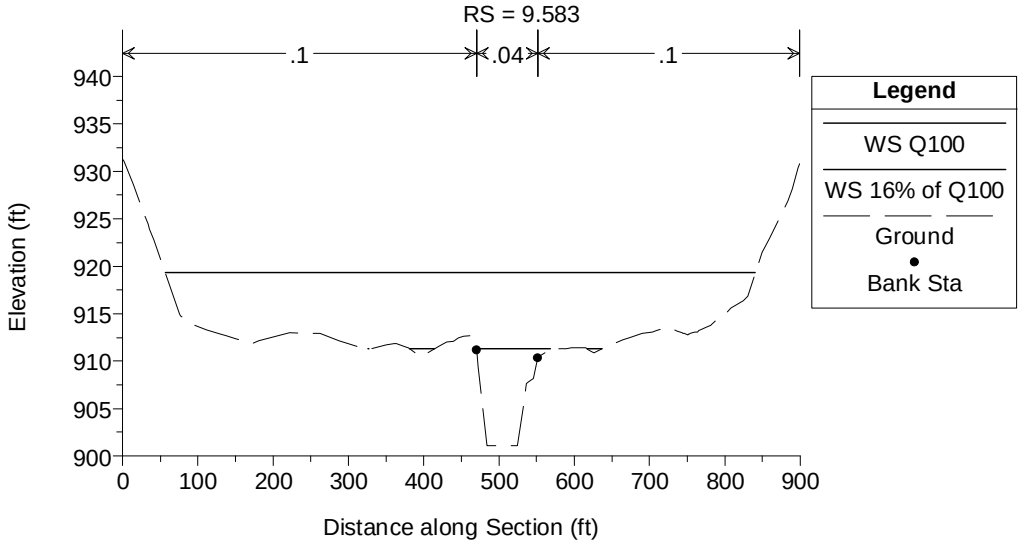

(f) Station 9.583 (miles)

Figure 5-14. Selected Cross-Sections, Reach No. 3 (cont.)

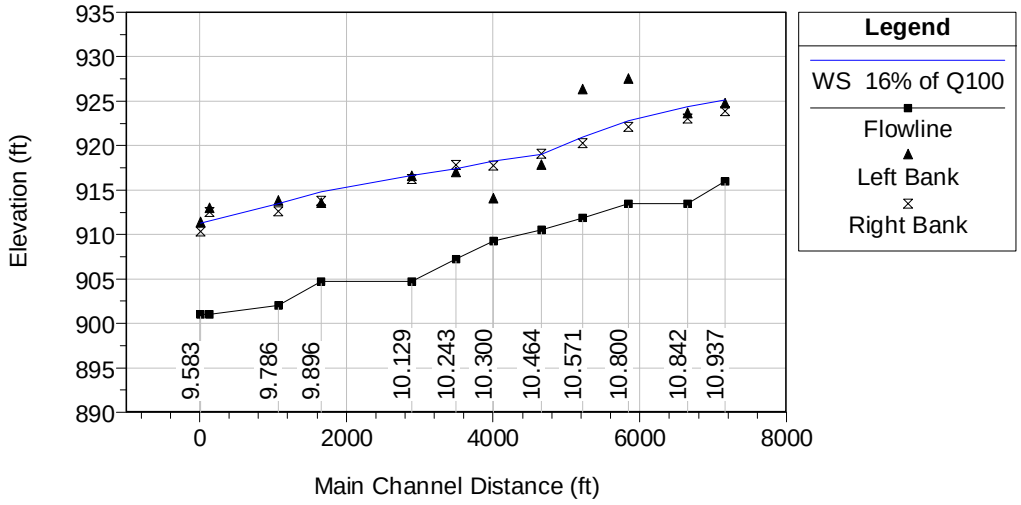

Figure 5-15. Profile of Left and Right Bank Stations, Reach No. 3

Table 5-7. Main-Channel Definition and Bank Stationing, Reach No. 3

Cross-Section Station	Width between Bank Stations (ft)	Depth from Lowest Bank Station to Flowline
10.937	92.1	7.9
10.842	102.1	9.6
10.800	94.5	8.6
10.571	93.8	8.4
10.464	75.3	7.1
10.300	90.1	4.7
10.243	108.9	9.6
10.129	75.9	11.5
9.896	76.3	8.7
9.786	60.8	10.6
9.607	78.9	11.5
9.583	81.2	9.3
Average (ft)	85.8	9.0
Std. Dev. (ft)	13.5	1.9

As expected on natural streams, the cross-sections within any of the four reaches show wide variations. Some sections are highly contained, with very little expansion of floodplain flows, whereas others contain very shallow main channels and broad overbanks. The relative diversity of the cross-sections in a single reach was viewed by plotting them all simultaneously on a graph of top width versus depth. The graph was created by exporting top width and flow depth information from the HEC-RAS steady state output, described in more detail later. Figure 5-16 shows this plot for the cross-sections in Reach No. 3, based on the final HEC-RAS geometry for that reach.

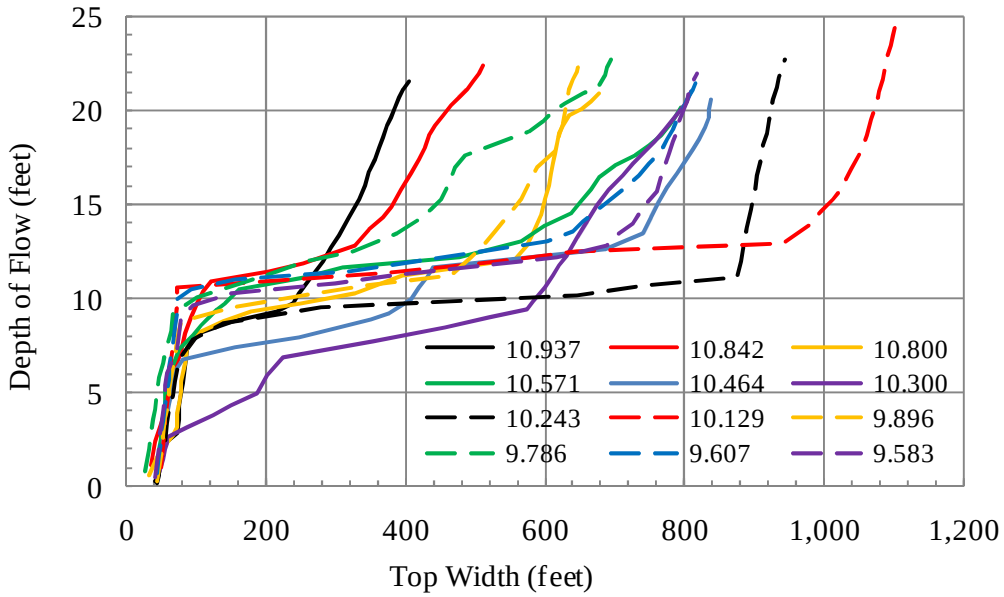

Figure 5-16. Top Width vs. Flow Depth for Cross-Sections in Reach No. 3

While the plotted ordinates of each line shown in the graph were dependent upon the specific flow rates calculated, the actual trend of the line and relationship between depth and top width for any given section is independent of the flow rates.

HEC-RAS in this instance serves as a convenient calculator of the channel geometry.

Most cross-sections show a sharp "break," where the steep profile of main-channel flow ends and the flattened overbank begins. For a majority of the cross-sections, the width of flow where this break occurs is between 70 and 90 feet. The depth at the "break" lies between 7 and 11 feet for most sections. These ranges correspond reasonably well with the 85.8 feet average width of channel between assigned bank stations and the 9.0 average depth of flow below the lowest assigned bank station elevations. The cross-section at Station 10.300 deviates significantly from the overall trend, with an initial widening of flow beginning near 3 feet of depth.

Moving further out, all of the cross-sections show an eventual steepening again of the top width vs. depth relationship, which was interpreted as beginning of the valley wall. Station 10.129 appears to have the widest available floodplain, extending to 940 feet of width before being contained by the valley wall. By contrast, Station 10.842 appears to be the most highly incised, with a floodplain width of no more than 320 feet before being contained by the valley wall.

5.5.1.7 Assigning Manning's n Roughness

As discussed previously, Manning's roughness values for the base line model were established for each reach using a presumed standard reference condition. The overbank Manning's n was set to 0.100 for both left and right overbank on all reaches. The main-channel was set to 0.040 for Reaches No. 2, No. 3 and No. 4 and 0.045 for Reach No. 1. The new Manning's roughness values for all cross-sections were then entered into the appropriate columns under **HEC-RAS | Edit | Geometric Data |**

Tables | Manning's n or k values.

5.5.1.8 Calculating Bed Slope

An effective hydraulic slope is required for unsteady flow modeling, both to define the geometry of simplified "representative" reach, and for use in setting the normal depth slope for downstream boundary conditions. For this study, the average bed slope was used to estimate this effective hydraulic slope. The minimum bed elevations from each cross-section were extracted from HEC-RAS, along with the downstream main-channel length, and imported into an **Excel** spreadsheet. A plot of the bed profile relative to the channel centerline was made and the linear trend-line feature used to plot a best fit line. The slope of the best-fit line was taken as an estimate of the main-channel bed slope. Figure 5-17 shows the bed profile and best fit slope line for Reach No. 3. The calculated bed slope was 0.0021 using this method. Bed slopes were rounded to two significant digits.

Bed slope can only be approximated in this manner. This method assumed that the planimetric data captured the actual low point of the stream, which was not always the case. The AIMS planimetric data were derived from planning-scale aerial photography, so the actual elevation being recorded is the water surface at the time of the aerial flight. For smaller streams, such as Reach No. 1 and No. 2, the depth of flow above that true flowline may be close. On the other hand, flowlines may be difficult to determine from aerial photography in small, heavily wooded streams.

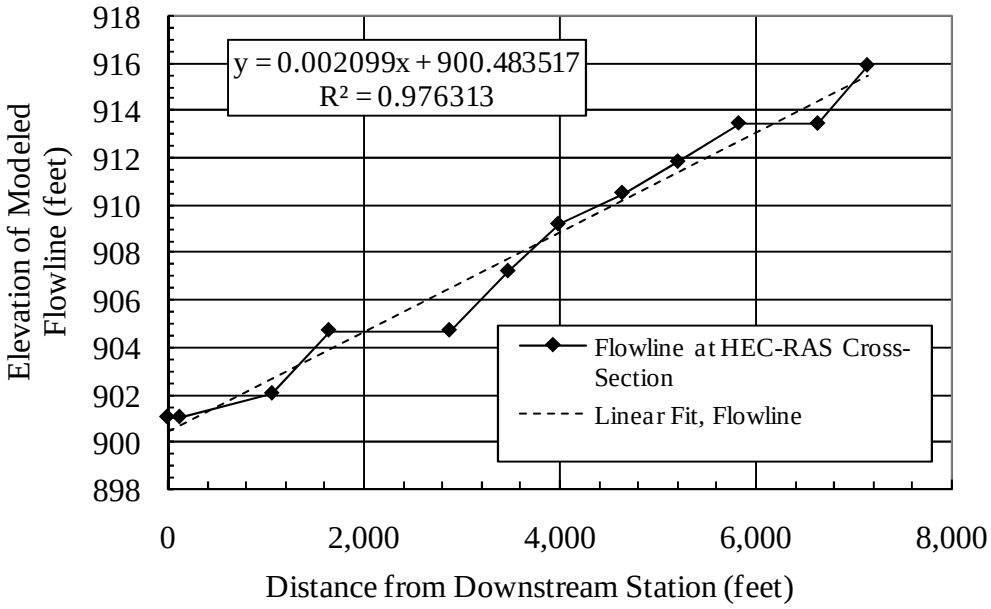

Figure 5-17. Bed Slope Profile, Reach No. 3

For larger streams, such as Reach No. 4 with 47.9 square miles of tributary area, the depth of channel that may be hidden due to larger base flow. The overall profile of the water surface during base flow conditions should be approximately parallel to the actual bed slope, however, particularly if it is evaluated over a large enough distance. Given a lack of field survey for these reaches, this slope calculation was assumed sufficient.

5.5.1.9 Establishing a Family of Reference Flows

As mentioned in the discussion of cross-sections, certain reach parameters must be evaluated with reference depths and flow areas appropriate to the expected range of flows. This means that some aspects of model development are iterative, with initial estimates being made to run the models, and then updated based on preliminary model results. To allow for these evaluations, a consistent family of

steady-state discharges was developed for all four reaches. The estimated 100-year peak discharge rate (Q_{100}) at the upstream end of the reach, as shown in Table 5-6 after rounding, was selected as a reference discharge. For Reach No. 3, the reference discharge was 24,000 cfs.

Based on this reference value, a family of 30 proportional steady-state discharge values was specified. These 30 values reflect flow conditions ranging from 0.1% to 140% of Q_{100}. The intermediate discharges are not uniformly spaced, but are segregated into ranges to allow greater clustering of values at low discharges and a more uniform spacing of the overall flow depths. These 30 discharge values were entered as separate profiles into a HEC-RAS steady-state flow file, to be used uniformly throughout the reach. Table 5-8 presents the relative flow rates used.

Table 5-8. Flow Rates Relative to Q_{100}, Used for Steady-State Profiles

0.1%	3%	10%	20%	50%	100%
0.5%	4%	12%	25%	60%	110%
1.0%	5%	14%	30%	70%	120%
1.5%	6%	16%	35%	80%	130%
2%	8%	18%	40%	90%	140%

5.5.1.10 Running HEC-RAS for Initial Geometry and Steady-Flow

Steady-state analyses were performed for each reach using HEC-RAS. The initial geometry file and family of discharge values were used. The downstream boundary conditions for each discharge profile were set as normal depth, using the reach-averaged bed slope as the hydraulic slope for calculation.

Results from the initial steady-state runs were used to refine the estimates of

reach properties, including valley length and bank stations. These results were also used to develop the top width versus depth relationships for each cross-section, shown previously. An iterative process was used to arrive at a final HEC-RAS file. Only one or two iterations were needed to obtain reasonably consistent results.

5.5.1.11 Revising the Valley Flow Path and Flow Distances

The initial valley flow path was based on a visual assessment of the valley planform and previously defined 100-year floodplain. After the initial HEC-RAS model was run, a revised estimate of the valley flow path could be defined that was less subjective.

In concept, the valley flow path represents the primary pathway followed by the flood flows that travel above the main-channel. Figure 5-14 showed selected cross-sections with the water surfaces for the 100-year discharge (Q_{100}) and the estimated bankfull discharge ($Q_{bankfull}$) plotted. The area lying between these profiles represents the portion of the 100-year flow that is traveling above the main-channel at the peak of the 100-year event. If the horizontal midpoint of this "above-bankfull" region was calculated for each section, the midpoints could be plotted in plan view and an alignment fitted through them. The resulting pathway could be treated as an approximation of the valley flow path.

The use of cross-sectional area is important because unsteady modeling relies heavily on conservation of volume for accuracy. By using a cross-sectional area based method, the valley flow-path calculation should allow for a reasonable estimate of the reach volume.

This process was followed in the current study to estimate a revised valley flow length. Various procedures could be used to calculate the horizontal midpoint location. For this study, the "Flow Distribution" feature in HEC-RAS was used to calculate cross-sectional areas for each profile (**HEC-RAS | Run | Steady Flow Analysis | Options | Flow Distribution Locations**). When using this feature, HEC-RAS divides each cross-section into a series of horizontal subsections and calculates the flow area for each. The horizontal divisions remain the same for all profiles, so the difference in flow area between the Q_{100} and $Q_{bankfull}$ profiles for each subsection can be calculated. The subsection containing the midpoint of flow can be isolated and linear interpolation used to estimate a specific location for the midpoint.

Table 5-9 summarizes the calculated midpoint values for Reach No. 3. Figure 5-18 displays a plot of these midpoints and the revised valley pathway that was fitted to them. The alignment does not fit precisely, since fitting a line through all of the midpoints would have involved some sharp localized curves. The revised line represents a reasonable fit of the midpoints and was used as the final alignment of the valley flow path. The main-channel centerline, cross-sections, and initial valley flow path are shown in Figure 5-18 for reference.

The valley midpoint calculation was based on an intermediate version of the HEC-RAS model for the reach. An iterative solution could have been used to refine the midpoint locations. However, the calculation and mapping of these midpoints was a laborious process, and the refinements that could be gained were judged to be minor. The valley flow paths revision from the first iteration was taken as final.

Table 5-9. Location of Valley Flow Midpoints, Reach No. 3

Cross-Section Identifier	Location of Valley Flow Midpoints, from Left Edge of Cross-Section (feet)
10.937	314
10.842	397
10.800	452
10.571	406
10.464	441
10.300	457
10.243	535
10.129	602
9.896	376
9.786	444
9.607	425
9.583	448

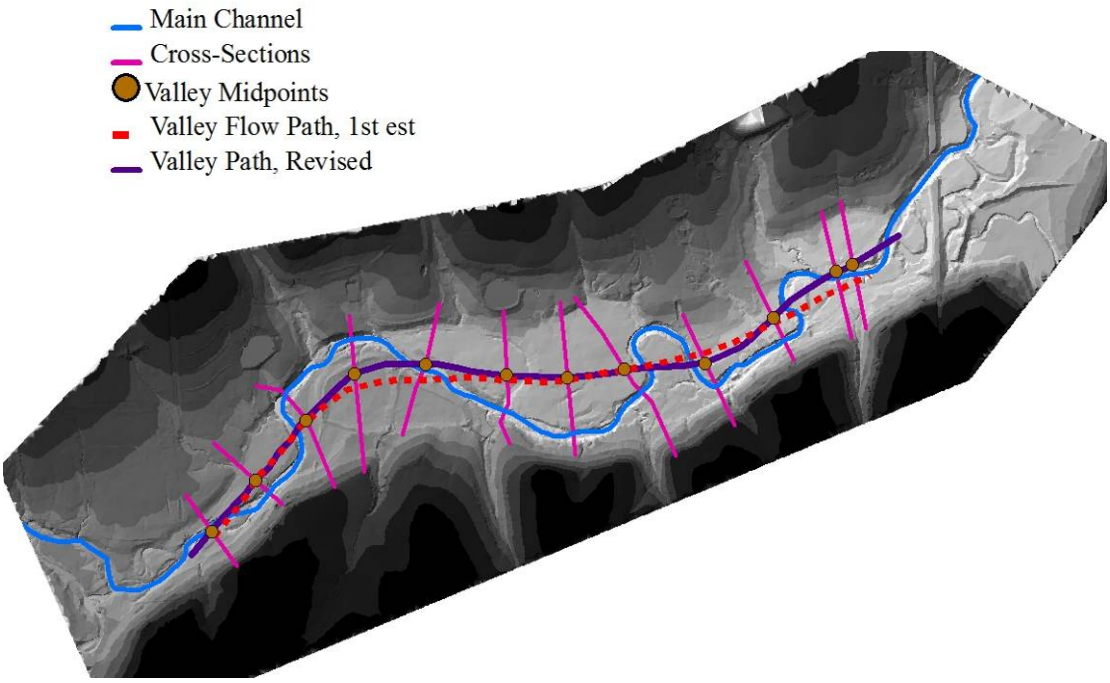

Figure 5-18. Valley Flow Midpoints and Revised Valley Path, Reach No. 3

For Reach No. 3, the total valley flow path length between bounding cross-sections was 5,174 feet. This is approximately 2.7% longer than the initial estimate of 5,039 feet. As can be seen in the figure, the revised flow path indicates some additional curvature to the valley flow path that was not shown in the initial estimate. This is reasonable since the initial estimate of the valley flow path was based purely on the midpoint of the floodplain with no consideration of the depth distribution across the overbanks.

The revised valley flow length is approximately 16% shorter than the average of the left and right overbank distances used in the original Blue River Watershed study (6,250 feet and 6,178 feet, respectively). This reduction in length has a direct impact on the storage volume estimates calculated by HEC-RAS.

HEC GeoRAS was used to calculate updated overbank distances, using the new valley flow-path alignment. A new **GeoRAS | RAS Geometry** project was developed and the **RAS Geometry** processing steps were then continued as before, with new downstream reach lengths for each cross-section were calculated. The updated values were exported to the working HEC-RAS model.

5.5.1.12 Finalizing the Base-Line Model

Once the bank stations were adjusted and the revised valley lengths calculated, the models were rerun and finalized. A selected set of final water-surface profiles for Reach No. 3 are given in Figure 5-19. The profiles are shown for discharges have the following values, based on the ratio to Q_{100}: 2%, 10%, 30% and 100%.

The results of this final model were used to define the surface and volume relationships for the reach under steady flow, as described in more detail in Section 5.6. Those relationships were used to derive a simplified equivalent reach, based on an 8-pt. cross-section, which is explained in Section 5.7. This model was also used as the base for developing the geometry file for unsteady flow routing in Chapter 6.

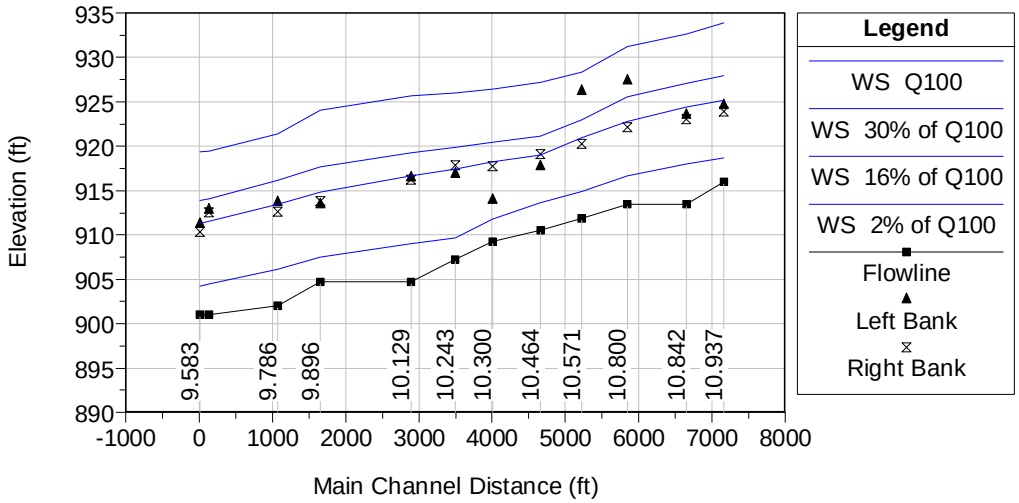

Figure 5-19. Water Surface Profiles for Selected Discharges, Reach No. 3

5.5.1.13 Calculating Sinuosity

As discussed in Chapter 4, sinuosity is an important parameter in describing the physical and hydraulic properties of a channel. Sinuosity is generally defined as the stream centerline length divided by the valley flow-path length (Leopold et al. 1964).

As seen from the previous discussion, the definition of valley length is not simple. The revised valley flow-path length calculated above was used for sinuosity

calculations. For Reach No. 3, between the bounding cross-sections, the stream centerline length was 7,149 feet and the revised valley flow path length was 5,174 feet, which results in a sinuosity of 1.38.

Other potential sinuosity ratios could have also been considered. The initial estimate of valley flow-path length was derived from a visual assessment of the reach meander, and might correspond to the reference valley length that would have been estimated in a less detailed study of the reach. In fact, in stream stability studies this is the valley flow path length that would typically be used. Had that path been used, the calculated sinuosity for Reach No. 3 would have been 1.42.

5.5.2 Summary of Base HEC-RAS Model for Each Reach

HEC-RAS models of the four reaches were developed using the procedures described in the previous section. A brief discussion of the input data and model characteristics for each reach is provided in this section. Key parameters are summarized on Table 5-10.

5.5.2.1 Reach No. 1

Figure 5-20 displays the TIN developed for Reach No. 1. Also displayed on the figure are the locations of the stream centerline, the final estimate of valley flow path, and the locations of all cross-sections used for analyses. An outline of the 100-year floodplain, as delineated in the original watershed study, is shown for reference.

Table 5-10. Summary of Steady-State HEC-RAS Model Parameters, All Reaches

Reach No.	1	2	3	4
Average Top Width of the Main-Channel (feet)	34.8	67.6	85.8	109
Average Height of Lowest Overbank Station above Channel Bottom (feet)	4.1	6.4	9.0	12.2
Reference Flow, 100-year Discharge, Q_{100} (cfs)	2,900	11,000	24,000	36,000
Approximate "Bankfull Flow" Discharge ($Q_{bankfull}$), as % of Q_{100}	10%	12%	16%	10%
Bed Slope, best fit (%)	0.54%	0.17%	0.21%	0.084%
Main-Channel Length (feet)	3,666	6,523	7,149	10,199
Valley Flow Length (feet)	2,121	4,303	5,174	7,520
Apparent Sinuosity	1.73	1.52	1.38	1.36

Figure 5-21 gives the station identifiers for all 11 cross-sections defined for this reach. The farthest upstream cross-section for this reach is at station 104+87 and the farthest downstream section is at station 68+21. Stationing for the Tomahawk Creek study was given in feet, unlike the other three reaches which were stationed in units of river miles.

Reach No. 1 required the most extensive modification from the original watershed study data. The seven cross-sections in the lower half of this reach were all redrawn to better align with the sinuosity of the meandering channel and overbank flows. A new cross-section at 68+21 was defined to serve as the downstream boundary. The four upstream-most cross-sections were kept in the same location as in the original Tomahawk Creek study. Blocked flow was established at one section

where a side tributary entered the flow and at another station where the cross-section intersected a large but isolated abandoned channel.

The geometry for the HEC-RAS cross-sections was created using the Geo-RAS procedures described above and the Johnson County data. As mentioned previously, this was the only reach of the four that was recreated in its entirety for this study.

Figure 5-22 displays selected cross-sections from Reach No. 1, with the water-surface profiles shown for 10% and 100% of Q_{100} discharge rates. The bank station locations as assigned in the final models are shown. For Reach No. 1, the 10% of Q_{100} discharge appeared to serve as the closest approximation to the bankfull discharge, $Q_{bankfull}$. Figure 5-23 presents the top width vs. depth relationship for all the cross-sections in Reach No. 1. Figure 5-24 presents the HEC-RAS profile view of this reach, including the bed elevations, elevations of left and right bank stations at each section, and final flow profiles for following ratios of Q_{100}: 2%, 10%, 30% and 100%.

5.5.2.2 Reach No. 2

Figure 5-25 displays the TIN developed for Reach No. 2, along with the stream centerline, valley flow path, cross-section locations, and original 100-year floodplain boundaries, similar to the figure given previously for Reach No. 1.

An index of the stationing for all 11 cross-sections used in Reach No. 2 is shown on Figure 5-26. Reach No. 2 is bounded by cross-section 13.664 (miles) on the upstream side and section 12.428 downstream.

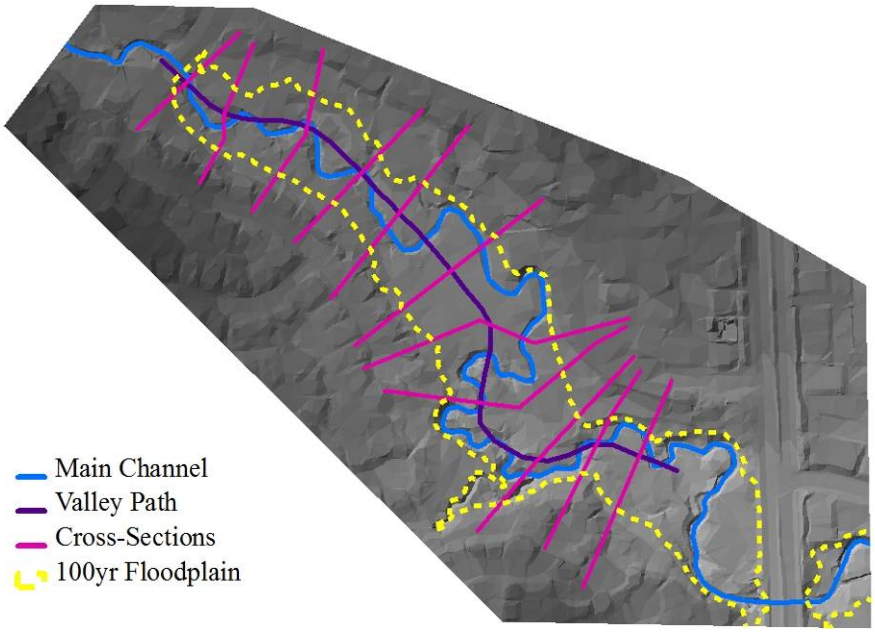

Figure 5-20. Plan View and TIN, Reach No. 1

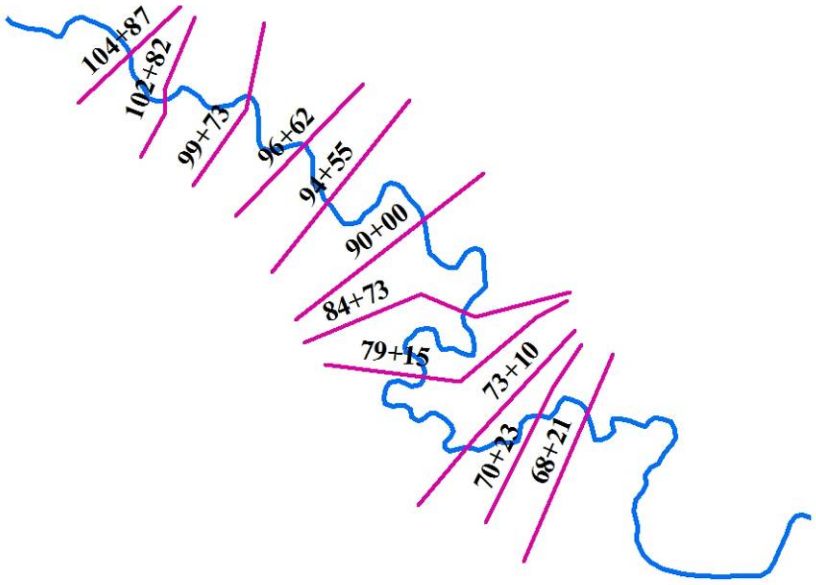

Figure 5-21. Cross-Section Index, Reach No. 1

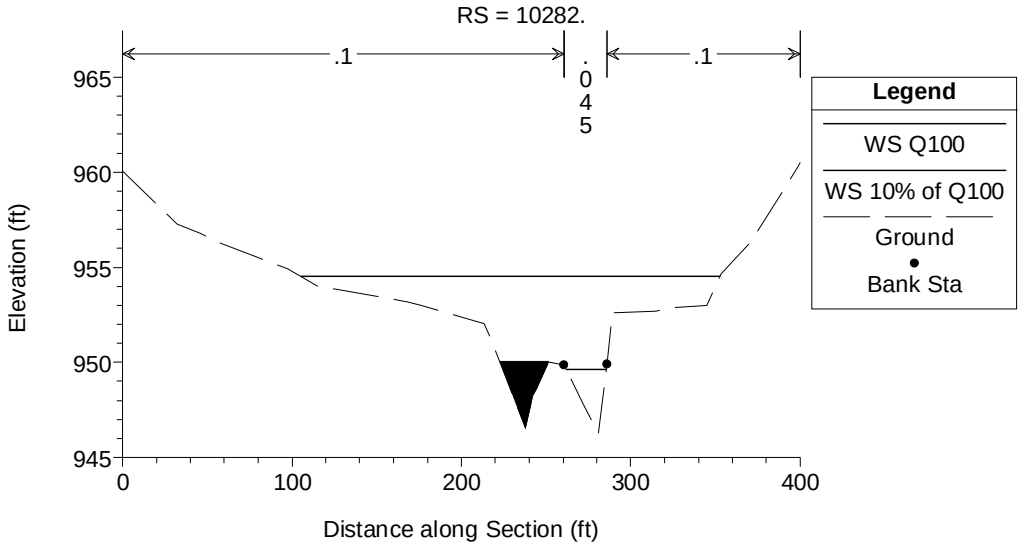

(a) Station 102+82 (feet)

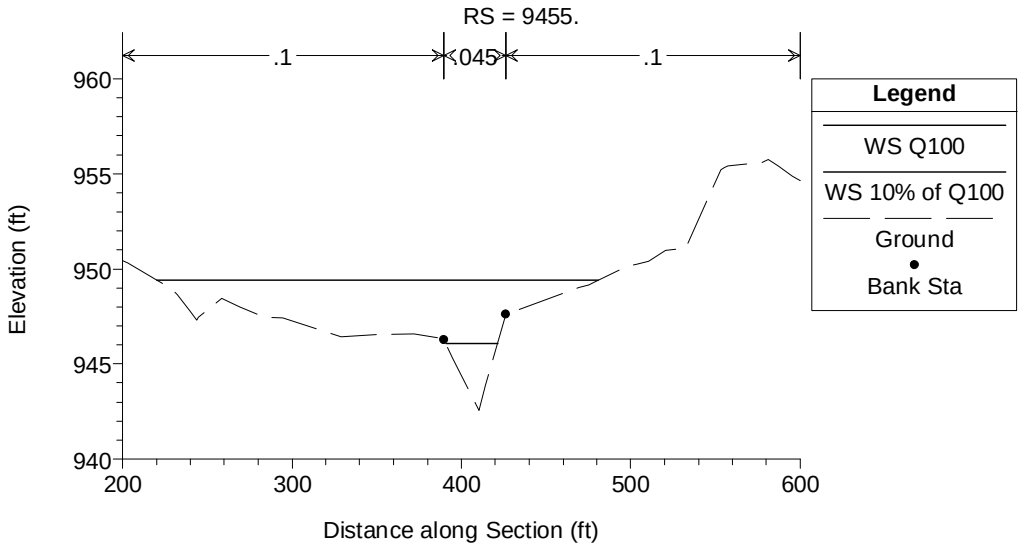

(b) Station 94+55 (feet)

Figure 5-22. Selected Cross-Sections, Reach No. 1

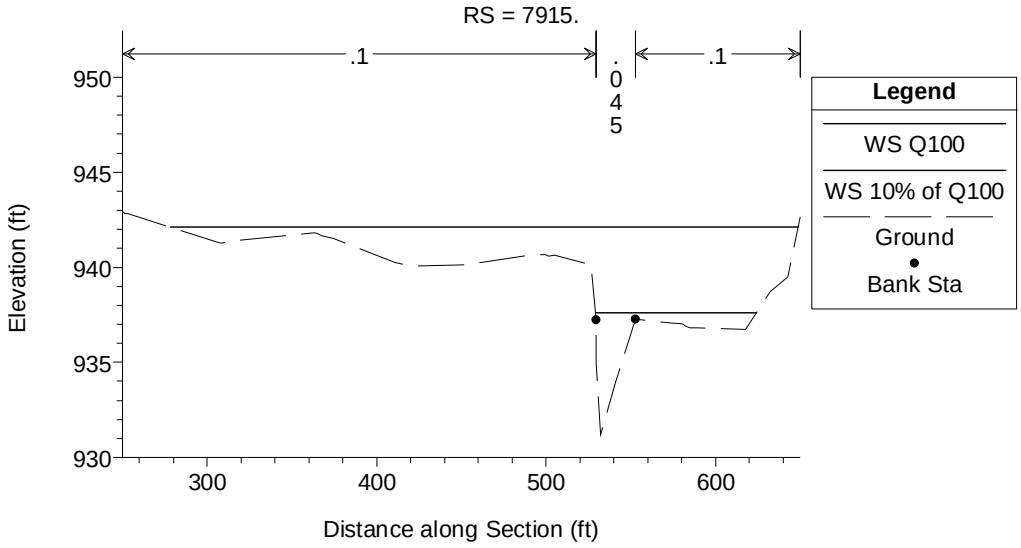

(c) Station 79+15 (feet)

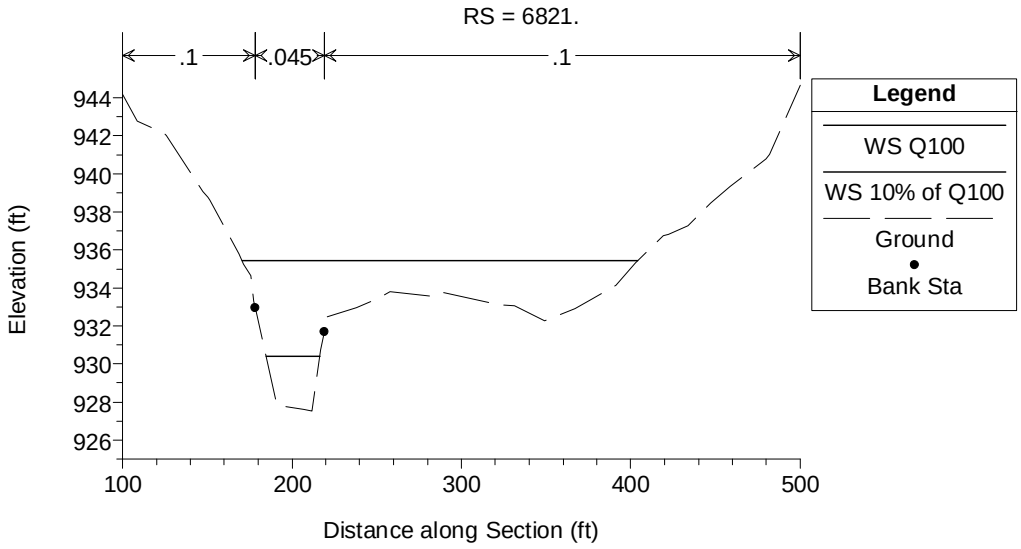

(d) Station 68+21 (feet)

Figure 5-22. Selected Cross-Sections, Reach No. 1 (cont.)

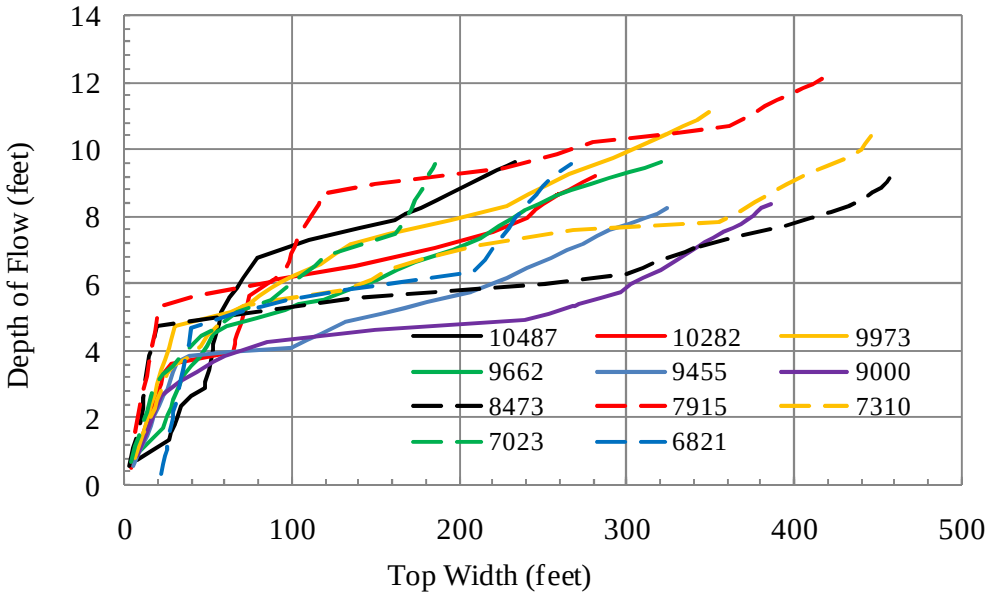

Figure 5-23. Top Width vs. Flow Depth for Cross-Sections in Reach No. 1

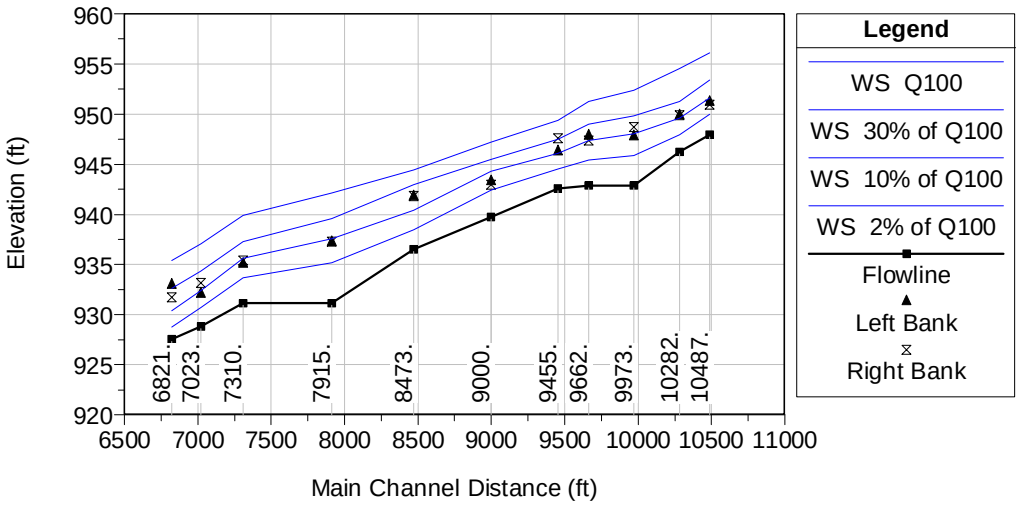

Figure 5-24. Water Surface Profiles for Selected Discharges, Reach No. 1

The cross-sections for this reach were primarily taken directly from the original Blue River Watershed Study. Two new cross-sections were added, one at Station 13.140 to better define conditions midway through the strong leftward bend in the creek, and a second at Station 12.655 to shorten the cross-sectional spacing in that area. Several other cross-sections were lengthened to fully capture the limits of flow, and the left overbank of one cross-section was adjusted so that it was oriented more perpendicular to the overall flow path. Blocked flow was added at three stations, based on the presence of a side tributary and an abandoned oxbow channel.

Figure 5-27 presents selected cross-sections from Reach No. 2, with the water-surface profiles shown for 14% and 100% of Q_{100}. For Reach No. 2, the bankfull discharge $Q_{bankfull}$ appeared to be best approximated by the steady-state discharge having a value of 14% of Q_{100}. Figure 5-28 presents the top width-vs.-depth relationship for all the cross-sections in Reach No. 2.

Figure 5-29 presents the HEC-RAS profile view of this reach, including the bed elevations, elevations of left and right bank stations at each section, and final flow profiles for following ratios of Q_{100}: 2%, 14%, 30% and 100%.

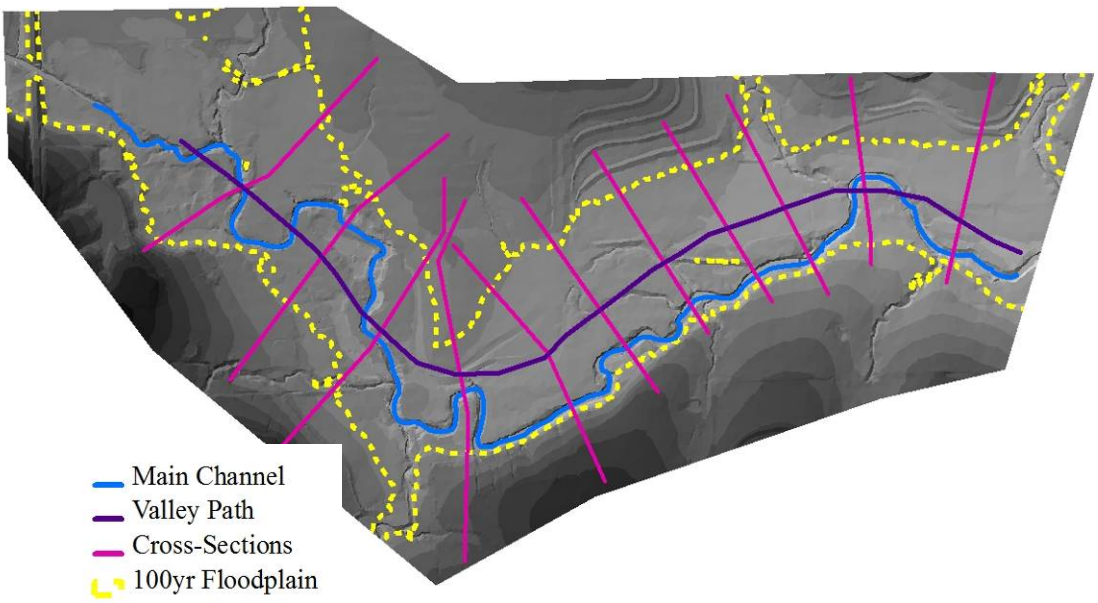

Figure 5-25. Plan View and TIN, Reach No. 2

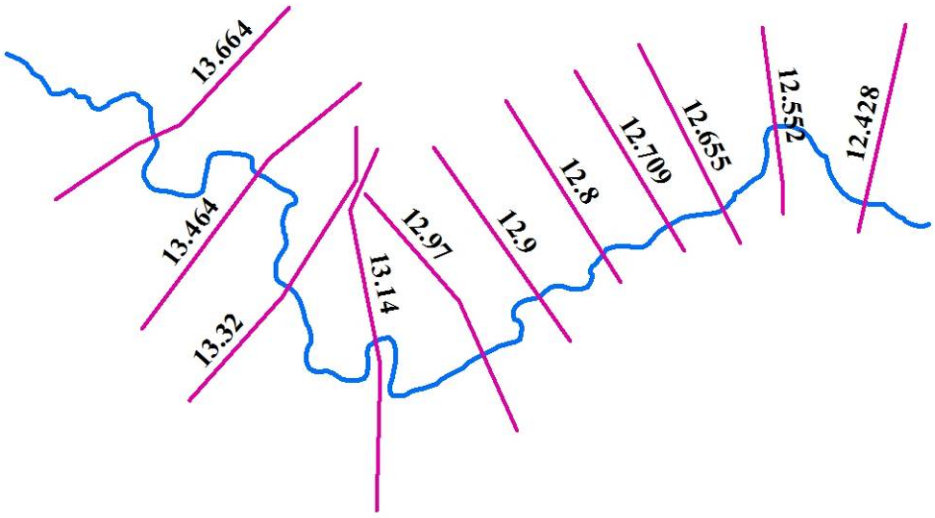

Figure 5-26. Cross-Section Index, Reach No. 2

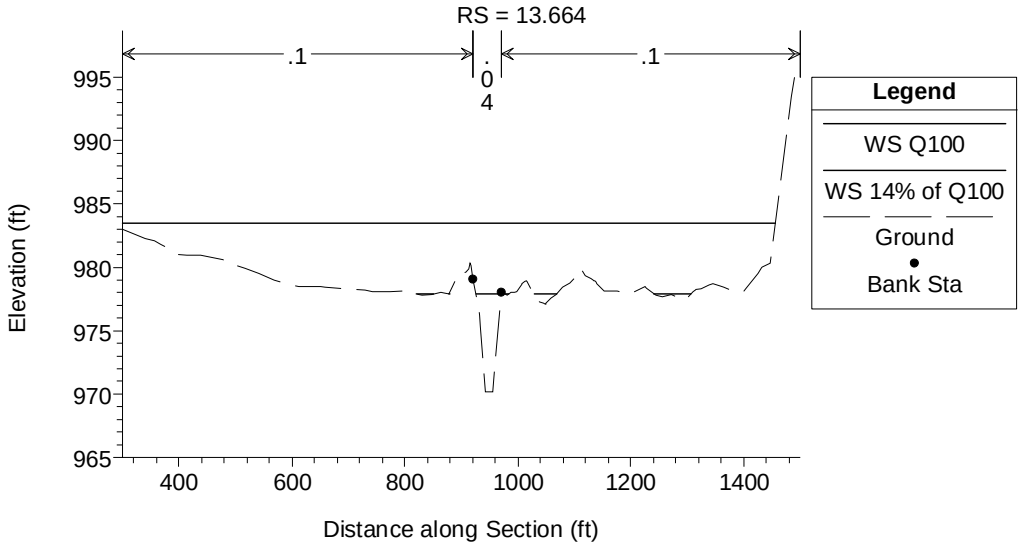

(a) Station 13.664 (miles)

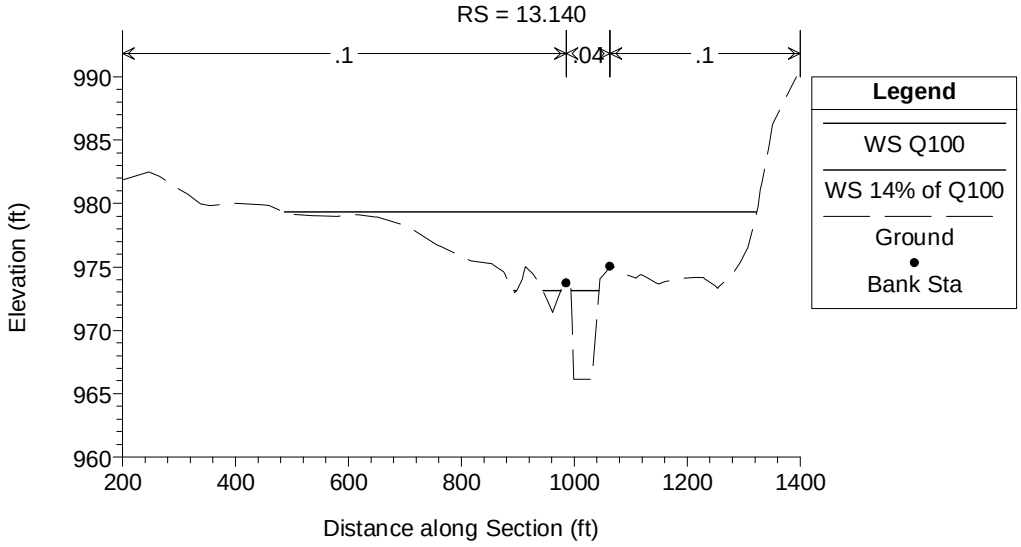

(b) Station 13.140 (miles)

Figure 5-27. Selected Cross-Sections, Reach No. 2

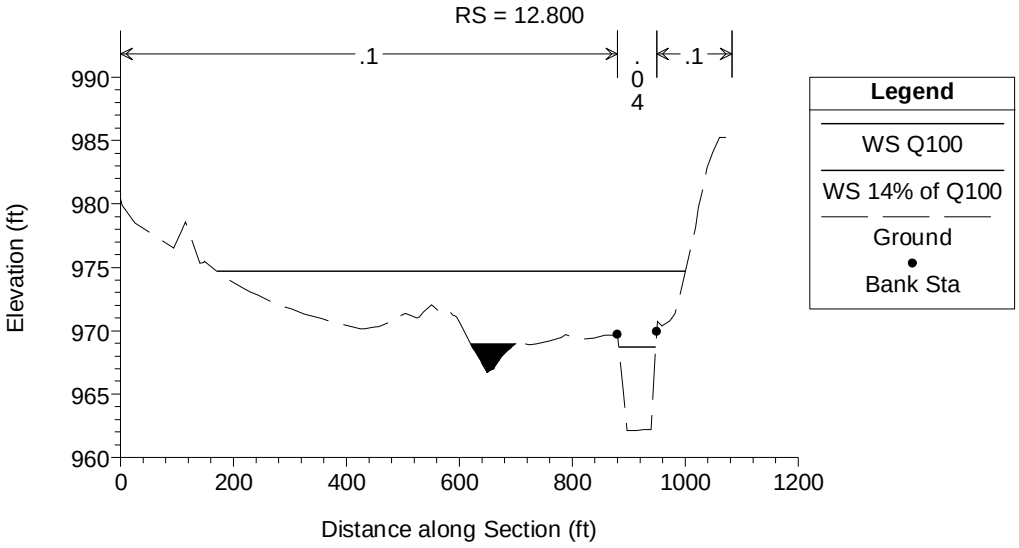

(c) Station 12.800 (miles)

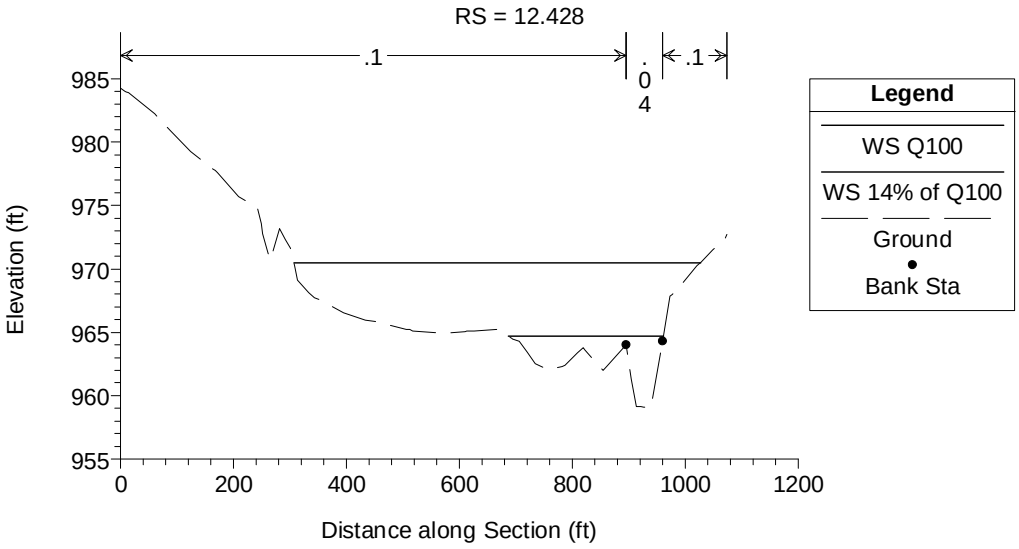

(d) Station 12.428 (miles)

Figure 5-27. Selected Cross-Sections, Reach No. 2 (cont.)

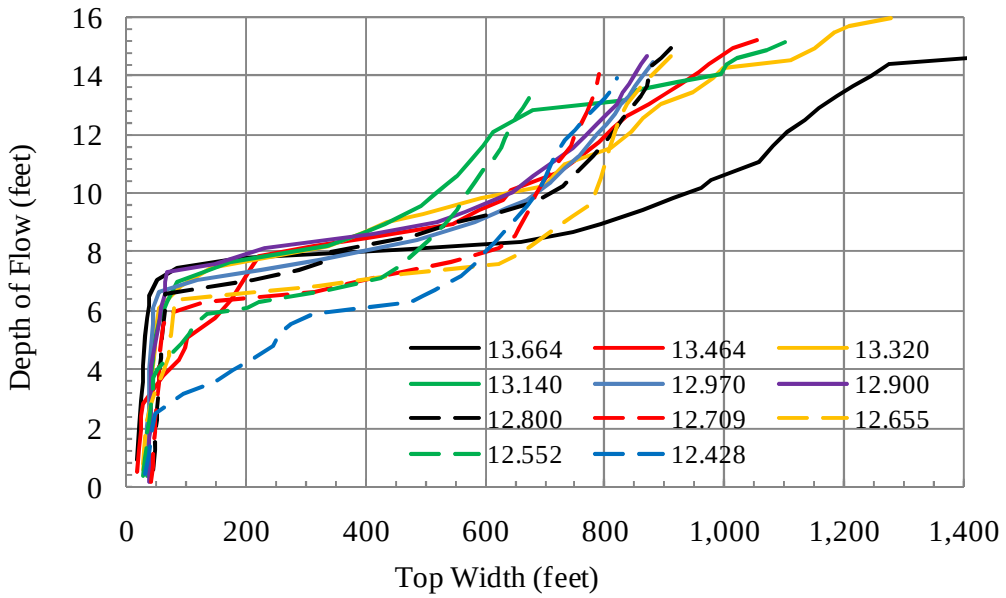

Figure 5-28. Top Width vs. Flow Depth for Cross-Sections in Reach No. 2

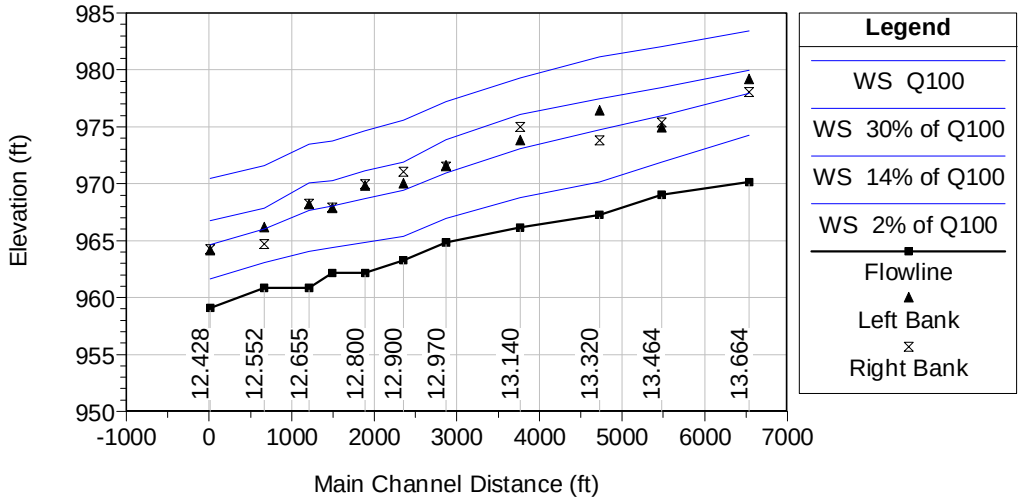

Figure 5-29. Water Surface Profiles for Selected Discharges, Reach No. 2

5.5.2.3 Reach No. 3

Reach No. 3 has already been discussed in detail in the previous sections. Figure 5-11 displayed the TIN as it was developed for Reach No. 3, along with the stream centerline, cross-section locations, and original 100-year floodplain boundaries. Figure 5-18 shows the final valley flow path, after revision. The index for cross-section identifiers is given in Figure 5-13 and selected cross-sections are shown in Figure 5-14. Reach No. 3 is bounded by cross-section 10.937 on the upstream side and section 9.583 downstream.

The bankfull discharge ($Q_{bankfull}$) for Reach No. 3 was estimated previously as 16% of Q_{100}. The top width vs. depth relationship for Reach No. 3 was given in Figure 5-16. Flow profiles are shown in Figure 5-19. The bankfull discharge ($Q_{bankfull}$) for Reach No. 3 was estimated previously as 16% of Q_{100}.

No new cross-sections were needed for Reach No. 3, nor were any section alignments adjusted. There was no need to established blocked flow areas on any of the cross-sections.

5.5.2.4 Reach No. 4

The TIN developed for Reach No. 4 is shown in Figure 5-30, along with the stream centerline, valley flow path, cross-section locations, and original 100-year floodplain boundaries.

The cross-section stations are shown on Figure 5-31. The bounding cross-sections are 6.870 upstream and 4.938 downstream. The cross-sections for this reach were all taken directly from the original Blue River Watershed Study. No new

sections or alignment adjustments were required. Blocked flow areas were added to one cross-section to eliminate an abandoned oxbow and at another to address a side tributary.

Figure 5-32 presents selected cross-sections from Reach No. 4, with the water-surface profiles shown for 10% and 100% of Q_{100}. The bankfull discharge $Q_{bankfull}$ in Reach No. 4 appeared to be best approximated by the steady-state discharge equal to 10% of Q_{100}.

Figure 5-33 presents the top width vs. depth relationship for all 11 cross-sections that were used to define Reach No. 4. An interesting characteristic of the reach can be seen in this figure. Rather than a single "bankfull" station and flattened overbank, it appears there are two levels of overbank flow, with a lower terrace that begins between 10 and 13 feet of flow depth, and a higher bench that is not reached until flows depths are 19 to 20 feet. This distinct terraced-type overbank is not seen in the other three reaches.

Figure 5-34 presents the HEC-RAS profile view of this reach, including the bed elevations, elevations of left and right bank stations at each section, and final flow profiles for following ratios of Q_{100}: 2%, 10%, 30% and 100%.

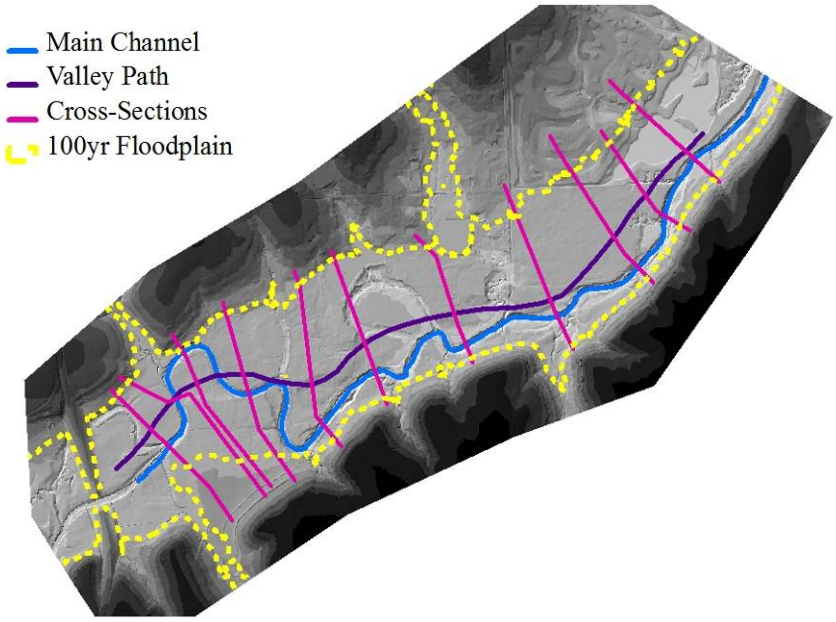

Figure 5-30. Plan View and TIN, Reach No. 4

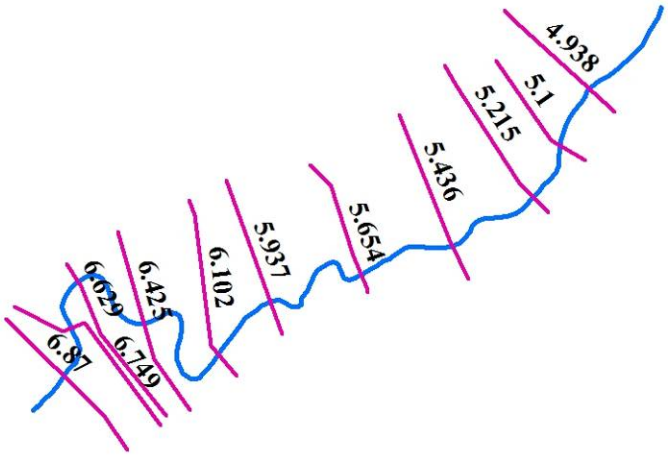

Figure 5-31. Cross-Section Index, Reach No. 4

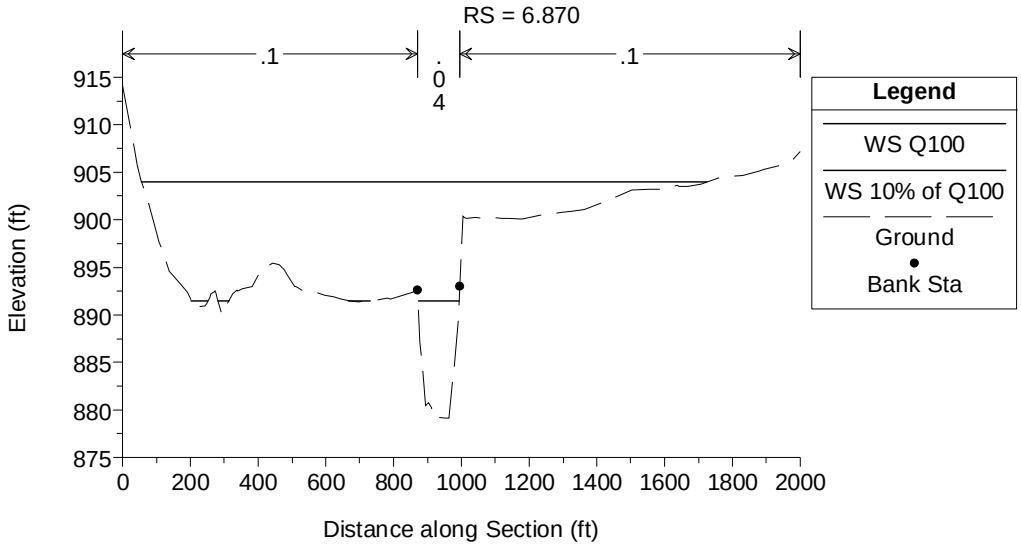

(a) Station 6.870 (miles)

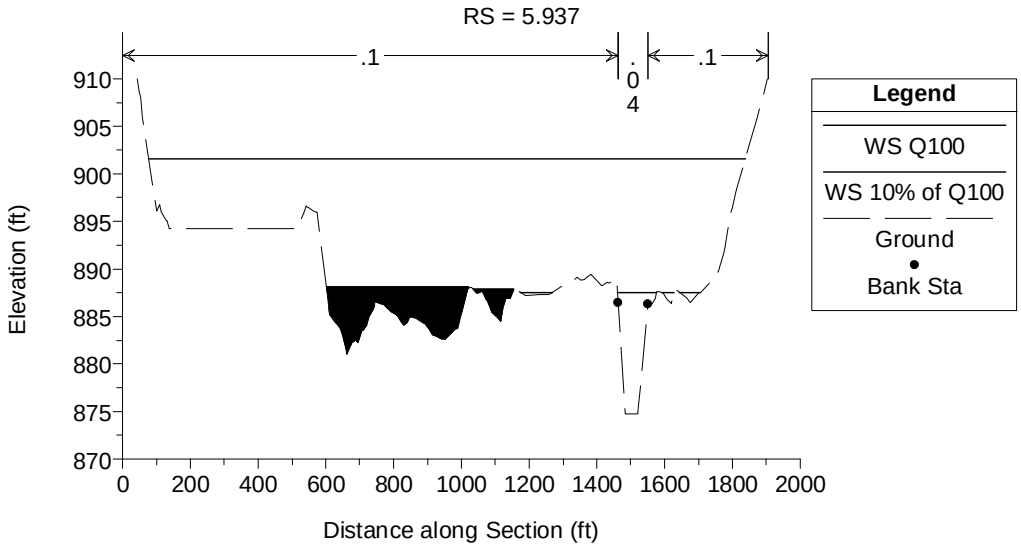

(b) Station 5.937 (miles)

Figure 5-32. Selected Cross-Sections, Reach No. 4

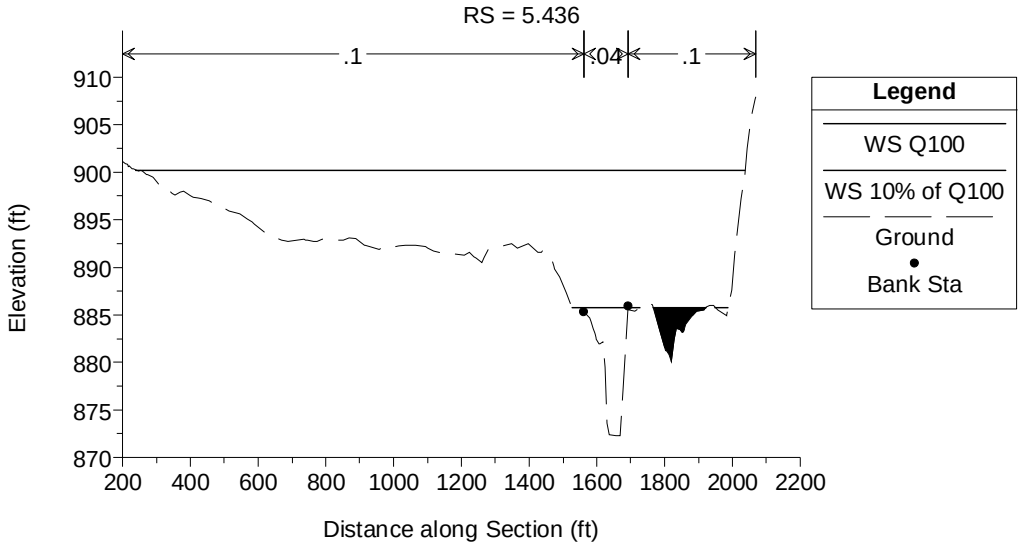

(c) Station 5.436 (miles)

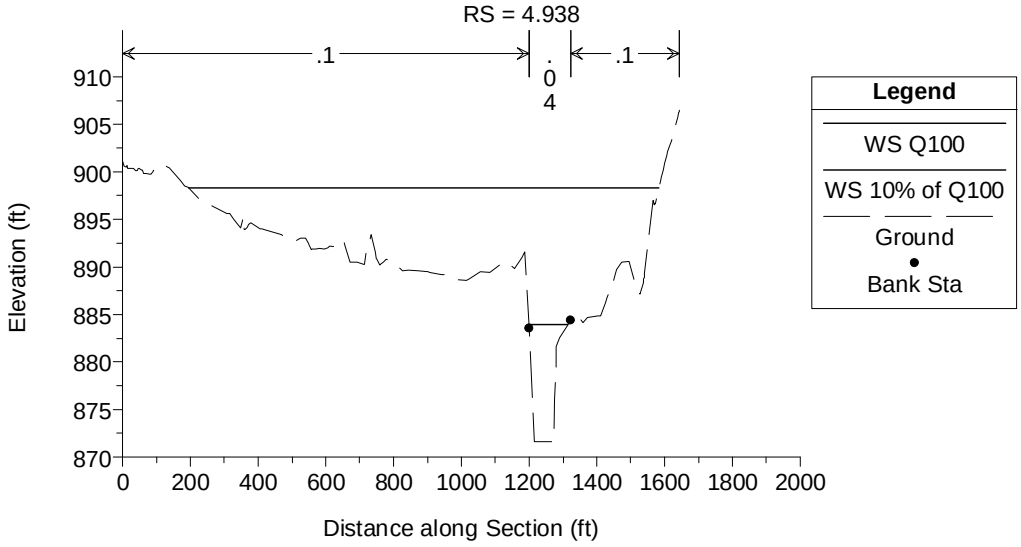

(d) Station 4.938 (miles)

Figure 5-32. Selected Cross-Sections, Reach No. 4 (cont.)

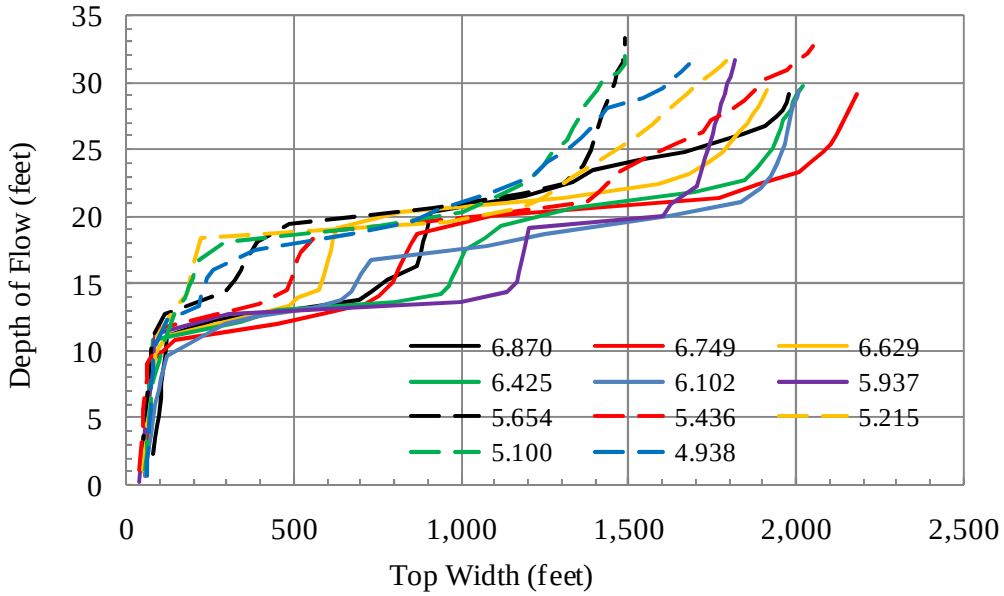

Figure 5-33. Top Width vs. Flow Depth for Cross-Sections in Reach No. 4

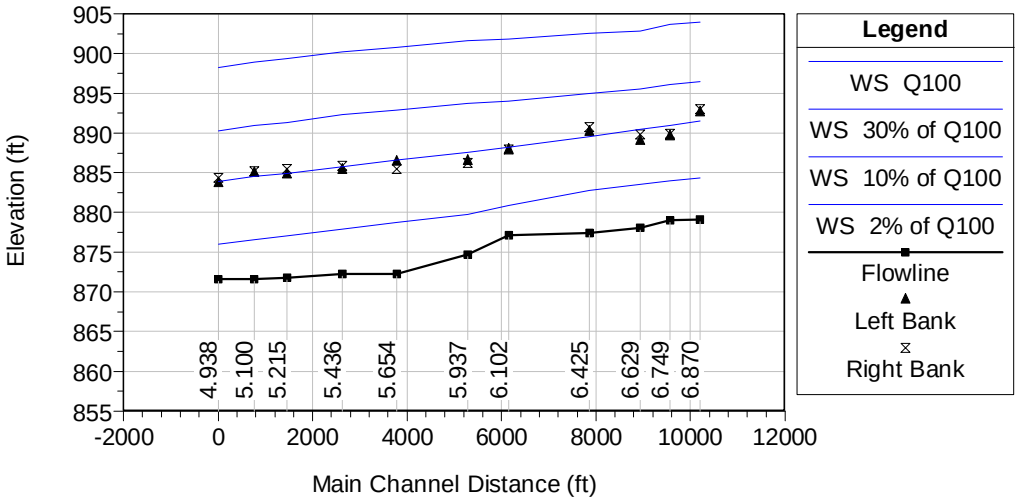

Figure 5-34. Water Surface Profiles for Selected Discharges, Reach No. 4

5.6 Preparation of Tabular Output Summary

Values for the characteristic reach length and kinematic wave speeds in a reach over a range of discharges can be calculated directly from tabular summaries of the volume, surface area, and steady-state discharge, as described in Chapter 3. This type of tabular data may be derived from the detailed output produced by HEC-RAS for steady-state runs. The tabular data may be used directly in the cascading reservoirs (CR) method or it may also be used to derive the properties of an equivalent, representative prismatic channel.

This information was generated by HEC-RAS for the 30 steady-state flow values discussed in the previous section. Also required are the length of the main stem of the channel and a representative value of the friction slope. The data is used first to derive values for K and N_o as shown in Eqs. (3-36) and (3-39), from which c_k and L_u can also be found, using Eqs. (3-40) and (3-41). The kinematic wave speed is given in units of feet per second (fps).

Tables 5-11 through 5-14 present a summary of the output data that was derived from the HEC-RAS runs for each of the four reaches, along with the results of subsequent calculations to be discussed.

Table 5-11. Steady State Output, Reach No. 1

Q (cfs)	VOL (acre-ft)	SA (acres)	$K_{backwards}$ (minutes)	$K_{prorated}$ (minutes)	N_o	c_k (fps)	L_u (ft)
3	0.24	0.53	--	--	--	--	--
15	0.75	0.97	--	--	--	--	--
29	1.20	1.20	22.5	21.3	27.9	2.87	131
44	1.60	1.36	20.0	18.8	23.9	3.25	153
58	1.95	1.49	17.5	16.5	22.3	3.70	164
87	2.57	1.72	15.5	15.1	18.8	4.03	195
116	3.16	1.92	14.8	14.3	16.7	4.28	220
145	3.71	2.12	13.8	13.4	15.7	4.56	234
174	4.23	2.43	13.0	13.4	15.0	4.56	245
232	5.33	3.04	13.8	13.5	13.9	4.52	263
290	6.39	3.73	13.3	13.9	13.3	4.40	276
348	7.55	4.43	14.5	14.0	13.1	4.36	281
406	8.6	4.99	13.5	13.3	13.3	4.58	277
464	9.7	5.44	13.1	14.0	12.1	4.38	304
522	10.9	6.26	14.8	14.6	11.8	4.17	312
580	12.0	7.17	14.5	13.5	13.1	4.51	279
725	14.5	8.07	12.6	11.8	13.6	5.18	270
870	16.7	8.65	11.0	10.5	13.6	5.82	269
1,015	18.7	9.03	10.0	9.9	12.9	6.18	284
1,160	20.7	9.74	9.8	9.9	12.2	6.19	300
1,450	24.7	11.21	9.9	10.1	11.0	6.05	333
1,740	28.8	12.48	10.3	9.9	10.5	6.20	350
2,030	32.5	13.73	9.4	9.7	10.0	6.31	365
2,320	36.5	14.61	9.9	9.8	9.2	6.21	399
2,610	40.4	15.36	9.8	9.2	9.2	6.63	399
2,900	43.8	15.78	8.7	8.5	9.2	7.20	398
3,190	47.2	16.17	8.3	8.3	8.8	7.34	419
3,480	50.5	16.57	8.3	8.2	8.4	7.49	437
3,770	53.7	16.95	8.0	7.7	8.4	7.95	436
4,060	56.6	17.29	7.4	--	--	--	--

L_c,	Length of Main-Channel (ft) =	3,666
S_o,	Main-Channel Slope =	0.54%
Z_r,	Vertical Drop in Bed Elevation Over Reach (ft.) =	19.8

Table 5-12. Steady State Output, Reach No. 2

Q (cfs)	VOL (acre-ft)	SA (acres)	$K_{backwards}$ (minutes)	$K_{prorated}$ (minutes)	N_o	c_k (fps)	L_u (ft)
11	1.88	4.35	--	--	--	--	--
55	5.08	4.76	--	--	--	--	--
110	7.94	5.10	37.75	34.91	10.7	3.11	610
165	10.37	5.38	32.08	30.56	8.6	3.56	759
220	12.57	5.66	29.04	29.11	7.1	3.74	917
330	16.99	7.06	29.17	28.08	6.1	3.87	1,064
440	21.08	8.20	26.99	25.74	5.8	4.22	1,119
550	24.79	8.82	24.49	23.60	5.5	4.61	1,192
660	28.23	9.26	22.70	22.44	5.0	4.84	1,296
880	34.95	10.80	22.18	22.16	4.5	4.91	1,463
1,100	41.66	12.41	22.14	22.75	4.0	4.78	1,634
1,320	48.74	16.49	23.36	27.14	3.7	4.01	1,760
1,540	58.1	24.92	30.92	35.15	3.7	3.09	1,760
1,760	70.0	34.09	39.37	39.68	3.9	2.74	1,660
1,980	82.2	39.83	40.00	38.91	4.2	2.79	1,567
2,200	93.6	44.77	37.82	36.74	4.5	2.96	1,463
2,750	120.6	54.83	35.67	35.05	4.6	3.10	1,424
3,300	146.7	62.18	34.43	33.23	4.6	3.27	1,429
3,850	171.0	66.23	32.04	30.76	4.5	3.53	1,449
4,400	193.3	68.44	29.49	28.65	4.4	3.79	1,493
5,500	235.5	73.16	27.82	26.51	4.0	4.10	1,615
6,600	273.7	75.62	25.19	24.41	3.8	4.45	1,726
7,700	309.5	77.72	23.63	23.06	3.5	4.72	1,851
8,800	343.5	79.84	22.49	22.09	3.3	4.92	1,973
9,900	376.4	82.12	21.69	22.22	3.0	4.89	2,171
11,000	410.9	85.61	22.75	21.50	2.9	5.06	2,238
12,100	441.5	87.23	20.25	20.05	2.9	5.42	2,253
13,200	471.6	90.47	19.85	20.58	2.7	5.28	2,433
14,300	503.9	92.85	21.32	20.24	2.6	5.37	2,525
15,400	532.9	95.06	19.15	--	--	--	--

L_{mc},	Length of Main-Channel (ft) =	6,523
S_o,	Main-Channel Slope =	0.17%
Z_r,	Vertical Drop in Bed Elevation Over Reach (ft.) =	11.1

Table 5-13. Steady State Output, Reach No. 3

Q (cfs)	VOL (acre-ft)	SA (acres)	$K_{backwards}$ (minutes)	$K_{prorated}$ (minutes)	N_o	c_k (fps)	L_u (ft)
24	4.01	6.73	--	--	--	--	--
120	10.30	7.52	--	--	--	--	--
240	16.04	8.21	34.73	32.19	11.6	3.70	617
360	20.94	8.73	29.65	28.04	9.4	4.25	758
480	25.31	9.17	26.44	25.08	8.3	4.75	861
720	33.15	9.95	23.72	22.85	6.6	5.21	1,085
960	40.42	10.81	21.99	21.66	5.7	5.50	1,262
1,200	47.47	11.54	21.33	21.57	4.9	5.52	1,471
1,440	54.68	12.44	21.81	20.98	4.5	5.68	1,593
1,920	68.00	13.30	20.15	19.53	3.9	6.10	1,849
2,400	80.50	14.51	18.91	19.43	3.4	6.13	2,108
2,880	93.69	18.54	19.95	21.54	3.3	5.53	2,194
3,360	109.0	28.26	23.13	26.09	3.5	4.57	2,035
3,840	128.2	38.28	29.06	30.27	3.6	3.94	1,991
4,320	149.0	46.10	31.48	32.69	3.6	3.64	2,009
4,800	171.4	56.50	33.91	32.72	3.9	3.64	1,824
6,000	223.6	62.35	31.54	29.89	3.8	3.99	1,887
7,200	270.2	67.78	28.25	27.10	3.8	4.40	1,888
8,400	313.2	70.06	25.96	25.23	3.6	4.72	1,984
9,600	353.6	73.07	24.49	23.52	3.5	5.07	2,027
12,000	428.2	78.55	22.55	21.67	3.3	5.50	2,171
14,400	496.9	80.77	20.79	20.17	3.0	5.91	2,359
16,800	561.5	82.39	19.55	19.27	2.8	6.18	2,577
19,200	624.3	84.25	18.99	18.40	2.6	6.48	2,750
21,600	683.1	85.78	17.80	17.12	2.5	6.96	2,827
24,000	737.5	86.95	16.43	16.11	2.5	7.39	2,917
26,400	789.7	88.12	15.79	15.57	2.3	7.65	3,059
28,800	840.4	89.35	15.34	15.09	2.2	7.90	3,189
31,200	889.4	90.53	14.83	14.65	2.2	8.13	3,312
33,600	937.3	91.74	14.47	--	--	--	--

L_{mc},	Length of Main-Channel (ft) =	7,149
S_o,	Main-Channel Slope =	0.21%
Z_r,	Vertical Drop in Bed Elevation Over Reach (ft.) =	15.0

Table 5-14. Steady State Output, Reach No. 4

Q (cfs)	VOL (acre-ft)	SA (acres)	$K_{backwards}$ (minutes)	$K_{prorated}$ (minutes)	N_o	c_k (fps)	L_u (ft)
36	9.99	11.01	--	--	--	--	--
180	26.36	12.38	--	--	--	--	--
360	40.59	13.34	57.39	52.90	4.4	3.21	2,341
540	52.59	14.09	48.40	46.40	3.5	3.66	2,916
720	63.60	14.88	44.41	42.06	3.1	4.04	3,337
1,080	83.29	16.02	39.71	38.15	2.4	4.46	4,217
1,440	101.43	17.10	36.58	35.94	2.1	4.73	4,962
1,800	118.93	18.26	35.29	35.59	1.8	4.78	5,754
2,160	136.73	19.73	35.90	34.88	1.6	4.87	6,262
2,880	170.32	23.71	33.87	44.48	1.2	3.82	8,859
3,600	224.95	54.30	55.09	59.35	1.6	2.86	6,452
4,320	288.04	81.33	63.62	64.25	1.8	2.65	5,596
5,040	352.4	94.83	64.89	65.37	1.8	2.60	5,697
5,760	417.7	102.70	65.84	64.51	1.7	2.64	5,933
6,480	480.3	106.12	63.17	62.04	1.6	2.74	6,212
7,200	540.8	108.36	60.91	59.94	1.6	2.84	6,531
9,000	686.9	116.60	58.96	61.23	1.3	2.78	7,750
10,800	844.4	164.36	63.49	68.19	1.4	2.49	7,348
12,600	1,025.1	204.73	72.89	70.36	1.4	2.42	7,101
14,400	1,193.3	216.50	67.83	65.16	1.4	2.61	7,106
18,000	1,503.1	240.26	62.48	60.93	1.4	2.79	7,485
21,600	1,797.5	268.25	59.37	57.47	1.3	2.96	7,588
25,200	2,073.0	281.21	55.57	54.07	1.3	3.14	7,946
28,800	2,333.8	289.28	52.58	51.12	1.2	3.33	8,345
32,400	2,580.0	294.42	49.65	47.98	1.2	3.54	8,659
36,000	2,809.7	299.49	46.31	45.57	1.1	3.73	8,983
39,600	3,032.0	303.38	44.83	44.01	1.1	3.86	9,420
43,200	3,246.1	306.80	43.18	42.40	1.0	4.01	9,789
46,800	3,452.4	310.54	41.61	44.66	0.9	3.81	11,036
50,400	3,689.0	315.46	47.70	--	--	--	--

L_{mc},	Length of Main-Channel (ft) =	10,199
S_o,	Main-Channel Slope =	0.084%
Z_r,	Vertical Drop in Bed Elevation Over Reach (ft.) =	8.6

The value for volume (*VOL*) and surface area (*SA*) for each corresponding steady-state discharge (*Q*) were taken directly from the "*Volume*," "*SA Total*" and "*Q Total*" variables in the HEC-RAS output reporting function. These variables give an accumulated total beginning from the downstream-most section of a defined HEC-RAS reach. The surface area calculations are based on the average top width and distance between sections, and the volume calculation is based on the average end areas and distances. The areas of the main channel and each overbank are calculated separately, based on the channel and overbank distances specified. In this study, each modeled stream reach corresponds to a separate HEC-RAS reach and the results from the HEC-RAS outputs were used directly. If the limits of a HEC-RAS reach had not corresponded exactly to the desired routing reach for unsteady modeling, the cumulative value of volume and surface area at the beginning and ending nodes could have been output and the difference calculated.

The value of *K*, which represents the rate of change in volume relative to discharge, is then approximated from the tabular values. *K* was originally defined in Eq. (3-29) as:

$$K = \frac{dVOL}{dQ} \tag{3-29}$$

The simplest estimate of K would be a linear finite difference between successive values in the table, as shown in Eq. (3-36). For a given discharge Q_i in the table, if the finite difference were backwards-looking, the estimate of K_i at that given discharge would be:

$$K_{backwards,i} \approx \frac{VOL_i - VOL_h}{Q_i - Q_h} \qquad (5\text{-}2)$$

and a forward-looking finite difference would be similar:

$$K_{forwards,i} \approx \frac{VOL_j - VOL_i}{Q_j - Q_i}$$

where the subscripts *h*, *i* and *j* indicate three successive lines of table entries, arranged from lowest to highest discharge. It is simple to note that $K_{forwards,i} = K_{backwards,j}$.

K is generally nonlinear, and so there will typically be a difference between the backward and forward difference estimates. If the table contained tightly spaced intervals of discharge, the difference may be negligible. For the tables developed in this study, only 30 discharge points were selected to describe the interval up to 100-year flows. From inspection of tables and graphs, it cannot be assumed that the differences are negligible.

A localized estimate of K for any given discharge in the tabular data could be made by assuming a smooth rate of transition and prorating the results from backwards-looking difference schemes for two successive entries in the table. Three primary assumptions are made: (1) the value of $K_{backward,i}$ is a reasonable estimate of the local value of *K* at discharge that is midway between the Q_h and Q_i; (2) that the value of $K_{backward,j}$ is a reasonable estimate of the local value of *K* at a discharge midway between Q_i and Q_j; and (3) that the rate of change in *K* is uniform between these two midpoints, i.e. that

$$\frac{dK}{dQ} = \frac{d^2VOL}{dQ^2} = Constant$$

If these assumptions are valid, then the prorated estimate of K for discharge Q_i is given by

$$K_{prorated,i} \approx K_{backwards,i} + \left(K_{backwards,j} - K_{backwards,i}\right)\left(\frac{\left(Q_i - Q_h\right)/2}{\left(Q_j - Q_h\right)/2}\right)$$

$$K_{prorated,i} \approx K_{backwards,i} + \left(K_{backwards,j} - K_{backwards,i}\right)\left(\frac{Q_i - Q_h}{Q_j - Q_h}\right) \qquad (5\text{-}3)$$

If the tabular values of Q are evenly spaced at intervals of ΔQ, then Eq. (5-3) reduces to a simple average the two entries,

$$K_{prorated,i} \approx \tfrac{1}{2}\left(K_{backwards,j} + K_{backwards,i}\right) \qquad (5\text{-}4)$$

In general, the tabular values exported from HEC-RAS were taken at even discharge intervals, except at few specific intervals where the spacing was adjusted. Eq. (5-3) was used to estimate the value of K for all four reaches. The tables present the appropriate value of $K_{backwards}$ for each entry as well.

A more sophisticated estimate of K might have been derived by fitting a polynomial through the *VOL* vs. Q points, with Q as the dependent variable, and then differentiating the polynomial as $\frac{dVOL}{dQ}$ directly. It was found through initial trials, however, that even a ninth-order polynomial did not generally produce a good enough fit to allow for successful derivation. The relationship of K vs. Q contains at least three distinct regions with sharp changes between them, as will be seen on the final plots. It was assumed that localized accuracy for the estimate of K is probably most important for the purposes of this study, and that the use of Eq. (5-3) was adequate.

The value for optimal number of sub-reaches N_o was then calculated using Eq. (3-39).

$$N_o = \left(\frac{SA}{K}\right)\frac{Z_r}{Q} \tag{3-39}$$

where $Z_r = L_{mc}(S_o)$ is total vertical drop in main-channel bed elevation over the reach, L_{mc} is the main-channel length, which is used as the reference length, and S_o is the bed slope, which is used as an estimate of the average water surface slope across the channel during steady-state conditions.

Once K and N_o are determined, the effective value for c_k and L_u are calculated using Eqs. (3-40) and (3-41).

$$c_k = \frac{L_{mc}}{K} \tag{3-40}$$

$$L_u = \frac{L_{mc}}{N_o} \tag{3-41}$$

5.7 Preparation of the 8-Point Equivalent Reaches

The variable-parameter Muskingum-Cunge (VMC) option within HEC-1 requires the specification of an equivalent reach based on a non-meandering alignment and a simplified, representative cross-section to evaluate the varying coefficients. The most appropriate option for floodplain routing in HEC-1 uses an *"eight-point (8-pt.) section."* An equivalent reach based on an 8-pt. section can be derived using the tabular reach data.

In HEC-1, an 8-pt. section is specified using eight pairs of station/elevation coordinates. Four of the coordinates define the main-channel, and the two additional coordinates on each side define the left and right overbank. The equivalent reach is assumed to be non-meandering, with the same the flow path lengths in the main-channel and each overbank. Separate roughness factors are specified for the main-channel and each overbank (USACE 1998).

Based on the derivation in Chapter 4, an acceptable 8-pt. equivalent reach for unsteady modeling is one that produces similar values of c_k and L_u as found for the original, natural reach. To do this, the equivalent reach should approximate the natural reach over the range of discharges for each of the following variables: surface area (*SA*), storage volume (*VOL*), and the rate of change in volume with respect to change in steady-state discharge (*K*). For simplicity, the equivalent reach is also generally assumed to have the same length and bed slope as the main-channel of the natural reach.

It was assumed that adequate resolution could be obtained with a symmetrical section. If so, the first four points of the 8-point section are then mirrored by the last four, and the same roughness values are specified in the left and right overbanks. The bottom of the channel is assumed to be flat, and the overbanks developed with two regions, an overbank bench which is typically flat, bounded by a steeper valley wall that continues upwards to fully contain the range of discharges modeled.

The cross-sectional geometry of this type of section could be specified completely by a set of four widths and three depths, as shown in Figure 5-35. The

location of the 8 specified cross-sectional coordinate points are also shown, labeled a through h.

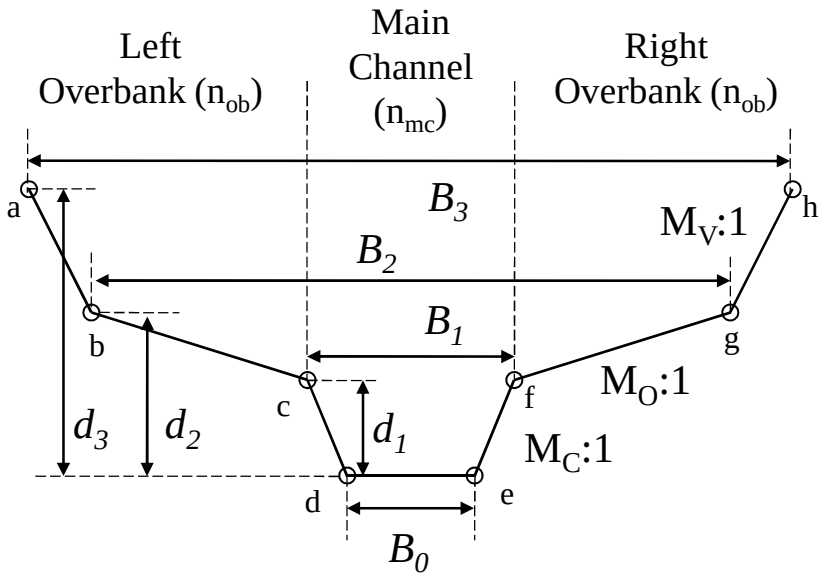

Figure 5-35. Dimensions for a Symmetrical 8-Pt. Cross-Sections

The three depths correspond to the depth of flow in the main-channel at each of three key conditions: bankfull flow in the main-channel (d_1), flow that just begins to reach the toe of the valley wall after inundating the overbank bench (d_2) and an arbitrarily selected deeper flow (d_3) that is bounded by the valley walls. The four widths correspond to the bottom width of the main-channel (B_0), and the top widths B_1, B_2, and B_3 that correspond to each of the three specified depths above.

From these seven variables, the side slopes of the three vertical regions on each section can be calculated. Those three slopes are the side slope of the main-

channel (M_C), the slope of the overbank bench (M_O) and the slope of the valley walls (M_V).

The geometry and hydraulic characteristics of the reach can then be completed by specifying the reach length of the main-channel, L_{mc}, the bed slope S_o of the main-channel, and the Manning's roughness coefficients for the main-channel (n_{mc}) and overbanks (n_{ob}) areas.

To illustrate how the tabular data from the natural reach can be used to specify this 8-pt. section, a detailed example for Reach No. 3 is presented below.

Initially a plot was made of the relationship between surface area (SA) and volume (VOL) from the natural reach, based on results at the 30 steady-state values summarized previously. Figure 5-36 presents this initial graph for Reach No. 3.

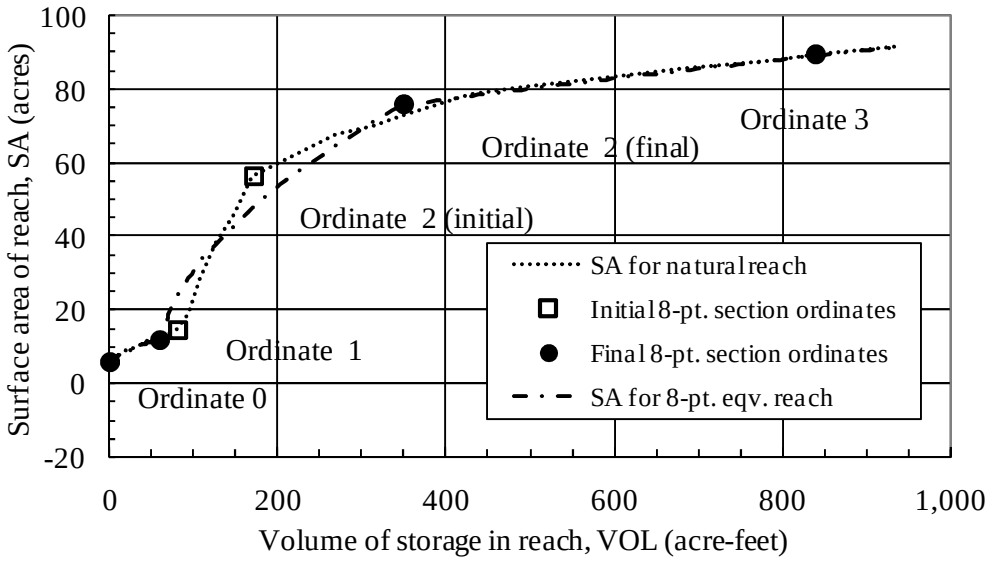

Figure 5-36. Surface Area vs. Volume Relationship for Reach No. 3

Shown on the plot are 4 separate points or ordinates, labeled 0 (zero) through 4, which are set on or near the line given for the SA vs. VOL relationship. These ordinates correspond to the breakpoints of a symmetrical 8-pt. section that would mimic the natural reach data. By dividing the reach volumes and surface areas by the channel length, the equivalent cross-sectional areas (XA_i) and top widths (B_i) associated with each ordinate can be derived. The relationship between XA_i and B_i are then used to dictate the necessary values of the depths of flow at each breakpoint, d_1, d_2, and d_3.

Ordinates 0 and 1 are very distinct on the graph, and should correspond to the exposed bottom width of the channel and the condition of "bankfull" flow, respectively. Ordinate 3 is an arbitrarily chosen upper limit, and Ordinate 2 is approximately located to give a good fit to the curvature of the surface area vs. volume graph. These ordinates are used to derive the geometry of a representative 8-pt. cross-section. All four of the ordinates require some trial and error to obtain a good approximation of the overall relationships, and the final ordinate selected will not necessarily fall directly on the underlying plot of the natural reach data. The graph shows the final location of all four ordinates, along with the initial trial values for Ordinates 1 and 2. Also shown on the graph is the SA vs. VOL relationship of the final version of the equivalent reach.

The final four ordinates selected and the associated calculations to derive the 8-pt. section for Reach No. 3 are summarized in Table 5-15.

Table 5-15. Example Calculation of 8-Pt. Equivalent Reach Geometry, Reach No. 3

Plotted Ordinates on the SA vs. VOL Plot, Used to Derive 8-Pt. Section			Calculation of 8-Pt. Section Shape					
Ord-inate, *i*	Surface Area, SA (acre)	Vol-ume, VOL (acre-ft)	Width, B (feet)	Cross-Section-al Area, XA (sf)	Change in XA over interval *i*-1 to i	Aver-age Width over interval	Change in Depth over interval	Total Depth, d (feet)
0	6.0	0.0	36.6	0.0				0.00
1	12.0	60.0	73.1	365.6	365.6	54.8	6.67	6.67
2	76.0	350.0	463.1	2,133	1,767	268.1	6.59	13.26
3	89.4	840.4	544.4	5,121	2,988	503.8	5.93	19.19
Channel Length = 7,149 feet								

Ordinate 0 corresponds to the bottom width when the flow depth is zero. Dividing the surface area at Ordinate 0 by the representative length gives the bottom width:

$B_0 = SA_0/L_{mc}$ = (6.0 acre/7149 ft)(43560 sf/acre) = 36.6 ft

Ordinate 1 is labeled where there is a dramatic change in slope of the surface area versus volume line. This change in slope represents the top of the main-channel and the beginning of overbank flow, as a small increase in flow depth in this range adds significantly more surface area relative to volume than was the case for lower depths. Ordinate 1, therefore, represents the "bankfull" condition.

Ordinate 1 was initially located at the actual breakpoint in the natural reach data, but it was found that a good overall fit of the region between Ordinates 1 and 2 could not be made. It was also found that relationships for Q, c_k, and L_u, to be

discussed later, were not as good when these initial values were used. For these reasons, Ordinate 1 was moved to the left and Ordinate 2 to the right. The top width of the main-channel is therefore dictated by the surface area at the final location of Ordinate 1, as follows:

$$B_1 = SA_1 / L_{mc} = (12.0 \text{ acre}/7149 \text{ ft})(43560 \text{ ft}^2/\text{acre}) = 73.1 \text{ ft}$$

The cross-sectional area of the main channel is determined based on the volume stored in the reach:

$$XA_1 = VOL_1 / L_{mc}$$

$$XA_1 = (60.0 \text{ acre-ft}/7149 \text{ ft})(43560 \text{ ft}^2/\text{acre}) = 365.6 \text{ ft}^2$$

Since top width, bottom width and area are known, the depth (d_1) of the main-channel can be determined:

$$XA_1 = (1/2)(d_1)(B_0+B_1)$$

$$365.6 \text{ ft}^2 = (1/2)(d_1)(36.6 \text{ ft} + 73.1 \text{ ft})$$

$$d_1 = 6.67 \text{ ft.}$$

At flows above bankfull (Ordinate 1), the surface area versus volume graph initially becomes very steep. Eventually, the steepness of the graph abates, which is interpreted as occurring when the flow eventually reaches the end of the flattened overbank surface and encounters the valley walls. The transition at the valley wall is much less abrupt that the change at bankfull, and a distinct breakpoint may not always exist. To specify the overbank geometry, two additional breakpoints are set: the toe of the valley wall (Ordinate 2); and an arbitrary upper limit along the valley wall that sets its slope (Ordinate 3).

The initial estimate for Ordinate 2 did not give a good fit to the overall set of relationships, and it was moved to the right, as discussed previously. The top width and total volume at Ordinate 2, based on the final location, are given similarly as before:

$$B_2 = SA_2 / L_{mc} = (76.0 \text{ acre}/7149 \text{ ft})(43560 \text{ ft}^2/\text{acre}) = 463.1 \text{ ft}$$

$$XA_2 = VOL_2 / L_{mc} = (350.0 \text{ acre-ft}/7149 \text{ ft})(43560 \text{ ft}^2/\text{acre}) = 2133 \text{ ft}^2$$

To find d_2, the following relationship is established for the incremental change in cross-sectional area:

$$(XA_2 - XA_1) = (1/2)(B_2 + B_1)(d_2 - d_1)$$

$$(2133 \text{ ft}^2 - 365.6 \text{ ft}^2) = (1/2)\,(463.1 \text{ ft} + 73.1\text{ft})(\, d_2 - 6.67)$$

$$d_2 = 13.26 \text{ ft.}$$

The top width, cross-sectional area, change in cross-sectional area and total depth at Ordinate 3 are calculated in a similar fashion, as summarized in Table 5-15.

Once the shape of the 8-pt. section has been established, Manning's formula is applied to calculate the discharge for the section at various depths. The objective of this step is to match the relationship between discharge (Q) and volume (VOL) between the 8-pt. equivalent section and the natural reach. Total discharges are calculated separately for the main channel and the two overbank subsections, and then added together.

The main-channel length and slope are given, so the only two variables that can be adjusted to provide this match are the Manning's roughness values in the

main-channel (n_{mc}) and the overbanks (n_{ob}). These values are arrived at through an iterative trial-and-error process.

A summary of the discharge calculations for the 8-pt. section representing Reach No. 3 is shown in Table 5-16. Calculations are provided for three specific depths, based on the final values chosen for the roughness coefficients. Discharges for each subsection are calculated using Manning's formula, using a form of the equation similar to Eq. (3-7) for English units:

$$Q = \frac{1.486}{n} A \left(\frac{A}{P_w} \right)^{2/3} (S_o)^{1/2} \qquad (5\text{-}5)$$

where Q is the discharge (in cfs) for the subsection, n is Manning's roughness coefficient, A is the cross-sectional area (in ft^2), P_w is the wetted perimeter, and S_o is the bed slope of the channel, which is used as friction slope for steady, uniform flow.

The average velocity (V) in each subsection is $V = \frac{Q}{A}$. The surface area and volume calculations for the equivalent reach are based on the main-channel length and the top widths and cross-sectional areas at each discharge. The full tables developed for this study used very small depth increments, so the simple backwards-looking finite difference scheme in Eq. (5-2) was used to approximate K. The values for c_k and L_u were then calculated using Eqs. (3-39) through (3-41).

Table 5-16. Example of Discharge Calculations for the 8-Pt. Equivalent Reach, Reach No. 3

Total Flow Depth, y (feet)	**6.67**	**12.80**	**18.05**
Reach Properties, Common to All Depths			
Length of Main-Channel, L_{mc} (ft)	7,149	same	same
Bed Slope, S_o	0.21%	same	same
Manning's n for Main-Channel, n_{mc}	0.050	same	same
Manning's n for Overbanks, n_{ob}	0.062	same	same
Hydraulic Calculations for the Main Channel			
Flow Depth, y_{mc} (ft)	6.67	12.80	18.05
Top Width, T_{mc} (ft)	73.1	73.1	73.1
Wetted Perimeter, $P_{w,mc}$ (ft)	75.5	75.5	75.5
Flow Area, A_{mc} (ft)	366	814	1,198
Discharge, Q_{mc} (ft)	1,427	5,416	10,313
Velocity, V_{mc} (ft/s)	3.90	6.65	8.61
Hydraulic Calculations for One Overbank			
Flow Depth, y_{ob} (ft)	0	6.13	11.38
Top Width, T_{ob} (ft)	0	181.4	227.8
Wetted Perimeter, $P_{w,ob}$ (ft)	0	181.5	228.3
Flow Area, A_{ob} (ft)	0	556	1,655
Discharge, Q_{ob} (ft)	0	1,288	6,814
Velocity, V_{ob} (ft/s)	0	2.32	4.12
Hydraulic Properties of Total Section (Main Channel plus Both Overbanks)			
Top Width, T (ft)	73.1	435.9	528.8
Flow Area, A (ft)	366	1,926	4,508
Discharge, Q (cfs)	1,427	7,993	23,941
Average Velocity, V (ft/s)	3.90	4.15	5.31
Volumetric Properties of Reach			
Surface Area, SA (acres)	12.0	71.5	86.8
Volume, VOL (acre-ft)	60.0	316.1	739.9
Unsteady Flow Routing Properties of Reach			
Kinematic Wave Speed, c_k (ft/s)	5.5	4.4	7.4
Characteristic Reach Length, L_u (ft)	1,697	1,975	2,931

To arrive at the final values for the roughness coefficient, the relationship between reach volumes and discharges were plotted over the entire range of discharges. This plot is best shown in combination with the surface area vs. volume data discussed previously. A combination plot in this format will be referred to as a *"Volume-Surface-Discharge Plot"* or *"VSQ plot."* The x-axis of the graph shows volume (*VOL*), while two separate variables are plotted on the y-axis: surface area (*SA*) and discharge (*Q*). The VSQ plot for Reach No. 3 is shown in Figure 5-37. The data for the 8-pt. reach in this plot reflect the final values chosen for the Manning's roughness.

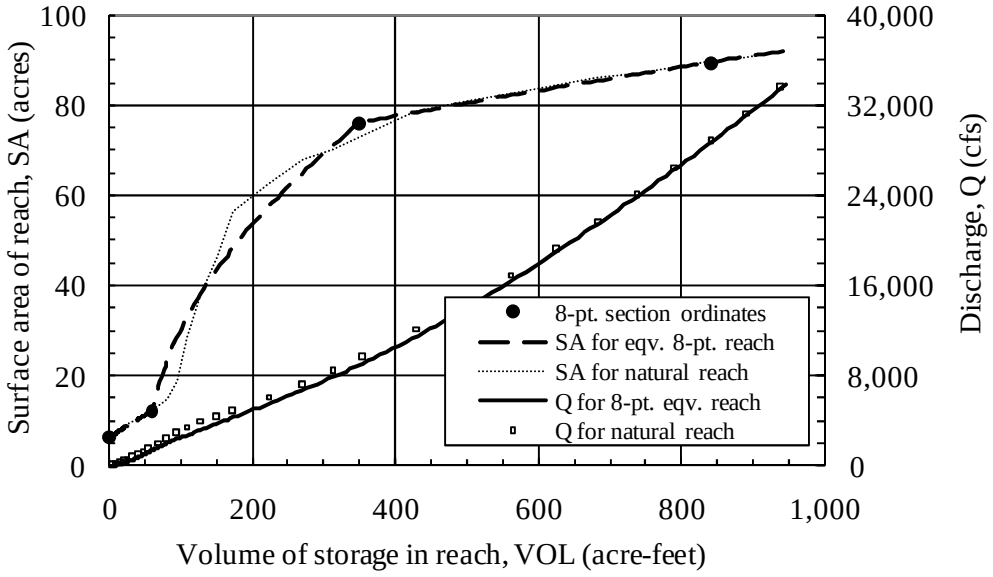

Figure 5-37. VSQ Plot, Reach No. 3

The main-channel roughness is established first to provide a good fit of volume versus discharge line for volumes between Ordinates 0 and 1. The overbank roughness is then selected to provide a good fit to the remainder of the curve. A

series of linked spreadsheets and dynamic VSQ plots were developed to allow rapid trial of roughness values.

Once the sections are established, another graphical method can be used to determine how well the 8-point cross-section matches the natural reach for the final variables of importance in river routing. A graph of discharge (Q) versus kinematic wave speed (c_k) and characteristic length (L_u) is prepared, which is referred to as the *"discharge-celerity-characteristic length plot"* or *"QCL plot"*. The QCL plot for Reach No. 3 is shown in Figure 5-38. This plot was examined as well during the trial-and-error process, and additional adjustments to the 8-pt. cross-sectional shape and the Manning's roughness factors were made to improve the fit of the lines given in the QCL plot. To the extent that a perfect fit between all four relationships could not be found, priority was given to the goodness-of-fit in the QCL plot.

The fit between the equivalent reach and the natural reach for Reach No. 3 is reasonably good. One item that is very noticeable on the QCL plot is the "surge" in values of c_k and L_u that occur around bankfull (Ordinate 1) discharge rates. This is apparently due to the sudden change in the surface area-versus-volume relationship. As discharges increase beyond bankfull, the relationship becomes much more smooth and regular, gradually increasing for both values of c_k and L_u. At discharges less than bankfull, the relationship becomes very steep, indicating large, but relatively smooth, changes in variables.

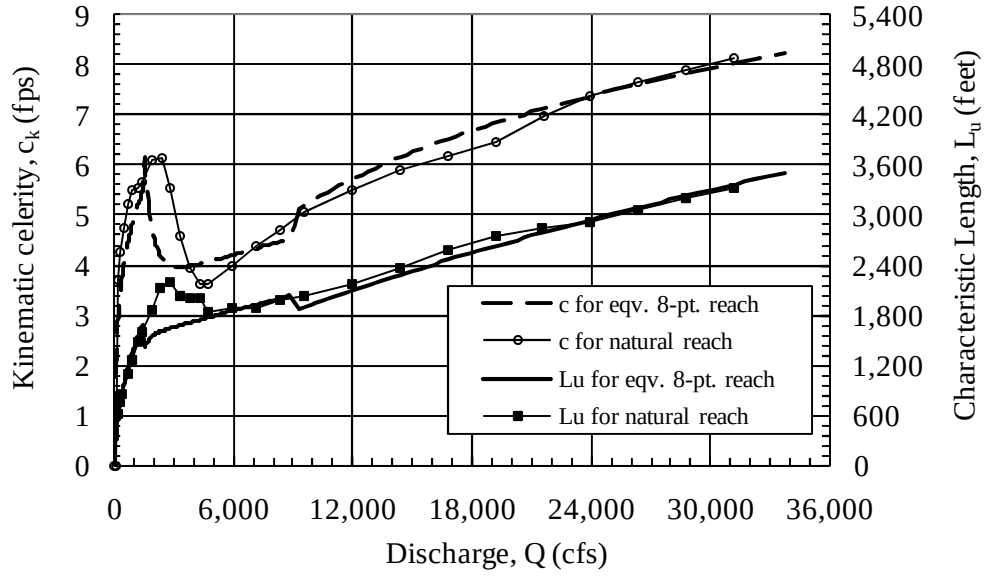

Figure 5-38. QCL Plot, Reach No. 3

A summary of the calculated properties of the 8-point cross-section for all four reaches is shown in Table 5-17. The VSQ and QCL plots for Reach Nos. 1, 2 and 4 are given in Figures 5-39 through 5-44.

Because the natural reaches are highly sinuous, the shape and roughness of the derived overbank should implicitly include an adjustment to account for the fact that the equivalent reach is non-meandering. The size of the overbank width and roughness values should not match the average widths and Manning's *n* values taken from the original HEC-RAS cross-sections. The equivalent reach should be reflect in some respect the section that would be developed using the "*modified overbank method*" discussed in Chapter 4.

Table 5-17. Summary of Geometric and Hydraulic Properties for the 8-Pt. Equivalent Reaches

Reach No.	**1**	**2**	**3**	**4**
Reach Length, L_{mc} (ft.)	3,666	6,523	7,149	10,199
Bed Slope, S_o (%)	0.54%	0.17%	0.21%	0.084%
Widths of Section at Ordinates (ft.)				
B_0	2.0	20.0	36.6	46.6
B_1	35.7	66.8	73.1	136.7
B_2	163.1	442.3	463.1	1,200
B_3	205.4	643.2	544.1	1,358
Depths of Section at Ordinates (ft.)				
d_1	4.03	5.85	6.67	12.59
d_2	7.15	9.34	13.26	24.11
d_3	8.70	14.14	19.19	30.15
Calculated Side Slopes, M:1 (Horizontal to Vertical)				
Main-Channel, M_C	4.17	4.00	2.74	3.58
Overbank Surface, M_O	20.4	53.8	29.6	46.2
Valley Wall, M_V	13.6	20.9	6.86	13.1
Manning's n for Equivalent Reach, as Fitted				
Main-Channel, n_{mc}	0.048	0.040	0.050	0.055
Overbank, n_{ob}	0.042	0.053	0.062	0.090
Surface Area of Section at Ordinates (acres)				
SA_0	0.17	3.00	6.00	10.9
SA_1	3.00	10.0	12.0	32.0
SA_2	13.7	66.2	76.0	281
SA_3	17.3	96.3	89.4	318
Volume of Section at Ordinates (acre-ft.)				
VOL_1	6.39	38.0	60.0	270
VOL_2	32.20	171.0	350.0	2,073
VOL_3	56.66	561.4	840.4	3,881
Discharge of Section at Ordinates (cfs)				
Q_1	281	935	1,427	3,684
Q_2	1,959	3,865	8,919	24,900
Q_3	4,015	16,500	28,590	54,260

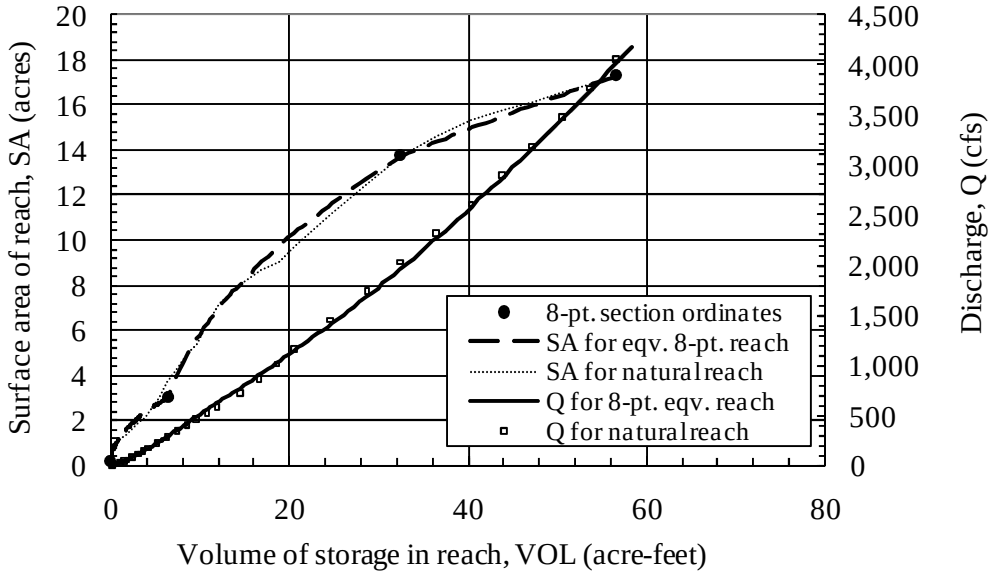

Figure 5-39. VSQ Plot, Reach No. 1

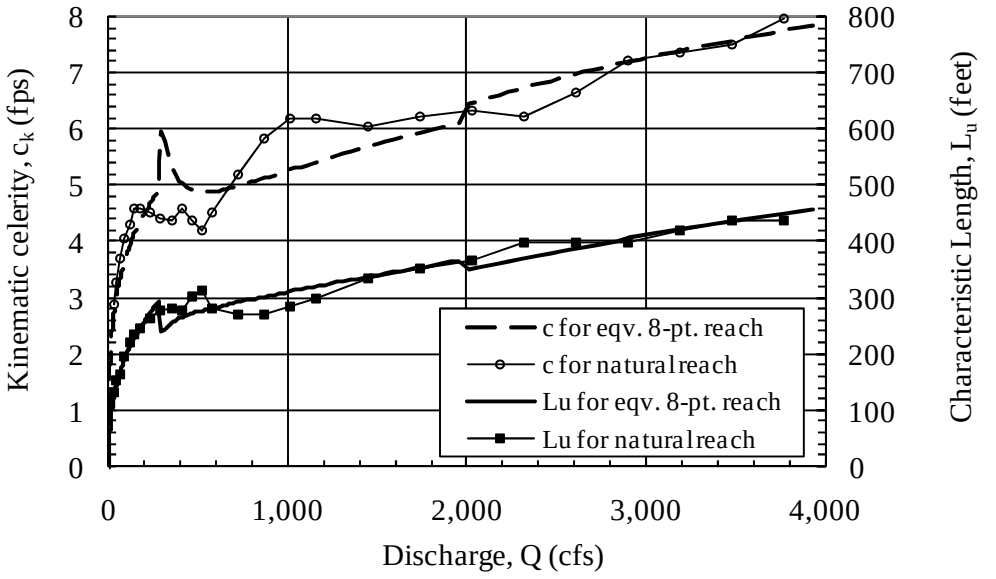

Figure 5-40. QCL Plot, Reach No. 1

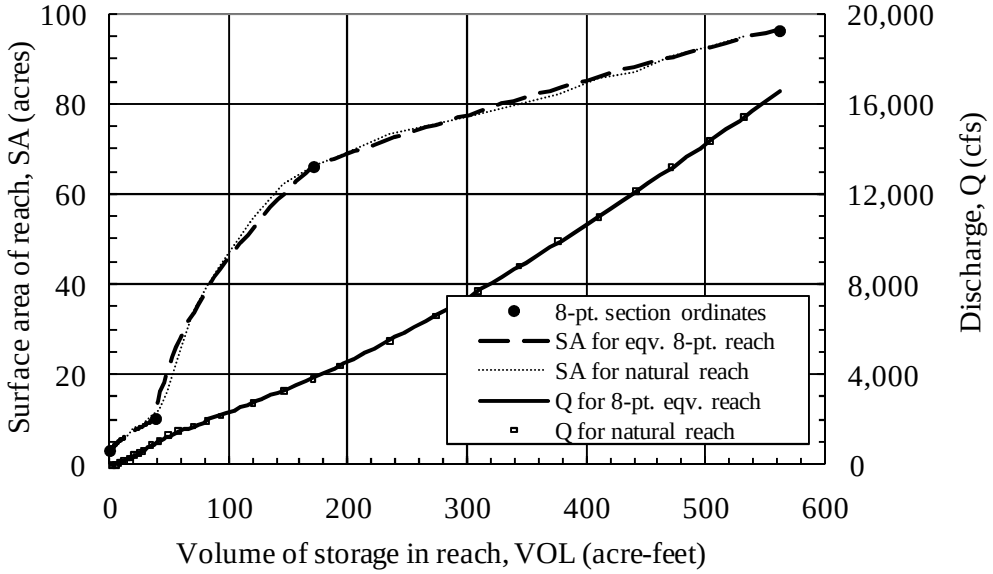

Figure 5-41. VSQ Plot, Reach No. 2

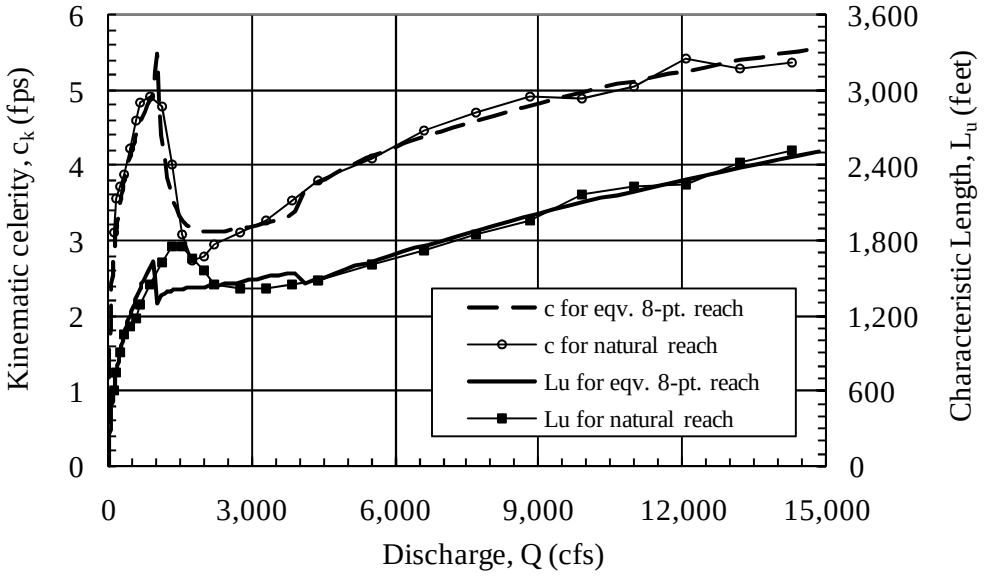

Figure 5-42. QCL Plot, Reach No. 2

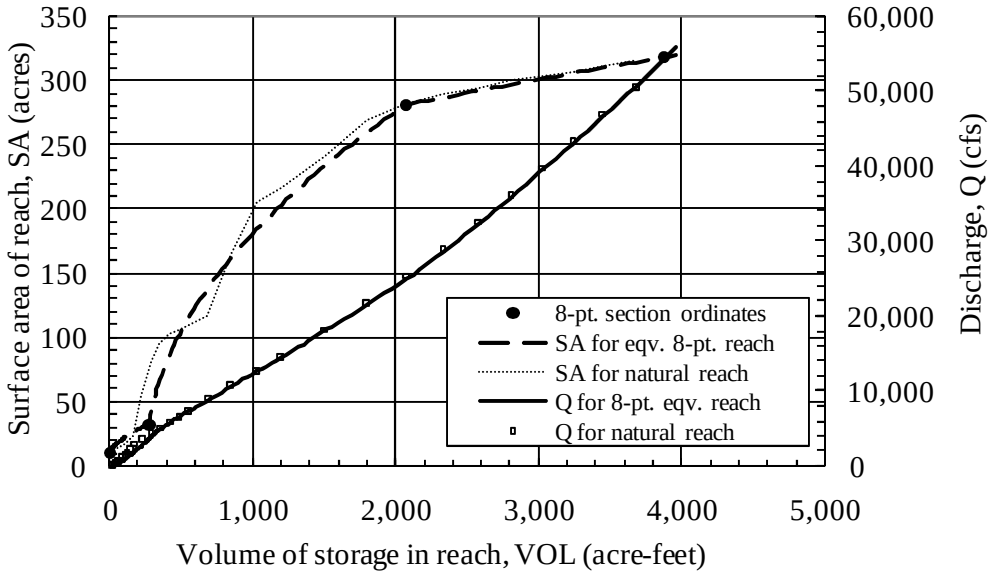

Figure 5-43. VSQ Plot, Reach No. 4

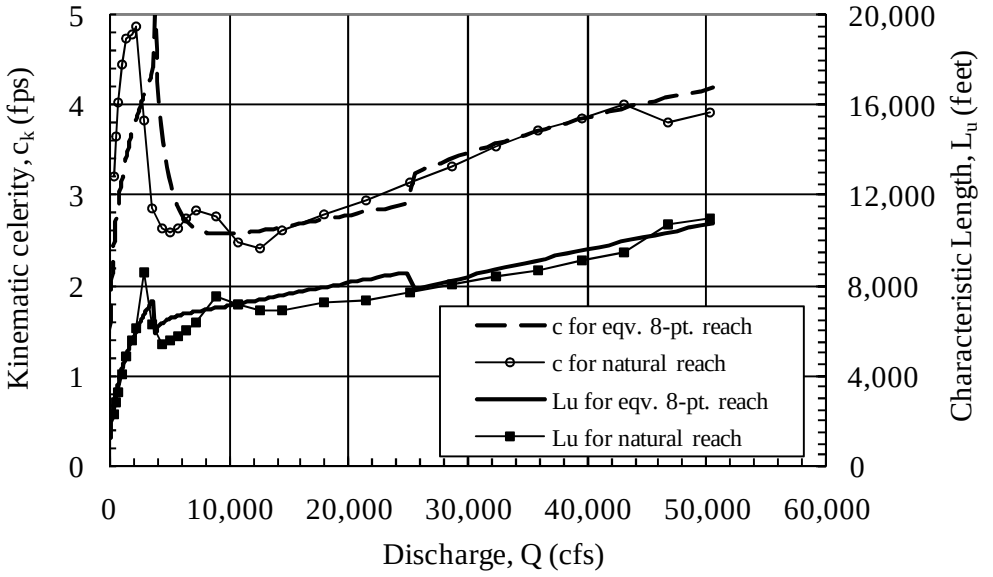

Figure 5-44. QCL Plot, Reach No. 4

In particular, the overbank roughness coefficients should be lower in the equivalent reach than used in the original HEC-RAS sections. Eq. (4-21) predicted that the modified roughness coefficient for the overbank (n_{obe}) should take on the following value,

$$n_{obe} = \frac{n_{ob}}{(SN)^{3/2}} \tag{4-21}$$

where SN is the sinuosity of the reach and n_{ob} is the roughness in an original prismatic 8-pt. section for which separate main-channel and overbank lengths and slopes were specified. The main-channel roughness found in the equivalent reach should be close to that specified for the natural reach, since the main-channel length was used as the reference condition in the equivalent reach. Table 5-18 presence a comparison of these roughness values.

Table 5-18. Comparison of Roughness Values, Natural vs. 8-Pt. Equivalent Reaches

Reach No.	**1**	**2**	**3**	**4**
Apparent Sinuosity, *SN*	1.73	1.52	1.38	1.36
Overbank Roughness, n_{ob}				
in Natural Reach Model	0.1000	0.1000	0.1000	0.1000
Predicted for Eqv. Reach Model, using Eq. (4-21)	0.0439	0.0534	0.0617	0.0631
Fitted for Eqv. Model	0.0420	0.0530	0.0620	0.0900
Relative Difference, Fitted vs. Predicted	-4.4%	-0.7%	0.5%	42.7%
Main-Channel Roughness, n_{mc}				
in Natural Reach Model	0.0450	0.0400	0.0400	0.0400
Fitted for Eqv. Model	0.0480	0.0400	0.0500	0.0550
Relative Difference, Fitted vs. Natural	6.7%	0.0%	25.0%	37.5%

For Reach Nos. 1, 2 and 3, the fitted value for the overbank roughness falls reasonably close to the predicted values, based on the apparent sinuosity estimated for the reach. The relative error is 5% for Reach No. 1 and is less than 1% for Reach Nos. 2 and 3. The error is much more pronounced for Reach No. 4, in which the actual fitted value for overbank roughness of 0.090 is 43% greater than the predicted value of 0.631.

Regarding the main-channel roughness values, the relative errors were more variable. Reach No. 2 was found a best fit using the original main-channel roughness, whereas Reach No. 1 has an error of approximately 7%. Reach Nos. 3 and 4 have much larger relative errors, 25% and 37.5%, respectively. In all cases where there is a discrepancy, the fitted roughness values were larger than the original values used in HEC-RAS.

A complete explanation for these differences was not discovered. Possible explanations may include the error introduced by using the bed slope as the estimate for hydraulic slope at all discharge levels. From Figure 5-34 for Reach No. 4, it can be seen that the water surface slope at high discharges is slightly flatter than at the low flows. Another explanation might include the impact of expansion and contraction losses, which are calculated separately in the original HEC-RAS model and which increase the effective losses of the channel, but which are not considered separately in the equivalent reach.

In general, it appears from the fitted data that some consideration of channel sinuosity must be made when developing “representative” sections based on a non-

meandering template. Eq. (4-21) appeared to provide a strong prediction for three of the four channels included in this study, but did not do well in predicting the value needed for Reach No. 4. Further research in this area is warranted.

Chapter 6

Application to Natural Streams

6.1 Testing Program for Natural Stream Reaches

To evaluate the effectiveness of the different flood routing methods, a series of numeric tests were run on the four stream reaches described in the previous chapter. The following computer models were used in these tests, with abbreviated designations that are used herein for all further discussions. (General information about each model was provided in Chapters 2 and 3.)

uRAS - The full-dynamic unsteady flow solver found in the Hydrologic Engineering Center's HEC-RAS model, using either the equivalent 8-pt. reaches developed in Chapter 5 or the original, natural reach geometry for input.

FLW - The National Weather Service FLDWAV model, using the implicit fully dynamic routing solution, based on the equivalent 8-pt. reaches.

VMC - The Variable-parameter Muskingum-Cunge method in the Hydrologic Engineering Center's HEC-1, using an equivalent 8-pt. reach.

CR - Cascading Reservoirs method, implemented using the modified-Puls option for channel routing in HEC-1. The equivalent reach based on 8-pt. cross-sections was used to populate the volume-discharge table, and the characteristic reach length at a reference flow of 2/3 the peak inflow was used to calculate the number of hypothetical subreservoirs.

Three rounds of testing were conducted and are described below.

6A – Comparison of uRAS and FLW - All four reaches were tested using uRAS and FLW to examine and validate the performance of the fully dynamic solvers. The baseline inflow hydrograph was used and outflow observations were recorded for eight routing lengths. All comparisons used the equivalent 8-point reach derived in Chapter 5.

6B - Comparison of VMC and CR to uRAS - The same testing program from Round 6A was extended to include VMC and CR methods, with comparison to the uRAS solution as the benchmark.

6C - Comparing uRAS Results on Natural Reach Data vs. the Equivalent Reach - A direct comparison of routing results in uRAS was made between the complex, natural reach data and the equivalent 8-pt. reaches analyzed in Round 6A. All four reaches were compared using the baseline inflow scenario. The effective length of routing in the natural reach was extended by iterative routing. Observations were recorded at the downstream end of the natural reach and at various multiples of further distance. Comparable locations on the equivalent reach were observed.

In general, uRAS was selected as the reference model, because it provides a solution to the fully dynamic equations and generally provides more convenient and robust utilities for output analyses.

Details regarding the methodology, results, and testing criteria for each round are presented in the following sections.

6.2 Comparison of uRAS and FLW (Testing Round 6A)

The four reaches were tested in Round 6A using uRAS and FLW. The goal of this round was to evaluate the performance of both fully dynamic solution methods. The following subsections explain the methodology and setup of each model. The set-up for Reach No. 3 is explained in detail as an example. Results are then presented and analyzed. For each of these models, the geometry was defined by the equivalent reach, based on non-meandering 8-pt. sections.

6.2.1 Geometric and Hydrologic Parameters (Round 6A)

In Round 6A, all four reaches are modeled as simple 8-pt. cross-sections, using the dimensions defined in Chapter 5. The total modeling length for each reach was extended to extreme distances to ensure that the inflow was routed to produce at least 50% attenuation.

Downstream observation locations were then established within that reach. Initial testing showed that a geometric progression of observation locations provided the easiest means of comparison. To simplify model development and comparison among reaches, a master sequence of observation location intervals was established, with each reach being evaluated over a sequence of 8 locations. For Reach No. 2 and Reach No. 3, the observation locations were set at 2,500 feet, 5,000 feet, 10,000 feet,

20,000 feet, 40,000 feet, 80,000 feet, 160,000 feet, and 320,000 feet downstream of the inflow location. This represents a total routing distance of 60.6 miles.

For Reach No. 1, the interval was shifted down one increment, with the observation location at 320,000 deleted and an observation location added at 1,250 feet. For Reach No. 4, the interval was shifted up one increment, with observations beginning at 5,000 feet and ending at 640,000 feet. These adjustments allowed for an efficient observation of routing results for each reach.

In setting these lengths, attention was paid to the characteristic reach length, L_u, determined for each reach. The modeling runs in this round were used again in Round 6B with VMC and CR methods. The ratio of the characteristic reach length to the total routing distance was calculated. Characteristic reach length was evaluated based on a discharge equal to the 100-year discharge, Q_{100}, which is also the peak inflow, I_p for the hydrograph in this testing round. Table 6-1 summarizes the observation stations established for the four reaches and the characteristic reach length ratio for each. The objective was to cover a range from 1 to 100 for the $\frac{L}{L_u}$ ratio. This objective was generally met, with minor exceptions on the lower end of Reach No. 1 and the upper end of Reach No. 4.

Table 6-1. Routing Lengths and Ratio to Characteristic Lengths, Rounds 6A and 6B

Reach No.	1	2	3	4
Total Length, L (feet)	Ratio L / L_u, for L_u Evaluated at I_p			
1,250	3.1	--	--	--
2,500	6.2	1.1	0.9	--
5,000	12	2.3	1.7	0.5
10,000	25	4.5	3.4	1.1
20,000	49	9.1	6.8	2.2
40,000	99	18	14	4.4
80,000	198	36	27	8.8
160,000	395	73	55	18
320,000	--	145	109	35
640,000	--	--	--	70
L_u (feet) at I_p	405	2,201	2,935	9,110
I_p (cfs)	2,900	11,000	24,000	36,000

The baseline inflow scenario discussed in Chapter 5 was used for each reach. The detailed model setup and methodology used in uRAS and FLW are presented in the following subsections. Table 6-2 summarizes the most important model parameters used in Testing Round 6A.

Table 6-2. Model Parameters, uRAS and FLW, Testing Round 6A

Reach No.	1	2	3	4
Inflow Hydrograph				
Peak Inflow, I_p (cfs)	2,900	11,000	24,000	36,000
Time to Peak, t_p (minutes)	36	88	124	160
Routing Parameters, Evaluated at Peak Inflow Discharge				
Kinematic Celerity, c_k (fps)	7.18	5.12	7.36	3.71
Characteristic Length, L_u (feet)	405	2,201	2,935	9,110
Time and Distance Step Analysis				
Computational Time Step, Δt (minute)	1	2	2	4
Computational Distance Step, Δx (feet)	156.25	625	625	1,250
Time Step Ratio, t_p / Δt	36	44	62	40
Distance Ratio, Δx / L_u	0.39	0.28	0.21	0.14
Total Routing Time and Distances				
Simulation Time (hours)	18	36	30	120
Station of 1st Observation Location (feet)	1,250	2,500	2,500	5,000
Total Distance to Last Obs. Location (feet)	160,000	320,000	320,000	640,000
Total No. of Computed Time Steps, N_T	1,080	1,080	900	1,800
Total No. of Computed Distance Steps, N_X	1,024	512	512	512
Matrix Size, $N_X \times N_T$	1E+06	6E+05	5E+05	9E+05
Downstream (DS) Boundary Condition				
Length of "Tail" from Last Obs. Location to Boundary	10,000	10,000	10,000	20,000
Slope Set for Normal Flow (%)	0.54%	0.17%	0.21%	0.084%

6.2.2 uRAS Model Setup (Round 6A)

An unsteady-flow HEC-RAS model (uRAS) was developed for each reach. A valid HEC-RAS model consists of a master project file and a number of subsidiary input files. For an unsteady flow model, three necessary file types are required: a *geometry* file, an *unsteady flow* file, and an *unsteady plan* file.

The geometry file contains the necessary physical description of the stream reach. The flow file describes the all flow inputs and related boundary conditions

needed for the unsteady flow analyses. A plan file designates the specific inputs to be used in an individual modeling run. A plan consists of one geometry file, one unsteady flow file, and control information such as time steps, calculations tolerances, certain variables, and output instructions. The contents of these files are illustrated in detail for Reach No. 3.

Geometry File, uRAS, Round 6A

The geometry file for Reach No. 3 consists of a series of designated 8-pt. cross-sections. Ten cross-sections are specified: one at the inflow point, 8 sections representing the 8 observation locations, and a downstream-most section where the boundary condition is applied.

The inflow cross-section was defined as “Station 0.” The uRAS model requires that all stationing increase in downstream-to-upstream order, so the other nine sections were stationed with negative numbers, based on their distance in feet from the inflow point. For Reach No. 3, this proceeds as -2500, -5000, -10000, etc.

A discharge rating curve was used as the downstream boundary condition. Downstream rating curves can produce unstable or erroneous results in their immediate vicinity. The HEC-RAS User's Manual recommends that downstream boundary conditions be applied some distance downstream from a study area to avoid introducing error in the area of interest (USACE 2002a). For Reach No. 3, the downstream-most cross-section was placed at Station -330000, which is 10,000 feet downstream of the last observation location. A visual review of the hydrographs and model simulations confirmed that this was sufficiently far downstream.

Eight pairs of station-elevation coordinates were entered at Station 0 to define the simplified 8-pt. cross-sections as described in Chapter 5. The channel flow-line elevation was set to an arbitrary elevation of 900 feet, which then established the datum for all other elevations. The station-elevation data were then copied to all other cross-sections and the elevations were adjusted based on distance between sections and the bed slope of the reach.

Bank stations, Manning's roughness values and channel lengths were then entered. The equivalent 8-pt. reaches developed in Chapter 5 are non-meandering, so the same length was entered for main channel, left overbank and right overbank.

The uRAS solver requires that a cross-section be used to represent every spatial node in the calculation. Therefore, the cross-section spacing is the same as the computational distance step, Δx, and must be relatively small. Because all of the user-defined cross-sections in the model have the same shape, the gaps between them were filled by automated interpolation (**HEC-RAS | Edit | Geometric Data | Tools | XS Interpolation**).

All models were developed with cross-sections spaced less than $\frac{L_u}{2}$, where L_u is the characteristic length evaluated at the inflow peak discharge for each reach. As discussed in Chapter 2, Perumal (1992) demonstrated that the use of distance steps longer than the characteristic reach length can result in negative inflows. The use of times steps smaller than L_u appeared to improve the stability of the models. In Chapter 7, the selection of cross-sectional spacing (distance steps), time steps, and other factors is examined in more detail.

Cross-sectional spacing was also set to ensure evenly-spaced intervals between designated observation locations. Table 6-2 summarized the spacing used for each of the four reaches. The same spacing was used for the FLW and uRAS testing in Round 6B. The spacing distance for Reach No. 3 was 625 feet.

Unsteady Flow File, uRAS, Round 6A

The unsteady flow file contains details on boundary conditions and initial conditions. The upstream boundary condition was an inflow discharge hydrograph at Station 0. For Reach No. 3, the inflow hydrograph has a peak discharge (I_p) of 24,000 cfs and a time to peak (t_p) of 124 minutes. As noted in Chapter 2, the HEC-1 User's Manual (USACE 1998) recommends that time steps be kept less than 1/20th the time to peak. For this round, a conservative criterion $\frac{t_p}{\Delta t} > 40$ was used. Table 6-2 presented the computational time steps used for all four reaches. A minor exception to the criterion was made for Reach No. 1 in order to keep the minimum time step at 1 minute.

Hydrograph ordinates were calculated separately in a Microsoft Excel™ spreadsheet, based on Eq. (5-1) and the time step specified. A baseflow value equal to 5% of the peak discharge superimposed on all hydrographs to maintain model stability. For Reach No. 3, with a 24,000 cfs peak discharge, the minimum base flow was 1,200 cfs.

The downstream boundary condition was also set as the depth under normal flow conditions, based on the overall reach slope. This condition was applied at the downstream-most cross-section, as discussed previously.

Unsteady Plan File, uRAS, Round 6A

The plan file contains control information for each individual model run. Most computational options and tolerances were left at the uRAS defaults, including the water-surface calculations tolerance (0.02 feet) and the maximum number of iterations (20). Theta (θ) is the implicit weighting factor for the spatial derivative described previously in Section 2.5.3. It was set equal to 0.6, the minimum value allowed by HEC-RAS. Further evaluation of the impact of different values of θ is found in Chapter 7.

Output formatting and post-processing options are also dictated by the plan file. Results from the uRAS solver in HEC-RAS are primarily stored in DSS format, a custom database designed for use with Corps of Engineers' water resources data (USACE 2002a). The uRAS solver only stores water-surface elevation (stage) and discharge data. More hydraulic detail can be obtained by post-processing the unsteady output. This post-processing step can be used to obtain estimates of secondary variables, such as velocities, flow area, shear stress or Froude number. The post-processing step also allows the hydrograph profiles to be examined in more detail and with the option of animating the flood wave.

6.2.3 FLW Model Setup (Round 6A)

Version 1.0.0 of the FLDWAV (FLW) model was also used to analyze test reaches. Like uRAS, a valid FLW model requires geometric data, flow data, and plan and control specifications. FLW does not include a convenient graphical interface or user-friendly input formatting. A single text-based input file is created by the user for each modeling scenario. This input file is then read by the program upon initiation, various lookup tables are generated and calculations performed. FLW is a DOS-based program.

Input/Output Structure for FLW

All input for a single FLW run is stored in a single input file. The input files for FLW are organized into structured data groups, and variables within a data group are entered in "free format." This means that they are separated by spaces; column location is not important. Also, some value must given to all variables called by a data group even if the default value is zero.

A total of 86 distinct data groups are defined, but rarely would all be used in a single model. Depending upon the data group and model setup, an individual data group may be needed once, be used multiple times, or be skipped. The program keeps track of which data groups are applicable to a project on the basis of various logical tests that are applied to inputs already logged. Unfortunately, this can mean that typographic errors in one portion of an input file can cause the program to fail in reading the input. Input files are not intuitive.

The input file requires that each data group be separated by a line of text. That intermediate line can either be blank or used for comments. For this study, a series of uniformly-styled comment lines were written to provide explanation and structure to the data input. Table 6-3 presents the input file developed in this testing round for Reach No. 3.

Once run, the output for a single run is stored to an output text file.

An explanation of the FLW input for Reach No. 3 is presented, including a description of the most relevant variables. Because FLW is not as widely known or user-friendly as the other programs in this study, detailed explanation of the input structure is provided. Full details of the input requirements are given in the FLDWAV User Documentation (Fread and Lewis 1998). Unless noted otherwise, the default recommended values were used for calculation options and tolerances.

All text above the "EOM" line is header information for the user. The "NO DESC" command instructs FLW to echo the input data in the output file. The detailed data group (DG) files then follow. Each line beginning "DG (n):" is a comment line developed for this study that explains the contents of the data group input that follows. The number in parenthesis indicates the data group identification, and the information following the colon is generally the variable name as defined for FLW. Certain variables are irrelevant for the tests conducted in this study and are omitted.

Table 6-3. FLDWAV Input File, Example for Reach No. 3

```
NWS FLDWAV Input File
Reach 3, Wolf Creek near OP
EOM
NO DESC
DG (1):  ESPY  THETA  F1    XFACT  DTHYD    DTOUT  METRIC
          .01    1       0.6    1        0.03333   0        0
DG (2):  JN  NU   ITMAX  KWARM  KLFP  NET  ICOND  IFUT3
          1    901  10       2         1      0     0        0 0 0
DG (3):  NYQD  KCG  NCG  KPRES
          0       0     0     1
DG (4):  NCS  KPL  JNK  KREVRS   NFGRF
          4     2     9    0          0
DG (5):  IOBS  KTERM  NP  NPST  NPEND
          0       0        0   0       0
DG (7):  TEH  DTHII    DTHPLT    FRDFR  DTEXP MDT(Time control)
          30    0.03333   0.03333    0.05    0        0
DG (10): NLEV  DHLV  DTHLV (Levee Info)
          0       0       0
DG (12): NBT NPT1 NPT2 EPQJ COFW VWIND WINAGL(XSection Control for main)
          10   1      10     10     0       0        0
DG (13): KU  KD  NQL NGAGE NRCM NQCM  IFUT4 (Bndry and Mannings n)
           2    4    0     10       1       0        0  0  0  0
DG (14): MXIF MUD KFTR ... (Specialties:  Mixed flow, mud, kalman filter, etc)
           0     0     0      0 0 0 0 0 0 0
DG (18, 19, 20): XT DXM KRCHT (Cross Sections: DG 18 gives location...
     0    2500   5000   10000   20000  40000  80000  160000   320000   330000
... and DG 19 gives max intermediate distance for computation, interpolating as needed
           625    625    625     625     625    625     625       625       625
... and DG 20 gives routing method, 0= implicit dynamic 1=implicit diffusion)
           0       0       0         0        0        0        0          0          0
DG (50, 52):  NGS STNAME (Observed stations: sequence and name)
       1 STA 0 INFLOW

       2 STA 2500
         [... additional station designations omitted]

DG (56):  ST1 (Discharges for Hydrograph as the Upstream Boundary)
1200    1200    1200    1200    1200    1200    1200    1200    1200    1200
1200    1200    1200    1380    1710    2080    2488    2933    3414    3928
4474    5049    5650    6274    6918    7580    8257    8944    9639    10340
        [... additional hydrograph ordinates omitted]
```

Table 6-3. FLDWAV Input File, Example for Reach No. 3 (cont.)

```
DG (70-74, 77): (XSections, repeat for each, begin with Sta 0, DG70 first)
            0          0          0         0
...DG 71 gives elevations
      900.00   906.67   913.26   923.00
...DG 72 gives channel top width at each elevation
        36.56     73.12    73.12     73.12
...DG 73 gives left overbank top width at each elevation, typ. all sections
         0.00      0.00   194.98   261.78
...DG 74 gives right overbank top width at each elevation, typ. all sections
         0.00      0.00   194.98   261.78
...DG 77 gives dead storage at each elevation, typ. all sections
            0          0          0         0
...Cross Section 2 (repeat DG 70-74,77, starting with DG 70)
            0          0          0         0
...DG71
      894.75   901.42   908.01   917.75
...DG72
        36.56     73.12    73.12     73.12
...DG73
         0.00      0.00   194.98   261.78
...DG74
         0.00      0.00   194.98   261.78
...DG77
            0          0          0         0
...Cross Section 3, (repeat DG 70-74,77, starting with DG 70)
```

[... additional section data omitted]

```
DG (78):  SNM (Sinuosity factor at each depth, for each interval)
            1          1          1         1
```

[... sequence repeated for each section, remaining lines omitted]

```
DG (79):  FKEC (Expansion Contraction Coefficients, by section interval)
            0    0    0    0    0    0    0    0    0
DG (80):  NCM (Subreach for same Mannings n distribution)
            1
DG (81-83):  CM (Manning's n at each depth interval, DG 81 for main channel)
         .050      .050       .050      .050
...and DG 82 for left overbank n
         .062      .062       .062      .062
...and DG 83 for right overbank n
         .062      .062       .062      .062
DG (85, 86) (Reach Names for output routines)
REACH 3 Wolf Creek

REACH 3
```

Plan and Control Data in FLW

Data groups DG (1) through (5) and DG (7) contain basic control and setup information. The variable "F1" has the same meaning as Theta (θ) in uRAS and is likewise set to 0.6. The variable labeled "THETA" in FLW has an entirely different meaning that is not applicable to this study. "EPSY" sets the depth tolerance in the iteration schemes (0.01 feet) and ITMAX sets the maximum number of iterations allowed (10). "XFACT" and "METRIC" together set the units to be used for measuring distance along the routing reach. XFACT=1 and METRIC=0 result in units set to feet.

The "KLFP" variable in DG (2) determines how the conveyance in the overbanks is handled. Setting KLFP=1 means that floodplain conveyance is calculated separately from the main channel, rather than treating the entire section as a single (composite) section. "KPRES" in DG (3) controls how the hydraulic radius is calculated. If set to zero (0), the top width is used as to approximate the wetted perimeter. It has been set to one (1) in this study so that a true calculation of the wetted perimeter is made. "KREVRS" in DG (4) is a low-flow filter; when set to zero it does not allow discharges less than the initial flow. This term is intended to improve the stability of most calculations by preventing negative or excessively shallow flow depths. It is examined in more detail in Chapter 7.

The “JNK” variable in DG (4) controls the level of output detail. The normal range is from 0 (no output) to 12. For most purposes, JNK=4 or 9 is adequate.

DG (10) is a required input line and gives levee information. DG (14) is also a required input line and relates to mud flows. These variables are set to zero for this study because neither condition applies.

Geometric Input in FLW

Geometric information is also intermixed in these first several data lines. The "JN" variable in DG (2) defines the number of separate river links to be modeled. In a dendritic system of channels, each branch would be defined as a separate river. For the simple cases in this study, JN=1. DG (12) contains detailed information describing each river link. This data group would be repeated the number of times required by "JN." For this study, it appears only once. In DG (12), the first variable "NBT" states the number of user-input cross-sections in that river link; this model uses ten. It is followed by two variables that give the beginning and ending cross-section numbers. Cross-sections are generally numbered consecutively in upstream-to-downstream order.

DG (18) gives the location (station) of each user-input cross-section (measured in feet for this study). The upstream cross-section is set to Station 0 (zero) and stationing increases downstream, which is opposite of the convention used in uRAS. Each of the eight observation locations are defined with a cross-section. The final cross-section is placed downstream of the last observation location and is used to specify the boundary condition. The same interval is used in FLW as was used for uRAS.

As with HEC-RAS, spatial nodes for computation must be specified as cross-sections. Interpolation is used to fill in gaps between user-defined sections. DG (19) specifies the maximum intermediate distance to use for interpolated cross-sections in each interval between user-input sections. The same computational distance step was used in FLW as in uRAS. For Reach No. 3, that distance was 625 feet. Since there are ten user-defined cross-sections, the value "625" must be entered nine times, once for each interval between user-defined sections.

The FLW model contains several different solution methods that can be used in individual reaches. The appropriate method is specified separately at DG (20) for each of the nine intervals between user-defined cross-sections. Values of zero (0) were assigned which instruct FLDWAV to solve the reach using an implicit four-point finite difference solution to the full St. Venant's equations. A value of one (1) invokes an implicit four-point finite difference solution to the diffusion method. Other options in FLW are provided to accommodate dam breaks, gate and reservoir operations, and local partial-inertial routing which is useful in supercritical or near-critical routings. Those additional options were not relevant to this study.

Data groups (50) and (52) allow for names or labels to be given to the user-defined sections. An entry must be provided for each of the 10 user-defined cross-sections.

Cross-Section Data in FLW

The geometric input continues at data group (70) where individual cross-sections are defined. Data groups (70) through (77) are input in series to describe the

upstream-most cross-section. That entire sequence is repeated for all remaining sections. DG (70) establishes a "flood stage" elevation for an individual cross-section to use as a flag. A zero value means no flag is set.

In FLW, cross-sections are defined by a user-input table of depths vs. top width. This is unlike uRAS, where station-elevation coordinates are provided. For an 8-pt. cross-section, a total of four elevation-width entries are needed. DG (71) for each cross-section gives the four elevations to be used. DG (72), (73), and (74) give the corresponding top widths of the main channel, left overbank, and right overbanks, respectively. DG (77) would give the widths to count as additional dead storage (i.e. ineffective flow). Dead storage is not used in this study, so DG (77) values are set to zero.

Data are defined first for the uppermost cross-section and then repeated for all the remaining ones. Elevations for each of the downstream cross-sections are lowered based on the routing distance and reach slope. A comment line was used to separate and label each section.

Data group DG (78) is used to specify a "sinuosity" factor "SNM" for adjusting to a cross-section based on the meander of the main-channel. FLW defines the base length of the channel as the dominant "valley length", with excess main-channel length caused by meandering in that valley given by a SNM ratio greater than 1.0. The sinuosity is then allowed to vary based on the depth of flow, with the theory being that the SNM factor should vary from full sinuosity at bankfull flow or less, but gradually taper down to 1.0 at very high stage flows. For this model, all 8-pt. cross-

sections are modeled as non-meandering, so SNM is set to “1”. Each line of data contains four entries (for each depth of flow), and 9 total lines of data are needed in this group to correspond to the 9 intervals between user-defined cross-sections.

Data group DG (79) gives expansion and contraction coefficients, which have been set to zero. Groups DG (80) through (83) define the Manning's n roughness values. Cross-sections are organized into sub-reaches for which the same distribution of Manning’s roughness values is modeled. For each sub-reach, the cluster of data groups DG (80) through DG (83) would be repeated. The identifier for the upstream-most section in each sub-reach is listed at DG (80). The Manning’s roughness to use in the main-channel at each depth increment of those sections is then listed at DG (81). Similar data is given at DG (82) and DG (83) for the left and right overbanks. The remaining lines of text in the input file give labeling information for outputs. Since the roughness values of all sections in this reach are the same, only one sub-reach was specified.

Flow Data and Boundary Conditions in FLW

The final input data needed for a valid FLW model are flow and boundary condition specifications. Returning to DG (1), "DTHYD" gives the time interval (in hours) for all input hydrographs. Hydrograph intervals were calculated for every computational time step, which for Reach No. 3 was 2 minutes (0.03333 hours). "NU" in DG (2) sets the total number of ordinates in the hydrograph. For Reach No. 3,901 ordinates are set, which provides for 30 hours of simulation time. In DG (7), the "TEH" variable sets the time (in hours) when the simulation will stop; this is also

set to 30 hours. "DTHII" defines the size of the computational time step (in hours), which as noted previously is 0.03333 hours for Reach 3. If set to zero, "DTHII" would default to the inflow interval, "DTHYD". "DTHPLT" can be used to set a larger time interval for plotting output data. When set to zero, the plotting interval defaults to "DTHII."

Boundary conditions are established on DG (13). The "KU" variable specifies the type of upstream boundary condition for each river. KU=2 means that a discharge hydrograph will be used. The "KD" variable specifies the downstream boundary condition. KD=4 means that a looped rating curve of discharge versus stage is defined, using the geometry of the downstream section and a friction slope computed from the momentum equation. This is a more sophisticated downstream boundary condition option than the normal depth option in uRAS. On relatively steep channels, it should make little difference. If multiple river links existed, DG (13) would be repeated for each.

DG (56) is a tabular input of all the ordinates to be used in the inflow hydrograph. The total number of entries must equal "NU" set at DG (2). As with HEC-RAS, these ordinates were calculated separately in a Microsoft Excel™ spreadsheet, using Eq. (5-1). Each of the separate flow scenarios were calculated and input into the relevant model input file.

6.2.4 Round 6A - Results

Results of Testing Round 6A for Reach Nos. 1 through 4 are given in Tables 6-4 through 6-12 and Figures 6-1 through 6-8.

Tables 6-4 through 6-7 present the peak outflow discharge and relative attenuation of the peak at the eight downstream observation stations for each of the four reaches. Results for both uRAS and FLW are shown. Relative attenuation is defined as:

$$Relative\ Attenuation = \frac{I_P - Q_P}{I_P} \times 100 \qquad (6\text{-}1)$$

where I_p is the peak discharge of the inflow hydrograph and Q_P is the peak discharge in the outflow hydrograph. Relative attenuation is expressed as a percentage. Relative attenuation is similar to the percent error in peak (PEP) criteria discussed in Section 2.4.1, but with the initial inflow peak used as the denominator, rather than the observed or reference outflow discharge. The advantage of the relative attenuation measure is that the denominator remains constant for all outflows observed, and the relative scale of the measure remains more consistent as different routing distances are evaluated. With the PEP criteria, the observed discharge in the denominator decreases with distance, whereas the absolute error between simulated and observed outflows generally increases, which makes it difficult to compare the actual error that is introduced over different routing distances. These tables also present the absolute difference in relative attenuation between uRAS and FLW.

Table 6-4. Peak Flow Results and Relative Attenuation for Reach No. 1, Testing Round 6A

Routing Distance (feet)	Peak Outflow Discharge, Q_p, by Given Model (cfs)		Relative Attenuation of Peak Outflow Discharge (%)		Diff. in Rel. Attenuation, FLW vs. uRAS (%)
	uRAS	FLW	uRAS	FLW	
Inflow, Peak 2,900 cfs at 36 minutes					
1,250	2,884	2,887	0.6%	0.4%	-0.1%
2,500	2,869	2,874	1.1%	0.9%	-0.2%
5,000	2,839	2,848	2.1%	1.8%	-0.3%
10,000	2,781	2,794	4.1%	3.7%	-0.4%
20,000	2,650	2,631	8.6%	9.3%	0.7%
40,000	2,339	2,283	19.3%	21.3%	1.9%
80,000	1,924	1,881	33.7%	35.1%	1.5%
160,000	1,478	1,499	49.0%	48.3%	-0.7%
				Average	0.3%
				Std. Dev.	1.0%

Table 6-5. Peak Flow Results and Relative Attenuation for Reach No. 2, Testing Round 6A

Routing Distance (feet)	Peak Outflow Discharge, Q_p, by Given Model (cfs)		Relative Attenuation of Peak Outflow Discharge (%)		Diff. in Rel. Attenuation, FLW vs. uRAS (%)
	uRAS	FLW	uRAS	FLW	
Inflow, Peak 11,000 cfs at 88 minutes					
2,500	10,831	10,823	1.5%	1.6%	0.1%
5,000	10,660	10,654	3.1%	3.1%	0.1%
10,000	10,312	10,327	6.3%	6.1%	-0.1%
20,000	9,649	9,684	12.3%	12.0%	-0.3%
40,000	8,446	8,406	23.2%	23.6%	0.4%
80,000	6,793	6,812	38.2%	38.1%	-0.2%
160,000	5,145	5,168	53.2%	53.0%	-0.2%
320,000	3,909	3,879	64.5%	64.7%	0.3%
				Average	0.0%
				Std. Dev.	0.2%

Table 6-6. Peak Flow Results and Relative Attenuation for Reach No. 3, Testing Round 6A

Routing Distance (feet)	Peak Outflow Discharge, Q_p, by Given Model (cfs)		Relative Attenuation of Peak Outflow Discharge (%)		Diff. in Rel. Attenuation, FLW vs. uRAS (%)
	uRAS	FLW	uRAS	FLW	
Inflow, Peak 24,000 cfs at 124 minutes					
2,500	23,868	23,889	0.5%	0.5%	-0.1%
5,000	23,742	23,777	1.1%	0.9%	-0.1%
10,000	23,491	23,549	2.1%	1.9%	-0.2%
20,000	22,982	23,066	4.2%	3.9%	-0.3%
40,000	21,858	21,868	8.9%	8.9%	0.0%
80,000	19,220	19,226	19.9%	19.9%	0.0%
160,000	14,952	14,903	37.7%	37.9%	0.2%
320,000	10,752	10,797	55.2%	55.0%	-0.2%
			Average		-0.1%
			Std. Dev.		0.2%

Table 6-7. Peak Flow Results and Relative Attenuation for Reach No. 4, Testing Round 6A

Routing Distance (feet)	Peak Outflow Discharge, Q_p, by Given Model (cfs)		Relative Attenuation of Peak Outflow Discharge (%)		Diff. in Rel. Attenuation, FLW vs. uRAS (%)
	uRAS	FLW	uRAS	FLW	
Inflow, Peak 36,000 cfs at 160 minutes					
5,000	34,026	33,983	5.5%	5.6%	0.1%
10,000	32,135	32,083	10.7%	10.9%	0.1%
20,000	28,729	28,781	20.2%	20.1%	-0.1%
40,000	23,731	23,754	34.1%	34.0%	-0.1%
80,000	18,710	18,874	48.0%	47.6%	-0.5%
160,000	14,426	14,584	59.9%	59.5%	-0.4%
320,000	10,969	11,047	69.5%	69.3%	-0.2%
640,000	8,006	8,014	77.8%	77.7%	0.0%
			Average		-0.1%
			Std. Dev.		0.2%

Table 6-8. Lag Time of Peak Outflow, Reach No. 1, Testing Round 6A

Routing Distance (feet)	Lag Time of Peak Outflow, Relative to Time of Peak Inflow (minutes)		Percent Error in Lag Time, FLW vs. uRAS
	uRAS	FLW	
1,250	2	3	67.1%
2,500	5	6	25.2%
5,000	11	12	11.2%
10,000	24	23	-4.1%
20,000	50	49	-1.6%
40,000	106	111	4.5%
80,000	230	227	-1.2%
160,000	482	487	1.1%

Table 6-9. Lag Time of Peak Outflow, Reach No. 2, Testing Round 6A

Routing Distance (feet)	Lag Time of Peak Outflow, Relative to Time of Peak Inflow (minutes)		Percent Error in Lag Time, FLW vs. uRAS
	uRAS	FLW	
2,500	6	8	29.0%
5,000	16	18	15.2%
10,000	34	36	7.1%
20,000	72	72	0.0%
40,000	152	152	0.0%
80,000	328	326	-0.5%
160,000	710	710	0.0%
320,000	1,544	1,554	0.6%

Table 6-10. Lag Time of Peak Outflow, Reach No. 3, Testing Round 6A

Routing Distance (feet)	Lag Time of Peak Outflow, Relative to Time of Peak Inflow (minutes)		Percent Error in Lag Time, FLW vs. uRAS
	uRAS	FLW	
2,500	4	6	50.0%
5,000	10	12	20.0%
10,000	22	24	9.1%
20,000	46	48	4.3%
40,000	100	98	-2.0%
80,000	218	222	1.8%
160,000	480	474	-1.3%
320,000	1,070	1,050	-1.9%

Table 6-11. Lag Time of Peak Outflow, Reach No. 4, Testing Round 6A

Routing Distance (feet)	Lag Time of Peak Outflow, Relative to Time of Peak Inflow (minutes)		Percent Error in Lag Time, FLW vs. uRAS
	uRAS	FLW	
5,000	20	24	20.0%
10,000	44	48	9.1%
20,000	96	100	4.2%
40,000	212	212	0.0%
80,000	456	452	-0.9%
160,000	952	936	-1.7%
320,000	1,928	1,892	-1.9%
640,000	3,744	3,644	-2.7%

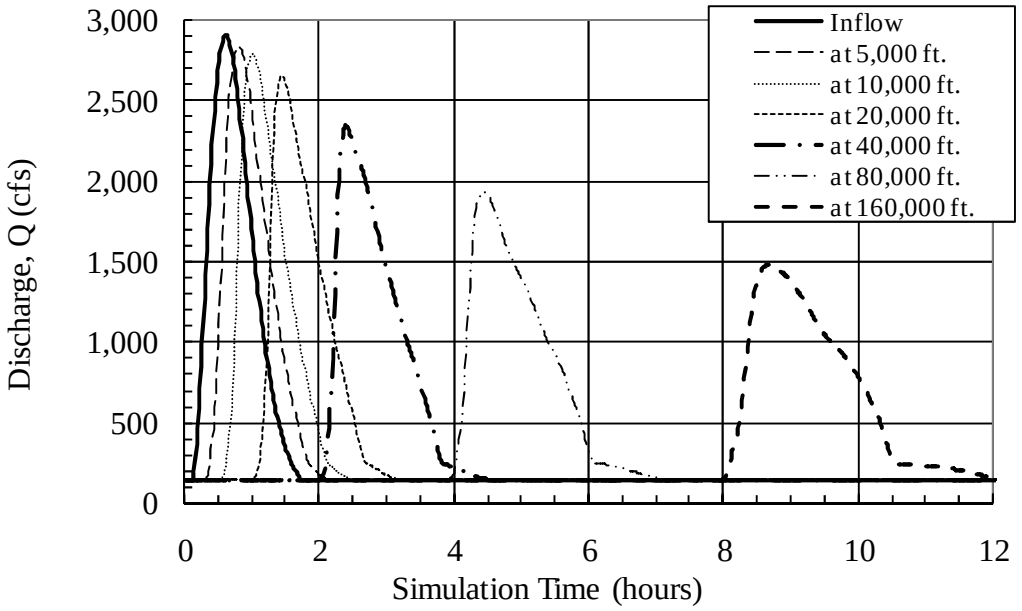

(a) Routed with uRAS

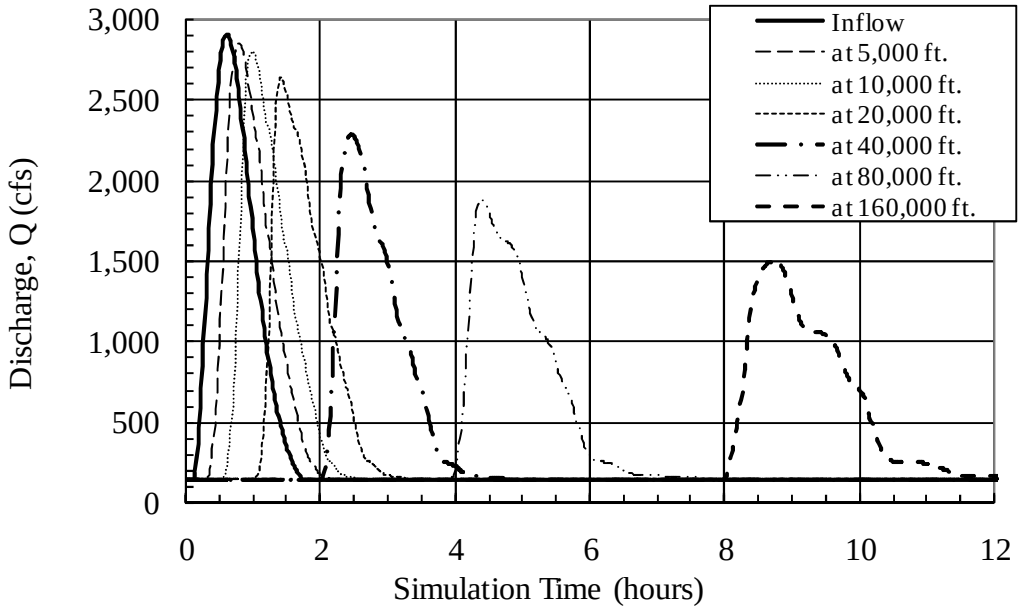

(b) Routed with FLW

Figure 6-1. Outflow Hydrographs for Reach No. 1, after Routing by uRAS and FLW

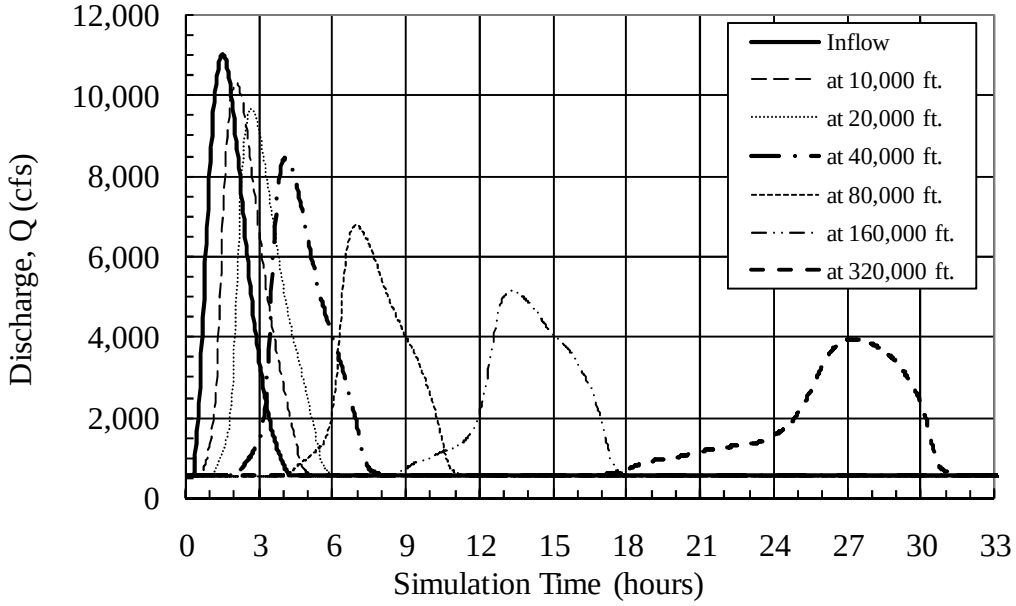

(a) Routed with uRAS

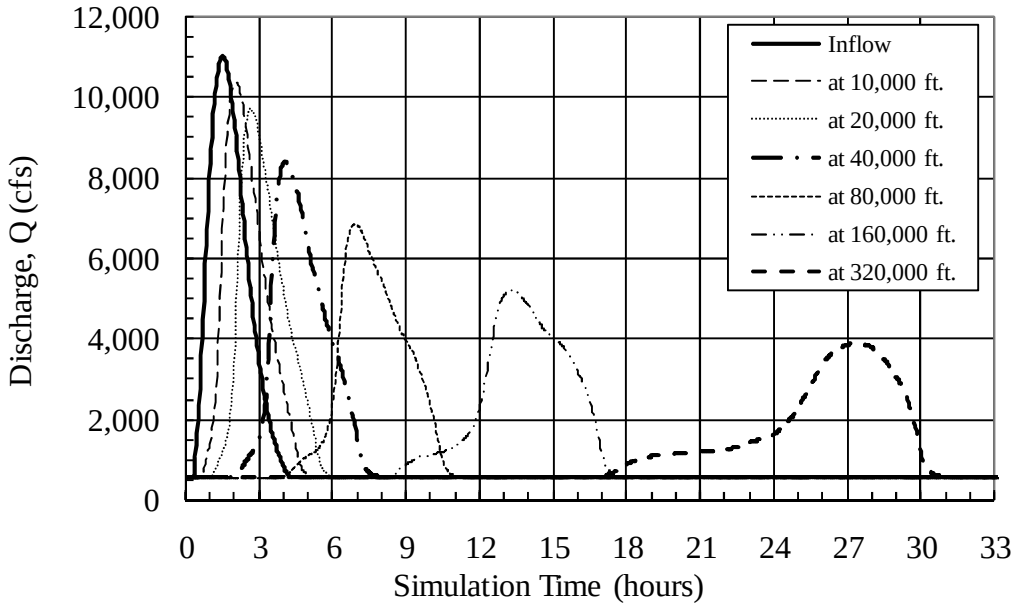

(b) Routed with FLW

Figure 6-2. Outflow Hydrographs for Reach No. 2, after Routing by uRAS and FLW

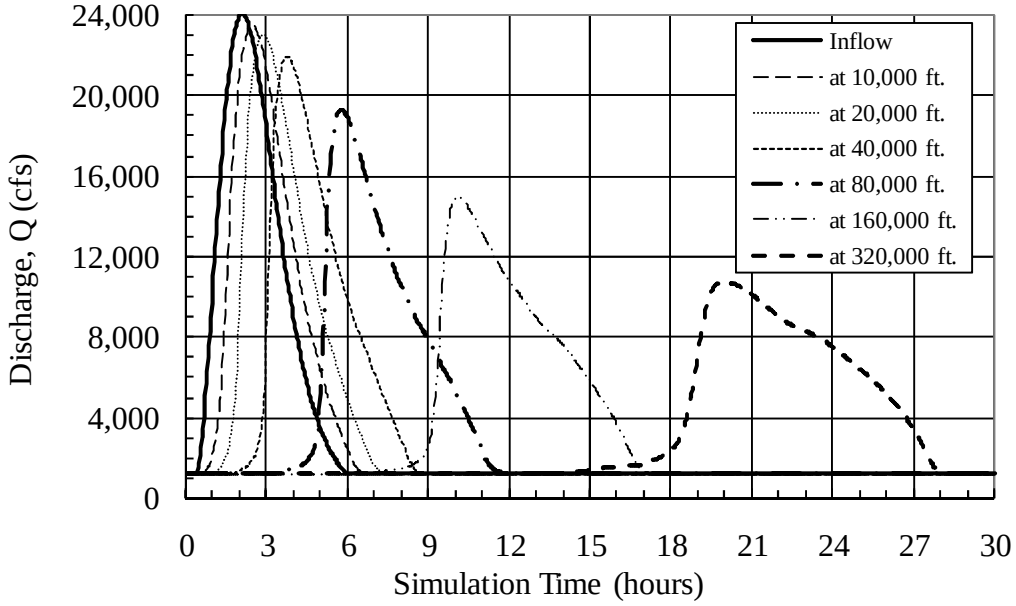

(a) Routed with uRAS

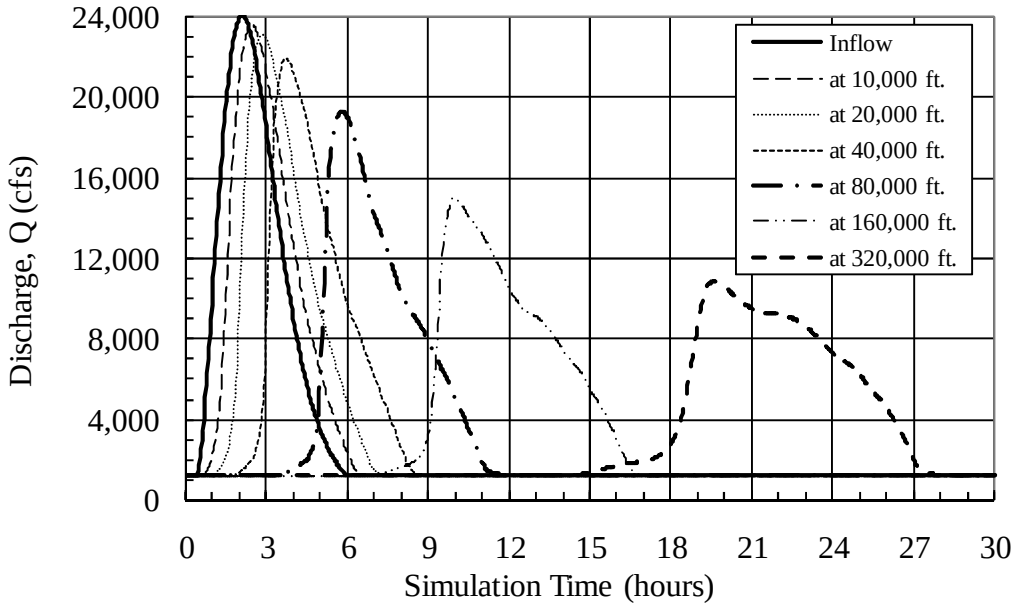

(b) Routed with FLW

Figure 6-3. Outflow Hydrographs for Reach No. 3, after Routing by uRAS and FLW

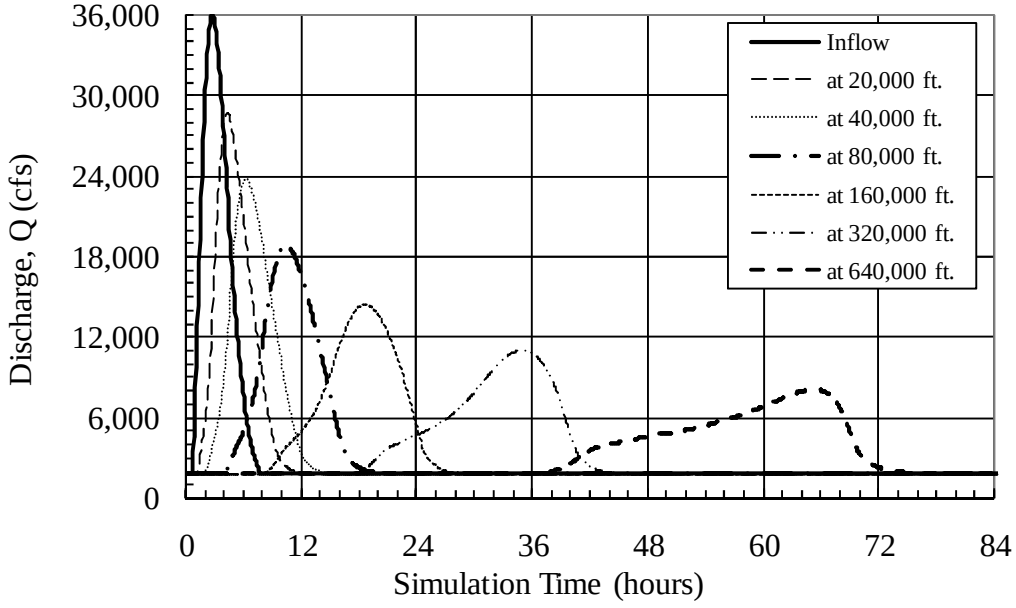

(a) Routed with uRAS

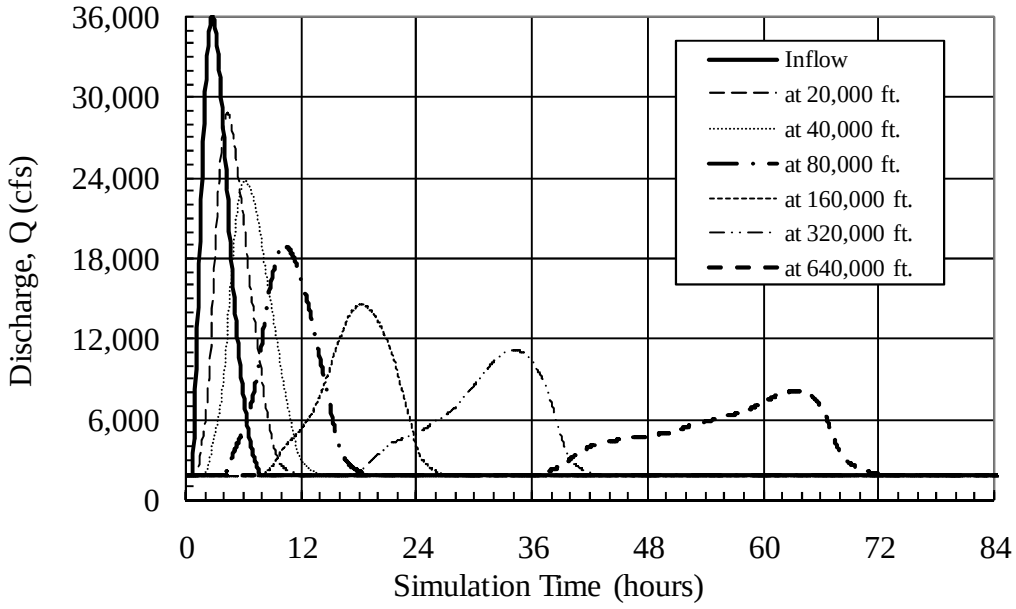

(b) Routed with FLW

Figure 6-4. Outflow Hydrographs for Reach No. 4, after Routing by uRAS and FLW

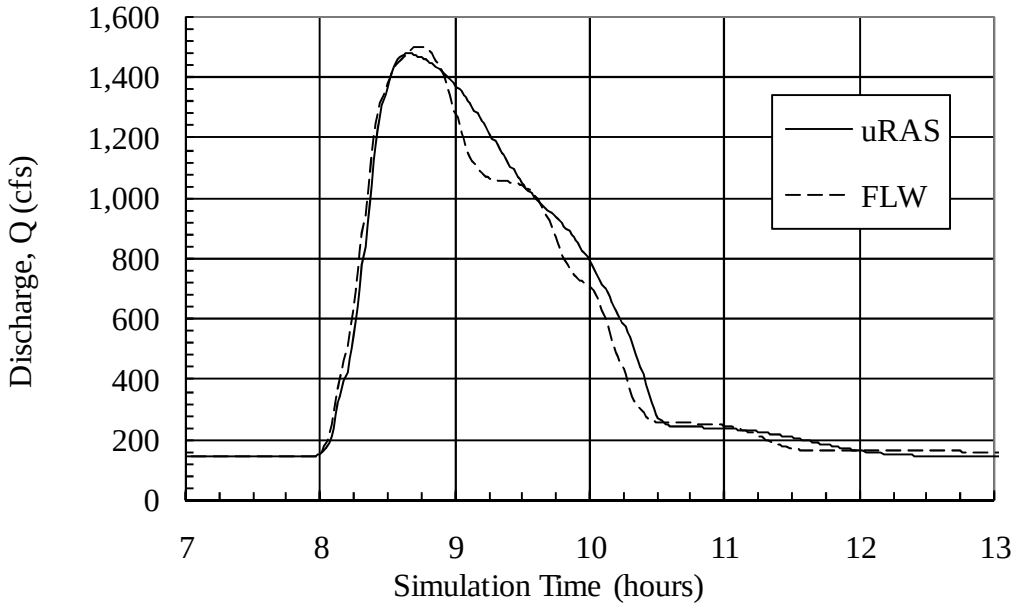

Figure 6-5. Hydrographs for Reach No. 1 after Routing 160,000 feet with uRAS and FLW

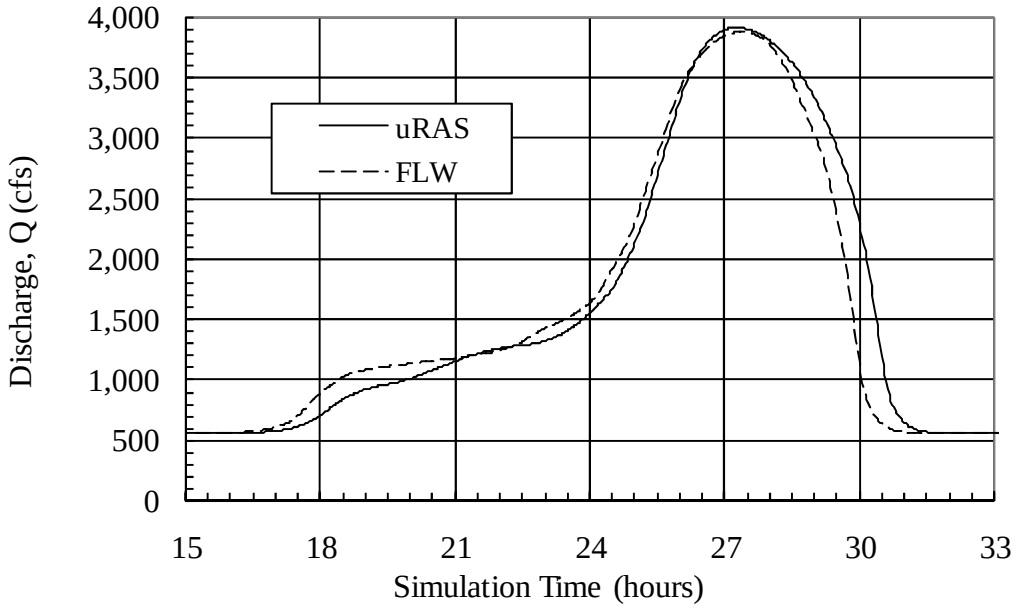

Figure 6-6. Hydrographs for Reach No. 2 after Routing 320,000 feet with uRAS and FLW

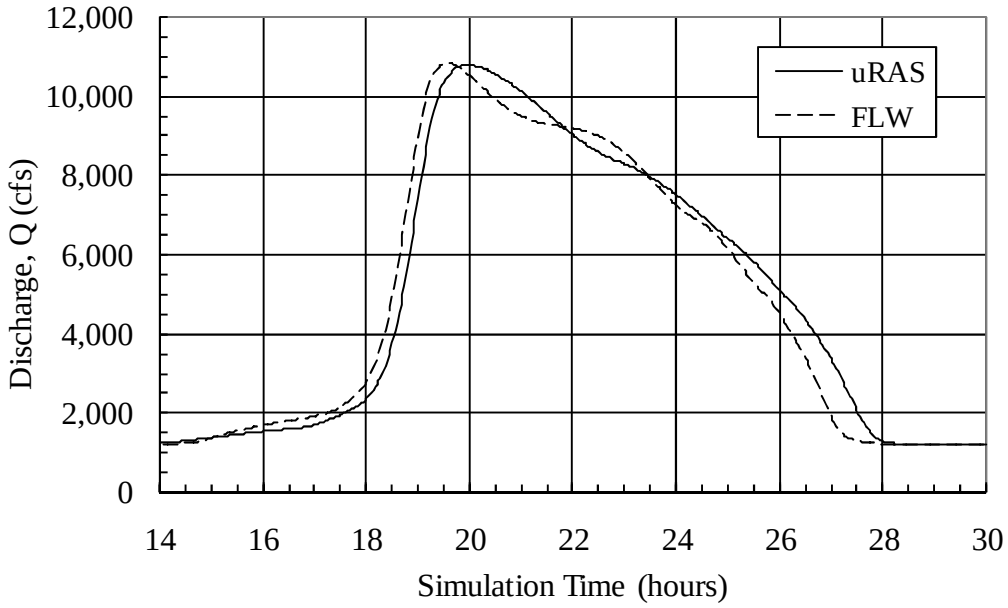

Figure 6-7. Hydrographs for Reach No. 3 after Routing 320,000 feet with uRAS and FLW

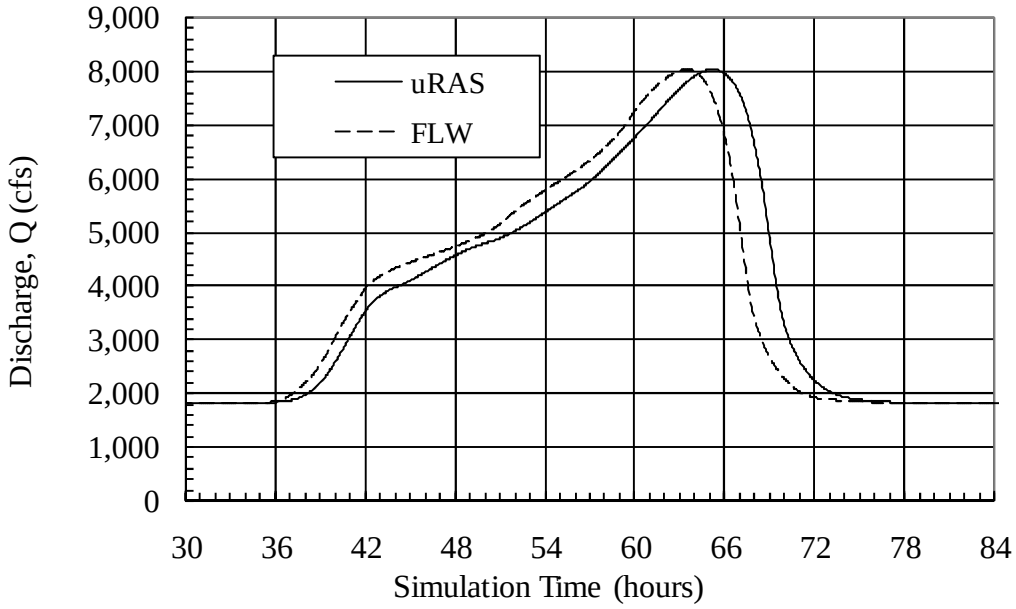

Figure 6-8. Hydrographs for Reach No. 4 after Routing 640,000 feet with uRAS and FLW

Table 6-12. Volume Losses During Outflow, Testing Round 6A

Reach No.	Routing Distance (feet)	Volume of Inflow Hydrograph, Excluding Baseflow (acre-feet)	Outflow Volume, Relative to Inflow, Excluding Baseflow (%)	
			uRAS	FLW
1	160,000	168.1	105.1%	100.1%
2	320,000	1570	102.6%	100.0%
3	320,000	4827	101.5%	100.0%
4	640,000	9343	102.1%	100.1%

As seen in these tables, the relative attenuation increases consistently with routing depth in all the reaches. For Reach No. 1, the hydrograph attenuated approximately 20% after 40,000 ft. of routing and almost 50% after 160,000 ft. For Reach No. 2, the attenuation was approximately 12% after 20,000 ft. and 53% at 160,000 ft. The attenuation rates were lower for similar distances in Reach No. 3, with only 4% attenuation after 20,000 ft. and 38% after 160,000 ft. On Reach No. 4, the attenuation was again more rapid, with approximately 20% attenuation after 20,000 feet and almost 60% attenuation at 160,000.

For each reach, the absolute difference in relative attenuation between uRAS and FLW was calculated, and the mean and standard deviation for set of observed values was calculated. Both FLW and uRAS gave very consistent results for relative attenuation. The average difference was within 0.1% for all reaches except Reach No. 1, which had an average difference of 0.3%. The standard deviation in the differences was approximately 0.2%. The maximum discrepancy was in Reach No. 1 at the 40,000 ft. routing length, with a difference of 1.9%.

Figure 6-1 gives a plot of the outflow hydrographs from uRAS and FLW for the 6 downstream-most observation stations for Reach No. 1. The two upstream-most stations are omitted for clarity. Figures 6-2 through 6-4 present similar plots for the remaining three reaches. These four figures show the progression of the flood waves.

In Reach Nos. 1 and 3, the peak of the hydrograph remains in the early portion of the hydrograph after long routing distances, with relatively longer falling limbs. By contrast, Reach Nos. 2 and 4 seems to show an elongated period of low to mid-level discharges prior to the outflow peak attenuation in each channel. This elongated initial period of discharge is most pronounced on Reach No. 2 (Figure 6-2). For the 320,000 ft. routing distance, the outflow runs at approximately 1,000 cfs between 18 and 23 hours of simulation before reaching the peak of 3,900 cfs at approximately 27 hours.

The overall pattern and shape of the hydrographs appear similar for both uRAS and FLW. On Reach No. 1, the FLW hydrographs appear to develop instabilities or oscillations on the falling limb, which are most noticeable for long routing distances. A similar but less pronounced oscillation also appears after long distance routing on Reach No. 3, but no such similar instabilities appear in Reach Nos. 2 and 4.

Figures 6-5 through 6-8 show a direct comparison between uRAS and FLW hydrographs for each reach at the downstream-most observation location. In the case of Reach No. 1 (Figure 6-5), the oscillation discussed above is especially noticeable, with the FLW result initially reaching a higher peak than the uRAS result, but then

falling in a less consistent fashion. A less pronounced oscillation on Reach No. 3 is also shown, though in that case the oscillation does not appear to cause much difference in peak flows. As noted before, the difference in relative attenuation between uRAS and FLW was greatest for Reach No. 1.

The overall shape and pattern of the hydrographs between uRAS and FLW on all four reaches are quite similar, even after extreme routing distances. This indicates that methods are capable of giving consistent results.

Another method of evaluating hydrograph consistency is to look at the lag time of the peak discharges. Table 6-8 through 6-11 present the relative lag in the timing of the peak outflows for the four reaches, where relative lag is defined as the difference between the time when the inflow hydrograph reaches its peak discharge and when the outflow hydrograph reaches its peak. Also shown in the tables is the percent error in lag times, using the uRAS solution as the reference condition. The percent error is calculated as:

$$Percent\ Error\ in\ Lag\ Time = \frac{LagTime_{sim} - LagTime_{ref}}{LagTime_{ref}} \qquad (6\text{-}2)$$

When short routing distances are observed, the percent error in lag time appears quite large. This is primarily a result of the relative coarseness of the results; the lag time of an individual hydrograph is rounded to the nearest model time step. The percent error declines with increasing routing distance. Based on the longer routing distances, the FLW model generally produces lag times within 5% of uRAS for all four reaches. The agreement between the models was best for Reach No. 2.

The lag-time response can also be evaluated from the hydrograph comparisons in Figures 6-5 through 6-8. From these figures, it appears that the best overall timing match occurs in Reach Nos. 1 and 2. In both Reach Nos. 3 and 4, the FLW solution appears to give a slightly faster overall routing.

The ability of uRAS and FLW to conserve volume during the routing was also examined. Volume conservation was measured as the proportion of volume in the outflow hydrograph relative to the inflow hydrograph. The hydrograph volumes were calculated based on the net volume above the minimum 5% baseflow that was superimposed in these simulations. The gross volume of the entire hydrograph was estimated by integrating the hydrograph ordinates using the trapezoidal rule. From that gross volume, the total volume of baseflow over the simulation period was deducted.

Volume conservation results are given in Table 6-12. The FLW solution provided almost perfect volume conservation, with errors at or less that 0.1% for all four reaches. The uRAS solution did not conserve volume as well. The outflow hydrographs on all four simulations appeared to gain volume relative to the inflow hydrograph, though the volume error was less than 3% for Reach Nos. 2, 3 and 4 and was 5.1% for Reach No. 1.

6.3 Comparison of VMC and CR to uRAS (Testing Round 6B)

In Round 6B, the fully dynamic solution using unsteady HEC-RAS (uRAS) is compared to the simplified variable-parameter Muskingum-Cunge (VMC) and Cascading Reservoirs (CR) routing methods. The goal of this round was to evaluate the performance of the simplified routing methods. As with Round 6A, the methodology and setup of each model is explained, using Reach No. 3 as an example. Results are presented and analyzed.

6.3.1 Basic Geometric and Hydrologic Parameters (Round 6B)

As in Testing Round 6A, all four reaches are modeled as simple 8-pt. cross-sections, using the dimensions defined in Chapter 5. The same total routing distances and observation locations are used. The baseline inflow hydrograph is used

6.3.2 uRAS Model Setup (Round 6B)

The uRAS model and results developed in the previous Round 6A are used for this comparison.

6.3.3 VMC Model Setup (Round 6B)

The variable parameter Muskingum-Cunge (VMC) test was performed in the HEC-1 hydrology model, version 4.1. HEC-1 provides an interconnected system of components to model individual elements of the rainfall-runoff process. The variable-parameter Muskingum-Cunge method is one of the options given for channel routing.

VMC is solved using the equation and coefficients given in Section 3.3. The Muskingum coefficients are derived from values of c_k, T, and Q calculated during the

computational step, based on normal depth flow from a user-defined channel section, roughness and slope. The most detailed section accepted by HEC-1 is the 8-pt. cross-section. An iterative 4-point box scheme is used to find a representative value for each of the three variables used in calculating the Muskingum-Cunge coefficients (USACE 1998).

HEC-1 relies on a single input file of text from which instructions and variables are read. Table 6-13 presents a condensed HEC-1 input file, demonstrating the inputs needed to route the baseline hydrograph through Reach No. 3 for one routing length, 20,000 feet.

Each line of text in a HEC-1 input file is called a "*record*." The first two-characters are a record identifier and call the process to be used during HEC-1 computations. After the record identifier, individual input variables are listed.

The default style in HEC-1 is "*fixed format*," in which each horizontal line of text is divided into ten fields defined by the horizontal character spacing. The horizontal location of numeric or text values is critical for proper reading of the file. Null or non-applicable values are left blank. Specific rules dictate the order in which records can be used. The initial records beginning with "ID" give the job title. The "IT" record then gives time control information. The first variable gives the primary computational time step to be used for the model. For Reach No. 3, the interval was two minutes. The remaining variables give the nominal date and clock time when the simulation begins ("0" indicating midnight). The final variable on that line states that 901 time steps will be calculated in simulation for Reach 3, resulting in a simulation

time of 30 hours. The "IO" record determines the degree of detail shown in output files.

Table 6-13. HEC-1 Input File for VMC Routing, Example for Reach No. 3

```
ID Variable-parameter Muskingum Cunge (VMC)
ID Reach 3, Wolf Creek, near OP Arboretum
IT     2 27JUL89    0000     901
IO     4        0
*
VS Input    V020K
VV  2.11     2.11
*
KK Input
KO     0        0
BA     1           24.000
IN     4
QI    50       50       50       50       50       50       50       71      104      142
QI   186      235      288      344      402      460      518      576      631      684
QI   734      781      823      861      895      923      947      967      982      992
QI   998     1000      998      993      984      972      957      940      921      900
QI   877      853      828      801      774      747      719      691      663      635
QI   607      580      553      527      501      476      451      428      405      383
QI   361      341      321      303      285      268      251      236      221      207
QI   194      181      169      158      148      138      128      120      111      104
QI    96       89       83       77       72       66       61       57       53       50
QI    50       50       50       50       50       50       50       50       50       50
QI    50       50       50       50       50       50       50       50       50       50
*
KK V020K
KO     0        0
RD
RC  .062     .050     .062    20000 .002100
RX119.94  186.74  381.72  400.00  436.56  454.84  649.82  716.62
RY 923.0  913.26  906.67  900.00  900.00  906.67  913.26  923.00
*
ZZ
```

A single asterisk followed by a space in lieu of a record identifier indicates a comment.

Individual calculation processes are grouped together at computation nodes. Nodes are described in the input file in the order that computation is needed. For HEC-1, all computations occur in upstream to downstream order, with branching reaches being calculated independently and the results combined as appropriate. For these simple simulations, no branched networks are involved. Individual computational nodes are identified by a "station computation identifier" designated after a "KK" record. HEC-1 does not require that an identifier be established for each process or that identifiers be unique, but the lack of a unique identifier limits the options for extracting output details from a given node.

Prior to the first "KK" card in this input file, a "VS" and "VV" record was provided. This instructs HEC-1 to generate tabular listing of the time history of flow or stages at a given node. This is convenient for exporting data to other programs for post-processing and analyses. The "VS" card specifies the station or stations to draw output from, using the identifier stated in the "KK" card. The "VV" card specifies the type of data to be exported, a value of 2 before the decimal indicating that calculated flow values are retrieved. The digits after the decimal place are set to "11" unless multiple "plans" or "ratios" have been defined for job. Those options are not used in the present study. Up to 10 separate stations can be designated using each "VS/VV" pair, and multiple "VS/VV" pairs can be used.

The first "KK" card in Table 6-13 defines an inflow hydrograph. The station identifier is "*Input*." As with the uRAS and FLW models, the ordinates of the baseline hydrograph were calculated in Microsoft Excel™ using Eq. (5-1) and the

inflow peak and time to peak for each hydrograph. The individual ordinates are then listed sequentially in left-to-right order in a series of one or more "QI" records. The "QI" record allows for direct input of hydrograph ordinates, bypassing the need for rainfall calculations or rainfall-runoff transformations.

The hydrograph defined in Table 6-13 is a dimensionless hydrograph normalized to a peak discharge of 1,000 cfs. Hydrograph ordinates were scaled to other values based on the multiplier. The numeric value given in the third field after the "BA" identifier is a multiplier which was applied to all the ordinates in the QI graph. To produce a peak of 24,000 cfs in Reach 3, a multiplier of 24.0 was used.

Following the "BA" record is an "IN" record, which gives the incremental time (in minutes) between individual ordinates in the "QI" series. When the hydrograph time step is different than the computational time step defined in the "IT" record, HEC-1 will interpolate. To reduce the size of the input file, the hydrograph interval was defined as twice the computational step. For Reach No. 3, the computational time step was 2 minutes and the hydrograph interval was 4 minutes.

Unlike the dynamic hydraulic equations being solved in uRAS and FLW, the VMC method in HEC-1 is not adversely affected by zero flow. To maintain consistency with the uRAS and FLW solutions, the 5% minimum flow rate was nevertheless applied. This minimum was calculated separately in Excel™ before transferring to the HEC-1 input file. The QI series in HEC-1 does not need to be specified for entire duration of the simulation. Once the falling limb of the

hydrograph has reach its minimum value, the QI series can be discontinued, and HEC-1 will automatically repeat the final value for all remaining ordinates.

The next process in the simulation is the routing of the inflow hydrograph through the river reach. A separate computational node designated "*V020K*" is defined by the second "KK" record. This designation specified the results of variable-parameter Muskingum-Cunge routing over a distance of 20,000 feet.

Muskingum-Cunge routing is invoked by the "RD" record. The next three records ("RC, RX, and RY") define the geometry of the 8-point cross-section. The "RX" card gives the horizontal coordinate for each of the eight points that define the section geometry. The "RY" card below it then gives the corresponding elevation coordinates. The first three fields after the "RC" identifier are the Manning's roughness for the left overbank, main-channel, and right overbank, respectively. All values were based on the 8-pt. section defined in Chapter 5 for each reach.

The last two fields in the "RC" card provide the length and slope of the routing reach. In this case, the length is 20,000 feet and the main-channel slope for Reach No. 3 was 0.0021.

HEC-1 internally calculates the computational time and distance steps used for VMC routing. This is one of the few subroutines in HEC-1 in which the overall computational time step set forth in record "IT" is subject to change. Results of the Muskingum-Cunge internal calculation are interpolated back to the overall model time step when finished. Generally speaking, the short time steps specified in the IT record are used, unless HEC-1 determines that a shorter interval is needed. For these

testing runs, the user-input model time step generally controlled. Likewise, HEC-1 internally determines the number distance steps into which the specified reach is divided. The specifications of time and distance steps are all internal to the HEC-1 model. They are not controlled by the user. The value chosen for time step is reported in the output file. The distance step is not reported. The criteria were given in Section 3.5

The condensed input file in Table 6-13 shows only the data needed for one routing length. The actual input files used for VMC in Testing Round 6B contained routing specifications for all eight routing lengths.

The final record a HEC-1 input file is an end-of-job record, "ZZ."

6.3.4 CR Model Setup (Round 6B)

The cascading reservoirs (CR) method was modeled in HEC-1 using the "modified Puls" or "storage routing" option (USACE 1998). The CR method treats the channel as a series of discrete, identical reservoirs in which discharge is a function of storage volume alone. By dividing the channel into subreaches with lengths close the characteristic length, L_u, the routing should come close to matching the results of VMC. This specified number of routing steps is denoted N.

The CR method does not allow for a perfect match to VMC. The value of N must be a whole integer, which means the actual length of subreach represented by each hypothetical reservoir is only approximately equal to L_u. Also, the subdivision remains consistent throughout the entire modeling run, even though L_u itself is a function of discharge. The selection of N therefore depends upon the selection of a

representative value of discharge. For this testing round (6B), a value of $\frac{2}{3} I_P$ for each inflow scenario was assumed as the reference discharge. This assumption is based on the fact that the peak conditions of the routing will be most influenced by conditions in the upper range of flow, but that the inflow peak itself occurs only for a very short time. Table 6-14 gives the calculated values of L_u and N for all of the reaches and routing distances used in Testing Round 6B.

Table 6-14. Values of *N* for CR Routing, Round 6B

Reach No.	1	2	3	4
Routing Length (feet)	Number of Subdivisions, *N*, Evaluated Using L_u at 2/3 of Peak Inflow (I_p)			
1,250	3	--	--	--
2,500	7	1	1	--
5,000	14	3	2	1
10,000	27	5	4	1
20,000	55	11	8	2
40,000	110	22	17	5
80,000	220	43	33	9
160,000	440	87	67	19
320,000	--	174	134	38
640,000	--	--	--	76
L_u (feet) at 2/3 I_p	364	1,842	2,395	8,471
2/3 I_p (cfs)	1,933	7,333	16,000	24,000

The HEC-1 input files for CR routing scenarios are very similar to those used for VMC. An example file for Reach No. 3 is given in Table 6-15.

Table 6-15. HEC-1 Input File for CR Routing, Example for Reach No. 3

```
ID Cascading Reservoirs (CR) Method
ID Reach 3, Wolf Creek, near OP Arboretum
IT      2 27JUL89     0000      901
IO      4        0
*
VS Input    C020K
VV  2.11     2.11
*
KK Input
KO      0        0
BA      1             24.000
IN      4
QI     50       50       50       50       50       50       50       71      104      142
QI    186      235      288      344      402      460      518      576      631      684
QI    734      781      823      861      895      923      947      967      982      992
QI    998     1000      998      993      984      972      957      940      921      900
QI    877      853      828      801      774      747      719      691      663      635
QI    607      580      553      527      501      476      451      428      405      383
QI    361      341      321      303      285      268      251      236      221      207
QI    194      181      169      158      148      138      128      120      111      104
QI     96       89       83       77       72       66       61       57       53       50
QI     50       50       50       50       50       50       50       50       50       50
QI     50       50       50       50       50       50       50       50       50       50
*
KK C020K
KO      0        0
RS      8               -1
RC  .062     .050     .062    20000 .002100
RX119.94   186.74   381.72   400.00   436.56   454.84   649.82   716.62
RY 923.0   913.26   906.67   900.00   900.00   906.67   913.26   923.00
*
ZZ
```

The specification of initial controls and inflow hydrographs was the same for CR as for VMC. The hydrograph given in the "QI" record is dimensionless, normalized at 1,000 cfs, and a multiplier of 24.0 is specified in the "BA" record. The ordinates given in the QI record are spaced at 4-minute increments. The peak value occurs at the 31st ordinate, corresponding to 124 minutes.

The inputs for a CR routing in Reach No. 3 over 20,000 feet of channel are illustrated at node "C020K", as labeled at the "KK" record. The "RS" card is used to invoke the storage-routing method. It takes the place of the "RD" card used in VMC.

In the CR routing method, two variables in the RS line are set. The first variable is the value for *N* (number of subdivisions) for the given reach. The value of "8" was taken from Table 6-14. The second field is left blank. The variable in third field defines the initial flow conditions in the routing reach. By setting that variable to "-1", HEC-1 is instructed to use the first flow value in the inflow hydrograph as the initial inflow.

The only remaining data needed is a storage volume-discharge table. The convention in HEC-1 is to establish a table based on the outflow discharge and the total volume of water in the entire reach. These overall storage volumes are then divided by *N* to establish a storage volume-discharge table for each individual subreservoir.

There are two methods available in HEC-1 for specifying the table. The first method is to directly input a table of volume and discharge values. These values would be entered using SV and SQ cards. This method is useful when routing data such as that shown for Reach No. 3 on Table 5-13 are directly available from a separate hydraulic study or detailed surveys. The actual values used would only be accurate for the original length of routing reach. If a modeler wished to use this tabular data to model routing over a fraction of the length or to extrapolate beyond the

original channel, the storage volumes in the table would have to be adjusted by the ratio of the modeled length to the original channel length.

Another option is to have HEC-1 generate a storage volume-discharge table automatically, given the 8-pt. cross-section described in the VMC method and assuming normal flow. This option was used in Round 6B because it enabled easier modification of the input file for different routing lengths. By using exactly the same geometry as the other three methods, it also eliminated a source of comparative discrepancy.

The 8-point section is specified using the "RC, RX and RY" cards as described with VMC. The actual input files contained a separate routing block for each of the 8 observation locations.

6.3.5 Round 6B – Results

Results of Testing Round 6B for Reach Nos. 1 through 4 are given in Tables 6-16 through 6-29 and Figures 6-9 through 6-22.

Figure 6-9 gives a plot of the outflow hydrographs from VMC and CR for the 6 downstream-most observation stations for Reach No. 1. The two upstream-most stations are omitted for clarity. Figures 6-10 through 6-12 present similar plots for the remaining three reaches.

Figure 6-13 provides a direct comparison of VMC, CR and uRAS hydrographs for Reach No. 1 at three select routing distances: 20,000 feet, 40,000 feet and 160,000 feet.

Table 6-16. Peak Flow Results for Reach No. 1, Testing Round 6B

Routing Distance (feet)	Peak Outflow Discharge, Q_p, by Given Model (cfs)		
	uRAS	VMC	CR
Inflow, Peak 2,900 cfs at 36 minutes			
1,250	2,884	2,885	2,887
2,500	2,869	2,871	2,878
5,000	2,839	2,844	2,855
10,000	2,781	2,786	2,806
20,000	2,650	2,653	2,708
40,000	2,339	2,362	2,404
80,000	1,924	1,939	1,887
160,000	1,478	1,516	1,475

Table 6-17. Relative Attenuation Results for Reach No. 1, Testing Round 6B

Routing Distance (feet)	Attenuation of Peak Outflow Discharge (%)			Diff. in Relative Attenuation, Compared to uRAS (%)	
	uRAS	VMC	CR	VMC	CR
1,250	0.6%	0.5%	0.4%	0.0%	-0.1%
2,500	1.1%	1.0%	0.8%	-0.1%	-0.3%
5,000	2.1%	1.9%	1.6%	-0.2%	-0.6%
10,000	4.1%	3.9%	3.2%	-0.2%	-0.9%
20,000	8.6%	8.5%	6.6%	-0.1%	-2.0%
40,000	19.3%	18.6%	17.1%	-0.8%	-2.2%
80,000	33.7%	33.1%	34.9%	-0.5%	1.3%
160,000	49.0%	47.7%	49.1%	-1.3%	0.1%
			Average	-0.4%	-0.6%
			Std. Dev	0.5%	1.1%

Table 6-18. Peak Flow Results for Reach No. 2, Testing Round 6B

Routing Distance (feet)	Peak Outflow Discharge, Q_p, by Given Model (cfs)		
	uRAS	VMC	CR
Inflow, Peak 11,000 cfs at 88 minutes			
2,500	10,831	10,814	10,794
5,000	10,660	10,637	10,739
10,000	10,312	10,281	10,355
20,000	9,649	9,585	9,786
40,000	8,446	8,386	8,570
80,000	6,793	6,822	6,755
160,000	5,145	5,323	5,037
320,000	3,909	3,945	3,823

Table 6-19. Relative Attenuation Results for Reach No. 2, Testing Round 6B

Routing Distance (feet)	Attenuation of Peak Outflow Discharge(%)			Diff. in Relative Attenuation, Compared to uRAS (%)	
	uRAS	VMC	CR	VMC	CR
2,500	1.5%	1.7%	1.9%	0.2%	0.3%
5,000	3.1%	3.3%	2.4%	0.2%	-0.7%
10,000	6.3%	6.5%	5.9%	0.3%	-0.4%
20,000	12.3%	12.9%	11.0%	0.6%	-1.2%
40,000	23.2%	23.8%	22.1%	0.5%	-1.1%
80,000	38.2%	38.0%	38.6%	-0.3%	0.3%
160,000	53.2%	51.6%	54.2%	-1.6%	1.0%
320,000	64.5%	64.1%	65.2%	-0.3%	0.8%
			Average	-0.1%	-0.1%
			Std. Dev	0.7%	0.9%

Table 6-20. Peak Flow Results for Reach No. 3, Testing Round 6B

Routing Distance (feet)	Peak Outflow Discharge, Q_p, by Given Model (cfs)		
	uRAS	VMC	CR
Inflow, Peak 24,000 cfs at 124 minutes			
2,500	23,868	23,868	23,892
5,000	23,742	23,745	23,793
10,000	23,491	23,489	23,588
20,000	22,982	22,968	23,157
40,000	21,858	21,796	21,963
80,000	19,220	19,166	19,266
160,000	14,952	15,082	14,607
320,000	10,752	11,370	10,322

Table 6-21. Relative Attenuation Results for Reach No. 3, Testing Round 6B

Routing Distance (feet)	Attenuation of Peak Outflow Discharge(%)			Diff. in Relative Attenuation, Compared to uRAS (%)	
	uRAS	VMC	CR	VMC	CR
2,500	0.5%	0.5%	0.4%	0.0%	-0.1%
5,000	1.1%	1.1%	0.9%	0.0%	-0.2%
10,000	2.1%	2.1%	1.7%	0.0%	-0.4%
20,000	4.2%	4.3%	3.5%	0.1%	-0.7%
40,000	8.9%	9.2%	8.5%	0.3%	-0.4%
80,000	19.9%	20.1%	19.7%	0.2%	-0.2%
160,000	37.7%	37.2%	39.1%	-0.5%	1.4%
320,000	55.2%	52.6%	57.0%	-2.6%	1.8%
			Average	-0.3%	0.1%
			Std. Dev	0.9%	0.9%

Table 6-22. Peak Flow Results for Reach No. 4, Testing Round 6B

Routing Distance (feet)	Peak Outflow Discharge, Q_p, by Given Model (cfs)		
	uRAS	VMC	CR
Inflow, Peak 36,000 cfs at 160 minutes			
5,000	34,026	33,059	34,348
10,000	32,135	30,570	30,580
20,000	28,729	26,707	26,602
40,000	23,731	21,953	22,677
80,000	18,710	17,230	17,331
160,000	14,426	12,801	13,526
320,000	10,969	9,023	10,221
640,000	8,006	6,542	7,523

Table 6-23. Relative Attenuation Results for Reach No. 4, Testing Round 6B

Routing Distance (feet)	Attenuation of Peak Outflow Discharge(%)			Diff. in Relative Attenuation, Compared to uRAS (%)	
	uRAS	VMC	CR	VMC	CR
5,000	5.5%	8.2%	4.6%	2.7%	-0.9%
10,000	10.7%	15.1%	15.1%	4.3%	4.3%
20,000	20.2%	25.8%	26.1%	5.6%	5.9%
40,000	34.1%	39.0%	37.0%	4.9%	2.9%
80,000	48.0%	52.1%	51.9%	4.1%	3.8%
160,000	59.9%	64.4%	62.4%	4.5%	2.5%
320,000	69.5%	74.9%	71.6%	5.4%	2.1%
640,000	77.8%	81.8%	79.1%	4.1%	1.3%
			Average	4.5%	2.8%
			Std. Dev	0.9%	2.0%

Table 6-24. Lag Time of Peak Outflow, Reach No. 1, Testing Round 6B

Routing Distance (feet)	Lag Time of Peak Outflow, Relative to Time of Peak Inflow (minutes)			Percent Error in Lag Time, Compared to uRAS	
	uRAS	VMC	CR	VMC	CR
1,250	2	3	3	66.7%	66.7%
2,500	5	6	6	25.0%	25.0%
5,000	11	13	12	22.2%	11.1%
10,000	24	26	25	7.5%	5.0%
20,000	50	54	51	8.4%	2.4%
40,000	106	115	107	8.5%	0.6%
80,000	230	243	233	5.7%	1.3%
160,000	482	505	483	4.9%	0.2%

Table 6-25. Lag Time of Peak Outflow, Reach No. 2, Testing Round 6B

Routing Distance (feet)	Lag Time of Peak Outflow, Relative to Time of Peak Inflow (minutes)			Percent Error in Lag Time, Compared to uRAS	
	uRAS	VMC	CR	VMC	CR
2,500	6	10	10	58.1%	58.1%
5,000	16	18	18	15.2%	15.2%
10,000	34	38	36	12.4%	7.1%
20,000	72	78	74	8.3%	2.5%
40,000	152	164	156	7.9%	2.8%
80,000	328	346	334	5.5%	1.8%
160,000	710	740	716	4.2%	0.8%
320,000	1,544	1,558	1,554	0.9%	0.7%

Table 6-26. Lag Time of Peak Outflow, Reach No. 3, Testing Round 6B

Routing Distance (feet)	Lag Time of Peak Outflow, Relative to Time of Peak Inflow (minutes)			Percent Error in Lag Time, Compared to uRAS	
	uRAS	VMC	CR	VMC	CR
2,500	4	6	6	50.0%	50.0%
5,000	10	12	12	20.0%	20.0%
10,000	22	26	24	18.2%	9.1%
20,000	46	52	50	13.0%	8.7%
40,000	100	108	104	8.0%	4.0%
80,000	218	232	224	6.4%	2.8%
160,000	480	506	490	5.4%	2.1%
320,000	1,070	1,114	1,080	4.1%	0.9%

Table 6-27. Lag Time of Peak Outflow, Reach No. 4, Testing Round 6B

Routing Distance (feet)	Lag Time of Peak Outflow, Relative to Time of Peak Inflow (minutes)			Percent Error in Lag Time, Compared to uRAS	
	uRAS	VMC	CR	VMC	CR
5,000	20	28	28	40.0%	40.0%
10,000	44	56	52	27.3%	18.2%
20,000	96	116	108	20.8%	12.5%
40,000	212	244	232	15.1%	9.4%
80,000	456	492	472	7.9%	3.5%
160,000	952	960	968	0.8%	1.7%
320,000	1,928	1,824	1,928	-5.4%	0.0%
640,000	3,744	3,316	3,700	-11.4%	-1.2%

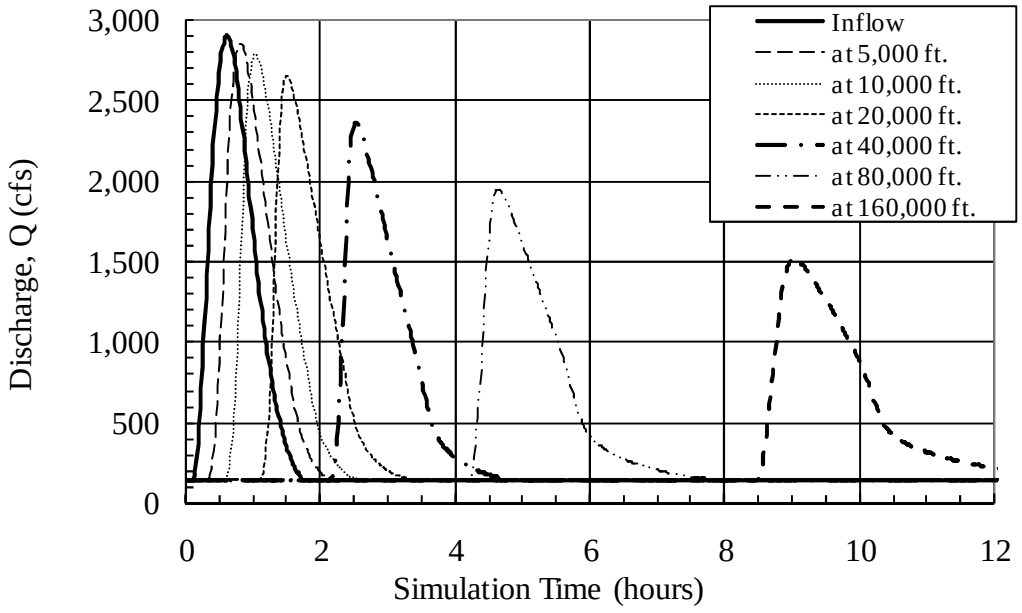

(a) Routed with VMC

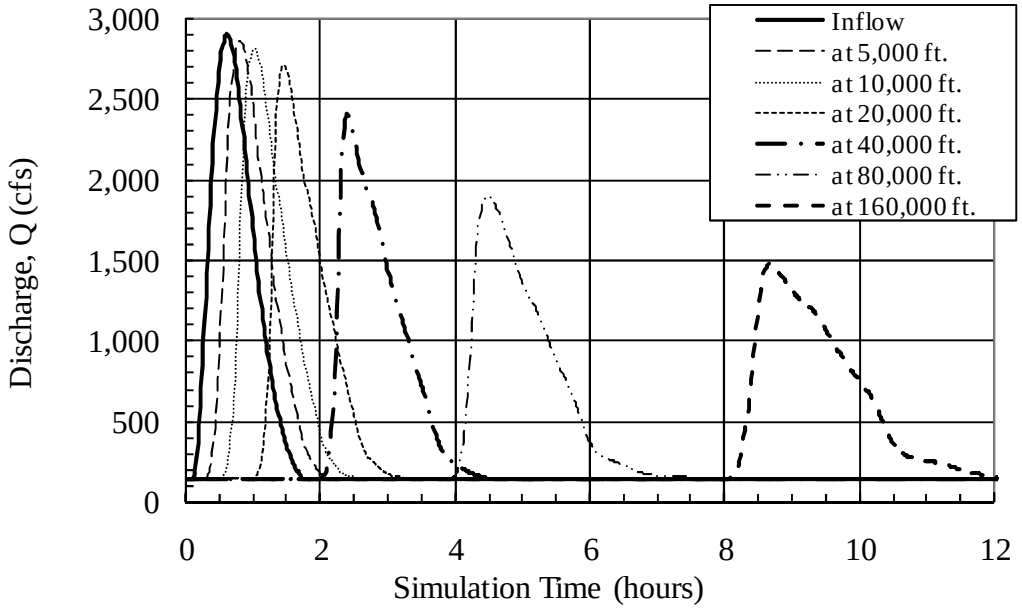

(b) Routed with CR

Figure 6-9. Outflow Hydrographs for Reach No. 1, after Routing by VMC and CR

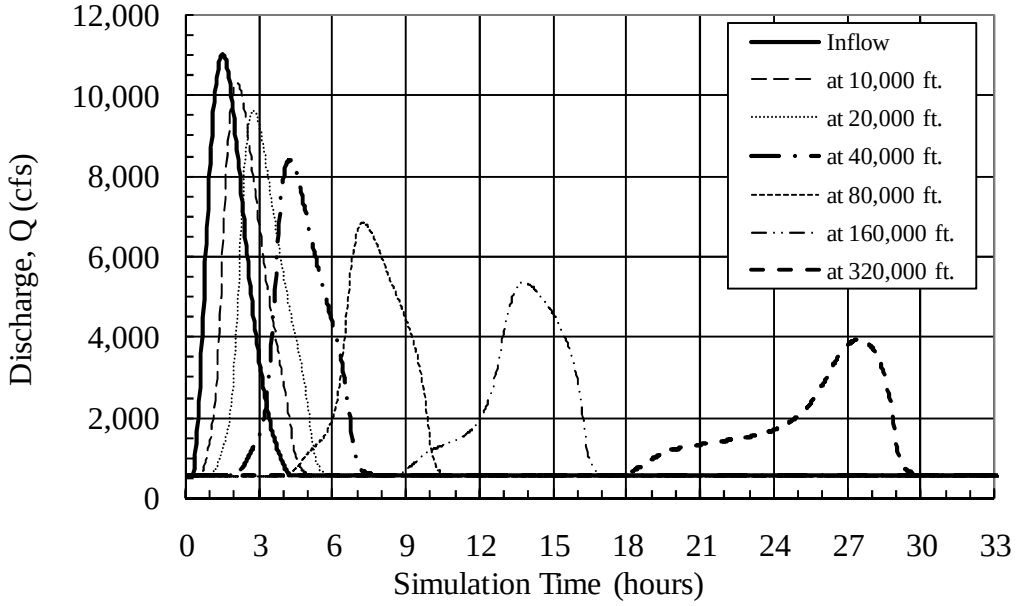

(a) Routed with VMC

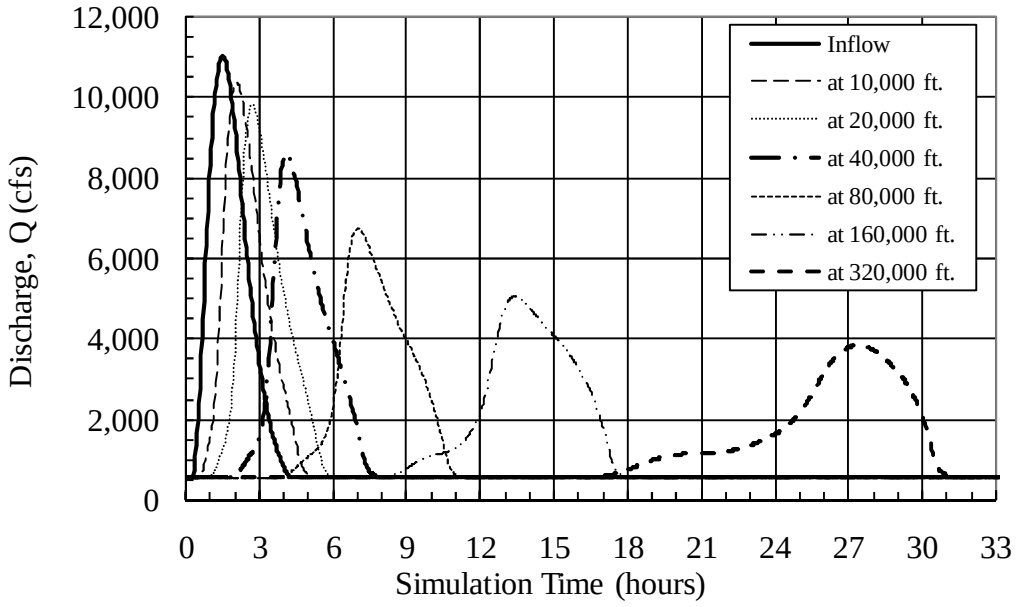

(b) Routed with CR

Figure 6-10. Outflow Hydrographs for Reach No. 2, after Routing by VMC and CR

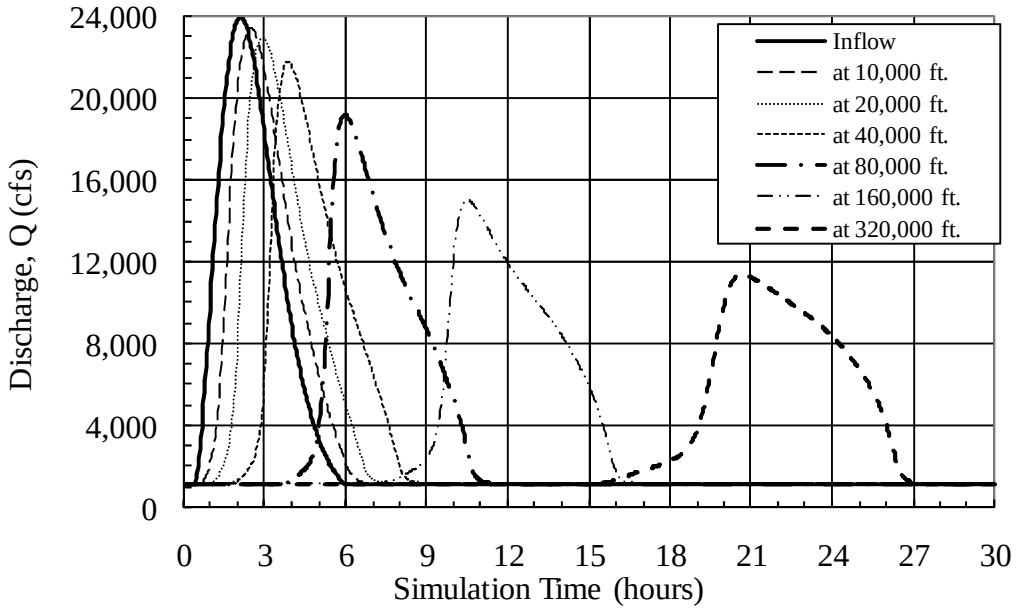

(a) Routed with VMC

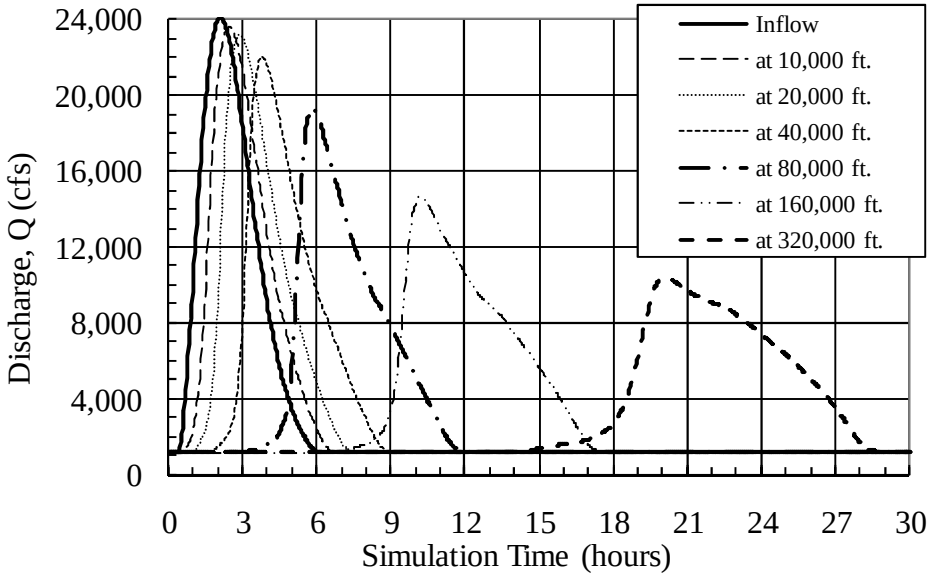

(b) Routed with CR

Figure 6-11. Outflow Hydrographs for Reach No. 3, after Routing by VMC and CR

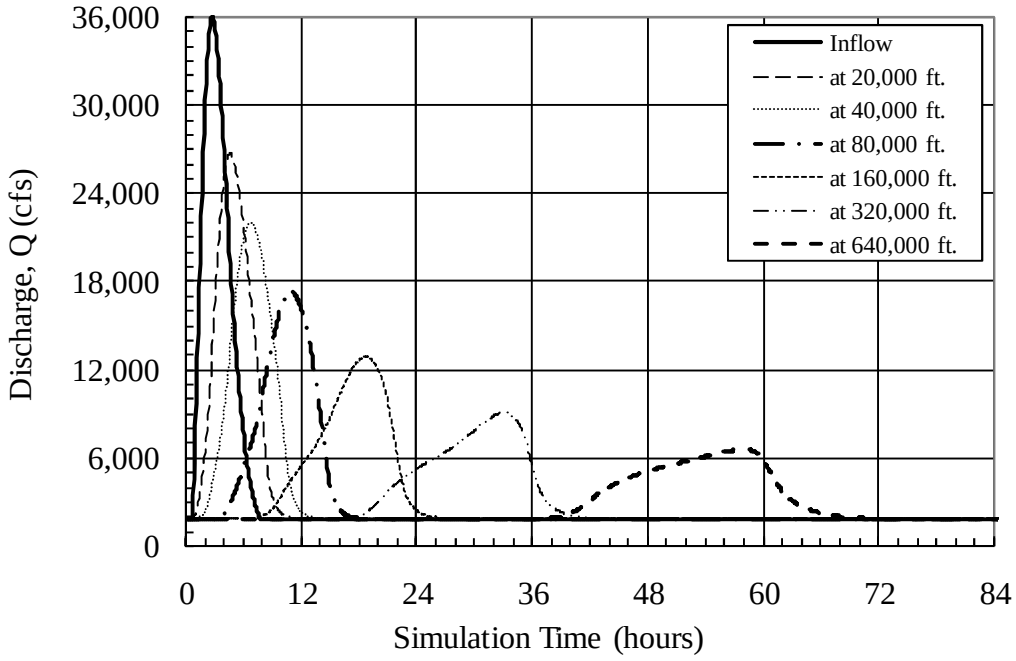

(a) Routed with VMC

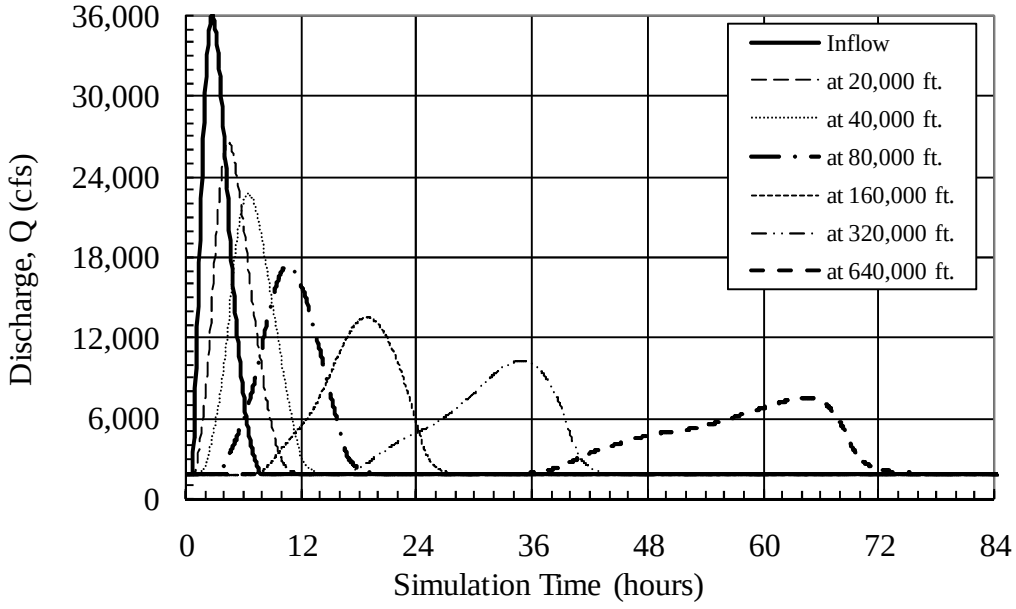

(b) Routed with CR

Figure 6-12. Outflow Hydrographs for Reach No. 4, after Routing by VMC and CR

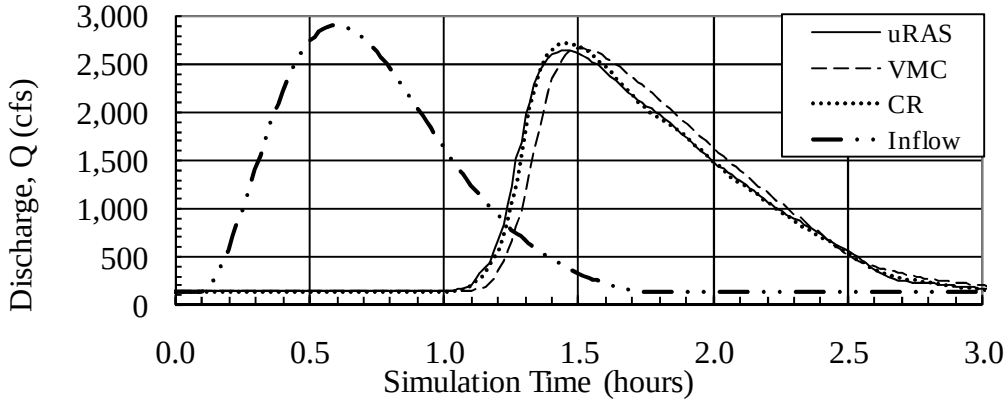

(a) Routed 20,000 feet

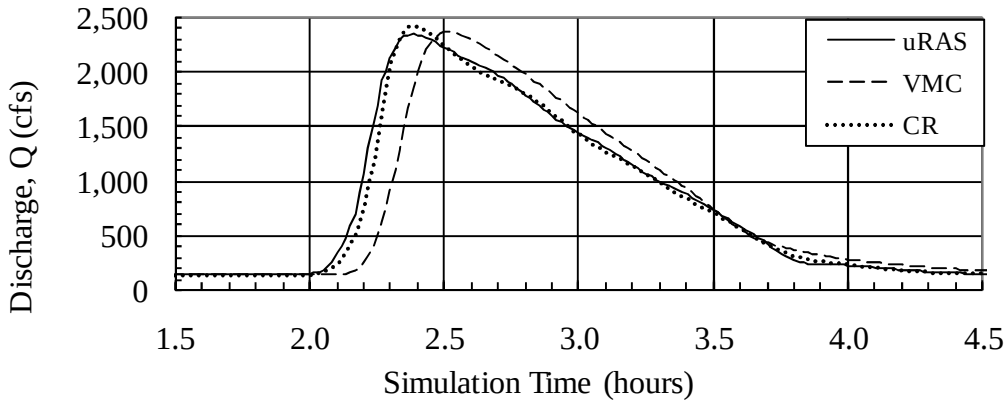

(c) Routed 40,000 feet

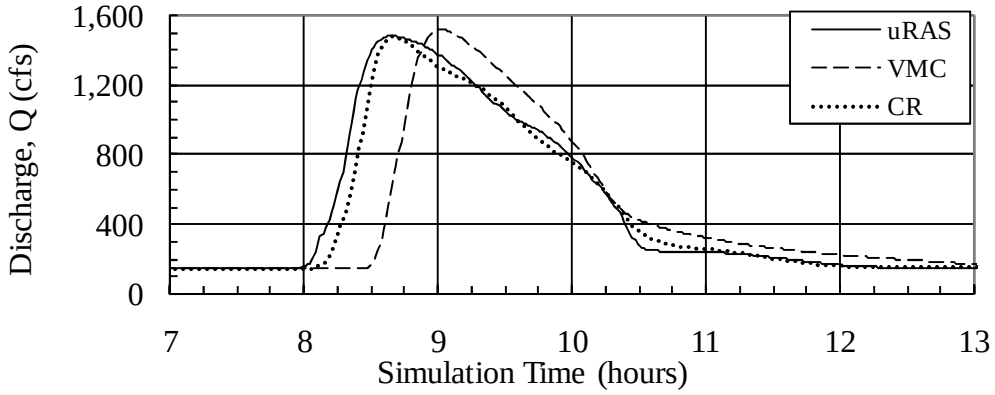

(c) Routed 160,000 feet

Figure 6-13. Hydrographs for Reach No. 1 after Routing with uRAS, VMC and CR

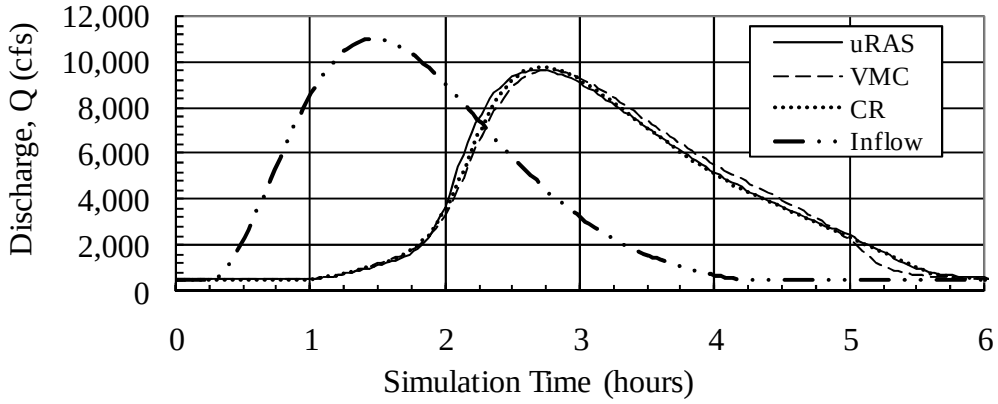

(a) Routed 20,000 feet

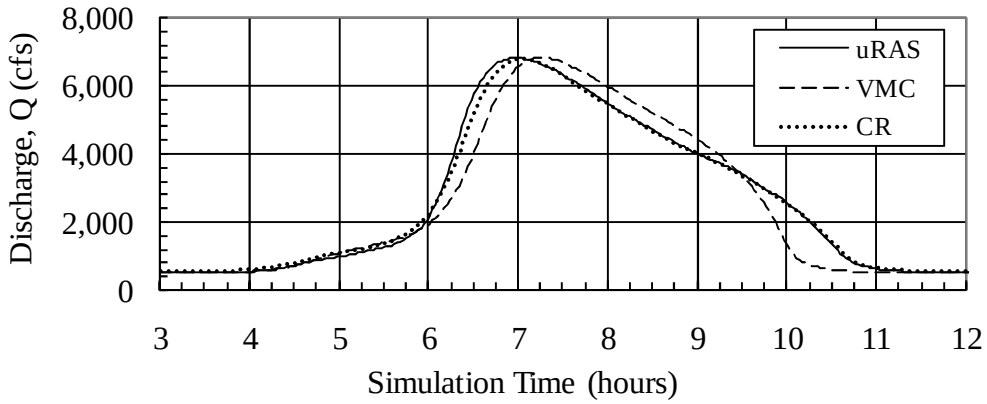

(b) Routed 80,000 feet

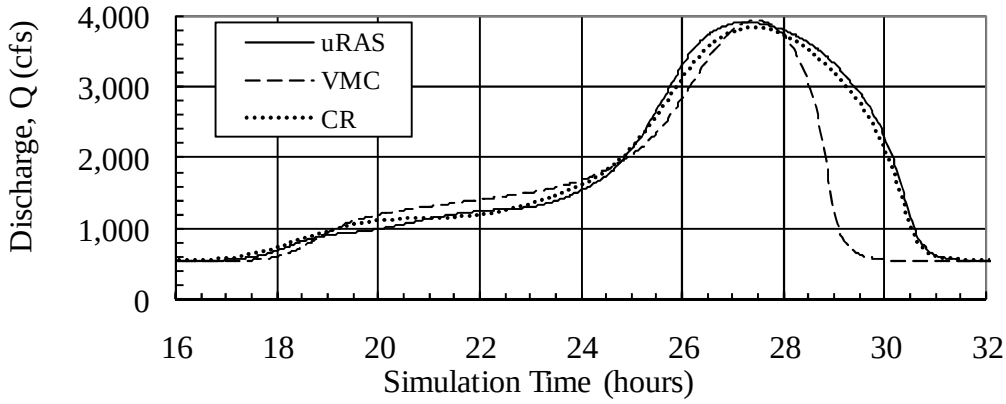

(c) Routed 320,000 feet

Figure 6-14. Hydrographs for Reach No. 2 after Routing with uRAS, VMC and CR

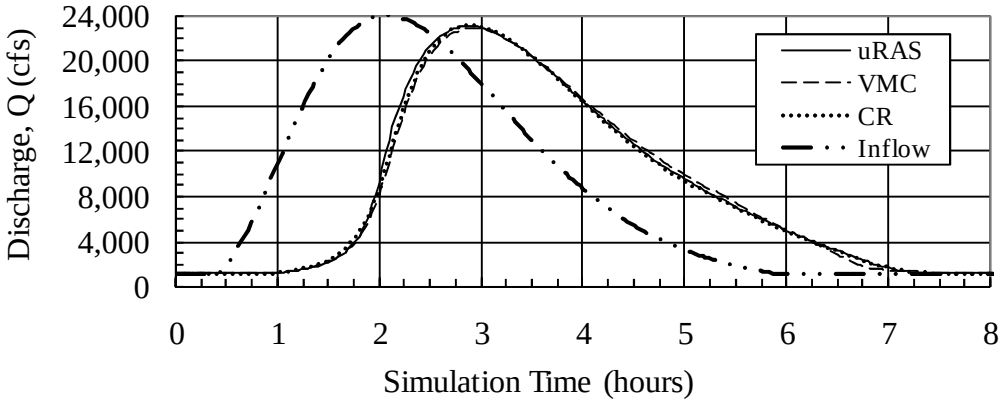

(a) Routed 20,000 feet

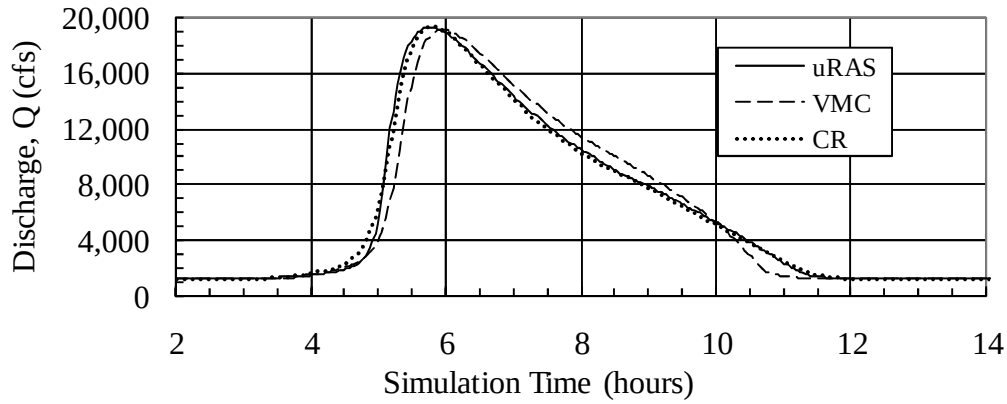

(b) Routed 80,000 feet

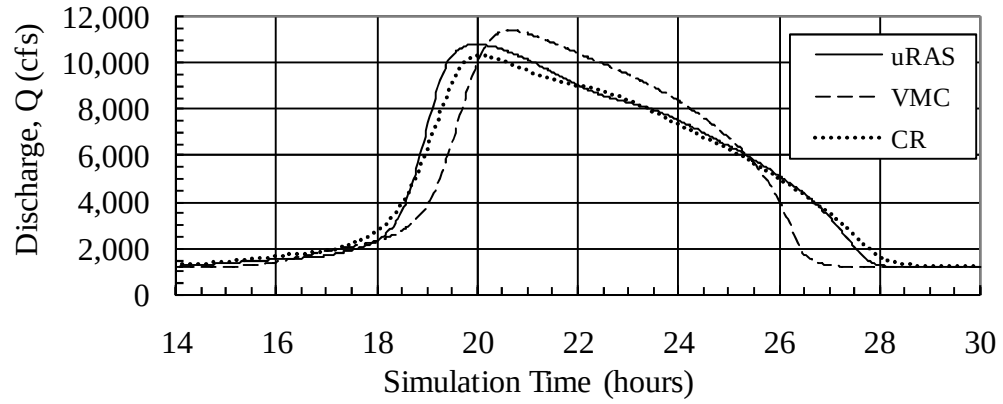

(c) Routed 320,000 feet

Figure 6-15. Hydrographs for Reach No. 3 after Routing with uRAS, VMC and CR

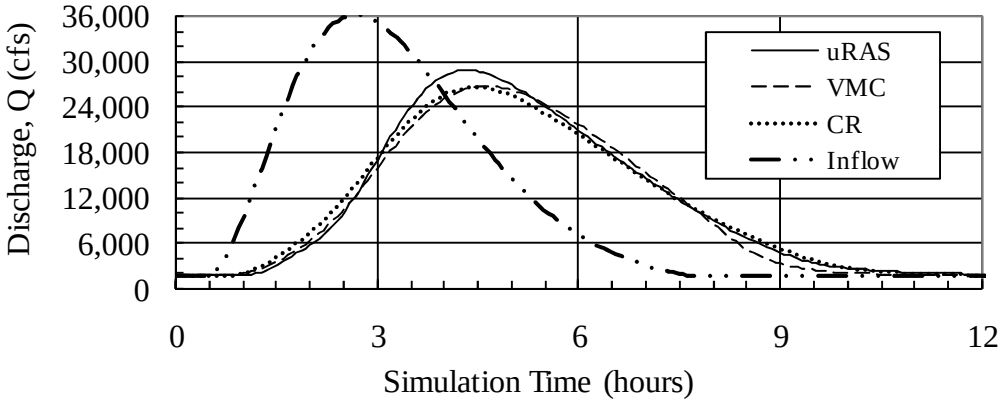

(a) Routed 20,000 feet

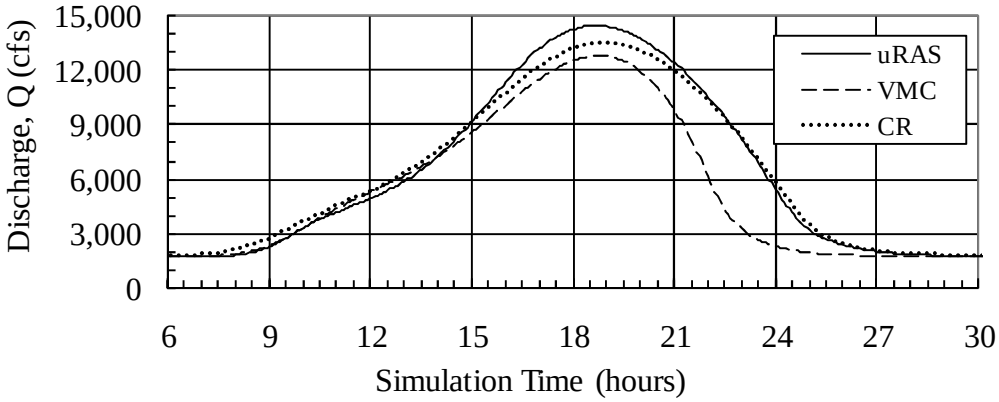

(b) Routed 160,000 feet

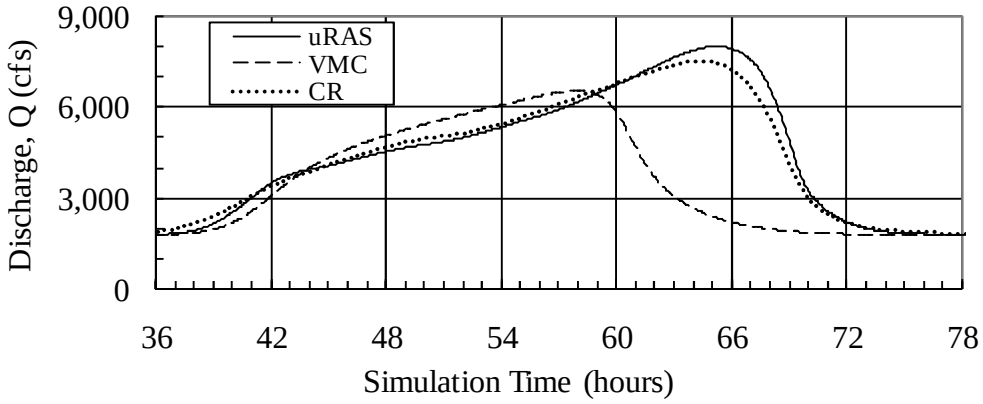

(c) Routed 640,000 feet

Figure 6-16. Hydrographs for Reach No. 4 after Routing with uRAS, VMC and CR

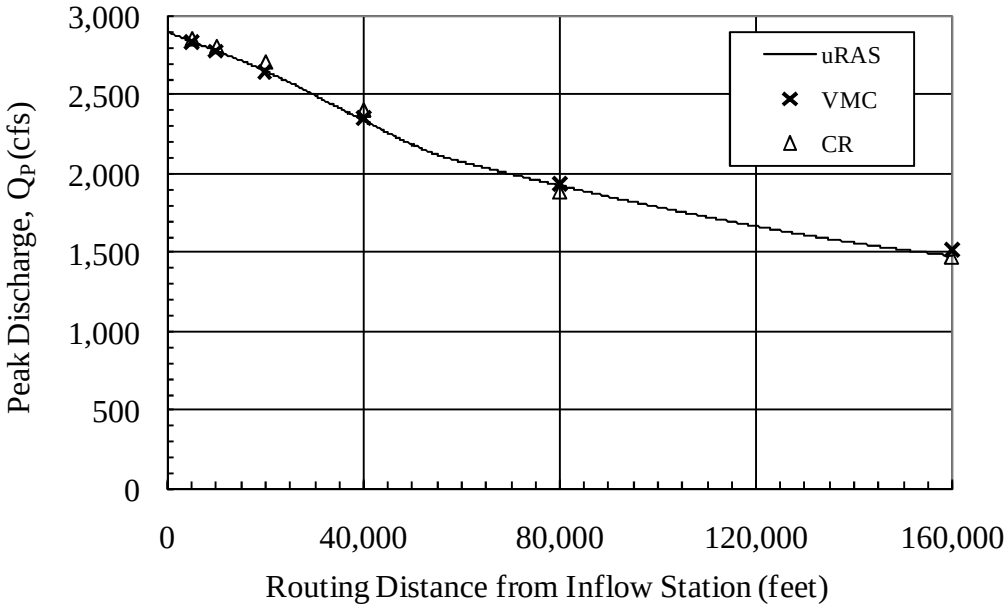

Figure 6-17. Decline of Peak Discharge over Distance, Reach No. 1, Comparing uRAS, VMC and CR

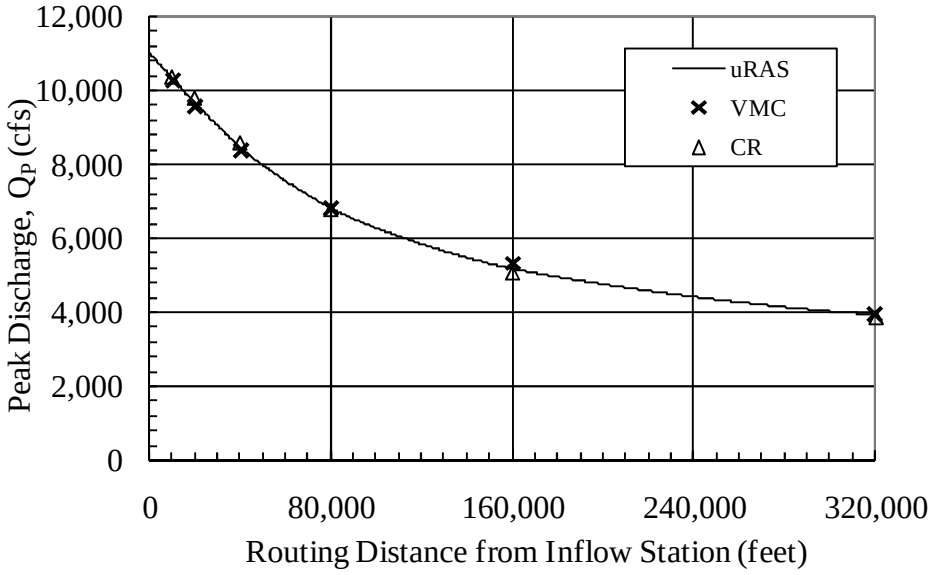

Figure 6-18. Decline of Peak Discharge over Distance, Reach No. 2, Comparing uRAS, VMC and CR

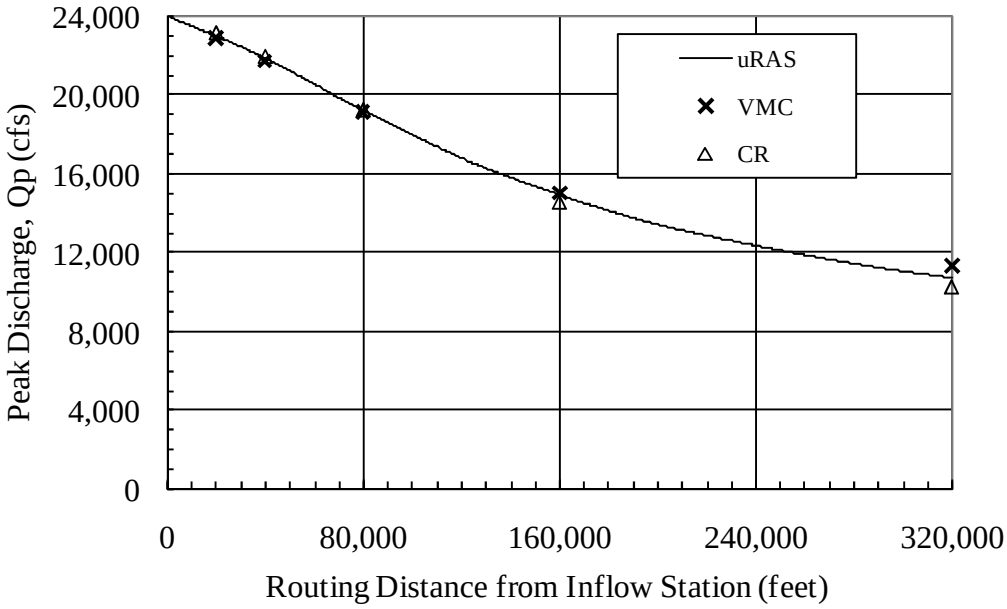

Figure 6-19. Decline of Peak Discharge over Distance, Reach No. 3, Comparing uRAS, VMC and CR

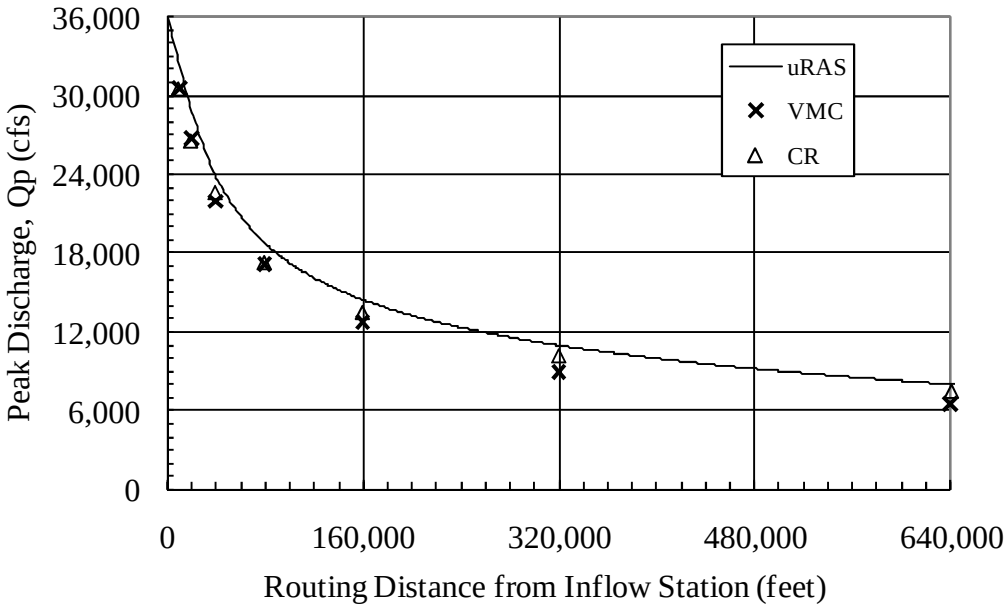

Figure 6-20. Decline of Peak Discharge over Distance, Reach No. 4, Comparing uRAS, VMC and CR

Table 6-28. Volume Losses During Outflow, Testing Round 6B

Reach No.	Routing Distance (feet)	Volume of Inflow Hydrograph, Excluding Baseflow (acre-feet)	Outflow Volume, Relative to Inflow, Excluding Baseflow (%)	
			VMC	CR
1	160,000	168.1	98.2%	100.0%
2	320,000	1570	84.5%	100.0%
3	320,000	4827	96.7%	100.0%
4	640,000	9343	68.6%	100.0%

Table 6-29. Volume Losses for VMC over Routing Length

Reach No.	1	2	3	4
Routed Length (feet)	Outflow Volume, Relative to Inflow, Excluding Baseflow (%)			
1,250	100.0%	--	--	--
2,500	100.0%	99.8%	100.0%	--
5,000	100.0%	99.7%	99.9%	99.0%
10,000	99.9%	99.4%	99.9%	98.0%
20,000	99.8%	98.9%	99.8%	95.9%
40,000	99.4%	97.9%	99.6%	92.0%
80,000	98.7%	96.0%	99.4%	86.4%
160,000	98.1%	92.2%	98.8%	79.4%
320,000	--	84.5%	96.7%	72.4%
640,000	--	--	--	68.6%

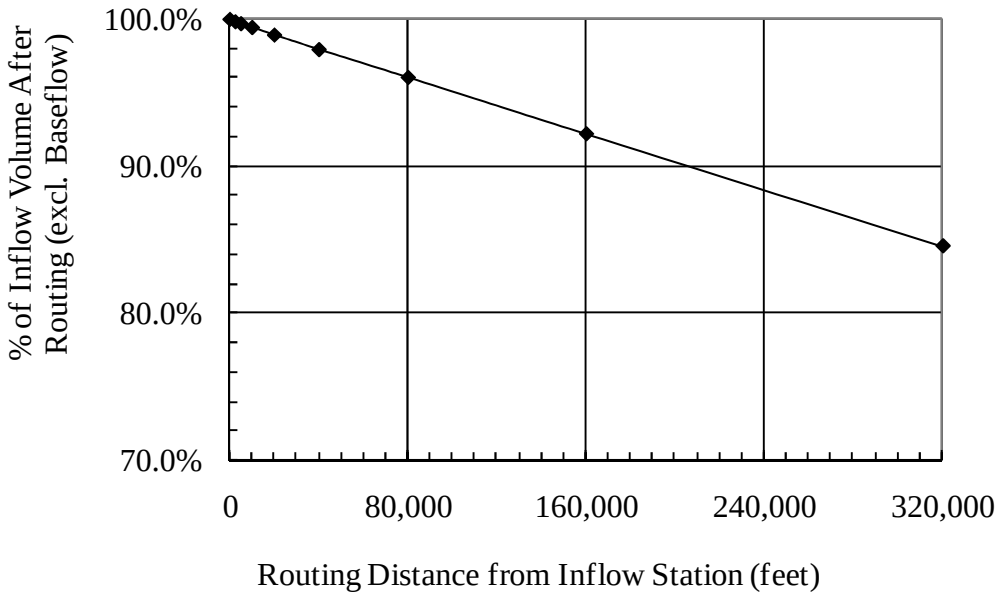

Figure 6-21. Volume Loss Over Routing Distance, Reach No. 2, using VMC Method

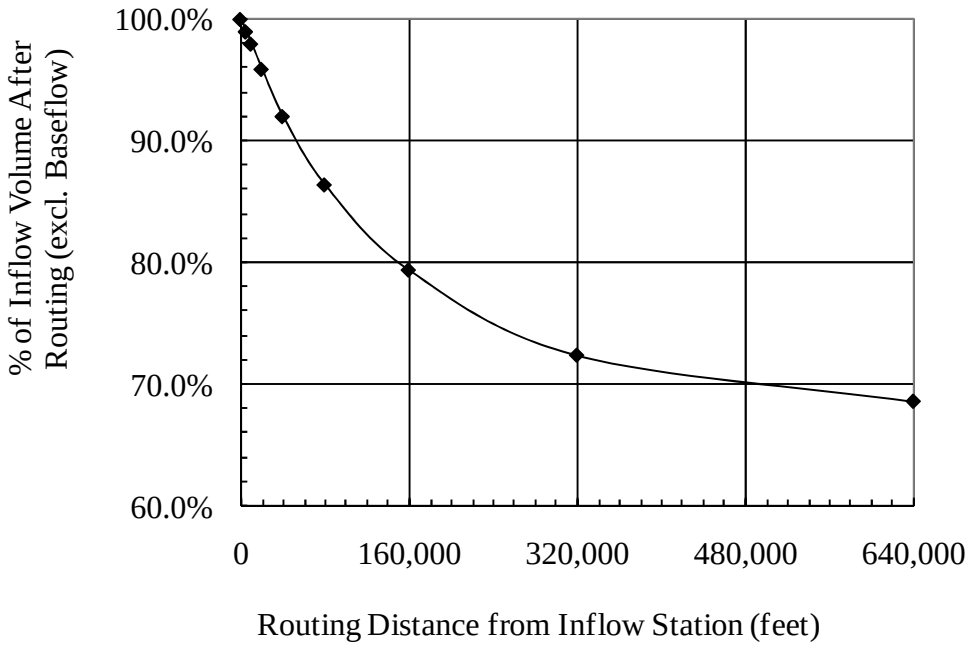

Figure 6-22. Volume Loss Over Routing Distance, Reach No. 4, using VMC Method

The relative differences between the two approximate methods and the fully dynamic solutions can be examined in detail at these three observation locations. Figures 6-14 through 6-16 display similar comparisons for Reach Nos. 2, 3, and 4, respectively.

From these figures, it can be seen that the VMC and CR methods each do a reasonably good job in producing outflow hydrographs similar to those produced by the uRAS method, particularly for the shorter routing reaches. For the 20,000 ft. routing distances on Reach Nos. 2 and 3 (Figures 6-14(a) and 5-15(a)), the agreement between the methods appears to be excellent throughout most of the range of interest.

As routing distances increase, several trends seem to emerge. For the VMC method, it generally appears that the outflow hydrograph begins to lag behind the uRAS output. Also, at very large distance, it appears that volume is being lost from the VMC method, with the falling limb of the outflow hydrograph suddenly tailing off. This is particularly notable on Figure 6-16(c) for Reach No. 4.

The CR method appears to track the general shape of the uRAS hydrograph better over the entire range of flows. On the other hand, the CR method appeared to experience more attenuation than the uRAS method and consistently gave outflow discharges less than uRAS.

Tables 6-16 through 6-23 present the peak outflow discharges and relative attenuation results at the eight downstream observation stations for each of the four reaches. Results for uRAS, VMC and CR are shown. Relative attenuation was defined previously at Eq. (6-1) during the presentation of Testing Round 6A results.

The VMC and CR methods provided the best results on the three smallest streams, Reach Nos. 1, 2, and 3, where the average differences in relative attenuation were less than 0.5% over the range of observation locations. By contrast, the average difference for Reach No. 4 was 4.5% for the VMC method and 2.8% for the CR method. Both VMC and CR produced hydrographs with relatively more attenuation that uRAS.

These results are presented graphically in Figures 6-17 through 6-20, which provide plots of the decline in peak outflow discharges over distance for each of the four reaches. The uRAS results are shown as a continuous line, based on the routing results recorded in the DSS database for each computational distance step. The VMC and CR results at the six downstream-most observation locations are also displayed. The two upstream-most observation locations are omitted for clarity. The general trend in attenuation is followed well in all four reaches, with the best matches occurring for Reach Nos. 1 and 2.

Tables 6-24 through 6-27 present the relative lag in the timing of the peak outflows for the four reaches, where relative lag was previously defined as the difference between the time when the inflow hydrograph reaches its peak discharge and when the outflow hydrograph reaches its peak. Also shown is the percent error in the lag time calculation, compared to uRAS. As with Round 6A, this measure is most useful for assessing differences over long routing distances.

As noted from the figures, the VMC method generally gives longer lag times (slower wave speed) than uRAS or CR method. The exception to this is Reach No. 4,

where the VMC results are inconsistent. On Reach No. 4, the VMC method gives relatively good agreement on lag times for the mid-range distances, but gives very early peaks for the longest routing distance, 640,000 ft. Examination of Figure 6-16(c) demonstrates that his discrepancy is a result of the overall volume loss problem, and not a result of a fundamentally faster travel time for the flood wave.

Table 6-28 presents the volume conservation analyses for VMC and CR for all four reaches. Hydrograph volumes and ratios were calculated using the same methodology described for Testing Round 6A. As can be seen in this table and Figures 6-14 and 6-16, the VMC method experienced considerable volume loss during the routing of flow through Reach No. 2 and No. 4 and slight losses in Reach No. 1 and No. 3. Table 6-29 provides a summary of the accumulated volume losses at each observation station for the four reaches under VMC routing. Figures 6-21 and 6-22 illustrate the volume losses over distance for Reaches 2 and Reaches 4 specifically.

6.4 Comparing uRAS Results on Natural Reach Data vs. 8-Pt. Sections (Testing Round 6C)

The third round of testing focused on the accuracy of using the non-meandering, equivalent 8-point reach derived in Chapter 5 as an approximation of the complex, meandering natural stream reach. Both geometries were tested using the fully dynamic solution to the St. Venant equations using uRAS.

A comparison was made of results for all four routing reaches. Routings were performed for various multiples of the original reach length. As with previous testing, the model set-up for Reach No. 3 is explained in detail.

6.4.1 uRAS Model for Natural Reach Data (Round 6C)

A special uRAS model was created for each of the four reaches, based on the actual cross-sections and natural, meandering geometry. The source geometry for each model was taken from the steady-state discharge models developed for each reach in Chapter 5. These models were based on those watershed models developed in the Tomahawk Creek Flood Study and Blue River Watershed Study, but restructured as described in Chapter 5. These steady-state models were the source data from which 8-pt. sections were derived.

Several modifications were needed to use these steady-state models in unsteady flow routing. The first modification was the extension of the downstream channel length, so that the downstream boundary conditions could lie some distance beyond the outflow observation location. To make the extension, a copy of the downstream-most original cross-section was placed further downstream to serve as the boundary condition location. The main-channel reach length of the extension was arbitrarily selected to be 2,000 feet. The meandering nature of the original stream was approximated by then setting shorter distances for the left and right overbank lengths between the sections. The overbank sections were set proportionally based on the overall reach sinuosity. The apparent sinuosity of Reach No. 3 was 1.38, so the overbank lengths were both set to (2,000 ft. / 1.38) = 1448 feet.

The elevations of all points on the new downstream cross-section were then lowered to match the 0.21% average bed slope of the upstream reach. The new downstream extension was stationed consistently with the upstream reach. The cross-section schematic lines were altered to show the new downstream section. The true downstream cross-section for this reach is located at Station 9.583 miles. The new downstream cross-section at the end of the extended tail was assigned to Station 9.228 miles. The inflow station at the upstream end of the reach is Station 10.937 miles.

The second modification was to add interpolated cross-sections to satisfy the stipulation that the computational distance steps be smaller than the characteristic reach length, L_u. Interpolation also minimizes abrupt changes in channel properties from one section to the next. The original cross-sections were cut from ground topography and exposed wide variations in channel slope, overbank width, and flow area. Sudden changes in these parameters from one section to another might introduce numeric errors or instability in the dynamic solution (USACE 2002a). The addition of several interpolated sections between the original cross-sections helps control instabilities brought on by sudden changes in the geometric parameters.

For this model run, the interpolation interval was set based on the minimum of $\frac{L_u}{2}$ or as needed to provide 1 to 2 interpolated sections between the actual cross-sections of the model. For Reach No. 3, a maximum interpolation distance of 300 feet was specified. This distance was based on an actual spacing of original cross-sections, which ranged between 500 and 800 feet. The characteristic reach length L_u

was much longer (2,935 feet when evaluated at the peak inflow of 24,000 cfs) and did not control. The actual spacing of computational distance steps ranged between 200 and 290 feet. A maximum spacing of 150 feet was used for Reach No. 1, 300 feet for Reach No. 2, and 500 feet for Reach No. 4.

Figure 6-23 shows the plan-view schematic in uRAS for Reach No. 3 after modifications. Flow is from left to right. Original cross-sections are shown in dark grey, with interpolated sections in lighter, dashed grey. The extended "tail" is shown on the right edge.

The actual lengths of the four reaches are too short to produce significant attenuation. For example, Reach No. 3 has an actual length of 7,149.37 feet (rounded to 7,149 ft in all previous tables). Based on the results for Reach No. 3 in Testing Round 6A, the attenuation expected over that length would only be 1 to 2 percent. An effective comparison of natural reach results requires longer routing distances. The effect of a longer routing reach was simulated by routing hydrographs through the same natural reach segment multiple times. The outflow hydrograph at the downstream end of the natural reach resulting from one iteration was cycled back as the inflow hydrograph in the next iteration. This allowed the hydrograph to undergo the attenuation it would have experienced if the original reach length were simply repeated multiple times, but without the need to actually create an artificially-lengthened geometry file.

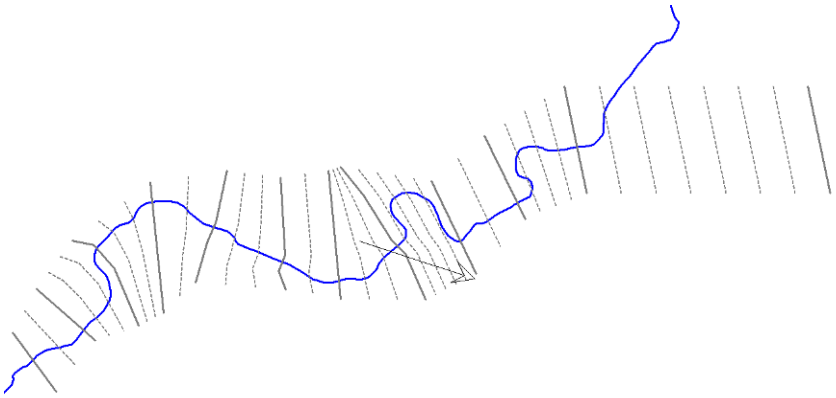

Figure 6-23. HEC-RAS Geometry Schematic for Reach No. 3, Natural Geometry, Unsteady Flow Routing

An initial unsteady flow file was created for each of the four reaches, based on the baseline inflow scenario. The same time steps, minimum flow settings, and initial conditions as described in Testing Round 6A were also used. The downstream boundary condition was set as normal depth, using the reach-averaged bed slope that was used to derive the 8-pt. section. For Reach No. 3, that slope was 0.21%.

As modeling progressed, an unsteady flow file was created for each iteration. The output ordinates from the downstream-most observation station were copied from the DSS database file and pasted into the unsteady flow file for the next iteration. For Reach No. 3, this downstream observation section was the original downstream section at Station 9.583. Observations were not made at the artificially-created downstream boundary at Station 9.228.

An unsteady plan file was created for each iteration, associating the geometry file with the appropriate unsteady flow file. Calculation tolerances and output settings were the same for all iterations. The same computational time step as used in Round 6A was retained. For Reach No. 3, this time step was 2 minutes.

The number of iterations was varied for each reach. The objective was to provide sufficient routing length to attenuate the inflow hydrograph by at least 25% to 30%. For Reaches No. 1 and No. 3, testing was discontinued after 15 iterations, with attenuations close to the target value. Seven iterations were used for Reach No. 4 and 10 were used for Reach No. 2.

6.4.2 uRAS Model for Equivalent Reach (Round 6C)

The unsteady routing results from the natural reach were compared to the results of routing in the simplified equivalent-reach modeled in Testing Rounds 6A and 6B. The equivalent reach consists of a non-meandering, prismatic reach in which each cross-section is defined by the symmetrical 8-pt. section derived previously in Chapter 5.

The uRAS modeling results from Testing Round 6A were used without modification.

The computational distance step intervals used in the natural reach did not match the distance steps used in this equivalent 8-pt. model. However both models used closely-spaced computational nodes, so the node in the 8-pt. reach that came closest to representing the routed length from the natural reach could used for comparison purposes.

6.4.3 Round 6C - Results

Results of Testing Round 6C for Reach Nos. 1 through 4 are given in Tables 6-30 through 6-33 and Figures 6-24 through 6-31.

Tables 6-30 through 6-33 present peak outflow discharges and relative attenuation results at the end of the natural reach after each routing iteration in uRAS. The equivalent routing distance is reported, as is the peak outflow and relative attenuation for the corresponding routing distance in the 8-pt. reach. Although reach lengths had been rounded to the nearest whole feet in all previous reports, the cumulative travel distances shown in these tables were based on a multiple of the actual HEC-RAS main-channel length, which were generally input in feet to two decimal places. The actual lengths used for Reach Nos. 1 through 4 were 3665.86 ft., 6,523.28 ft, 7,149.37 ft., and 10,199.26 ft., respectively.

The peak outflow data for the equivalent reach was adjusted by linear interpolation to correspond to the equivalent routing distance. Figures 6-24 through 6-27 display this same data graphically over the entire range of natural-reach data for each of the four reaches. The relative locations of the natural-reach end points are shown on the figures.

For Reach No. 1, the 8-pt. reach initially experiences slightly less attenuation (i.e. has a greater peak out flow) than the natural-reach, then the trend reverses. The difference in relative attenuation remains within 1% for routing distances up to approximately 28,000 ft (7 to 8 times the original channel length), then it begins to diverge rapidly. After 15 iterations, the relative attenuation in the 8-pt. reach is

26.9% while the natural reach has only experienced 21.6% attenuation, a difference of 5.3%.

Reach Nos. 2 and 3 likewise show a consistent trend of deviation between the 8-pt. reach and the natural reach. By contrast, Reach No. 4 appears to show good agreement between the natural reach and 8-pt. equivalent scenarios, with deviations in relative attenuation of no more than 1.3%.

Figure 6-28 provides a direct comparison of two select outflow hydrographs after routing through the natural reach versus the 8-pt. equivalent reach for Reach No. 1. The hydrographs selected were those at the downstream end of the reach after the 5^{th} and 15^{th} iteration of routing. A hydrograph for the closest corresponding computational point in the equivalent reach is also provided. There is a slight difference in the routed lengths between the natural reach and the equivalent reach, due to different spacing of the computational distance steps.

Figures 6-29 through 6-31 provide corresponding comparisons for Reach Nos. 2 through 4. From these hydrographs, it appears that the discrepancies in peak outflow discharge arise in part from slower wave speeds (greater lag time) in the 8-pt. equivalent reach for Reach Nos. 1, 2 and 3.

A complete explanation for this discrepancy has not yet been discovered; this topic merits further research.

Table 6-30. Peak Flow Results and Relative Attenuation, Reach No. 1, Testing Round 6C

Routing Iteration	Effective Routing Distance (feet)	Peak Outflow Discharge, Q_p, (cfs), uRAS Routing		Attenuation of Peak Outflow Discharge (%)		Diff. in Relative Attenuation, 8-pt. vs. Natural Reach (%)
		Natural Reach	8-Pt. Equivalent Reach	Natural Reach	8-Pt. Equivalent Reach	
Inflow, Peak 2,900 cfs at 36 minutes						
1	3,666	2,849	2,855	1.8%	1.6%	-0.2%
2	7,332	2,801	2,811	3.4%	3.1%	-0.3%
3	10,998	2,755	2,768	5.0%	4.5%	-0.4%
4	14,663	2,710	2,724	6.5%	6.1%	-0.5%
5	18,329	2,668	2,675	8.0%	7.8%	-0.3%
6	21,995	2,627	2,621	9.4%	9.6%	0.2%
7	25,661	2,584	2,569	10.9%	11.4%	0.5%
8	29,327	2,542	2,510	12.3%	13.5%	1.1%
9	32,993	2,500	2,449	13.8%	15.5%	1.7%
10	36,659	2,461	2,391	15.1%	17.6%	2.4%
11	40,324	2,422	2,333	16.5%	19.6%	3.1%
12	43,990	2,382	2,274	17.9%	21.6%	3.7%
13	47,656	2,346	2,217	19.1%	23.6%	4.4%
14	51,322	2,309	2,166	20.4%	25.3%	4.9%
15	54,988	2,275	2,120	21.6%	26.9%	5.3%

Table 6-31. Peak Flow Results and Relative Attenuation, Reach No. 2, Testing Round 6C

Routing Iteration	Effective Routing Distance (feet)	Peak Outflow Discharge, Q_p, (cfs), uRAS Routing		Attenuation of Peak Outflow Discharge (%)		Diff. in Relative Attenuation, 8-pt. vs. Natural Reach (%)
		Natural Reach	8-Pt. Equivalent Reach	Natural Reach	8-Pt. Equivalent Reach	
Inflow, Peak 11,000 cfs at 88 minutes						
1	6,523	10,647	10,556	3.2%	4.0%	0.8%
2	13,047	10,279	10,102	6.6%	8.2%	1.6%
3	19,570	9,907	9,676	9.9%	12.0%	2.1%
4	26,093	9,543	9,267	13.2%	15.8%	2.5%
5	32,616	9,204	8,873	16.3%	19.3%	3.0%
6	39,140	8,887	8,495	19.2%	22.8%	3.6%
7	45,663	8,590	8,152	21.9%	25.9%	4.0%
8	52,186	8,319	7,852	24.4%	28.6%	4.2%
9	58,710	8,071	7,576	26.6%	31.1%	4.5%
10	65,233	7,841	7,319	28.7%	33.5%	4.7%

Table 6-32. Peak Flow Results and Relative Attenuation, Reach No. 3, Testing Round 6C

Routing Iteration	Effective Routing Distance (feet)	Peak Outflow Discharge, Q_p (cfs), uRAS Routing		Attenuation of Peak Outflow Discharge (%)		Diff. in Relative Attenuation, 8-pt. vs. Natural Reach (%)
		Natural Reach	8-Pt. Equivalent Reach	Natural Reach	8-Pt. Equivalent Reach	
Inflow, Peak 24,000 cfs at 124 minutes						
1	7,149	23,656	23,633	1.4%	1.5%	0.1%
2	14,299	23,293	23,273	2.9%	3.0%	0.1%
3	21,448	22,931	22,909	4.5%	4.5%	0.1%
4	28,597	22,552	22,524	6.0%	6.1%	0.1%
5	35,747	22,158	22,114	7.7%	7.9%	0.2%
6	42,896	21,754	21,676	9.4%	9.7%	0.3%
7	50,046	21,336	21,217	11.1%	11.6%	0.5%
8	57,195	20,916	20,736	12.9%	13.6%	0.7%
9	64,344	20,496	20,240	14.6%	15.7%	1.1%
10	71,494	20,087	19,761	16.3%	17.7%	1.4%
11	78,643	19,685	19,306	18.0%	19.6%	1.6%
12	85,792	19,292	18,861	19.6%	21.4%	1.8%
13	92,942	18,911	18,418	21.2%	23.3%	2.1%
14	100,091	18,538	17,979	22.8%	25.1%	2.3%
15	107,241	18,177	17,548	24.3%	26.9%	2.6%

Table 6-33. Peak Flow Results and Relative Attenuation, Reach No. 4, Testing Round 6C

Routing Iteration	Effective Routing Distance (feet)	Peak Outflow Discharge, Q_p, (cfs), uRAS Routing		Attenuation of Peak Outflow Discharge (%)		Diff. in Relative Attenuation, 8-pt. vs. Natural Reach (%)
		Natural Reach	8-Pt. Equivalent Reach	Natural Reach	8-Pt. Equivalent Reach	
Inflow, Peak 36,000 cfs at 160 minutes						
1	10,199	31,607	32,061	12.2%	10.9%	-1.3%
2	20,399	28,134	28,607	21.8%	20.5%	-1.3%
3	30,598	25,409	25,769	29.4%	28.4%	-1.0%
4	40,797	23,236	23,583	35.5%	34.5%	-1.0%
5	50,996	21,569	21,928	40.1%	39.1%	-1.0%
6	61,196	20,216	20,601	43.8%	42.8%	-1.1%
7	71,395	19,085	19,500	47.0%	45.8%	-1.2%

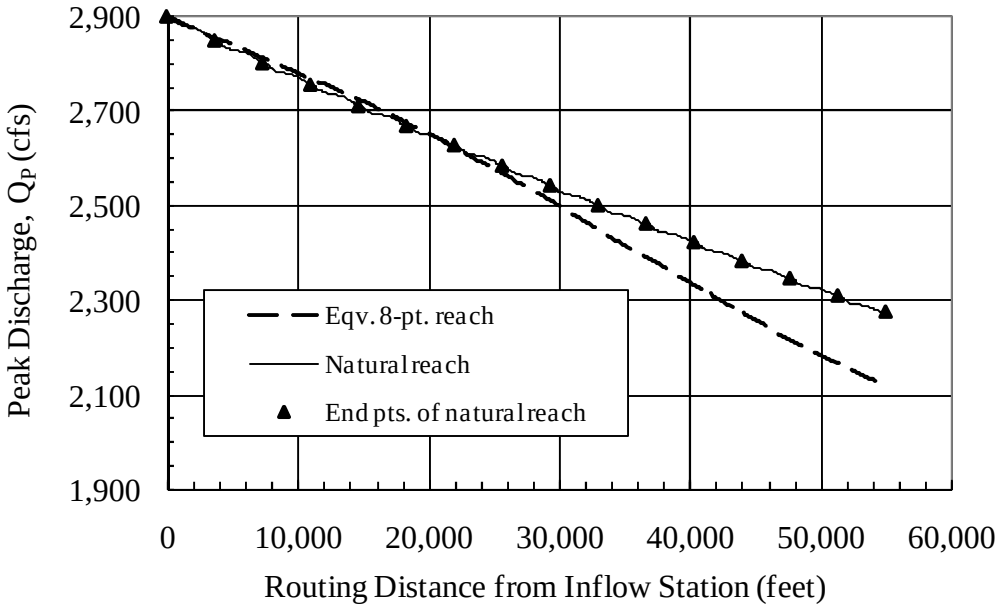

Figure 6-24. Decline of Peak Discharge over Distance, Reach No. 1, Comparing Natural vs. Equivalent Reach for uRAS Routing

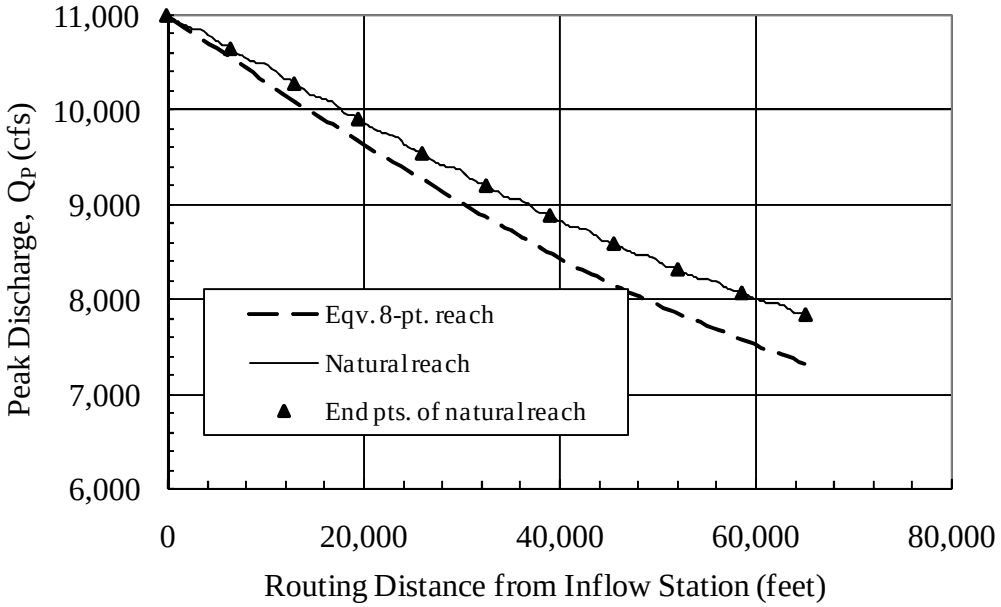

Figure 6-25. Decline of Peak Discharge over Distance, Reach No. 2, Comparing Natural vs. Equivalent Reach for uRAS Routing

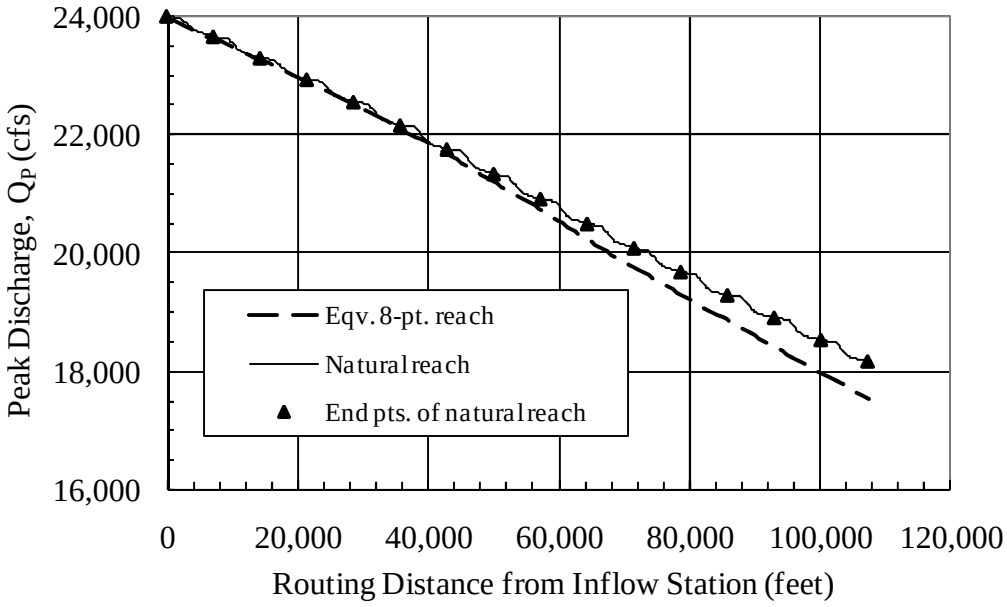

Figure 6-26. Decline of Peak Discharge over Distance, Reach No. 3, Comparing Natural vs. Equivalent Reach for uRAS Routing

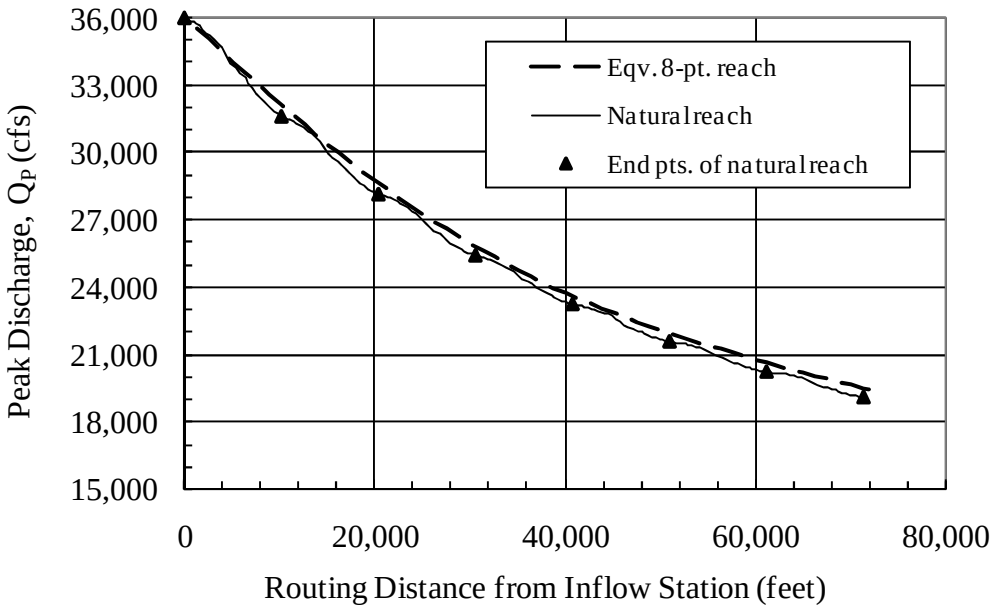

Figure 6-27. Decline of Peak Discharge over Distance, Reach No. 4, Comparing Natural vs. Equivalent Reach for uRAS Routing

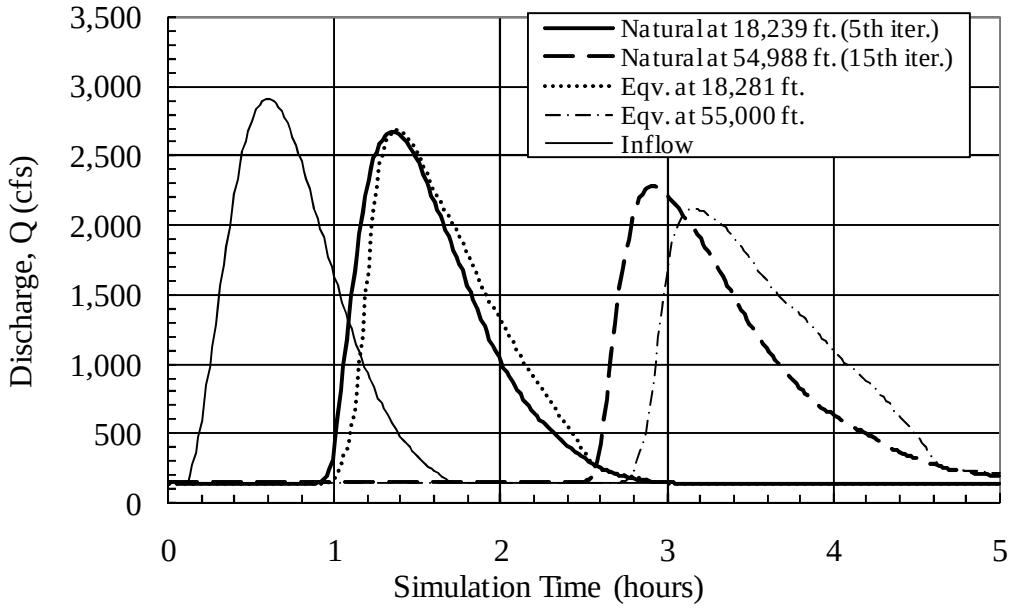

Figure 6-28. Natural vs. Equivalent Reach Routing by uRAS, Comparison of Select Hydrographs, Reach No. 1

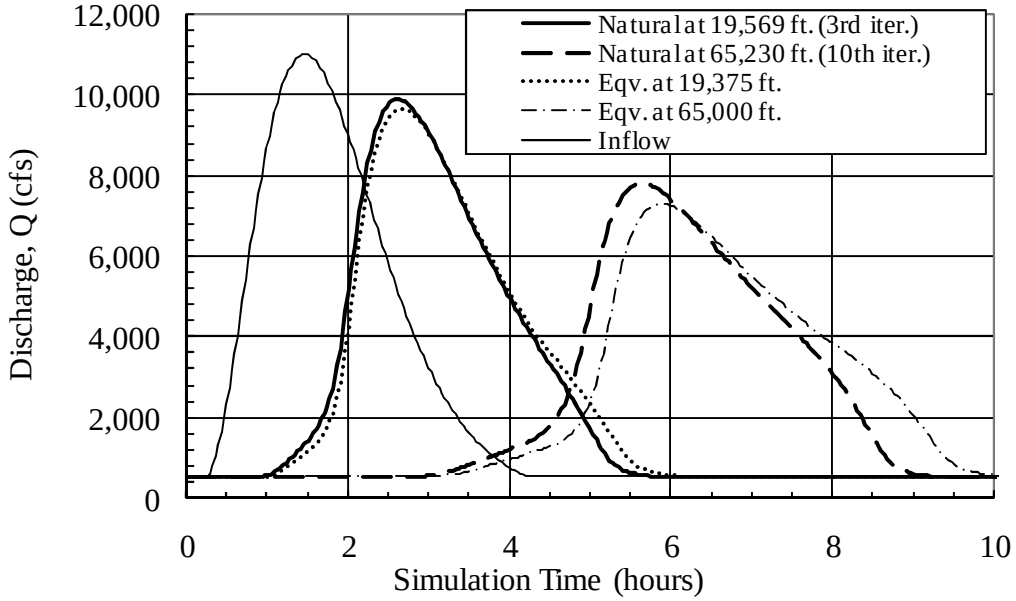

Figure 6-29. Natural vs. Equivalent Reach Routing by uRAS, Comparison of Select Hydrographs, Reach No. 2

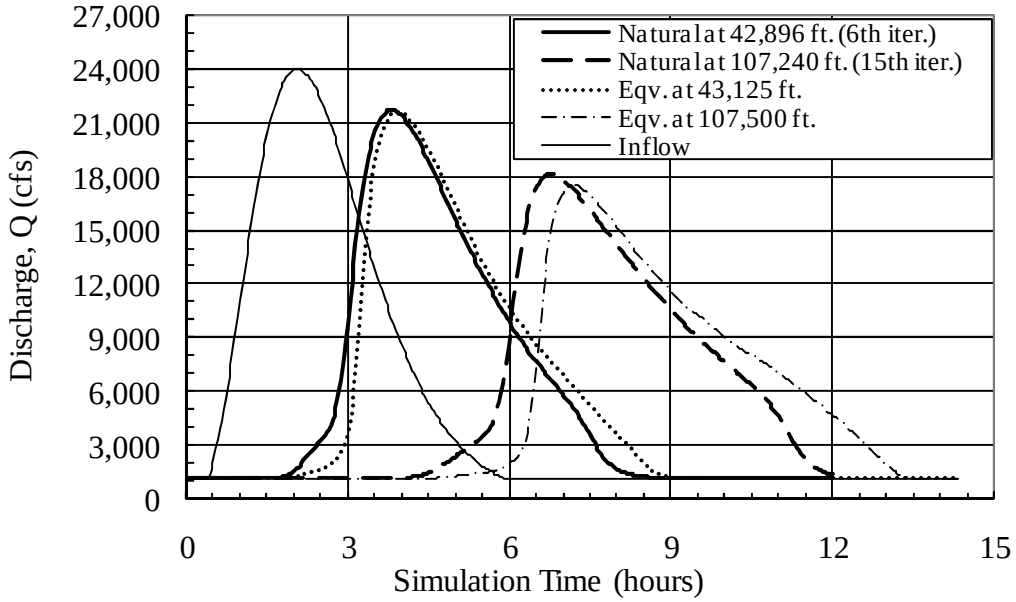

Figure 6-30. Natural vs. Equivalent Reach Routing by uRAS, Comparison of Select Hydrographs, Reach No. 3

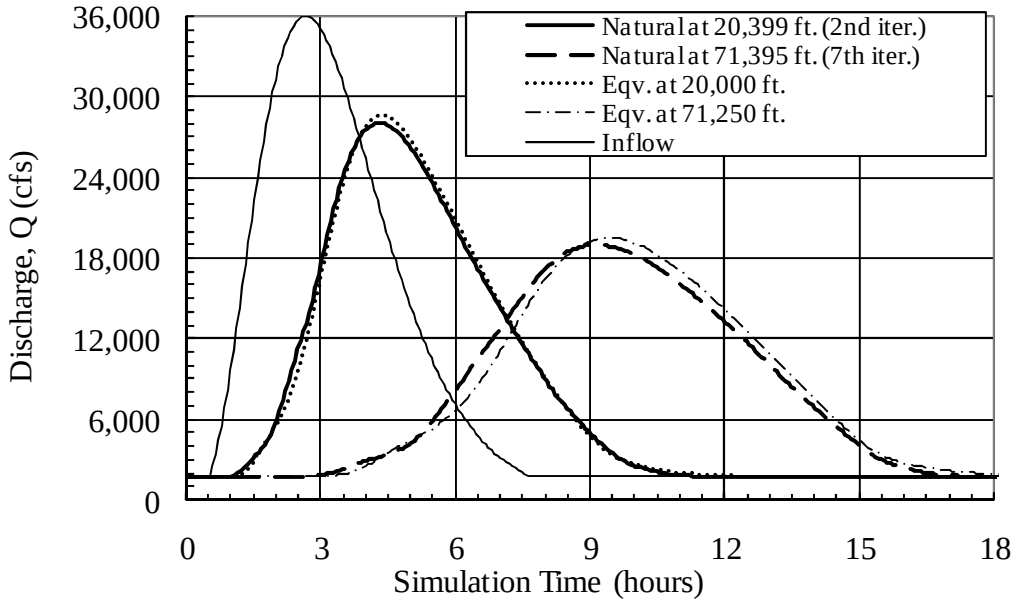

Figure 6-31. Natural vs. Equivalent Reach Routing by uRAS, Comparison of Select Hydrographs, Reach No. 4

6.5 Analysis and Recommendations

Testing Round 6A demonstrated the similarity of routing results that could be obtained for 8-pt. equivalent reaches when using either the unsteady HEC-RAS solution (uRAS) or the FLDWAV program (FLW). Both methods appeared to agree within an average of 0.1 to 0.3% for all four reaches over an extreme distance of flood routing. The FLW method appeared to give near perfect volume conservation, with only 0.1% error maximum after routing distance of 30 to 120 miles. On the other hand, two of the reaches suffered from oscillations in the falling limb of the hydrograph when FLW was used. The origin of these oscillations was not determined, but merits further study.

Testing Round 6B showed further that the two approximate methods also gave reasonably good agreement to the fully dynamic solution. The two approximate methods were the variable-parameter Muskingum-Cunge method (VMC) and the Cascading Reservoirs (CR) method. The agreement was strongest for the shorter and medium length routing lengths, and was best for three smaller reaches, Reach Nos. 1, 2 and 3. The VMC method suffered on two of the reaches from excessive problems with volume conservation. In general, the VMC method appeared to lose volume during routing, whereas the CR method gave excellent conservation. The primary difference in the methods lies in the fact that the value of L_u and thus "X" varies during the routing when using VMC, which is not the case in the CR method. Further research into the volume loss on natural streams is warranted.

Rounds 6A and 6B were each based on the equivalent reach defined using 8-pt. sections. Round 6C examined the correlation between uRAS results when using the equivalent reach versus the original natural stream data. For Reach No. 4, the two methods of defining the reach gave similar results over the routing distances examined, with the differences in relative attenuation less than or equal to 1.3%. By contrast, a systematic divergence occurred in Reach Nos. 1, 2 and 3, with the natural reach method consistently producing less attenuation (higher peak discharges) than the 8-pt. equivalent reach over the longer routing distances.

Chapter 7

Sensitivity Testing of Modeling Controls

7.1 General Considerations

In Chapter 6, a comprehensive comparison was made of the Muskingum-Cunge method and fully dynamic solutions of the St. Venant equations. Actual model results are dependent in part on the stability of the dynamic solution and upon the particular values chosen for certain modeling parameters. In an ideal situation, only adjustments in variables that represented physical phenomena would impact model results. In reality, certain non-physical parameters were found to have an important impact. In this chapter, the role of four specific parameters are investigated: time step (Δt), distance step (Δx), the finite-difference weighting coefficient (θ or theta), and the minimum or baseflow discharge of the hydrograph.

The sensitivity of uRAS and FLW model results to these four parameters is examined. The analyses are limited to Reach No. 3. Four (4) rounds of testing were conducted, as follows:

7A – Distance Steps and Minimum Flows Using uRAS – Reach No. 3 was tested using uRAS for five different computational distance steps and two assumptions of minimum baseflow. The comparisons were made using the "equivalent 8-pt. reach" used previously in Testing Round 6A.

7B – Distance Steps and Low-Flow Filters Using FLW – A similar testing program to that in Round 7Awas made for FLW. Five distance step options were evaluated, and comparison made between the option of activating the low flow filter option. Only one baseflow assumption was used in this testing round.

7C – Time-Step Variations Using uRAS and FLW - A direct comparison of routing results on Reach No. 3 using uRAS and FLW was made for three time steps ranging from 30 seconds to 6 minutes.

7D – Variations of Theta (θ) Using uRAS and FLW - A direct comparison of routing results on Reach No. 3 using uRAS and FLW was made for three choices of finite-difference weighting factors, theta (θ), ranging from 0.6 to 1.0.

Details of the methodology, results, and testing criteria for each round are presented in the following sections.

7.2 Distance Step and Minimum Baseflow Relationships, using uRAS (Testing Round 7A)

The first round of sensitivity testing focused on the impact of different distance steps on stability and performance in unsteady HEC-RAS modeling (uRAS). Five (5) different computational distance steps were selected, as shown in Table 7-1. The smallest distance step, 625 feet, matches the value used in the testing rounds described in Chapter 6.

Table 7-1. Computational Distance Steps to Evaluate, Reach No. 3, Testing Round 7A

Computational Distance Step, Δx (feet)	Ratio Δx / L_U, Evaluated for Given Flow Condition		
	Peak Inflow, I_P	5% of I_P	20% of I_P
625	0.2	0.4	0.4
2,500	0.9	1.6	1.4
5,000	1.7	3.2	2.8
10,000	3.4	6.4	5.6
20,000	6.8	12.8	11.3
L_U (feet)	2,935	1,563	1,771
Q (cfs)	24,000	1,200	4,800

Table 7-1 also shows the ratio of the distance step to characteristic reach length, $\frac{\Delta x}{L_U}$. Ratios are calculated for various flow conditions, including the peak inflow discharge, I_P, and for smaller flows having values of 5% and 20% of I_P. These smaller flows correspond to the minimum baseflow values evaluated in this testing round.

The $\frac{\Delta x}{L_U}$ ratio was tested over the range from 0.2 to 6.8, based on L_u evaluated at the peak discharge, I_P. When evaluated at a discharge of 5% of I_P, the ratio covered the range from 0.4 to 12.8.

As is shown in the modeling results from this round, the uRAS model is sensitive to instabilities caused by large distance steps. One technique for overcoming these instabilities is the setting a larger minimum flow (baseflow) on the inflow hydrograph. The modeling in Chapter 6 set the baseflow equal to 5% of the

peak inflow. For Reach No. 3, the peak inflow is 24,000 cfs and the baseflow was therefore 1,200 cfs. To explore the relationship between distance step size and baseflow, an alternate inflow hydrograph was investigated which had a baseflow equal to 20% of the peak inflow.

The combination of 5 distance steps and 2 baseflow levels produces 10 computational scenarios in uRAS. All the scenarios used in this testing round utilized a weighting coefficient of $\theta = 0.6$ and a computational time step of 2 minutes. These parameters mirror those used in Chapter 6. More information on the role of the weighting coefficient, θ, is provided later in the discussion of Testing Round 7D.

The first computational scenario uses a distance step of 625 feet and a baseflow of 5% of the peak inflow. This is the scenario that matches the testing conducted in Chapter 6 and is reference condition against which other scenarios were evaluated.

All outflow results are examined at the observation station located 160,000 feet downstream of the inflow point. This observation point is unrealistic in a physical sense because it is unlikely that any natural steam reach with an initial drainage area of 24.5 square miles would flow that distance without a dramatic increase in channel dimensions and lateral inflow. As with the testing in Chapter 6, however, this distance is useful for sensitivity testing. The routing distance is large enough to allow small errors to propagate and produce more obvious deviations in results.

7.2.1 uRAS Model Setup (Round 7A)

The uRAS model used in this testing round is based on the model parameters described in Testing Round 6A in the previous chapter. To allow for easier comparison of results, all 10 testing scenarios were incorporated as separate *unsteady plans* in a single HEC-RAS project.

The geometry files were all based on the non-meandering 8-point cross-section geometry file developed for Testing Round 6A. The inflow enters the channel reach at Station 0 and is routed downstream a total of 320,000 feet. The downstream boundary condition is the normal-depth flow option applied at the end of the 10,000 foot "tail" appended to the end of the reach.

The initial geometry file from Round 6A was modified to remove the intermediate sections previously located at 2,500, 5,000, 10,000 and 20,000 feet downstream of the inflow point. This modification made it easier to adjust the interpolation interval on the overall reach. The interpolation interval in uRAS sets the computational distance step. Five separate geometry files were created, one for each computational distance step listed in Table 7-1. All five distance steps are even divisors of 20,000 feet, which allows a common comparison of longer reach intervals.

The flow file from Testing Round 6A was also retained. This file contained the inflow hydrograph for Reach No. 3, which has a peak discharge of 24,000 cfs, a time-to-peak of 124 minutes, and a shape matching the gamma distributions with m equal to 3.7. The original flow file used a minimum baseflow of 1,200 cfs, (5% of the baseflow). A second flow file was created in which the baseflow was set to 4,800

cfs (20% of the peak inflow). The minimum discharges values were entered into the "*min. flow*" field on the input screen at **HEC-RAS | Edit | Unsteady Flow Data | Boundary Condition | Flow Hydrograph** for the upstream boundary at Station 0. The same value was also entered in the "*Initial Flow*" field on the input screen at **Unsteady Flow Data | Initial Conditions**.

A separate plan file was created for each of the 10 scenarios. The time step (Δt) and finite-difference factor (θ) were assigned. Each plan was uniquely named and structured to export the outflow hydrograph to a DSS file. The DSS file format is an external database file that HEC-RAS can read. HEC-RAS provides for limited output analyses tools, including graphical plots and tabular summaries of the data.

7.2.2 Round 7A – Results

Results of Testing Round 7A for are given in Tables 7-2 and 7-3 and in Figures 7-1 and 7-2.

Table 7-2 presents the peak outflow discharges and relative attenuation results for each of the 5 distance step sizes selected, as evaluated after routing the inflow hydrograph in uRAS for 160,000 feet. Results are given for two inflow scenarios: one with a minimum baseflow of 5% of the inflow peak and another with a baseflow of 20% of the inflow peak. The outflow peak in the reference scenario is 14,952 cfs, which represents a 37.7% relative attenuation of the inflow peak of 24,000 cfs.

For the 5% scenario, uRAS failed to produce usable results for the two largest distance steps, 10,000 and 20,000 feet. In both cases, the program reported that it reached the maximum number of iterations for most computations. Inspection of

output results showed erratic flow results with frequent spikes that were orders of magnitude larger than the inflow. These two scenarios were neglected in further analyses. The largest distance step that was successfully routed was 5,000 feet, which produced a relative attenuation of 38.2%, within 0.5% of the reference scenario.

By contrast, the scenarios with a 20% baseflow all successfully produced output results. In general, these scenarios all experienced less attenuation than the 5% baseflow scenarios.

For the two scenarios with $\Delta x = 625$ ft., the 20% baseflow scenario had a relative attenuation that was 5.8% less than the 5% baseflow scenario. As distance step increased, the general trend was towards greater attenuation, with a relative attenuation of 35.5% when the distance step was 20,000 ft.

Table 7-3 provides a summary of the volume balance in the discharge hydrographs for these same scenarios. Volume balance is defined as the proportion of volume in the outflow hydrograph relative to the inflow hydrograph, with the volume associated with the minimum baseflow excluded. The volumes were calculated by integration of the hydrograph ordinates using the trapezoidal rule, as described previous with Testing Round 6A.

Table 7-2. Sensitivity of Peak Flow Results to Distance Step Size, Based on uRAS Routing on Reach No. 3, Testing Round 7A

Computational Distance Step, Δx (feet)	Peak Outflow Discharge, Q_p, (cfs) for Given Scenario, after Routing 160,000 ft. in uRAS		Attenuation of Peak Outflow Discharge (%)		Diff. in Relative Attenuation, Relative to the Reference Scenario (%) *	
	5% Baseflow	20% Baseflow	5% Baseflow	20% Baseflow	5% Baseflow	20% Baseflow
Inflow, Peak 24,000 cfs at 124 minutes						
625	14,952	16,352	37.7%	31.9%	*Reference Scenario**	-5.8%
2,500	14,956	16,307	37.7%	32.1%	0.0%	-5.6%
5,000	14,836	16,185	38.2%	32.6%	0.5%	-5.1%
10,000	n/a **	15,854	--	33.9%	--	-3.8%
20,000	n/a **	15,473	--	35.5%	--	-2.2%

** The Reference Scenario uses Δx = 625 ft and 5% baseflow.*

*** uRAS failed to compute valid results for these two scenarios.*

Table 7-3. Sensitivity of Volume Changes to Distance Step Size, Based on uRAS Routing on Reach No. 3, Testing Round 7A

Computational Distance Step, Δx (feet)	Outflow Volume, Relative to Inflow, Excluding Baseflow (%), for Given Scenario after Routing 160,000 ft. in uRAS	
	5% Baseflow	20% Baseflow
625	100.8%	101.0%
2,500	101.3%	101.2%
5,000	100.0%	101.3%
10,000	n/a *	101.4%
20,000	n/a *	102.5%
Inflow Volume, Excluding Baseflow (acre-feet)	4,827	3,464

** uRAS failed to compute valid results for these two scenarios*

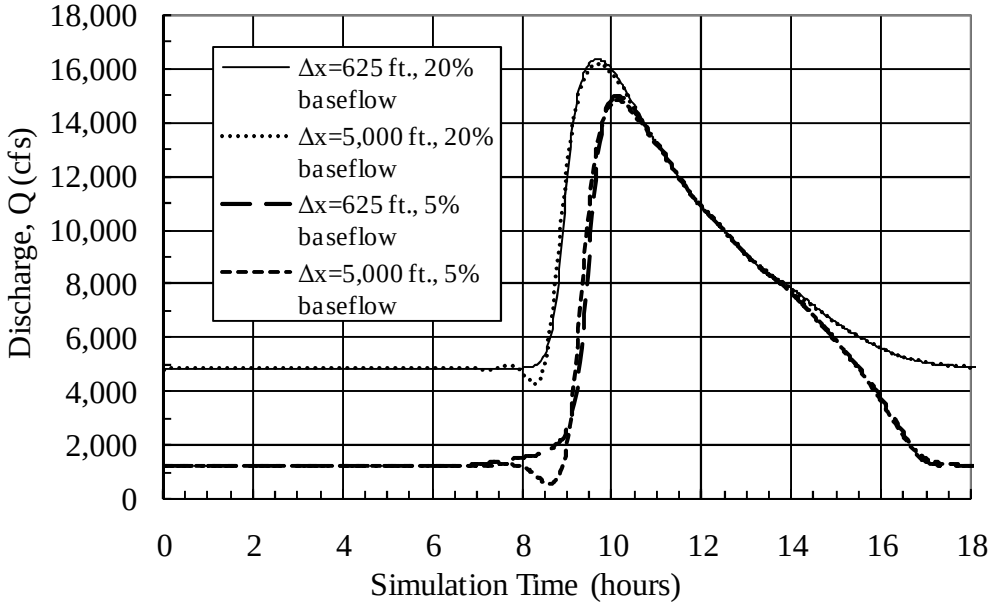

(a) 625 and 5,000 ft. Distance Steps (Δx), 5% and 20% Baseflows

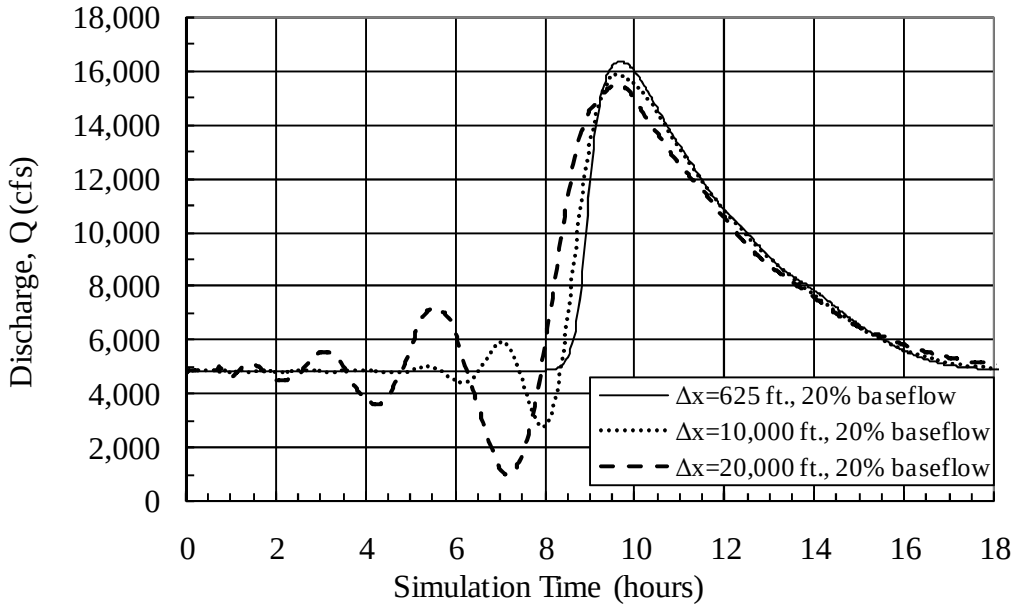

(b) 10,000 and 20,000 ft. Distance Steps (Δx), 20% Baseflow only

Figure 7-1. Outflow Hydrographs for Reach No. 3, after Routing 160,000 feet in uRAS, Various Distance Steps and Minimum Baseflows

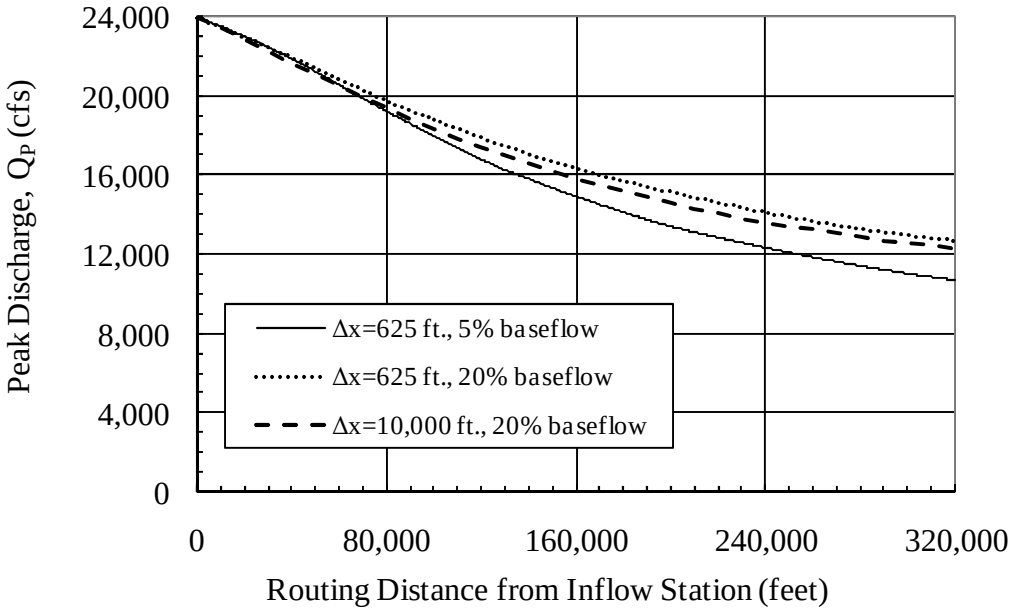

Figure 7-2. Decline of Peak Discharge over Distance, Reach No. 3, Comparing uRAS Results for Select Distance Steps and Baseflows

In general, there was no significant trend in volume balance. The outflow hydrographs all appeared to gain a slight amount of volume during routing, but the maximum increase was 2.5% when Δx = 20,000 feet and baseflow was 20%.

Figure 7-1 provides a plot of the outflow hydrographs from these scenarios after routing a distance of 160,000 feet. Figure 7-1(a) compares the two baseflow scenarios for two of the shorter distance steps, 625 ft. and 5,000 feet. The hydrograph for the Δx = 2,500 ft. distance step scenario is omitted because it was almost identical to the Δx = 625 ft. scenario.

For a constant baseflow, increasing the distance step to 5,000 feet had only minor impacts on most of the hydrograph and very little impact on the peak discharge. A noticeable "dip" emerged, however, at the base of the rising limb of the

hydrograph for the 5,000 ft. distance step. The dip occurred under both baseflow conditions, though it appeared relatively more pronounced in the 5% baseflow scenario.

For a constant Δx, the impact of using an increased baseflow was more significant. In both cases, the 20% baseflow scenario began to rise earlier and reached a larger outflow peak. The falling limbs of all four hydrographs, however, were almost identical at flows well above the baseflow.

Figure 7-1(b) presents the hydrographs for the two larger distance steps, 10,000 ft. and 20,000 ft., based on the 20% baseflow scenario. The hydrograph for $\Delta x = 625$ ft, 20% baseflow scenario is also shown for reference. Rather than the "dip" that was present in the $\Delta x = 5{,}000$ ft. scenario, these hydrographs suffer from significant oscillations that precede the rising limb. Once the initial period with oscillations passes, the remainder of the hydrographs follows the reference condition reasonably well. It appears that a residual effect of the initial instability is increased attenuation of the peak discharge. The falling limbs of all three hydrographs plot reasonably well together.

The impacts of these oscillations are offset to some degree by the large minimum baseflows established in the inflow hydrograph. The baseflow served to absorb the lower component of each cycle, preventing the model from experiencing negative or near-zero discharges. As shown in Figure 7-1(b), the largest oscillation in the $\Delta x = 20{,}000$ ft scenario drops to a minimum discharge of 978 cfs, which is 3822 cfs below the baseflow level. Relative to the inflow peak of 24,000 cfs, this is a

swing of 16%. The 5% baseflow scenario would not have been able to absorb such a large dip.

The characteristic reach length Reach No. 3 was 2,935 ft. when evaluated based on the full initial peak discharge of 24,000 cfs. The initial dip is not present in the scenarios with $\Delta x = 625$ and $\Delta x = 2{,}500$, which represent conditions where the computational distance step is smaller than the characteristic reach length. A dip is present when $\Delta x = 5{,}000$ ft, which has a $\frac{\Delta x}{L_U}$ ratio of 1.7. For the two largest time steps, which experience repeated oscillations prior to the rising limb, the $\frac{\Delta x}{L_U}$ ratios are 3.4 and 6.8.

The characteristic reach lengths evaluated at the 5% and 20% baseflow levels are 1,563 and 1,771 ft, respectively. These lengths are almost half the value of L_u at the initial peak. Based on the value of L_u in the 5% scenario, the hydrograph begins to dip somewhere between $\frac{\Delta x}{L_U}$ ratios of 1.6 and 3.2, whereas full-scale oscillations begin somewhere between $\frac{\Delta x}{L_U}$ ratios of 3.2 and 6.4.

Perumal (1992) explored the issue of negative inflow values in Muskingum-Cunge routing and concluded that the appearance of a dip was related to fact that the distance step exceeded L_u. These results suggest that a similar situation may also be true of fully dynamic routing solutions and that the characteristic reach length, L_u, may serve as a good guideline for selecting computational distance steps here as well.

Figures 7-2 presents a plot of the decline in peak outflow discharges over distance for three select scenarios. The first two scenarios are based on $\Delta x = 625$ ft and compare the attenuation of peak discharges for the 5% and 20% baseflow scenarios. In general, an increase in baseflow from 5% to 20% led to decreased attenuation of the discharges as routing proceeds downstream.

The third scenario plotted is for $\Delta x = 10{,}000$ ft and 20% baseflow. In comparing the two scenarios with 20% baseflow, it appears that changing distance steps has relatively less effect on the accuracy of peak outflow calculations throughout the entire range modeled.

7.3 Distance Steps and Low-Flow Filter, using FLW (Testing Round 7B)

In the second round of sensitivity testing, a similar evaluation of distance steps was made for the FLW program. The same range of five computational distance steps was evaluated. FLW was found to be more stable than uRAS in its handling of low-flow conditions. For that reason, a complete evaluation of the two baseflow scenarios was unnecessary and all primary FLW evaluations were made using the 5% baseflow scenario. One model test using the 20% baseflow scenario was created to allow for a direct comparison between uRAS and FLW on the largest distance step.

FLW provides a “low-flow filter” option which is designed to prevent output hydrographs from falling below a reference value. The performance of this filter was examined in this testing round.

The combination of five distance steps and two filter options (low-flow filter set on or off) produced 10 computational scenarios in FLW. As with Round 7A, all the tests conducted in this testing round utilized $\theta = 0.6$ and a computational time step of 2 minutes. These values mirror those used in Chapter 6. Outflows were examined at the observation station located 160,000 feet downstream of the inflow point.

7.3.1 FLW Model Setup (Round 7B)

The FLW input files for these tests were based on the original model developed in Testing Round 6A. The original input file for Reach No. 3 under the baseline hydrograph was the starting point. An example of this file was given in Table 6-3. The weighting factor theta (θ) was set 0.6 in all the runs. (In FLDWAV, theta is specified by the F1 variable in DG (1)).

This original input file was adjusted to remove the cross-sections at Stations 2500, 5000, 10000 and 20000 ft. These particular sections were removed to allow for easier experimentation with alternate interpolation intervals.

The removal of these sections required numerous changes to individual lines in the FLW input files. The cross-sections themselves were found in blocks labeled DG (70) through (77) values near the end of the input file. The sections were deleted and the remaining sections renumbered. The lengths to individual stations assigned at DG (18) were updated. The list of cross-section labels found at data groups DG (50) and (52) provided labels was adjusted. In data group DG (12), the total number of sections was reduced from ten to six (variable NBT), which also resulted in a similar change to variable NPT2 on the same line and to NGAGE on DG (13).

Several data groups give input data separately for each interval between sections. Specific examples include the maximum interpolation intervals called out in DG (19), the routing method to use in each interval listed at DG (20), the sinuosity factors at DG (78), and the expansion/contraction coefficients at DG (79). The values previously listed separately for the intervals from 0 to 20,000 were consolidated into one interval.

Having made these initial changes, a series of 10 individual input files was written, based on the five distance steps and the two low-flow filter options. Data group DG (19) defines the minimum computational distance step between cross-sections. The original input data files for Testing Round 6A used 625 feet. Separate files were created for the other distance step options shown in Table 7-1. A paired series of input files was then created for each of the five distance-step scenario, based on the two low-flow filter options.

The low-flow filter is defined by the variable KREVRS variable in DG (4). This filter prevents water surface elevations and discharge values from falling below the initial conditions. It is described in the FLDWAV User's Documentation as a "*safety net*" which "*maintains computational robustness*" (Fread and Lewis 1998). The default in FLDWAV is to have this filter activated, which occurs when KREVRS=0. The filter was active for all testing conducted previously in Round 6A.

The uRAS model does not contain a similar feature. To maintain comparability between the uRAS and FLW testing, the reference scenario in Round 7B is to have the low flow filter turned off, which occurs when KREVERS=1.

7.3.2 Round 7B - Results

Results of Testing Round 7B are given in Tables 7-4 and 7-5 and in Figures 7-3 through 7-6.

Table 7-4 presents the peak outflow discharges and relative attenuation results for each of the 5 distance step sizes selected, as evaluated after routing the inflow hydrograph in FLW for 160,000 feet. All results are based on a minimum baseflow of 5%. Results were examined for both conditions when the low flow filter was off (the reference condition) and when the filter was on. The outflow peak in the reference scenario was 14,903 cfs, which represents a 37.9% relative attenuation from the inflow peak of 24,000 cfs. This attenuation is within 0.2% of the relative attenuation found using uRAS for the same conditions.

The FLW program, unlike uRAS, was able to produce results for all five distance steps when using a 5% baseflow. This was true for both low-flow filter options. When the filter was used, the peak flow discharge and relative attenuation results all remained within 1% of the reference scenario, with no clear trend in the data. By contrast, when the filter was not used, there was a trend towards increased attenuation with larger distance steps, with a maximum relative attenuation of 43.7% when Δx = 20,000 ft, which is 5.8% greater than the reference condition. This trend towards increasing attenuation when no filter is used is similar to the trend found in the uRAS results in Testing Round 7A.

Table 7-5 provides a summary of the volume balance in the discharge hydrographs for these same scenarios. When the low-flow filter was not used, FLW

appeared to conserve volume to a high degree of accuracy, with any losses less than 0.1%. When the filter was activated, the method no longer conserved volume well, with 1.9% increase in volume appearing when Δx = 5,000 ft and increasing to a 36% increase in volume when Δx =20,000 ft.

Figure 7-3 provides a plot of the outflow hydrographs from these scenarios after routing a distance of 160,000 feet. The 625 ft., 5,000 ft., and 20,000 ft. distance steps are shown. Figure 7-3(a) shows the hydrographs when no filter is used, whereas Figure 7-3 (b) shows the same scenarios when the filter is activated. The hydrograph for the Δx = 2,500 ft. distance step scenario was omitted because it was almost identical to the Δx = 625 ft. scenario. The Δx = 10,000 ft. scenario is omitted from this graph for clarity but is presented separately in Figure 7-4.

Figure 7-3 sheds light on the routing results given in Tables 7-4 and 7-5. As shown in Figure 7-3 (a), the Δx = 5,000 ft scenario in FLW displays the same tendency to "dip" as was found when routing with uRAS. The low-flow filter option acts to prevent the dip, as shown in Figure 7-3 (b).

Table 7-4. Sensitivity of Peak Flow Results to Distance Step Size, Based on FLW Routing on Reach No. 3, Testing Round 7B

Computational Distance Step, Δx (feet)	Peak Outflow Discharge, Q_p, (cfs) for Given Scenario after Routing 160,000 ft. in FLW		Attenuation of Peak Outflow Discharge (%)		Diff. in Relative Attenuation, Relative to the Reference Scenario (%) *	
	No Low-Flow Filter	With Filter	No Low-Flow Filter	With Filter	No Low-Flow Filter	With Filter
Inflow, Peak 24,000 cfs at 124 minutes						
625	14,903	14,903	37.9%	37.9%	*Reference Scenario**	0.0%
2,500	14,817	14,819	38.3%	38.3%	0.4%	0.3%
5,000	14,681	14,794	38.8%	38.4%	0.9%	0.5%
10,000	14,034	14,989	41.5%	37.5%	3.6%	-0.4%
20,000	13,520	15,084	43.7%	37.2%	5.8%	-0.8%

** The Reference Scenario uses Δx = 625 ft. with no low flow filter. All scenarios used a 5% Baseflow*

Table 7-5. Sensitivity of Volume Changes to Distance Step Size, Based on FLW Routing on Reach No. 3, Testing Round 7B

Computational Distance Step, Δx (feet)	Outflow Volume, Relative to Inflow, Excluding Baseflow (%), for Given Scenario, after Routing 160,000 ft. in FLW	
	No Low Flow Filter	With Filter
625	100.0%	100.0%
2,500	100.0%	100.0%
5,000	100.0%	101.9%
10,000	100.0%	114.0%
20,000	n/a *	136.0%
Inflow Volume, Excluding Baseflow (acre-feet)	4,827	

** FLW failed to produce a complete hydrograph.*

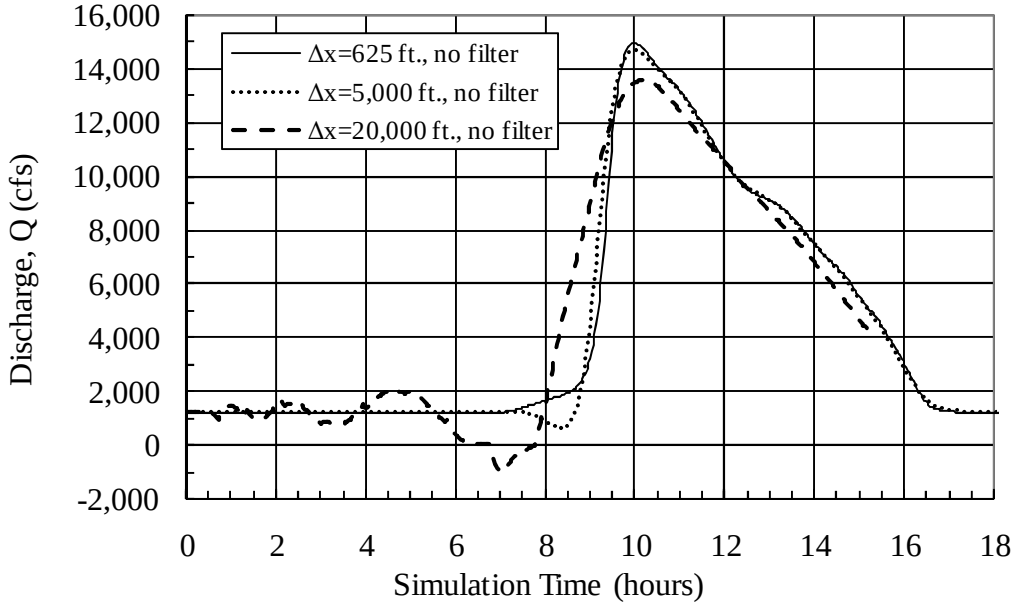

(a) 625, 5000, and 20000 ft. Distance Steps (Δx), No Low Flow Filter

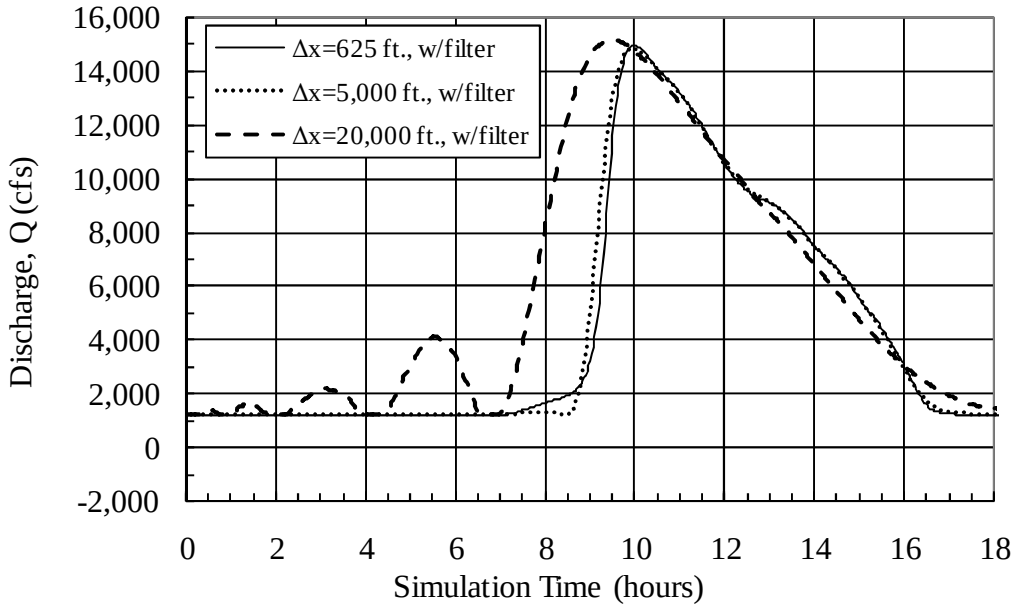

(b) 625, 5000, and 20000 ft. Distance Steps (Δx), Low-Flow Filter Activated

Figure 7-3. Outflow Hydrographs for Reach No. 3, after Routing 160,000 feet in FLW, Various Distance Steps

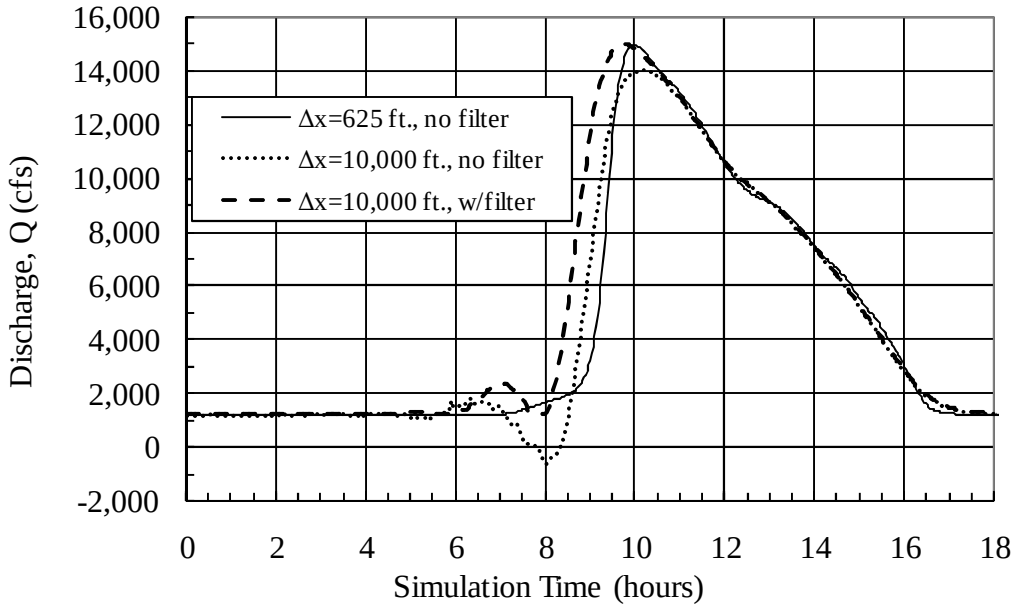

(a) for 10,000 ft. Distance Steps

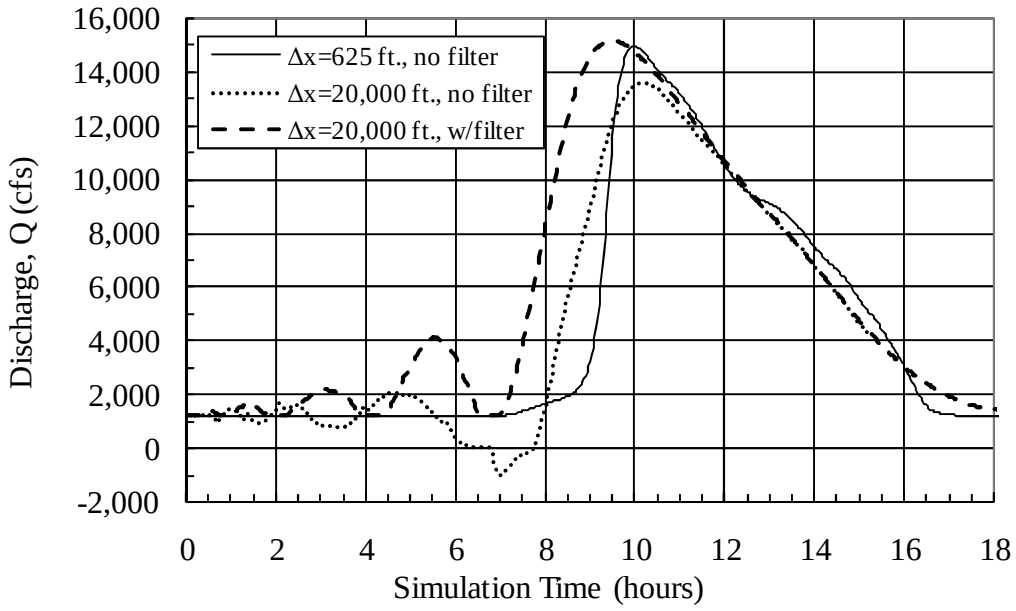

(b) for 20,000 ft. Distance Steps

Figure 7-4. Outflow Hydrographs for Reach No. 3, after Routing 160,000 feet in FLW, Comparison of Low-Flow Filter Options

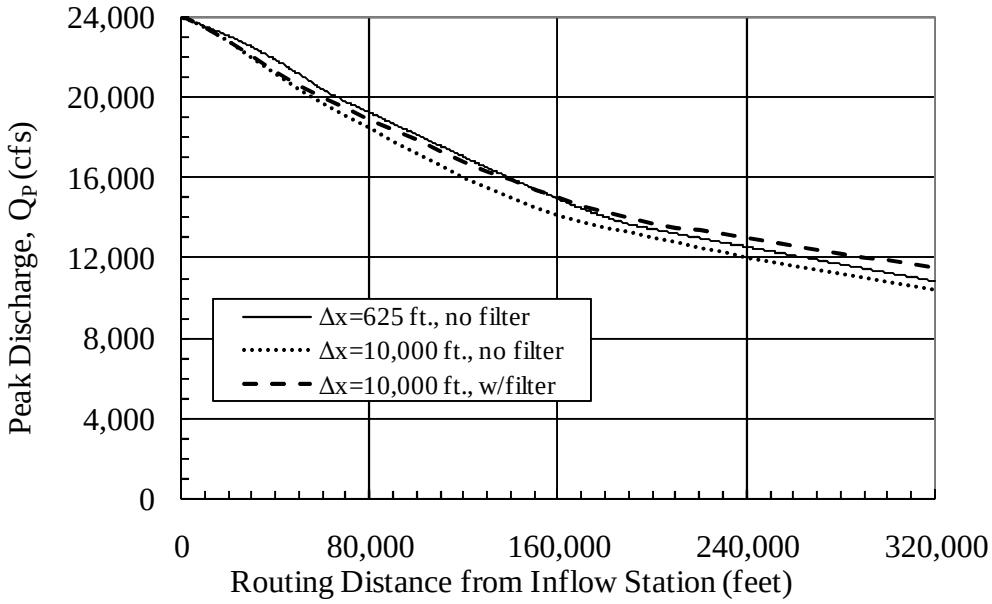

Figure 7-5. Decline of Peak Discharge over Distance, Reach No. 3, Comparing FLW Results for Select Distance Steps and Filter Options

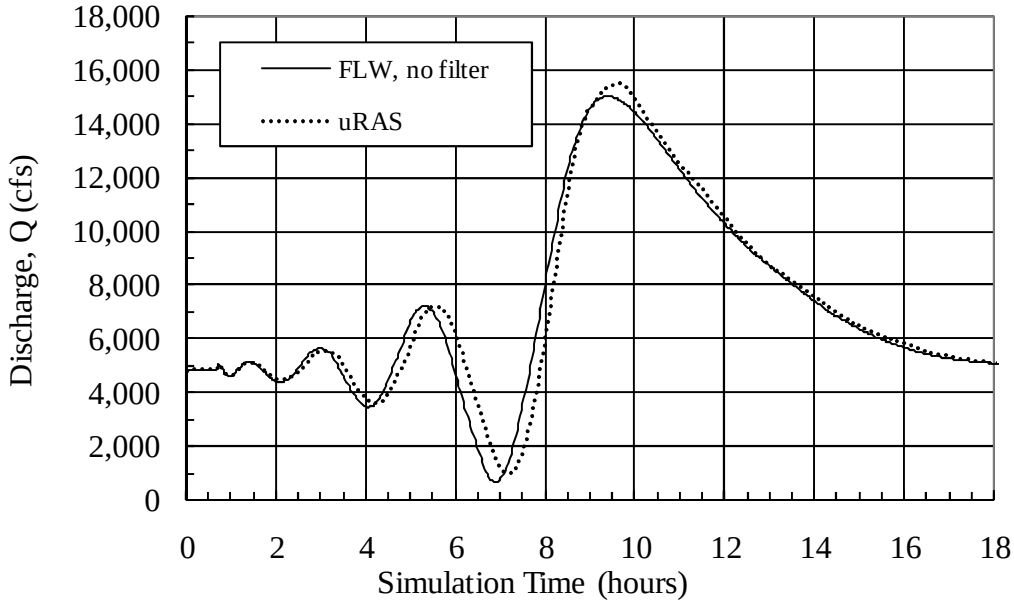

Figure 7-6. Outflow Hydrographs for Reach No. 3, after Routing 160,000 feet, Comparing FLW and uRAS Results for Δx = 20,000 ft. and 20% Baseflow

Likewise, the Δx =20,000 ft. scenario the dip gives way to full-scale oscillations in the time period before the arrival of the rising limb. Unlike uRAS, FLW appears to be capable of handling negative flow ordinates without becoming unstable, which explains why results were obtained for the two largest distance steps when routing in FLW, even though they were not obtained in uRAS. When the low flow filter is activated for the Δx =20,000 ft scenario, the lower component of each oscillation cycle is clipped off, but the upper portion of each cycle remaining and apparently being amplified relative to the "no filter" condition.

Figure 7-4 provides a direct comparison of the filter and no-filter scenarios for the 10,000 ft. and 20,000 ft. distance steps. The "Δx =625, no-filter scenario" is also shown for comparison. The Δx =10,000 ft. scenario also experiences leading oscillations, though to a lesser degree than for the 20,000-ft scenario. The low-flow filter prevents discharges from falling below the baseflow value, but at the cost of increasing the magnitude of the oscillation above baseflow.

When the "no filter" option is used, both hydrographs in Figure 7-4 rise to a smaller peak discharge than in the reference condition. The "with filter" option appears to come closer to matching the peak discharge predicted by the reference condition, but not necessarily with a similar hydrograph shape or timing. For the Δx = 20,000 option particularly, the ability to match the peak discharge comes at the cost of increased hydrograph volume. It appears that when oscillations appear in a hydrograph, there is a trade-off between matching peak discharges and conserving

volume. The falling limbs of all hydrographs plotted in Figures 7-3 and 7-4 seem to match well.

Figures 7-5 presents a plot of the decline in peak outflow discharges over distance for three select scenarios. The first two scenarios were based on the "no-filter" scenario, comparing results for Δx = 625 ft. and for Δx = 10,000 ft. The first scenario was the reference condition for this testing round. The larger distance step generally resulted in a slightly lower peak discharge throughout the routing range.

The second and third scenarios were both based on Δx = 10,000 ft, but compare the results of using the low-flow filter. For small routing distances, both scenarios plotted closely together, but as routing distance expands, the "no filter" option consistently produced smaller peak discharges.

In comparing the first and third scenarios, it is shown that the use of the low-flow filter was not a cure for problems associated with large distance steps. At a routing distance of 160,000 ft., the two scenarios gave similar results, but that appears to be a coincidence. The general trends for these two scenarios were not the same. At routing intervals less than 160,000 ft, the third scenario generally predicted greater attenuation than the first (reference scenario). Beyond 160,000 ft., the third scenario over-predicted the peak discharge.

The last issue examined in this testing round was a comparison of the uRAS and FLW routing results for the largest distance step modeled, Δx = 20,000 ft. To provide for a direct comparison, a FLW analyses was made for the 20% baseflow

condition. The low-flow filter was turned off so that the oscillations could develop fully.

Figure 7-6 presents the outflow hydrograph after routing 160,000 ft. for this condition. For the given inflow conditions on Reach No. 3, both uRAS and FLW give comparable results, including oscillations with similar amplitudes and frequencies.

7.4 Sensitivity to Time Step (Testing Round 7C)

Testing Rounds 7A and 7B demonstrated strong relationships between distance step and model stability. Round 7C was designed to evaluate the sensitivity of model results to the time step. A default scenario was identified based on a distance step of 625 feet, a time step of 2 minutes, $\theta = 0.6$ and a 5% baseflow. Two alternate time steps were then evaluated: 30 seconds (0.5 minutes) and 6 minutes. The time step ratios, $\frac{t_p}{\Delta t}$, for these three time steps are therefore 248, 62, and 21, respectively, based on the inflow time-to-peak, t_p, of 124 minutes.

7.4.1 uRAS Model Setup (Round 7D)

The uRAS project developed for Testing Round 7A was extended to accommodate this analysis. No adjustments to the geometry or unsteady flow input files were required. The computational time step was adjusted by selecting the appropriate "*computation interval*" at **HEC-RAS | Run | Unsteady Flow Analysis** input screen. For the 30-second time-step scenario, the "*hydrograph output interval*"

was left at 2 minutes. This field controls the level of detail found in the output files. For 6-minute time step scenario, the output interval was also changed to 6 minutes.

7.4.2 FLDWAV Model Setup (Round 7D)

The FLDWAV input files for this round 7C were derived from the input files developed in Round 7B, which used a computational time step of 2 minutes. To adjust the computational time steps, the value of DTHII in DG (7) was modified. The units of measure for DTHII is hours, so for a time step of 30 seconds and 6 minutes, the input must be 0.008333 and 0.10 hours, respectively. For the 30-second time step scenario, the plotting interval DTHPLT on that same line was left unchanged at 2 minutes (0.0333 hours). For 6-minute scenario, the plotting interval DTHPLT was changed to 0.10 hours.

7.4.3 Round 7C – Results

Results of Testing Round 7C for are given in Tables 7-6 and 7-7 and in Figures 7-7 and 7-8. Table 7-6 presents the peak outflow discharges and relative attenuation results for each of the 3 time step sizes selected. As before, the routing distance is 160,000 feet, and routing results are presented for both the uRAS and FLW models. Table 7-7 presents the volume balance for these same conditions, where volume balance is measured relative to the inflow hydrograph, after excluding the baseflow component.

From the tables, it appears that the model gave similar results over this range of time steps. There was a slight tendency for the smallest time step (30 seconds) to produce the highest discharges, but the total difference in relative attenuations

between the 30 second time step and the 6 minute time steps was only 0.6% for uRAS and 1.6% for FLW.

Likewise, volume conservation between the different scenarios was similar. The FLW program continued to demonstrate a superior ability to conserve volume, gaining only 0.3% relative to the inflow hydrograph for the 6-minute time step. For uRAS, the greatest change was a 2.6% increase in volume for the 6-minute time step.

Figure 7-7 presents a plot of the outflow hydrographs after 160,000 ft. of routing for all three time steps. Results for routing by uRAS and FLW are both shown. These plots reinforce the relative insensitivity of modeling results to time step, at least for the range evaluated.

Figure 7-8 presents two plots of the decline in peak outflow discharges over distance for three time-step scenarios for both uRAS and FLW modeling. These plots reinforce the conclusion that time steps chosen did not produce significant variations in modeling accuracy.

Table 7-6. Sensitivity of Peak Flow Results to Time Step Size, Based on Routing of Reach No. 3 by uRAS and FLW, Testing Round 7C

Time Step, Δt (minutes)	Peak Outflow Discharge, Q_p (cfs) by Given Model after Routing 160,000 ft.		Attenuation of Peak Outflow Discharge (%)		Diff. in Relative Attenuation, for Each Method, Compared to the Δt=2 min. Scenario (%)	
	uRAS	FLW	uRAS	FLW	uRAS	FLW
Inflow, Peak 24,000 cfs at 124 minutes						
0.5	15,020	15,013	37.4%	37.4%	-0.3%	-0.5%
2	14,952	14,903	37.7%	37.9%	--	--
6	14,881	14,649	38.0%	39.0%	0.3%	1.1%

Table 7-7. Sensitivity of Volume Changes to Time Step Size, Based on Routing of Reach No. 3 by uRAS and FLW, Testing Round 7C

Computational Time Step, Δt (min)	Outflow Volume, Relative to Inflow, Excluding Baseflow (%), for Given Method after Routing 160,000 ft.	
	uRAS	FLW
0.5	100.4%	100.1%
2	100.8%	100.0%
6	102.6%	100.3%
Inflow Volume, Excluding Baseflow (acre-feet)	4,827	

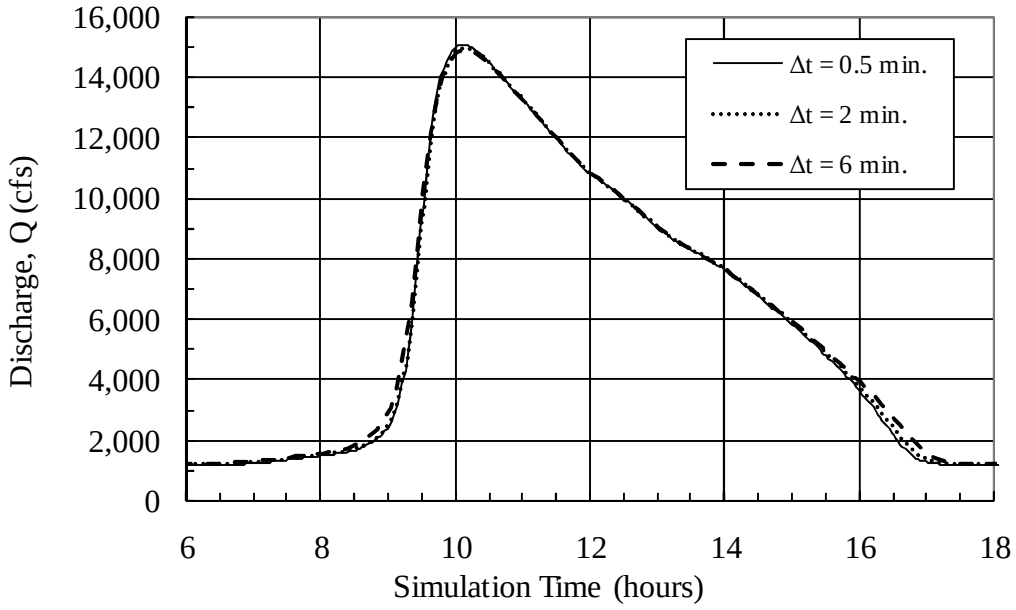

(a) Routed by uRAS

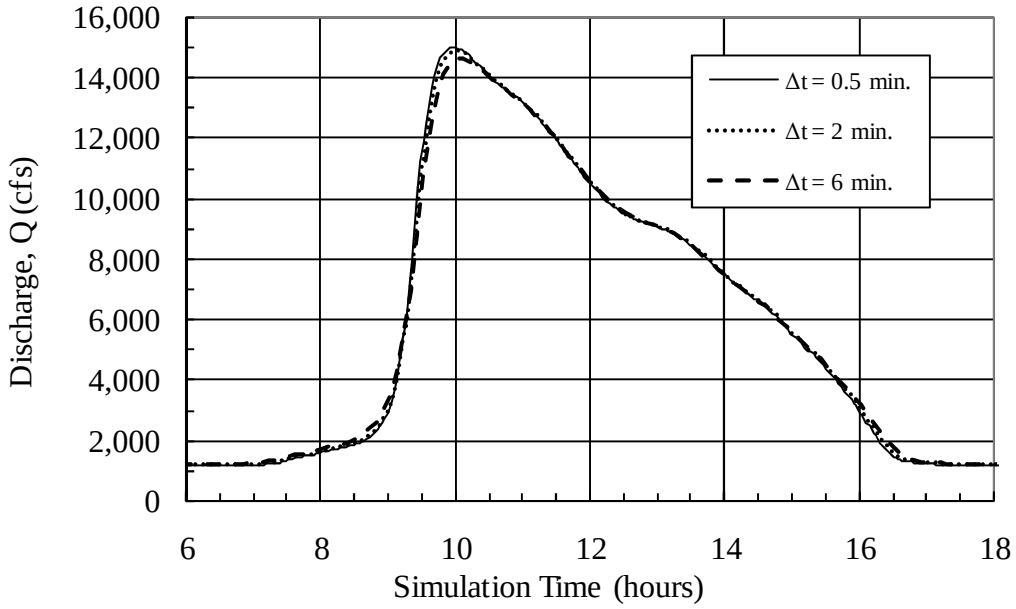

(b) Routed by FLW

Figure 7-7. Outflow Hydrographs for Reach No. 3, after Routing 160,000 feet, Sensitivity to Time Step Size for uRAS and FLW

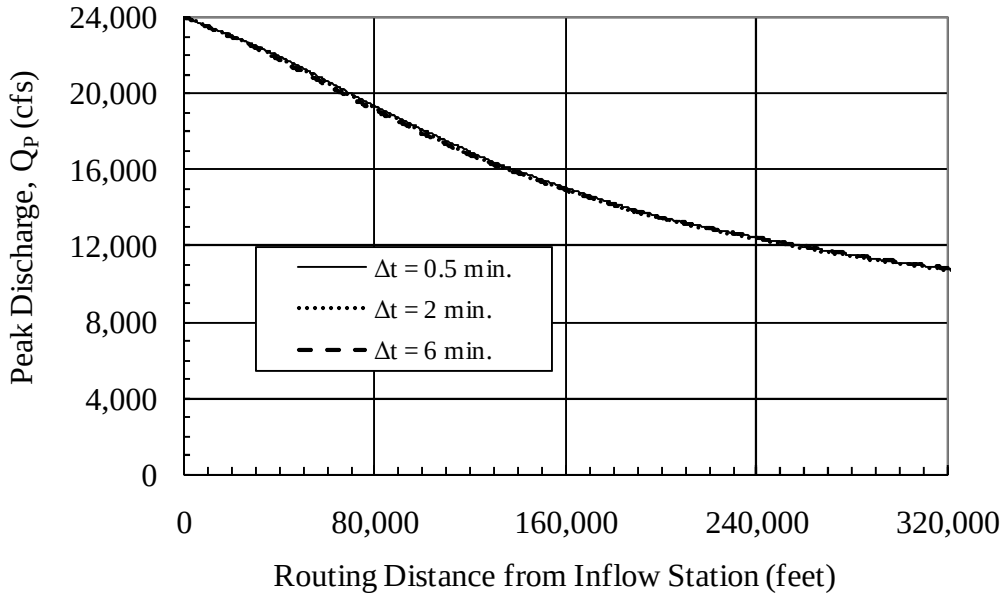

(a) Routed by uRAS

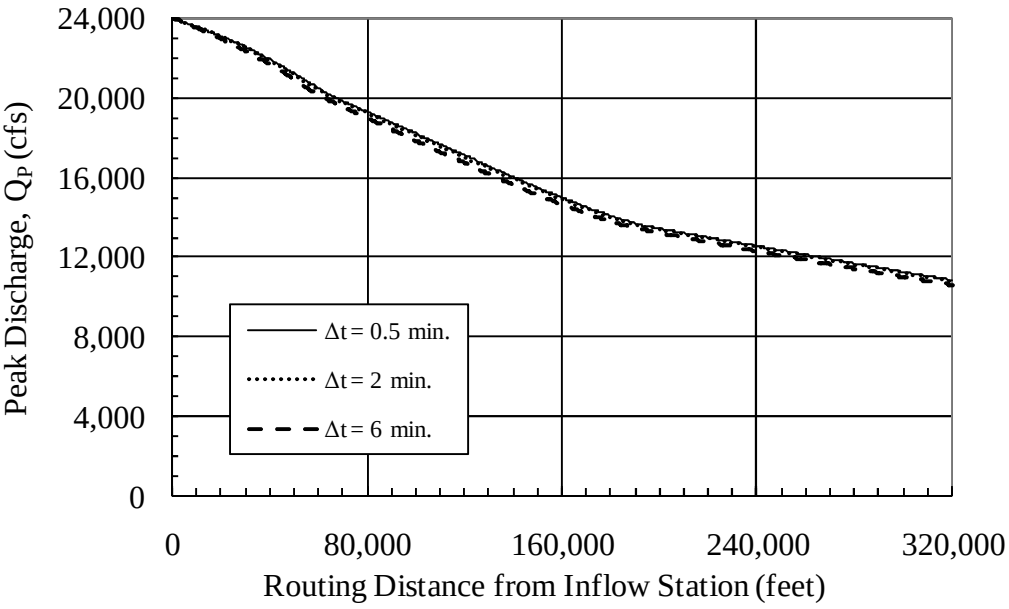

(b) Routed by FLW

Figure 7-8. Decline of Peak Discharge over Distance, Reach No. 3, Comparing Sensitivity to Time Step Size for uRAS and FLW

7.5 Sensitivity to Theta (Testing Round 7D)

Theta (θ) is the weighting factor used to approximate the spatial derivative term in the four-point implicit box scheme used to solve uRAS and FLW. A theta of 0.5 would estimate the spatial derivative over a time step as the even weight of the approximate value at the beginning and end. A theta of 1.0 would give all the weight to the projected value of the spatial derivative at the end of the time step.

Theory would generally support the use 0.5 for theta, but as discussed previously, experiments have shown that stability issues can arise when this is done. The FLDWAV User Documentation recommends a theta of 0.55 or 0.6 (Fread and Lewis 1998) and the UNET User's Manual recommends a theta of 0.6 when possible, or greater if model stability requires (Barkau 1997). uRAS does not allow the input of theta less than 0.6.

In this testing round, a direct investigation is made of the influence of theta on the accuracy or variability in modeling results. A reference modeling scenario was identified used a time step of 2 minutes, a distance step of 625 feet, and a minimum baseflow of 5% the peak flow. This reference scenario was then evaluated for theta equal to 0.6, 0.8 and 1.0.

7.5.1 uRAS Model Setup (Round 7D)

The uRAS project developed for Testing Round 7C was expanded for to include this testing round. No adjustments to geometry or unsteady flow files were required. Two new plans were then saved, one for θ=0.8 and one for θ=1.0. The value of theta is adjusted in HEC-RAS by opening the **HEC-RAS | Run | Unsteady**

Flow Analysis | Options | Calculation Options and Tolerances menu. Both the primary theta value and the value used during warm-up were changed.

7.5.2 FLDWAV Model Setup (Round 7D)

Two additional FLW input files were created for the alternate values of theta. The value for theta is given by variable F1 in data group DG (1). No other changes to the input file were needed.

7.5.3 Round 7D – Results

Results of Testing Round 7D for are given in Tables 7-8 and 7-9 and in Figures 7-9 through 7-11.

Table 7-8 presents the peak outflow discharges and relative attenuation results, for each three values of θ selected, after 160,000 feet of routing using both uRAS and FLW. The table shows a tendency for the relative attenuation to increase (peak discharges decrease) as θ increases. For uRAS, the relative attenuation at θ=0.6 was 37.9%, but increased 3.2% when θ=1.0. For FLW, the relative attenuation went from 37.9% to 40.3% when θ increased from 0.6 to 1.0, a change of 2.4%.

Table 7-9 presents the volume balance for these same conditions. The FLW scenarios experienced no change in volume for any of the θ values examined. The uRAS modeling appeared to experience a slight volume loss when theta was increased. For θ=1.0, the volume loss was 2.2%. By contrast, when θ=0.6, the uRAS model produced a gain of 0.8%. As seen in previous rounds of sensitivity testing, the uRAS model appears to be subject to minor errors in volume conservation.

Figure 7-9 presents plots of the outflow hydrographs after 160,000 ft. of routing for all three choices of θ. Figure 7-10 presents two plots of the decline in peak outflow discharges over distance for three time-step scenarios for both uRAS and FLW modeling. Both sets of figures demonstrate that increased values of θ lead to a small increase in the degree of attenuation experienced during routing. The impact appeared to be slight for the scenarios in this evaluation. Overall, the hydrograph and peak discharge trends were similar for the three weighting factors.

The final issue investigated in this testing round was the effectiveness of θ in stabilizing the oscillations produced by long distance steps. As discussed previously, the primary reason for using larger values of θ is to produce greater computational stability in a model. Whether θ can produce this stability when the source of error is an overly large distance step was of interest.

Figure 7-11 presents the results of a single model comparison that was made to investigate this issue. The modeling results are both drawn from uRAS for Δx = 20,000 feet, Δt=2 minutes, and a baseflow of 20%. A comparison of the hydrograph is provided after 160,000 feet of routing for two values θ, 0.6 and 1.0. In general, the larger value of θ dampens the oscillations slightly, but it does not eliminate the oscillation, nor does it appear to alter the cycle frequency. From this observation, it appears unlikely that adjustments to θ would be useful in addressing instabilities that are caused by poor distance-step selection.

Table 7-8. Sensitivity of Peak Flow Results to Weighting Factor, θ Based on Routing of Reach No. 3 by uRAS and FLW, Testing Round 7D

Finite Difference Weighting Factor, θ	Peak Outflow Discharge, Q_p (cfs) by Given Model after Routing 160,000 ft.		Attenuation of Peak Outflow Discharge (%)		Diff. in Relative Attenuation, for Each Method, Compared to the θ=0.6 Scenario (%)	
	uRAS	FLW	uRAS	FLW	uRAS	FLW
Inflow, Peak 24,000 cfs at 124 minutes						
0.6	14,952	14,903	37.7%	37.9%	--	--
0.8	14,543	14,605	39.4%	39.1%	1.7%	1.2%
1.0	14,176	14,328	40.9%	40.3%	3.2%	2.4%

Table 7-9. Sensitivity of Volume Changes to Weighting Factor, θ, Based on Routing of Reach No. 3 by uRAS and FLW, Testing Round 7D

Finite Difference Weighting Factor, θ	Outflow Volume, Relative to Inflow, Excluding Baseflow (%), for Given Method after Routing 160,000 ft.	
	uRAS	FLW
0.60	100.8%	100.0%
0.80	99.1%	100.0%
1.00	97.8%	100.0%
Inflow Volume, Excluding Baseflow (acre-feet)	4,827	

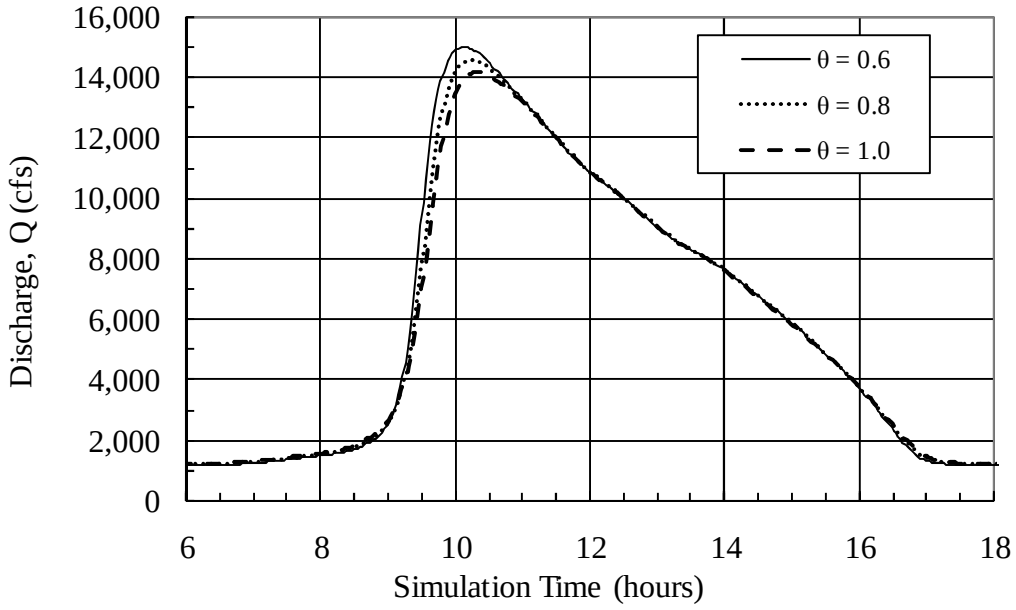

(a) Routed by uRAS

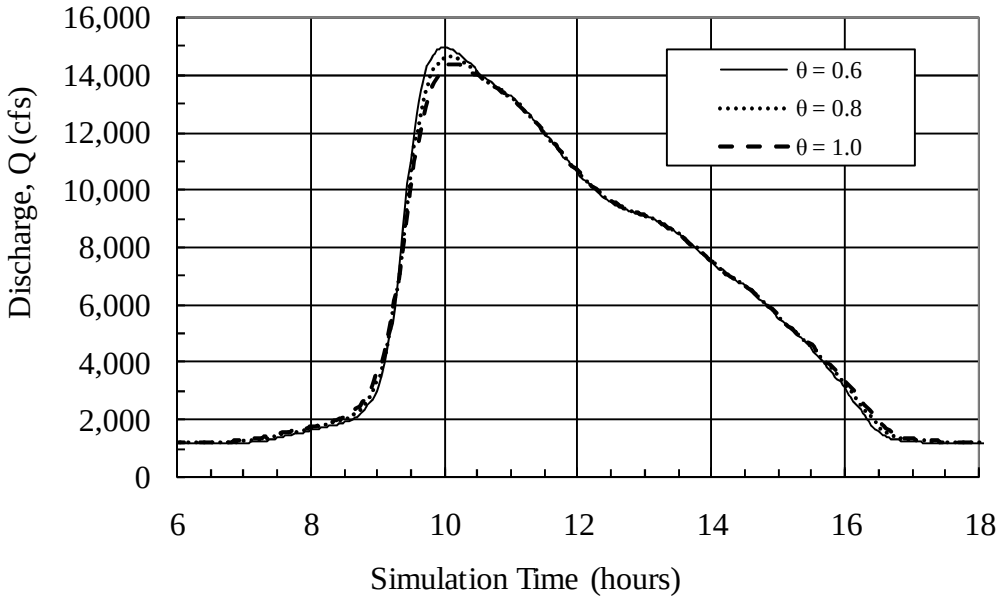

(b) Routed by FLW

Figure 7-9. Outflow Hydrographs for Reach No. 3, after Routing 160,000 feet, Sensitivity to Weighting Factor, θ for uRAS and FLW

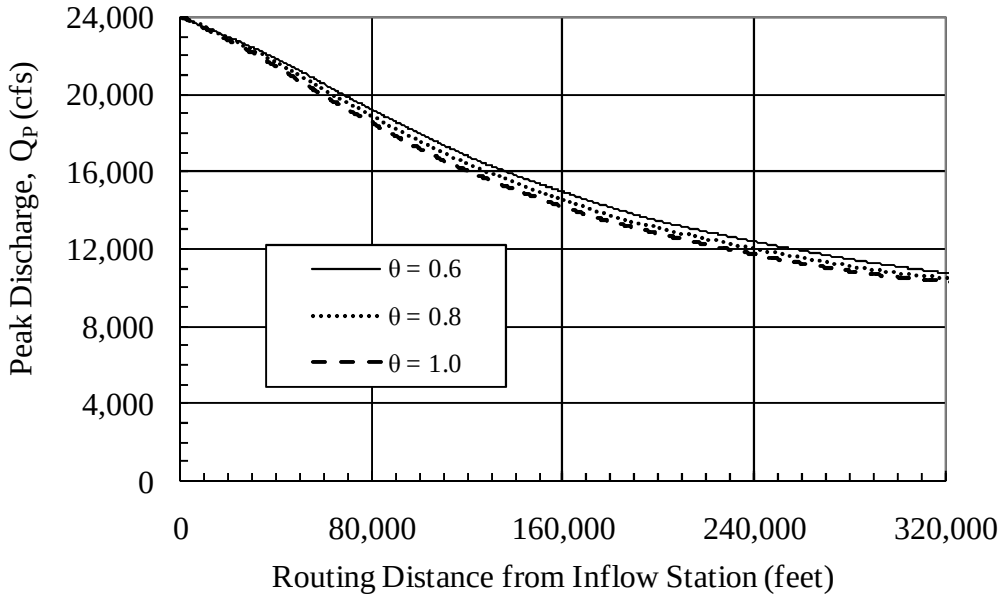

(a) Routed by uRAS

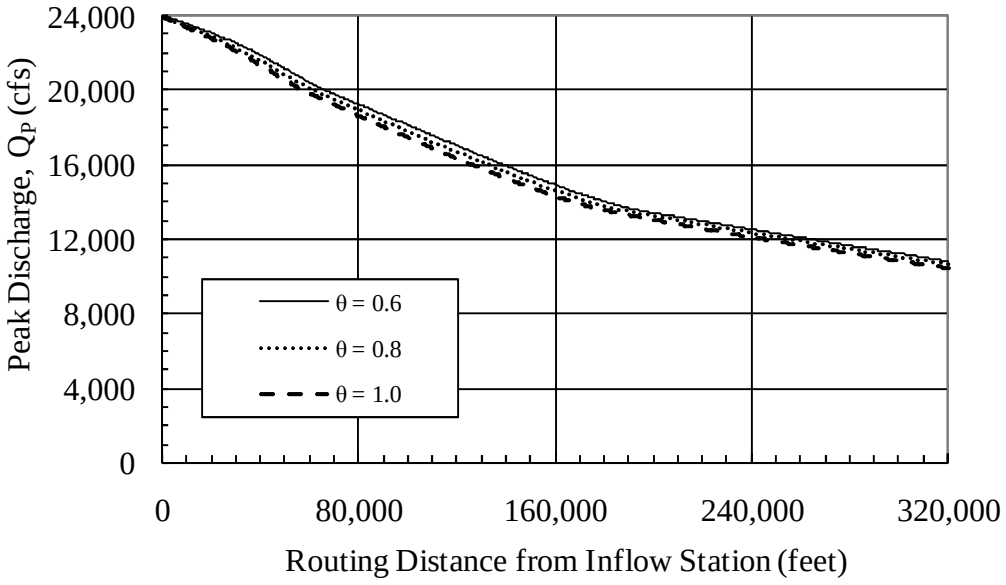

(b) Routed by FLW

Figure 7-10. Decline of Peak Discharge over Distance, Reach No. 3, Comparing Sensitivity to Weighting Factor, θ for uRAS and FLW

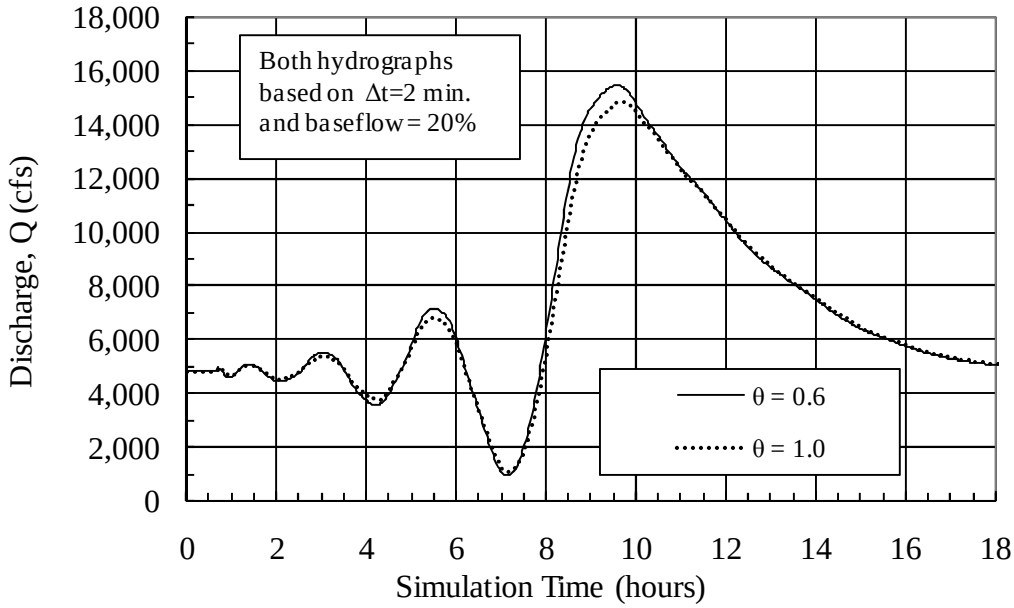

Figure 7-11. Effect of Increased θ on Routing Stability, Comparing Outflow Hydrographs for Reach No. 3 after Routing 160,000 feet with uRAS, Using Δx = 20,000 ft

7.6 Analysis and Recommendations

Testing Rounds 7A and 7B demonstrated a strong relationship between the size of the computational distance step and the stability of the model. In particular, short distance steps were needed to prevent the appearance of oscillations in the baseflow preceding the rising limb of the hydrograph. For Reach No. 3, the initial appearance of a "dip" begins for distance steps between 2,500 and 5,000 feet. The structure of the Muskingum-Cunge equation and previous investigations by Perumal (1992) suggest a relationship between the characteristic reach length, L_u, and the avoidance of initial instabilities. The instability in Reach No. 3 appeared to begin when the $\frac{\Delta x}{L_U}$ ratio was close to 1.7 and stability worsened as the ratio increased, where L_u, was evaluated for a discharge equal to the peak inflow. The instabilities occur, however, when the actual discharge rates are much lower, at whatever minimum or baseflow value has been assumed. If the $\frac{\Delta x}{L_U}$ ratios had been evaluated based on a baseflow equal to 5% of the peak discharge, the instability appears to begin at ratios between 1.6 and 3.2.

In the event that a model is developed with distance steps that are too large, two compensating approaches could be used: the minimum baseflow could be increased to absorb the leading oscillations or the program could be designed to filter out any results that fell below a threshold. The first option was evaluated in Testing Round 7A using uRAS, whereas the second option is available in FLW and was examined in Round 7B. In both situations, the use of these mitigating techniques did

allow for results to be obtained from otherwise unstable models. In each case, however, there was a cost to be paid in terms of accuracy of the peak discharges or in the conservation of the hydrograph volume. From these conclusions, it appears that successful models should first give primary attention to the selection of appropriately small distance steps. These other techniques would then be used only as a fail-safe, or as a trial condition to isolate problem areas during the initial development of models.

Based on the preliminary review conducted for Reach No. 3, and in conjunction with other observations made during this study, it is recommended that computational distance steps be kept smaller than the characteristic reach length, L_u, for a given reach. As a conservative assumption, all computational distance steps in Chapter 6 were kept smaller than $\frac{L_U}{2}$.

By contrast, the models appear to be less sensitive to the computational time step used or to the value given to θ, the finite-difference weighting coefficient. The sensitivity to computational time step was negligible, with only a 1 to 2% difference in relative attenuations for the scenarios tests, based on time step variations ranging from 30 seconds to 6 minutes. For θ, the recommended values of 0.6 gave the highest levels of peak discharge, whereas greater values up to the maximum 1.0 show a slight decrease in peak discharges (i.e. an increase in attenuation).

Given these results, it is recommended that time steps be developed in line with general modeling guidance of $\frac{t_p}{\Delta t}$ ratios greater than 20 and that the values of θ

be set to 0.55 or 0.6 whenever possible. If instabilities should arise under those conditions, the first response should be to review the distance step intervals. While some degree of minimum baseflow is needed to guard against near-zero or negative flow depths, the size of that baseflow need not be large, provided the distance steps are appropriate. The use of a 5% minimum baseflow in Chapter 6 appears to be reasonable.

Chapter 8

Summary, Conclusions and Recommendations

8.1 Summary and Conclusions

The first part of this research was a comprehensive review of the theoretical basis of the Muskingum-Cunge equation. A simplified, physically intuitive derivation of the Muskingum-Cunge equation was presented, as synthesized from the works of Perumal, Montes and others. This derivation illustrated the importance of the little-known concept of "characteristic reach length." The characteristic reach length is the length of river that must be isolated if one is to treat the stream reach as the equivalent of a reservoir in storage routing.

Based on this derivation, a clear link was established between the Muskingum-Cunge method and the "Cascading Reservoirs" approximation, also known as "modified-Puls method for river routing" in Corps of Engineer's literature. The derivation illustrated a flaw in the Corps' guidance on the appropriate number of subdivisions (N) to use when employing the Cascading Reservoirs method. It also provides a method for determining the correct value of N based on characteristic reach length.

The Muskingum-Cunge derivation was extended to explicitly handle two-stage meandering channels. The expanded derivation accounts for the differences in main-channel and overbank lengths. The derivation was based on the idea that the main-channel and overbank floodplains form "parallel channels" with flow balanced

between each based on the difference in conveyance and hydraulic slope. A conceptual framework was developed for altering typical sections from meandering flow data to equivalent, non-meandering sections, using either a "modified-overbanks" or "equivalent-lengths" approach. The derivation showed that in either case, the geometry and roughness values for overbanks and/or main-channels must be adjusted.

The governing equations for the unsteady routing method in HEC-RAS were reviewed. This unsteady routing module is based on the earlier UNET model developed by Barkau. A conceptual error was discovered in the handling of the momentum term in meandering sections where overbank and channel lengths are different. A correction was proposed that relies upon the "parallel channels" concept and results in a simpler governing equation than that used in the HEC-RAS unsteady flow module. A similar error was also discovered in the weighted length term used for the steady-state HEC-RAS solution and an alternate equation was proposed.

In the second part of this research, detailed procedures were developed to reduce complex, natural stream data down to the essential reach-averaged values of volume, surface area and discharge as needed for flood-routing methods. The data reduction methods included the development of simplified reaches based on 8-point cross-sections that represent a geometric average of the original natural stream. The methods developed in this study provide an 8-point cross-section that is representative of the dominant flood-routing parameters: volume, surface area and

discharge of a natural channel reach. This 8-point cross-section takes channel meanders into account.

The detailed procedure first involves the development of plots of volume versus discharge and surface area versus discharge for a range of steady-state flow profiles for the natural stream of interest. These steady-state flow profiles are developed using HEC-RAS. The 8-point cross-section is then defined to give an initial "best match" to the plots for the natural stream reach. A final step involves adjusting the 8-point cross-sections to fit the relationships of kinematic wave speed vs. discharge (c_k vs. Q) and characteristic reach length vs. discharge (L_u vs. Q).

These procedures were applied to four small streams in Johnson County, Kansas. The tributary area of these streams ranged between 1 and 48 square miles. Several typical patterns in the variation in kinematic wave speed (c_k) and characteristic reach length (L_u) were shown, including the clear presence of a "bankfull" break in the data values for both parameters.

The third and final part of this research examined the flood-routing characteristics of these four reaches, using four separate flood-routing methods. Two fully dynamic solution methods were used: the unsteady HEC-RAS model developed by the U.S. Army Corps of Engineers (USACE) and the FLDWAV model developed by the National Weather Service. Two simplified methods were also evaluated: the variable-parameter Muskingum-Cunge method and the "Cascading-Reservoirs" method (as corrected). Both of the simplified methods were used as formulated in the HEC-1 hydrology program developed by the USACE. Tests were conducted to

mimic a realistic 100-year discharge event, based on the simplified 8-point cross-sections for each stream.

The tests demonstrated that the two dynamic solvers give nearly equivalent results. The average difference in relative attenuation was within 0.1% for three of the reaches and was within 0.3% for the fourth. The FLDWAV model appeared to conserve hydrograph volume better than the unsteady HEC-RAS solution.

The two approximate methods (Muskingum-Cunge and Cascading Reservoirs) also demonstrated a strong ability to reproduce the peak, translation and general shape of downstream hydrographs for very long distances. Some systematic differences in the approximate methods were demonstrated. The VMC method appeared to show more distortion over distance as routing continues. It also tended to lose volume in certain situations, causing accuracy to decrease.

A comparison was also made of direct routing results using unsteady HEC-RAS based on simplified sections and actual complex, meandering geometry. One of the channels showed excellent agreement based on the simplifications proposed, whereas three showed a minor but definite diverging trend in the results for increased routing distances. This issue is identified as requiring further research.

This type of detailed evaluation of routing of flows for small, two-stage meandering rivers is rare in the literature. This study demonstrates the methods and analytic techniques that could be used to explore additional river systems and better organize and communicate the flood-routing characteristics of natural streams.

Finally, a sensitivity test was made of the influence of different model controls (distance steps, time steps, minimum baseflow, and finite difference weighting factor (theta)) on modeling stability and accuracy within unsteady HEC-RAS and FLDWAV. Recommendations for setting distance steps in fully dynamic solutions is provided, based on maintaining stability in calculations and avoiding an initial 'dip" of negative inflow. These recommendations specify that distance steps should be kept smaller than the characteristic reach length.

8.2 Recommendations for Further Research

Based on the findings of this investigation, further research is suggested into the following topics:

- Representative values of kinematic wave speed and characteristic reach length for actual natural channels should be developed, to assist modelers in calibrating unsteady models. It is expected that such representative values would be strongly related to the geology and geomorphology of regions and would show a correlation to drainage area.
- Further investigation into the distance-step criteria for Muskingum-Cunge and fully dynamic solutions should be undertaken, to verify whether the guidance given for characteristic reach is of general applicability, and to determine the appropriate ratios of distance step to characteristic reach length to use in model design.
- The origin of the volume loss in the variable-parameter Muskingum-Cunge method should be investigated in further detail. The literature has previously

focused errors introduced by the 3-point or 4-point finite difference averaging scheme. This research suggests that the errors could be related instead to the use of a variable value for characteristic reach length during routing.

References

ASCE Task Committee on Definition of Criteria for Evaluation of Watershed Models of the Watershed Management Committee, Irrigation and Drainage Division. (1993). "Criteria for evaluation of watershed models." *Journal of Irrigation and Drainage Engineering,* 119(3), 429-442.

Barkau, R. L. (1997). *UNET One-Dimensional Unsteady Flow Through a Full Network of Open Channels, User Manual, Version 3.2.* U.S. Army Corps of Engineers, Hydrologic Engineering Center, Davis, California.

Bras, R. L. (1990). *Hydrology: An Introduction to the Hydrologic Science.* Addison-Wesley Publishing Company, Reading, Mass.

Bedient, P. B. and Huber, W. C. (1992). *Hydrology and Floodplain Analysis, 2nd Ed.* Addison-Wesley Publishing Company, Reading, Mass.

Booth, B. (2000). *Using ArcGIS 3D Analyst*. Environmental Research Systems Research Institute, Inc. (ESRI), Redlands, California.

Camp, Dresser, & McKee, Inc. (CDM) (2005). *Blue River Watershed Study.* Prepared for Johnson County, Kansas. Revised Final Report, December 2005.

Chow, V. T. (1959). *Open-Channel Hydraulics*. McGraw-Hill, New York.

Crago, R. D. and Richards, S. M. (2000). "Nonkinematic effects in storm hydrograph routing." *Journal of Hydrologic Engineering*, 5(3), 323-326.

Cunge, J. A. (1969). "On the subject of a flood propagation computation method (Muskingum method)." *Journal of Hydraulic Research,* 7(2), 205-230.

Dooge, J. C. I. (1973). *Linear theory of hydrologic systems*. U.S. Department of Agriculture, Technical Bulletin 1468. Washington, D.C.

Dooge, J. C. I., Strupczewski, W. G., and Napiorkowski, J. J. (1982). "Hydrodynamic derivation of storage parameters of the Muskingum model." *Journal of Hydrology*, 54, 371-389.

Ervine, D. A., Babaeyan-Koopaei, K., and Sellin, R. H. J. (2000). "Two-dimensional solution for straight and meandering overbank flows." *Journal of Hydraulic Engineering*, 126(9), 653-669.

Franz, D. D., and Melching, C. S. (1997). *Full Equations (FEQ) model for the solution of the full, dynamic equations of motion for one-dimensional unsteady flow in open channels and through control structures.* U.S. Geological Survey Water-Resources Investigations Report 96-4240.

Fread, D. L. and Lewis, J. M. (1998). *NWS FLDWAV Model: Theoretical Description and User Documentation.* National Weather Service, Office of Hydrology, Hydrologic Research Laboratory, Silver Spring, Maryland.

Garbrecht, J. and Brunner, G. (1991). "Hydrologic channel-flow routing for compound sections." *Journal of Hydraulic Engineering*, 117(5), 629-641.

Green, I. R. A. and Stephenson, D. (1986). "Criteria for comparison of single event models." *Hydrological Sciences Journal*, 31(3), 395-411.

Heatherman, W. J. (2004). "Muskingum-Cunge revisited." *Proceedings, World Water and Environmental Resources Congress 2004, Salt Lake City.* Sponsored by ASCE, Reston, Va.

Henderson, F. M. (1966). *Open Channel Flow*. Prentice Hall, Upper Saddle River, New Jersey.

Kalinin, G. P. and Milyukov, P. A. (1958). "On the computation of unsteady flow along the channels by the use of reach-travel curves." (in Russian), *Meteorologiya i gidrologiya.* USSR.

Leopold, L.B., Wolman, M. G., and Miller, J.P. (1964). *Fluvial Processes in Geomorphology*. W.H. Freeman and Company, San Francisco.

Lighthill, M. J. and Whitham, G. B. (1955). "On kinematic waves. I. Flood movement in long rivers." *Proceedings of the Royal Society of London, Series A, Mathematical and Physical Sciences*, 229(1179), 281-316.

Miller, W. A., and Cunge, J. A. (1975). "Simplified Equations of Unsteady Flow." Chapter 5 in *Unsteady Flow in Open Channels, Vol. I.* Mahmaud, K. and Yevjevich, V, editors. Water Resources Publications, Fort Collins, Colo., 216-242.

Montes, S., (1998). *Hydraulics of open channel flow*. ASCE Press, Reston, Va., 564-580.

Nash, J. E. (1959). "A note on the Muskingum flood-routing method." *Journal of Geophysical Research*, 64(8), 1053-1056.

Natural Resources Conservation Services (NRCS). (2007). *National Engineering Handbook, Part 630, Hydrology, Chapter 16, Hydrographs.*" March 2007.

Ormsby, T., Napoleon, E., Burke, R., Groessl, C., and Feaster, L. (2004). *Getting to Know ArcGIS, 2nd Ed*. ESRI Press, Redlands, Ca.

Perumal, M. (1992). "The cause of negative initial outflow with the Muskingum method." *Hydrological Sciences Journal,* 37(4), 391-401.

Perumal, M. (1994a). "Hydrodynamic derivation of a variable parameter Muskingum method: 1. Theory and solution procedure." *Hydrological Sciences Journal,* 39(5), 431-442.

Perumal, M. (1994b). "Hydrodynamic derivation of a variable parameter Muskingum method: 1. Verification." *Hydrological Sciences Journal,* 39(5), 443-458.

Perumal, M. and Ranga Raju, K. G. (1999). "Approximate convection-diffusion equations." *Journal of Hydrologic Engineering,* 4(2), 160-164.

Phelps Engineering, Inc. (PEI) (1997). *Tomahawk Creek Flood Study.* Prepared for the Cities of Overland Park, Leawood, and Olathe and Johnson County, Kansas. December 1997.

Patra, K. C. and Kar, S. K. (2000). "Flow interaction of meandering river with floodplains." *Journal of Hydraulic Engineering,* 126(8), 593-604.

Ponce, V. M. and Simons, D. B. (1977). "Shallow wave propagation in open channel flow." *Journal of the Hydraulics Division*, 103(12), 1461-1476.

Ponce, V. M., Li, R. M., and Simons, D. B. (1978a). "Applicability of kinematic and diffusion models." *Journal of the Hydraulics Division*, 104(3), 353-360.

Ponce, V. M. and Yevjevich, V. (1978b). "Muskingum-Cunge method with variable parameters." *Journal of the Hydraulics Division*, 104(12), 1663-1667.

Ponce, V. M. (1980). "Linear reservoirs and numerical diffusion." *Journal of the Hydraulics Division*, 106(5), 691-699.

Ponce, V. M. and Theurer, F. D. (1982). "Accuracy criteria in diffusion routing." *Journal of the Hydraulics Division*, 108(6), 747-757.

Ponce, V. M. (1989). *Engineering Hydrology: Principles and Practices*. Prentice-Hall, Upper Saddle River, New Jersey.

Ponce, V. M. (1990). "Generalized diffusion wave equation with inertial effects." *Water Resources Research*, 26(5), 1099-1101.

Ponce, V. M. (1991). "New perspective on the Vedernikov number." *Water Resources Research*, 27(7), 1777-1779.

Ponce, V. M. and Chaganti, P. V. (1994). "Variable-parameter Muskingum-Cunge method revisited." *Journal of Hydrology*, 162(3-4), 433-439.

Ponce, V. M. and Lugo, A. (2001). "Modeling looped ratings in Muskingum-Cunge routing." *Journal of Hydrologic Engineering*, 6(2), 119-124.

Roberson, J. A., Cassidy, J. J., and Chaudhry, M. H. (1988). *Hydraulic Engineering*. Houghton Mifflin Company, Boston.

Roberson, J. A. and Crowe, C.T. (1990). *Engineering Fluid Mechanics, 4th Ed.* Houghton Mifflin Company, Boston.

Seddon, J. A. (1900). "River hydraulics." *Transactions, American Society of Civil Engineers*, 43, 179-229.

Strelkoff, T. (1980). *Comparative analysis of flood routing methods (Research Document 24)*. U.S. Army Corps of Engineers, Hydrologic Engineering Center, Davis, California.

Szel, S. and Gaspar, C. (2000). "On the negative weighting factors in the Muskingum-Cunge scheme." *Journal of Hydraulic Research*, 38(4), 299-306.

Stephenson, D. and Kolovopoulos, P. (1990). "Effects of momentum transfer on compound channels." *Journal of Hydraulic Engineering*, 116(12), 1512-1522.

Tang, X. N., Knight, D. W., and Samuels, P. G. (1999a). "Volume conservation in variable parameter Muskingum-Cunge equation." *Journal of Hydraulic Engineering*, 125(6), 610-620.

Tang, X. N. and Knight, D. W. (1999b). "Variable parameter Muskingum-Cunge method for flood routing in a compound channel." *Journal of Hydraulic Research*, 37(5), 591-613.

Toebes, G. H. and Sooky, A. A. (1967). "Hydraulics of meandering rivers with floodplains." *Journal of Waterway and Harbor Division*, 93(2), 213-236.

United States Army Corps of Engineers (USACE) (1994). *Flood Runoff Analysis (EM 1110-2-1417)*. August 1994.

USACE, Hydrologic Engineering Center (HEC) (1998). *HEC-1 Flood Hydrograph Package User's Manual, Version 4.1*. June 1998.

USACE, HEC (2000). *Hydrologic Modeling System, HEC-HMS, Technical Reference Manual, Version 2.0*. pp. 80-99.

USACE, HEC (2002a). *HEC-RAS River Analyses System, User's Manual, Version 3.1 (CPD-68).* November 2002.

USACE, HEC (2002b). *HEC-RAS River Analyses System, Hydraulic Reference Manual, Version 3.1 (CPD-69).* November 2002.

USACE, HEC (2005). *HEC-GeoRAS, GIS Tools for support of HEC-RAS using ArcGIS, User's Manual, Version 4 (CPD-83).* September 2005.

Younkin, L. M. and Merkel, W. H. (1988). "Evaluation of diffusion models for flood routing." *Proceedings, 1988 National Conference on Hydraulic Engineering, Colorado Springs, Colo.* Sponsored by ASCE, Reston, Va. 674-680.

Wang, G. T., Chen, S., and Singh, V. P. (2003). "Nonlinear convection-diffusion equation with mixing-cell method for channel flood routing." *Journal of Hydrologic Engineering*, 8(5), 259-265.

Weinmann, P. E. and Laurenson, E. M. (1979). "Approximate flood routing methods: a review." *Journal of the Hydraulics Division*, 105(12), 1521-1535.

Wormleaton, P. R. and Merrett, D. J. (1990). "An improved method of calculation for steady uniform flow in prismatic main channel/floodplain sections." *Journal of Hydraulic Research*, 128(2), 157-174.